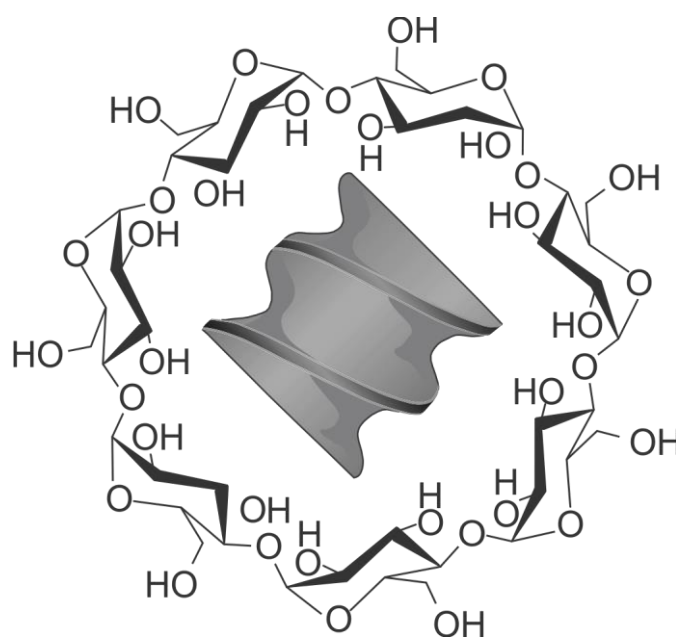


Solvent-Free Processes for the Formation of β -Cyclodextrin Inclusion Complexes Within a Melt-Twin-Screw- Extruder



Doctoral Thesis Submitted in the Fulfilment of the Requirements for the Degree of Doctor in Natural Sciences
at Kiel University, Germany

By

Annika Kristin Heel

Kiel 2018

Reviewer: Prof. Dr. Hartwig Steckel
Co-Reviewer: Prof. Dr. Regina Scherließ

Date of Defense: 06.04.2018
Accepted for publication: 10.04.2018

sgd. Prof. Dr. Natascha Oppelt
(Dean)

Für meine Eltern,
Sibylle und Kai-Detlef Heel

Parts of this work were previously published in conference contributions:

Conference Poster Presentations

- ❖ Heel, A., Steckel, H., Inclusion Complex Formation by Hot-Melt Extrusion with β -Cyclodextrin and Itraconazole - A First Approach -, 8th Polish-German Symposium on Pharmaceutical Sciences, Kiel, Germany, May 2015
- ❖ Heel, A., Steckel, H., Development of Hot-Melt-Extrusion Process with β -Cyclodextrin and Itraconazole for Inclusion Complex Formation - A First Approach -, 4th European Conference on Cyclodextrins, Lille, France, October 2015
- ❖ Heel, A., Steckel, H., Hot-Melt Extrusion and Hot-Melt Granulation of beta-Cyclodextrin and Itraconazole Blend – A Comparative Study -, 10th World Meeting on Pharmaceutics, Biopharmaceutics and Pharmaceutical Technology, Glasgow, Scotland, April 2016
- ❖ Heel, A., Steckel, H., Polymer- and Solvent-Free Processes for the Continuous Production of β -Cyclodextrin/Itraconazole Inclusion Complexes Via Hot-Melt Granulation By a Melt-Twin-Screw-Extruder, 22nd Annual Meeting of the Controlled Release Society (Germany Local Chapter), Halle, Germany, March 2018

Flash Oral Presentation

- ❖ Heel, A., Steckel, H., Development of Hot-Melt-Extrusion Process with β -Cyclodextrin and Itraconazole for Inclusion Complex Formation - A First Approach -, 4th European Conference on Cyclodextrins, Lille, France, October 7th 2015; Best Presentation Award

Oral Presentation

- ❖ Heel, A., Steckel H., Solvent-Free Inclusion Complex Formation in Hot-Melt Granulated β -Cyclodextrin/Itraconazole Blend to Improve Itraconazole Dissolution, 5th European Conference on Cyclodextrins, Lisbon, Portugal, October 5th 2017

*Aus der Wahrheit Feuerspiegel
Lächelt sie den Forscher an.
Zu der Tugend steilem Hügel
Leitet sie des Dulders Bahn.
Auf des Glaubens Sonnenberge
Sieht man ihre Fahnen wehn,
Durch den Riß gesprengter Särge
Sie im Chor der Engel stehn.*

An die Freude, Friedrich Schiller

Lack of a specific mark or a reference to a trademark or a patent does not imply that this work or part of it can be used or copied without copyright permission.

Table of Contents

ABSTRACT (GERMAN)	a
ABSTRACT	c
I. Introduction and Definition of Objectives	1
I.1. Introduction	1
I.2. Objectives	3
II. Theoretical Background	5
II.1. Solubility and Solubility Rate Enhancement of Active Pharmaceutical Ingredients	5
II.2. Solid Dispersions by Hot-Melt Extrusion and Hot-Melt Granulation	8
II.2.1. Solid Dispersions	8
II.2.2. Hot-Melt Extrusion	10
II.2.3. Hot-Melt Granulation	14
II.3. Inclusion Complexes with Cyclodextrins	15
III. Material and Methods	19
III.1. Material	19
III.1.1. Itraconazole	19
III.1.2. Sempera [®] /Sporanox [®] Capsules.....	21
III.1.3. β -Cyclodextrin and Hydroxypropyl- β -Cyclodextrin	22
III.1.4. Soluplus [®]	26
III.1.5. Polyethylene Glycol 6000	27
III.1.6. Xylitol.....	28
III.1.7. Hydroxypropyl Methylcellulose	28
III.2. Methods	30
III.2.1. Preparative Methods.....	30
III.2.1.1. Preparation of Powder Blends	30
III.2.1.2. Kneading and Wet Granulation	31
III.2.1.3. Hot-Melt Extrusion and Hot-Melt Granulation	32
III.2.1.3.1. Pharma 11 Twin Screw Extruder	32
III.2.2. Analytical Methods	37
III.2.2.1. Phase Solubility Analyses and Data Interpretation	37
III.2.2.2. Thermal Analysis	40
III.2.2.2.1. Differential Scanning Calorimetry	40

III.2.2.2.2.	Thermal Gravimetry	41
III.2.2.3.	Itraconazole Content Evaluation.....	42
III.2.2.3.1.	UV-Spectroscopy	42
III.2.2.3.2.	High Performance Liquid Chromatography	43
III.2.2.3.3.	f_1 and f_2 -Concept	43
III.2.2.4.	Quantification of Cyclodextrins.....	44
III.2.2.5.	X-ray Powder Diffraction	45
III.2.2.6.	Attenuated Total Reflectance Fourier-Transform-Infrared Spectroscopy Implementation and Data Evaluation	47
III.2.2.6.1.	Data Evaluation for Inclusion Complex Detection	48
III.2.2.7.	Laser Diffraction	50
III.2.2.8.	Scanning Electron Microscopy.....	50
III.2.2.9.	Dissolution Testing.....	51
III.2.2.10.	Storage Stability	53
IV.	Results and Discussion	55
IV.1.	Phase Solubility Measurements Results.....	55
IV.1.1.	Evaluation of Phase Solubility Diagrams and Discussion	55
IV.1.2.	Concluding Remarks about Phase Solubility Measurements	60
IV.2.	Development of Binary Hot-Melt Process.....	61
IV.2.1.	Binary Hot-Melt Extrusion Process.....	61
IV.2.1.1.	Physico-Chemical Characterisation of Raw Material and Powder Blend ...	61
IV.2.1.2.	Preliminary Hot-Melt Extrusion Trials and Optimisations.....	64
IV.2.1.2.1.	Different Die Arrangements: 2 mm Standard Die	65
IV.2.1.2.2.	Different Die Arrangements: 3 mm and 6 mm Variable Systems	67
IV.2.1.2.3.	Development of 6 mm Conical Die and Utilisation.....	69
IV.2.1.3.	Characterisation of Extrudates for Content Evaluation and Amorphousness ..	71
IV.2.1.4.	Concluding Remarks about the Hot-Melt Extrusion Process.....	73
IV.2.2.	Binary Hot-Melt-Granulation Process	73
IV.2.2.1.	Hot-Melt Granulation Parameters	73
IV.2.2.2.	Characterisation of Hot-Melt-Granules	74
IV.2.3.	Closing Remarks about the Hot-Melt-Granulation Procedure	75
IV.3.	Comparative Evaluation of Hot-Melt Extrusion and Hot-Melt Granulation Procedures	76
IV.3.1.	Physico-Chemical Comparison of Melt Extrudate and Granules	76
IV.3.2.	Solubility Measurements and Itraconazole Dissolution.....	77
IV.3.3.	Inclusion Complex Detection in Melt Extrudates and Granules.....	80
IV.3.3.1.	ATR-FT-IR Results and Discussion	80

IV.3.4.	Concluding Remarks and Decision for Hot-Melt Procedure Gold Standard	84
IV.4.	Hot-Melt Granulation Process Optimisation	85
IV.4.1.	Experimental Set-Up and Processability	86
IV.4.2.	Physico-Chemical Characterisation of HMG Trial A - D.....	87
IV.4.3.	Dissolution Testing and Inclusion Complex Formation Evaluation of HMG Trial A - D	94
IV.4.4.	Concluding Remarks about HMG Trial A - D.....	99
IV.5.	Investigating Hot-Melt-Granulation against Physical Inclusion Complex Formation Methods	99
IV.5.1.	Kneading Process and Wet Granulation Processability	99
IV.5.2.	Physico-Chemical Characterisation of KN and HMG Trial WG.....	100
IV.5.3.	Dissolution Testing and Inclusion Complex Formation Evaluation of KN and HMG Trial WG	104
IV.5.4.	Concluding Remarks about KN and HMG Trial WG	106
IV.6.	Examination of the Influence of Hydroxypropyl-β-Cyclodextrin on Product Quality	107
IV.6.1.	Hot-Melt Granulation Process.....	107
IV.6.2.	Physico-Chemical Characterisation of HMG Trial HP	108
IV.6.3.	Dissolution Testing and Inclusion Complex Formation Evaluation of HMG Trial HP.....	111
IV.6.4.	Concluding Remarks about HMG Trial HP	113
IV.7.	Influence of a Polymer Matrix in Hot-Melt Granulation	114
IV.7.1.	Hot-Melt-Granulation Process Parameters and Processability	114
IV.7.2.	Physico-Chemical Characterisation of HMG Trial SOLU	116
IV.7.3.	Dissolution Results of HMG Trial SOLU	120
IV.7.4.	Concluding Remarks about HMG Trial SOLU.....	121
IV.8.	Comparison of Hot-Melt Granulation Procedure against the Marketed Formulation	122
IV.8.1.	Physico-Chemical Characterisation of SEMP and Pellet Dissolution	122
IV.8.2.	Concluding Remarks about SEMP	125
IV.9.	Ternary Additives as Possible Dissolution Enhancers	126
IV.9.1.	Case Study Polyethylene Glycol 6000	127
IV.9.1.1.	Preparation and Behaviour During Hot-Melt-Granulation of Polyethylene Glycol 6000 Blends.....	127
IV.9.1.2.	Physico-Chemical Characterisation of HMG Trial PEG, PEG10 and PEG20	128
IV.9.1.3.	Dissolution Results and Inclusion Complex Formation Evaluation of HMG Trial PEG, PEG10 and PEG20.....	131

Table of Contents

IV.9.1.4.	Outcome of Case Study Polyethylene Glycol 6000	134
IV.9.2.	Case Study Hydroxypropyl Methylcellulose	134
IV.9.2.1.	Preparation and Behaviour During Hot-Melt Granulation of Hydroxypropyl Methylcellulose Blends	135
IV.9.2.2.	Physico-Chemical Characterisation of HMG Trial HPMC, HPMC10 and HPMC20.....	136
IV.9.2.3.	Dissolution Results and Inclusion Complex Formation Evaluation of HMG Trial HPMC, HPMC10 and HPMC20	138
IV.9.2.4.	Outcome of Case Study Hydroxypropyl Methylcellulose.....	141
IV.9.3.	Case Study Xylitol.....	141
IV.9.3.1.	Preparation and Behaviour During Hot-Melt Granulation of Xylitol Blends .	142
IV.9.3.2.	Physico-Chemical Characterisation of HMG Trial XYL, XYL10 and XYL20 .	143
IV.9.3.3.	Dissolution Results and Inclusion Complex Formation Evaluation of HMG Trial XYL, XYL10, XYL20	146
IV.9.3.4.	Outcome of Case Study Xylitol.....	148
IV.9.4.	Concluding Remarks About the Addition of Ternary Additives.....	149
IV.10.	Storage Stability	150
IV.10.1.	Chosen Samples	150
IV.10.2.	Stability over Six Months	150
IV.10.2.1.	Changes in Physico-Chemical Properties	150
IV.10.2.2.	Variations in Dissolution and ATR-FT-IR Spectroscopic Changes.....	160
IV.10.3.	Concluding Remarks about the Stability Study.....	170
V.	Comparative Summary and Overall Discussion	172
V.1.	Hot-Melt Processes and Formulation Approaches	172
VI.	Conclusion and Perspectives.....	183
VI.1.	Final Denouement and Scientific Significance of the Developed Formulation.....	183
VI.2.	Future Possibilities	184
VII.	Appendices	186
VII.1.	Abbreviations, Units and Variables	186
VII.2.	Analyser Materials.....	191
VII.3.	Methods for Content Evaluation	192
VII.3.1.	HPLC Method for Itraconazole Content Evaluation	192
VII.3.2.	HPLC Method for Cyclodextrin Content Evaluation	192
VII.3.3.	Comparison of Methods for Itraconazole Content Evaluation.....	193
VIII.	Literature References	I

ABSTRACT (GERMAN)

Eine der größten Herausforderungen für die Formulierungsentwicklung in der pharmazeutischen Technologie ist die häufig schlechte Wasserlöslichkeit von Wirkstoffen (WS). Nur ein im Körper gelöst vorliegender WS wird seine Wirkung voll entfalten können. Nach der oralen Gabe einer festen Arzneiform und deren Disintegration im Gastrointestinaltrakt (GIT) muss der WS so schnell in Lösung gehen können, dass er während der Passagezeit durch den GIT absorbiert werden kann. Besonders in den letzten Jahrzehnten wurden vielfältige Technologien entwickelt, um Lösungsansätze hierfür zu finden. Zwei gängige Techniken, die Herstellung einer festen Dispersion mit einhergehender Amorphisierung des WS, sowie die Erzeugung von Einschlussverbindungen (EV) mit Cyclodextrinen (CD), wurden im Rahmen dieser Arbeit untersucht. Die festen Dispersionen oder gegebenenfalls feste Lösungen wurden hierbei mit den Methoden der Schmelzextrusion (SE) und Schmelzgranulation (SG) mit einem Zweischneckenschmelzextruder erhalten. Das sehr schlecht wasserlösliche Antimykotikum Itraconazol (ITR) diente in der vorliegenden Arbeit als Modellarzneistoff. Während üblicherweise thermoplastische Polymere als Matrixsubstanzen in Schmelzprozessen dienen, wurde hier vorwiegend β -Cyclodextrin (β CD) als Träger verwendet. Zudem lag der Fokus darauf, möglichst auf ternäre Zusätze zu verzichten und eine reine ITR- β CD-Formulierung zu gewinnen. Wie in Schmelzprozessen üblich, wurde vollständig auf die Zugabe von potentiell toxischen Lösungsmitteln verzichtet. Aber auch die Zugabe von Wasser, welches die mikrobielle Anfälligkeit einer Formulierung erhöhen kann, wurde vermieden. All dies ermöglichte einen kontinuierlichen, kostengünstigen und ökologisch attraktiven Herstellungsprozess.

Die Entwicklung einer solchen Formulierung und nicht zuletzt die Entwicklung des dazugehörigen stabilen Schmelzprozesses ist in der Literatur bisher nicht oder nur sehr marginal beschrieben worden und wird in den meisten Reviews nicht behandelt. Trotz der patentierten Anwendung von β CD als Träger in Schmelzprozessen werden EV mit WS fast ausschließlich im wässrigen Milieu gewonnen. Feste EV entstehen nachfolgend durch Gefriertrocknung oder vergleichbare Verfahren. Die Kombination von Schmelzprozessen und CD-EV ist zudem bis auf sehr wenige Ausnahmen nur im Beisein von Polymeren untersucht worden. Sowohl die komplett flüssigkeitsfreie Erzeugung von EV als auch die polymerfreie SE oder SG wurden bislang nicht umfassend charakterisiert, obwohl sich viele formulierungstechnische Vorteile in einer solchen Methodik vereinen. Daher lag es im be-

sonderen Interesse, synergistische oder additive Effekte dieser beiden Technologien auf die grundsätzlichen Eigenschaften des Produkts sowie vor allem auf die Löslichkeit beziehungsweise Lösungsgeschwindigkeit von ITR *in-vitro* zu untersuchen.

In der vorliegenden Arbeit konnte gezeigt werden, dass zum einen unter Zuhilfenahme einer eigens hierfür entwickelten Düsengeometrie eine stabile SE möglich war und zum anderen, dass gleichwertige Produkte mit einer stabilen SG erhalten werden konnten, die einfacher handzuhaben war. Es wurde ein optimales Temperaturprofil für die Herstellung des Schmelzgranulats gefunden, dessen Maximaltemperatur ca. 10 °C über dem Schmelzpunkt (T_m) von ITR lag. Dieses vereinte die Amorphisierung des ITR mit einer fast quantitativen WS-Freisetzung nach 120 min in 0,1 N HCl. Anhand der kombinierten Auswertung mehrerer Methoden war es möglich, auf das Vorhandensein von EV im Schmelzgranulat zu schließen. Auch die Verarbeitung deutlich unter dem T_m von ITR zeigte aufschlussreiche Ergebnisse, da sich dabei mit ca. 86 % die höchste relative Verbesserung der Freisetzung über 4 h nachweisen ließ. Da ITR hier vollständig kristallin vorlag, war der Nachweis von EV vor allem durch die Infrarotspektroskopie durchführbar.

Zudem wurden weitere Optimierungsansätze untersucht. Für Vergleichszwecke kamen polymerische Zusätze sowie ein Zuckeralkohol zum Einsatz. Des Weiteren wurden Sempera[®]-Kapseln, ein deutsches orales ITR-Marktprodukt, als Referenz analysiert. Einzig ein geringer Hydroxypropylmethylcellulose-Zusatz in der SG war in der Lage, die Freisetzungsgeschwindigkeit des ITR im Vergleich zum binären Schmelzgranulat zu erhöhen. Jedoch zeigte sich in diesem ternären System Segregation der Pulvermischung während der Fütterung des Schmelzextruders. Mit dem zur Verfügung stehenden Equipment war die Stabilität dieses Optimierungsansatzes nicht ausreichend gesichert. Eine kontrollierte Substanzzuführung über mehrere Fütterstationen könnte diese festgestellte Problematik jedoch beheben. Darüber hinaus wurden Stabilitätsuntersuchungen bei Stressbedingungen (40 °C/75 % relative Luftfeuchte) über sechs Monate bei fast allen hergestellten Proben durchgeführt. Hierbei konnte kein substantieller Qualitätsabfall der Produkte beobachtet werden.

Im Kontext dieser Arbeit konnte dargestellt werden, dass der entwickelte Schmelzgranulierungsprozess ein neuartiger, innovativer Ansatz für eine kontinuierliche Verarbeitung von CDs ist, um simultan wasserfrei EV zu erzeugen.

ABSTRACT

One of the major challenges in the field of pharmaceutical technology is the poor aqueous solubility of active pharmaceutical ingredients (APIs). Most of the time, the API can only come to full effect in the body if it is dissolved in physiological fluids. After oral administration of a solid dosage form and the following disintegration in the gastrointestinal tract (GIT), the dissolution kinetics of the API need to be fast enough so that API molecules can be absorbed during GIT passage. Especially in the last decades, a plethora of techniques were developed to resolve this. Two well-established technologies were combined in this project. Firstly, the manufacture of solid dispersions during which the API was transformed to its amorphous state and secondly, the formation of inclusion complexes (ICs) with cyclodextrins (CDs). For obtaining the solid dispersions or, if applicable, solid solutions, hot-melt extrusion (HME) and hot-melt granulation (HMG) were employed. Thereby, a melt twin-screw extruder was utilised. Throughout this thesis, the poorly water-soluble antifungal drug itraconazole (ITR) served as model API. Traditionally, the matrix component in melt processes is a thermoplastic polymer. Different from this, in this project, β -cyclodextrin (β CD) was investigated as carrier in HME and HMG. Moreover, the focus was put on trying to avoid ternary additives in the formulation as the overall aim was a binary product of ITR and β CD. As customary in melt processes, no potentially toxic liquid was added during manufacturing. Furthermore, the use of water was omitted since this can alter the microbiological susceptibility of the formulation. All of this ensured a continuous, cost-effective and ecologically attractive manufacturing process.

The development of such a formulation as well as the development of the stable melt process have only been described marginally in the literature. Most reviews do not even cover the possibility of this special application. Even though β CD has been patented for the use as matrix substance in HME, nearly all ICs are formed in an aqueous milieu. Solid ICs are successively obtained by freeze drying or comparable techniques. With only very few exceptions, the combination of melt processes and ICs with CDs has only been investigated in the presence of polymers. Both, the completely dry formation of ICs, as well as polymer-free melt processes have not been comprehensively characterised. This is surprising as both techniques unite diverse advantages for the formulation. Consequently, in this project, there was a strong interest to investigate synergistic and additive

effects that both of these technologies would have on the solubility or rather solubility rate of ITR *in-vitro* and on the general product.

In this present work, it was shown that it was possible to achieve a stable SE-process with β CD as matrix. For this, a self-developed die geometry was utilised. Also it was presented that products with the same quality could be obtained by a stable HMG procedure which was simpler to operate. An optimal HMG temperature profile was found. The maximum temperature was approximately 10 °C higher than the melting point (T_m) of ITR. By this, amorphisation of ITR was achieved as well as nearly quantitative ITR dissolution in 0.1 N HCl after 120 min. By using the combined results of different methods, it was possible to conclude the presence of ICs in the melt granules. Processing below ITR T_m also yielded informative results as the relatively highest increase in ITR dissolution over 4 h (86 %) was determined for such a sample. Since ITR was completely crystalline in this specimen, ICs could be verified by infrared spectroscopy.

Additionally, different optimisation approaches were investigated. Polymeric additives as well as a sugar alcohol were examined. Moreover, Sempera[®] capsules, an oral ITR formulation on the German market, was analysed as reference. Merely the minor addition of hydroxypropyl methylcellulose in HMG resulted in faster ITR dissolution compared to the binary product. However, during this HMG procedure, segregation of the powder blend occurred in the feeding system of the extruder. The available equipment did not allow sufficient and reproducible stability of this optimisation approach. Nonetheless, this phenomenon could probably be resolved by applying a more controllable feeding system with separate feeding units. Finally, a stability study was conducted at elevated conditions (40 °C/75 % relative humidity) for six months. Nearly all manufactured samples were subjected to this stability investigation. No substantial loss in product quality was seen.

In this thesis, it became obvious that the developed HMG process is a novel and innovative approach for the continuous processing of CDs during which solvent-free IC formation can be achieved.

I. Introduction and Definition of Objectives

I.1. Introduction

Since recent years the pharmaceutical industry faces new obstacles in regard to the development of innovative, acceptable formulations. The main objection for pharmaceutical technologists probably is the increasing amount of active pharmaceutical ingredients (APIs) with poor aqueous solubility. This can lead to inadequate dissolution and, consequently, bioavailability. Due to advanced high throughput screening techniques, these days, new APIs, also called new chemical entities (NCEs), are often developed backwards by identifying a target and then creating a molecule for interaction. By this, the amount of NCEs with high lipophilicity oftentimes increases. It is estimated that over 40 % of marketed drugs are poorly water-soluble as well as about 60 % of NCEs, coming directly out of the synthesis laboratories [1]. These poorly soluble NCEs can be categorised according to the Biopharmaceutics Classification System (BCS) by assigning them either in class II or class IV [2]. APIs categorised into BCS class IV possess poor aqueous solubility as well as insufficient intestinal permeability, whereas BCS class II compounds exhibit good permeability properties.

BCS class II APIs are most applicable for solubility enhancement by formulation design opposing to BCS class IV drugs that are more likely candidates for changes on the chemical level, such as addition of functional groups or synthesising them as pro-drugs [3]. For BCS class II compounds, the rate limiting step regarding bioavailability is either their absolute solubility or their dissolution rate as it is proposed that after being dissolved in the gastrointestinal tract (GIT), absorption is rapidly following [4]. Therefore, formulation design of BCS class II drugs has to be carried out carefully to overcome the deficiency in aqueous solubility. Depending on the desired dosage form, different techniques can be used for this solubility enhancement, such as micronisation, nanosizing, crystal engineering, solid dispersions by hot-melt extrusion (HME), hot-melt granulation (HMG) and formation of inclusion complexes (ICs) with cyclodextrins (CDs) [5].

Even though formulation research constantly brings forward innovative approaches for non-invasive systemic drug delivery such as dermal, pulmonary or nasal application, the most common for drug administration still is the oral route which also shows highest patient adherence [6]. Solid forms comprise the largest

share of oral formulations, since they combine different positive properties both for the patient as well as for the pharmaceutical manufacturer, like simple administration or cost-effective transportation.

After oral administration of a solid form, the API needs to dissolve in the GIT and will then most likely be absorbed in the small intestine before it can take effect [7]. The oral bioavailability of APIs can vary strongly between different patients but also for each individual itself due to e.g. change in gastric pH or liquid in the GIT. The formulation comprises an additional factor which could possibly be responsible for therapeutic failure. Many medications already on the market show insufficient and fluctuating bioavailabilities. For instance, when administering diclofenac or glibenclamide, the oral bioavailability is strongly dependent on the formulation and situated between 30 - 80 % and 50 - 90 %, respectively [7]. When no alternatives are at disposal, patients have to cope with the risk of either inadequate API efficacy or on the other hand, more adverse reactions. By guaranteeing that the absorbed API shows the desired therapeutic effect, doses may have to be determined higher than necessary with improved formulation design. This shows that, although much research has been and still is conducted in the field of solubility and dissolution rate enhancement of orally administered drugs, there is definitely room for improvement. Most inquiries only deal with one single solubility enhancing technique. Combinational approaches are rarely reported and reviews usually discuss procedures as stand-alones [1,5,8].

Over the years, pharmaceutical production has constantly become more regulated which on the one hand is positive for the consumer as it further ensures product quality but on the other hand, regulatory, manufacturing and maintaining costs have risen for the pharmaceutical companies. As the development of new formulations and NCEs is very costly and patent protection often expires already a few years after the medication has entered the market, the originator company has only limited time to earn the necessary turnover from the product. A key factor in ensuring this is to keep manufacturing processes as cost-effective and simple as possible whereby at the same time upholding high product quality. Traditionally, pharmaceutical production was carried out in batch mode. Recently, continuous manufacturing has become more and more important as it has been recognised by the Food and Drug Administration (FDA) of the United States of America (US) [9]. HME and HMG are processes eligible for this. By applying

these techniques, it is technically possible to operate production endlessly, resulting in cost savings. With the proper downstream equipment, it is theoretically possible to obtain the final dosage form directly after HME/HMG. Moreover, analytical tools can be applied to monitor product quality throughout the whole procedure. This is an advantage compared to most batch processes where ordinarily samples of specified size are drawn during manufacturing for in-process controls. In batch production mode, there is rarely the possibility of a full-batch control, especially in volume production where millions of units are produced in a few hours.

Taking all of the points previously mentioned into account, it becomes clear that important aspects regarding the future of pharmaceutical technology can be identified. First of all, solubility enhancing formulation design should be available not only for innovative dosage forms but also for the most utilised oral solids. By this, satisfactory oral bioavailability may be ensured for BCS class II drugs and other substances that show deficiencies in that area. The chosen techniques to achieve this should not be applied as solitaires but rather be combinatorically investigated to expose synergistic and additive effects for the joint product. Secondly, the thereby invented formulations should be producible in a cost-effective, quality-upholding manner, in the best case by a continuous manufacturing process.

In consequence, this thesis presents an innovative approach in the development of a solid, oral formulation and optimisation thereof which conflates all of these identified needs. The present project targets the solid dispersion technique by HME and HMG combined with the encapsulation by CDs to improve the aqueous solubility of a model BCS class II API. Furthermore, this combinational approach will be attempted simultaneously during continuous hot-melt procedures.

I.2. Objectives

The present work aims at developing a novel oral solid formulation for the BCS class II model compound itraconazole (ITR). The oral bioavailability of ITR shows great variability and is situated at an average 55 % for the marketed capsule-based formulation Sporanox[®] [10]. Here, ITR spray-coated neutral pellets with an ITR mass fraction (drug load) of approximately 22 % are prepared in multi-stage batch production (see section III.1.2.). In this thesis, emphasis will be put on continuously preparing a formulation with ITR that exhibits higher drug load

than the marketed counterpart. To pursue advances in ITR dissolution, two solubility enhancing methods will be intertwined. Solid dispersions will be prepared by hot-melt procedures within a melt-twin screw extruder (mTSE). Thereby, the API can become trapped in a usually polymeric matrix in its amorphous state, resulting in strong dissolution improvement. Apart from the traditional use of polymers as matrices, CDs will be investigated as matrix to additionally enhance ITR solubility by forming ICs within the mTSE.

Generally, inclusion complex formation (ICF) occurs in the presence of water, mostly in solution [11]. Thus, the merging of these two techniques, utilisation of an mTSE as well as solvent-free formation of solid ICs during HME or HMG are innovative approaches in formulation design. Through this combinational approach, possible additional and synergistic effects on API solubility and the general product can be investigated. To ensure cost-effectiveness, unmodified β CD will be utilised predominantly, as it is a considerably inexpensive sustainable excipient.

Based on this overall aim of the current study, the following chronological targets can be ascertained:

Firstly, a stable operating mTSE process has to be developed and optimised to yield products with sufficient characteristics. This includes the exhibition of ICs as well as enhanced ITR dissolution. To detect solid ICs, data of different analytical tools will be interpreted in a self-constructed coordinated scheme. Preformulation studies will be carried out and evolved into a final hot-melt procedure. The melt-processed product will be characterised thoroughly.

Secondly, the developed formulation will be compared with the marketed formulation, alternative methods of ICF as well as varying hot-melt matrix or ternary components to put the formulation's results into a wider scientific perspective. The products' storage stability will be evaluated to gain insights into their behaviours at different storage conditions and, moreover, to identify differences between the examined alternatives.

Finally, it will be possible to assess the newly developed formulation's future perspectives and to choose the most promising formulation design approach of all the diverse investigated specimen.

II. Theoretical Background

The subsequent chapter gives insights into the necessary theoretical facts for the deeper understanding of this thesis.

II.1. Solubility and Solubility Rate Enhancement of Active Pharmaceutical Ingredients

As mentioned, different strategies can be taken for improving the solubility of poorly soluble substances such as BCS class II compounds. For full comprehension, a schematic view of the different BCS classes is shown in Figure II.1..

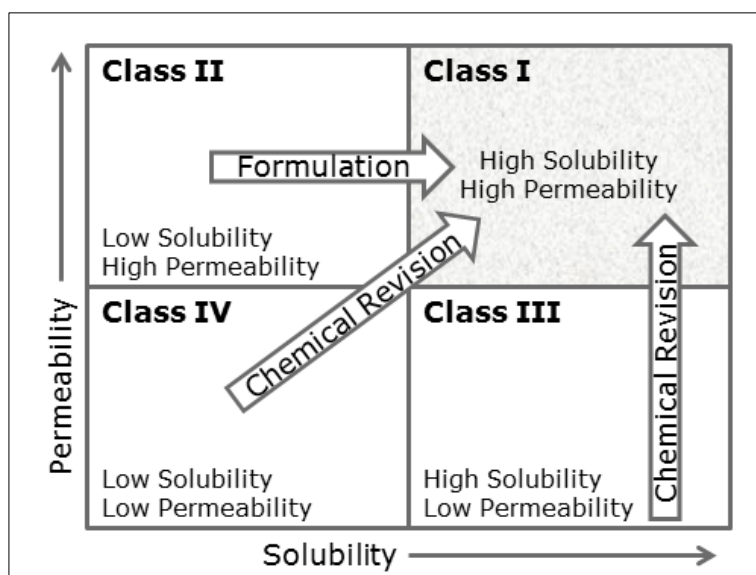


Figure II.1. - Schematic representation of the four different divisions in the Biopharmaceutics Classification System according to [3].

This project concentrates on the solubility and dissolution rate enhancements of the BCS class II model drug ITR. Recently, Butler and Dressman further divided BCS class II in class IIa and class IIb in their so-called "Developability Classification System" (DCS) [12]. Hereby, class IIa substances show dissolution rate limited absorption in the body whereas class IIb drugs are absorbed solubility limited. This means that a class IIa API will most likely achieve complete oral absorption even when its saturation solubility is reached in the intestines without the need for complex formulation technologies. Class IIb drugs tend to only show full absorption if the formulation design achieves an already solubilised form. Generally, class IIb APIs prove the greater challenge in formulation development [12]. According to Butler, ITR belongs to DCS class IIb [13].

Table II.1. gives a detailed overview of different techniques for solubility enhancement, categorised according to either physical or chemical modifications on the drug in question.

Table II.1. - Different approaches for enhancing drug solubility or enlarging the available surface area for improving dissolution rate, combined and modified after [14,15].

Physical modifications	<i>Particle size by</i>
	<i>Micronisation</i>
	<i>Nanosuspensions</i>
	<i>Crystal engineering</i>
	<i>Creation of polymorphs</i>
	<i>Creation of co-crystals</i>
	<i>Creation of pseudopolymorphs, including solvates</i>
	<i>Complexation, solubilisation and delivery systems</i>
	<i>With surfactants</i>
	<i>Micelles</i>
<i>Emulsions and microemulsions</i>	
<i>Self-emulsifying systems</i>	
<i>With cyclodextrins</i>	
<i>Liposomes and niosomes</i>	
<i>Further micro/nanoparticles</i>	
<i>Drug dispersion in different carriers (mostly polymeric)</i>	
<i>Eutectic mixtures</i>	
<i>Solid dispersions (non-molecular)</i>	
<i>Solid solutions</i>	
Chemical modifications	<i>Soluble pro-drugs</i>
	<i>Salts</i>
	<i>Changes in lipophilic/hydrophilic moieties in synthesis</i>

The first step in understanding solubility enhancement is the definition of solubility. The Pharmacopoeia Europaea (Ph. Eur.) defines solubility as the saturated concentration of a solute (e.g. drug) in regard to the volume of a given sol-

vent (e.g. gastric fluids) between 15 - 25 °C [16]. This illustrates that the solubility of a substance is a constant at specific conditions. Thus, the term solubility enhancement can somewhat be misleading as true solubility enhancement is generally only possible by changing the substance on a molecular level such as by altered synthesis or by changing the crystal habit (see Table II.1.). In most other cases, it is only the solubility/dissolution rate (DR) which is improved, such as by enlarging the surface area of the API. An exception to this is the creation of a supersaturated solution. By using different excipients, the API is kept from precipitating in a solution where its concentration exceeds its actual solubility. Examples for these excipients are surfactants or CDs. The modified Noyes-Whitney equation (*equation 1*) explains the relationship between important factors relevant for dissolution of poorly soluble compounds in the GIT [17].

$$DR = \frac{dX}{dt} = \frac{A \cdot D}{h} \cdot \left(C_s - \frac{Xd}{V} \right) \quad \text{equation 1}$$

Here, dX is the amount of dissolved drug during a specified time period dt , A is the surface area of the API, D the diffusion coefficient, h the effective boundary layer thickness, C_s the saturation concentration of the API in the gastric conditions, V the volume of the surrounding fluid and X_d the amount of drug already dissolved in this fluid. Figure II.2. shows a simplified model of how a drug is absorbed after being orally ingested. The solid dosage form has to disintegrate and subsequently release the API which can then become dissolved. At all times, a certain amount of drug will deteriorate in the gastric environment, possibly by enzymatic reactions or hydrolysis. Therefore, the release from the dosage form, the dissolution and the absorption of the API have to occur fast enough or else all of the drug will be metabolised without significant absorption and effect.

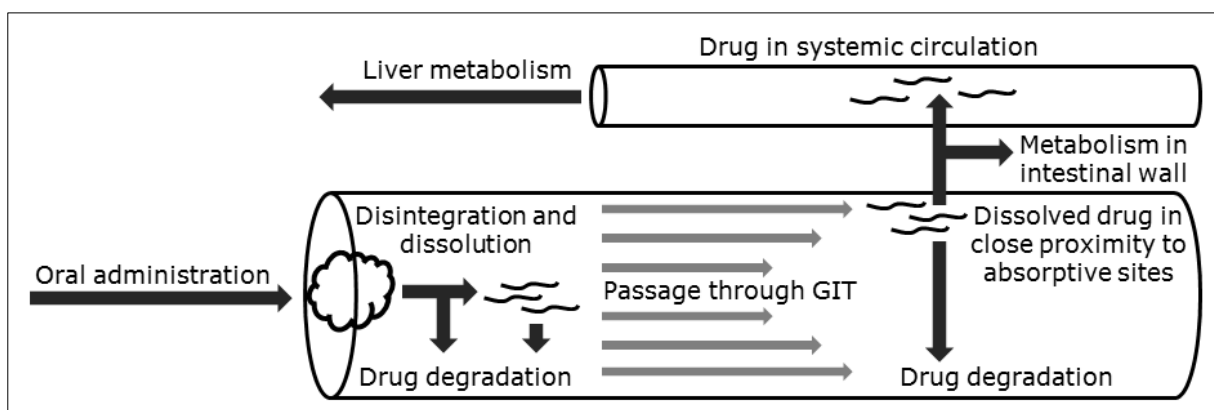


Figure II.2. - Following the simplified different occurrences after administering a solid oral dosage form, modified after [7,17].

The dissolved drug molecules are passing the intestinal wall, where most absorption takes place. From there, the drug can enter the blood circulation and reach its target site. Simultaneously, the drug undergoes metabolism in the liver and in the gut wall. The degree of these metabolisms is strongly dependent on drug properties. As mentioned, for BCS class II or rather DCS class IIa drugs, the absorption rate is often controlled by the dissolution rate [3]. They have to dissolve during GIT passage so that they can still reach the absorptive sites. From there, absorption is generally very fast. This explains why so many of the techniques mentioned in Table II.1. utilise an enhancement of surface area. This improves the wettability of the drug and consequently the dissolution rate (see *equation 1*). For DCS class IIb drugs like ITR, additional techniques such as complexation, solubilisation or amorphisation may be necessary to achieve a supersaturated state or improve solubility. By this, the (supersaturated) solution enables API molecules to reach the absorptive sites.

Usually, the above-named applications are singularly employed. In this project, an innovative approach was sought out: the combination of two of these well-established methods to possibly detect synergistic and additive effects on the solubility and dissolution rate of ITR. Solid dispersion technique is known to improve ITR's bioavailability [13]. Apart from this, there is an oral solution on the market employing ICF with CDs [10]. Therefore, encapsulation by β CD was utilised to create a supersaturated API system. Moreover, β CD served as matrix component in which ITR was supposed to be delicately dispersed. This dispersion was attempted by using HME and HMG processes. Besides the ability to create solid dispersions and solutions by HME/HMG, there is the possibility of API amorphisation which can further enhance drug solubility. The following subsections will focus on these applications that were carried out within this work.

II.2. Solid Dispersions by Hot-Melt Extrusion and Hot-Melt Granulation

II.2.1. Solid Dispersions

In 1971, Chiou and Riegelman defined a solid dispersion as a dispersion of one or more APIs in an inert carrier or matrix system in the solid state. They only referred to systems that were prepared by melting, solvent or melting-solvent methods [18]. However, due to the development of new technologies, especially

in the field of nanoparticles, the line between solid dispersions and other formulation approaches has become blurred. In recent times, solid dispersion mostly refers to a glassy solution of a drug in an amorphous carrier with high glass transition temperatures (T_g) [19]. The matrix substance in these formulations is in almost all cases polymeric. Nonetheless, different subtypes of solid dispersions are known and are presented in Table II.2..

Table II.2. - Different subtypes of solid dispersions according to [20].

Subtype of Solid Dispersion	Carrier	API	Phases
I Eutectics	<i>crystalline</i>	<i>crystalline</i>	2
II Amorphous precipitates in crystalline matrix	<i>crystalline</i>	<i>amorphous</i>	2
III Solid solutions			
<i>a Continuous vs. discontinuous</i>	<i>crystalline</i>	<i>molecularly dispersed</i>	1 or 2
<i>b Substitutional vs. interstitial</i>	<i>crystalline</i>	<i>molecularly dispersed</i>	1 or 2
IV Glass suspension	<i>amorphous</i>	<i>crystalline</i>	2
V Glass suspension	<i>amorphous</i>	<i>amorphous</i>	2
VI Glass solution	<i>amorphous</i>	<i>molecularly dispersed</i>	1

Whereas for the carrier, where only the crystalline and the amorphous state are recognised, the drug can also be molecularly dispersed or rather “dissolved” in the matrix. If the solubilising capability of a matrix is large enough to dissolve all API molecules, the result is a solid solution with only one phase with one T_g where the T_g s of the sole components cannot be distinguished anymore. Eutectics are mixtures of very fine crystals of the components. If the carrier is highly water-soluble and the eutectic mixture is given into an aqueous environment, the carrier will rapidly dissolve, causing a large surface of the freed API particles. This increases the dissolution rate [15]. The same mechanism can be assumed for type II solid dispersions.

For solid solutions, two different categories with two subcategories each are known. These depend either on the miscibility of the substances (type IIIa, see Table II.2.), or on the API’s position in the crystal lattice (type IIIb). In a continuous solid solution, all components are completely miscible whereas in a discontinuous solid solution, there are only proportions in which a true solid solution can be reached. In other ratios, the components are not miscible. A substitution-

al solid solution is based on the theory that the solute drug substitutes for matrix molecules in the crystal lattice. In interstitial systems, the drug solutes will be situated in the interstitial spaces between matrix molecules [15]. In glass suspensions or solutions, the drug molecules can be either homogeneously dispersed in the carrier or situated in API-rich regions. If the drug was turned amorphous during manufacturing of solid dispersions or solutions, the saturation solubility will most likely increase. The main disadvantage of the amorphisation, however, is the fact that often, products are only metastable. As the crystalline state is mostly energetically favourable, amorphous systems tend to recrystallise directly after production or during storage. This recrystallisation is especially common when drug clusters are present in type V solid dispersions [20]. The chosen carrier can help to immobilise the drug molecules, hindering recrystallisation, e.g. due to viscosity or interactions with the API [20].

II.2.2. Hot-Melt Extrusion

As previously mentioned, for the preparation of solid dispersions, two technologies are recognised, melting and solvent methods. There are important disadvantages regarding the solvent method. Generally, it is time consuming due to long processing. Furthermore, drying steps are often necessary. With this, high costs arise as well as insecurity about product quality. As organic solvents are used frequently, it is crucial that no residuals of these often poisonous substances stay in the formulation [1,18]. Moreover, the use of toxic components could endanger personnel during production.

In the last decades, a particular melting technique, HME, has been gaining more and more ground in the creation of solid dispersions and solutions in the pharmaceutical field. It has been regularly applied industrially for at least a century. In the beginning, HME was employed in the plastics as well as in the food industry. Up to date, more than half of all plastic products are processed by HME. Examples for these products include pipes, bags, tape, fibres or sheets. The first industrial use of HME was in the mid-nineteenth century for the fabrication of plastic insulation of wires [21,22]. This already indicates that HME is a well-known and established technology in the field of polymer science. Nonetheless, its application in the pharmaceutical industry only dates back a few decades. Especially in the last twenty years, HME has advanced to being a platform technology when it comes to the development of solid dosage forms [23].

Figure II.3. shows the issued patents for the pharmaceutical employment of HME between 1983 and 2006 as well as an international scope where these patents were issued. Germany and the US together hold over 50 % of the market. But it is obvious that HME is a field that is internationally focused on.

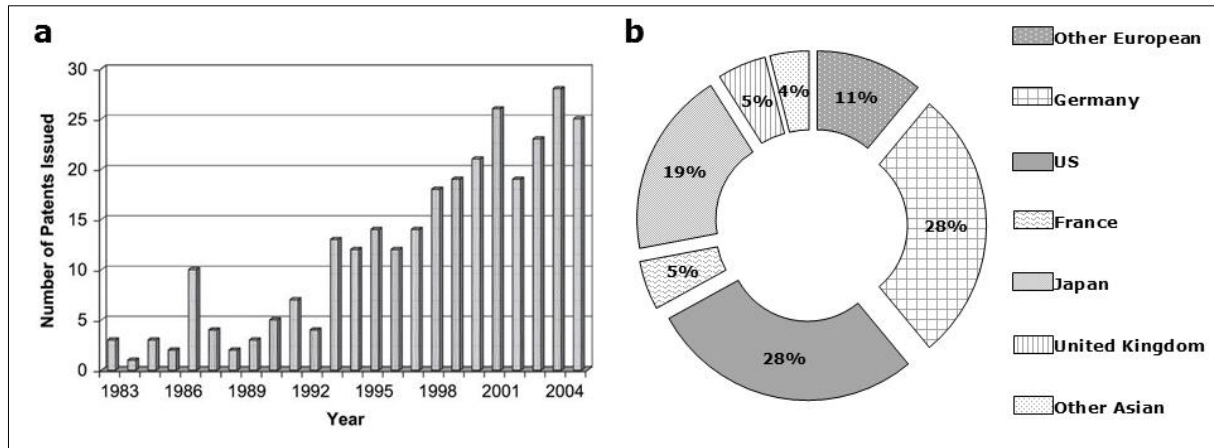


Figure II.3. - Patents regarding the pharmaceutical utilisation of HME issued between 1983 and 2006; a) shown in numbers per year and b) shown in percentage by country/continent; according to [21].

Extrusion in general is a procedure where raw material is fabricated into a product with consistent shape and density. These uniform properties are achieved by forcing the material through a die at specified conditions [24]. Whereas in wet extrusion, a liquid binder is used to agglutinate the material so that it forms a new shape after being deformed in the die, HME is a solvent-free technique. Here, the deformation is caused by applying controlled heat to the material. This is a strong advantage against solvent methods. The HME procedure can be divided into four different operations. Firstly, the material has to be fed to the extruder through a feeding system, also called a hopper. Secondly, it has to be transported through the extruder barrel while being mixed, grinded and kneaded. If necessary, ventilation ports for vapour discharge can be applied here. Thirdly, the material has to be pressed through the die and lastly, the product leaving the die, now called extrudate, has to be downstream processed, e.g. by calendaring, cutting or shaping in moulds [25].

HME is carried out utilising either melt-single screw extruders (mSSE), melt-twin screw extruders (mTSE), melt-multi screw extruders or ram extruders. This means that either one lone screw is rotating in the heated barrel or two or more screws which can be co- or counter-rotating and (non)intermeshing. In ram extrusion, a piston is used to press the material through the die. Hereby, the aris-

ing pressures are often very high [21,23]. Each of these set-ups has its own advantages and disadvantages. The most commonly applied is the mTSE with intermeshing co-rotating screws. This has positive effects on the mixing capability of the system. Additionally, intermeshing screws exhibit a so-called self-wiping effect which eliminates stagnation in the barrel and allows a more confined residence time of the material during HME. In this project, an intermeshing co-rotating mTSE set-up was employed. Figure II.4. shows a schematic view of this typical mTSE system.

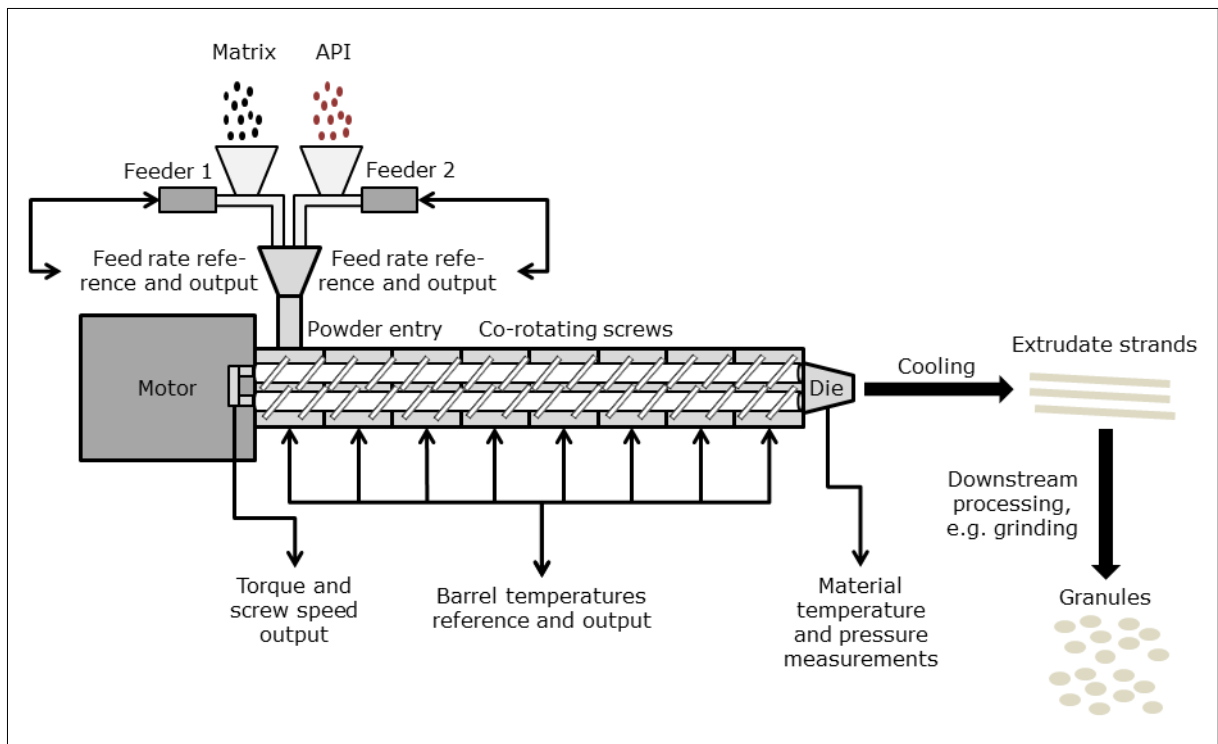


Figure II.4. - Scheme of typical HME procedure with an mTSE, adapted from [26].

The API and the matrix can either be pre-blended or fed into the mTSE by two separate hoppers. The zone of the powder entry is customarily not heated to avoid blockages. The other barrel zones are usually separately heated so that the ingredients follow a specified temperature profile along the barrel. Thereby, the material is melted, plasticised, mixed and compressed. The energy input is not only caused by the heated barrel but also due to shear and frictional forces by the screws and barrel walls [27]. In most cases, the screws can be assembled by combining different screw elements, such as kneading or conveying elements. The screw configuration has a large impact on the energy input during HME and thus, is also mostly chosen individually. The same applies for the chosen screw speed. The torque of the mTSE as well as the actual screw speed can be moni-

tored. At the end of the barrel the die is located. Different kinds of dies can be employed such as flat dies, circular dies or annular dies. Generally, the chosen die structure predicts the shape of the resulting product [27]. After leaving the die, the finished extrudate can be cooled under defined conditions or simply be air-cooled. Afterwards, downstream equipment can be used such as pelletisers or grinding equipment. The whole process of HME from feeding to the final formulation can be applied in a continuous fashion. Even though the classic solid dispersion or solution prepared by HME only necessitates an API as well as the matrix, other excipients can be added to the formulation to optimise product stability. Possible substances can e.g. belong to the classes of plasticisers, anti-oxidants or thermal lubricants [21].

The main disadvantage of HME is the thermal stress which is applied to the material [24]. Highly thermo-labile components cannot be processed by HME. Nonetheless, by the application of mTSE, the mean residence time of the substances in the barrel is kept relatively short. In some cases, this can allow the operation with generally thermo-labile molecules. The advantages of this technique outweigh the disadvantages by far. Reproducible, continuous manufacturing with simple equipment are only a few. No solvents are needed in this process. Additionally, HME enables constant monitoring and documentation of the process. Different parameters which are chosen at the beginning of the procedure are recorded continually such as feed rate, temperatures in the barrel, pressure at the die, extrudate temperature or the torque. This contributes to the FDA's process analytical technology (PAT) initiative. Hereby, products in pharmaceutical processes should be constantly monitored in-line, e.g. by employing UV spectroscopy, near infra-red spectroscopy (NIR) or Raman spectroscopy [24,27].

Pharmaceutically, HME is mainly used for solid dosage forms such as granules, pellets, spheres, tablets, capsules, transdermal and transmucosal films or implants [28–32]. Dominantly, polymers are used as matrices in these case studies. Very often, the target under investigation is not immediate drug release but rather modified or sustained drug delivery systems. Hereby, the choice of matrix is especially important as it usually controls the dissolution rate of the drug.

II.2.3. Hot-Melt Granulation

Another hot-melt process is HMG. Per definition, HMG is construed as an agglomeration process where a molten or softened binder (hydrophilic or hydrophobic) is added to fine solid particles [33]. Solid bridges can form when the molten material solidifies. Generally, the meltable binder should exhibit a T_m between 50 - 100 °C and should be present in the mixture in an amount of 10 - 30 % [34]. Applications for HMG are similar to HME, since the choice of binder can influence the drug release from the produced granules. Mostly, HMG is carried out by utilising high-shear mixers or fluidising granulators. The application of extruders is not impractical, albeit not the most common technique [34]. Recently, HMG is gaining more interest, as it can be operated as a continuous manufacturing process, e.g. by applying an mTSE. Shah and Repka stated that high shear mixers and fluidised bed granulators are inferior to mTSE regarding the flow mechanics and heat transfer in the barrel. The heat transfer within mTSE is easier to control and localise. Furthermore, the high uniformity allows simpler up-scaling [23]. Richter explained that it is possible to perform HMG with an mTSE by removing the die from the extruder barrel. By this, the material is granulated without rising pressure [35].

Batra et al. investigated the behaviour of different polymeric binders in HMG to achieve favourable compactibility of the produced granules [36]. They differentiated HME and HMG according to the following premises:

- i. in HME, the polymer content is usually > 60 % due to the formation of solid dispersions/solutions, whereas in HMG, it should be around 10 %,
- ii. in HME, the API can be miscible in the polymer,
- iii. in HMG, the process is carried out above T_g of the polymer and below T_m of the drug, whereas in HME, it is possible to operate the procedure while both substances are molten/softened,
- iv. HME products are usually extrudate strands [36].

Richter investigated two different polymeric binders with the same mTSE used in this project (see section III.2.1.3.) with a commercial granulation kit. She

found that processing below T_g resulted in unstable processes and thus, agreed with the postulations of Batra et al. [35,36].

It has to be noted that the procedure communicated as HMG in this thesis does not meet the conditions mentioned above. The ratio between API and matrix was always in the favour of the matrix. Additionally, processes were partly carried out above T_m of the model drug ITR and, depending on the used carrier, below $T_{g/m}$ of this component. No specified molten binder was used in this project. The molten API mostly served this purpose. Furthermore, in most experiments, no polymeric carrier was used as matrix system but rather the oligosaccharide β CD. These facts all indicate that no HMG was carried out in its traditional sense. However, for the lack of a better term for the innovative processes developed, they will still be referred to as HMG throughout this study whenever the mTSE was operated without a die.

II.3. Inclusion Complexes with Cyclodextrins

In addition to the HME/HMG technologies, in this work, the complexation with CDs was employed for solubility and dissolution rate enhancement of ITR. As stated, this oftentimes results in super-saturated drug systems. This subsection will focus on the improvement of oral bioavailability of APIs by ICF with CDs. The chemical structure and properties of the used CDs will be explained in more detail in section III.1.3.. It should be noted that the pharmaceutical application of CDs is not only limited to the enhancement of API solubility. Moreover, CDs can be used for taste masking, masking odours, increasing product stability or decreasing tissue irritation [37]. Over 30 different pharmaceutical formulations are marketed world-wide containing CDs, not only for oral delivery but also for a variety of other administrative routes [38]. However, it has to be added that one of the main advantages of CDs is also an important drawback when it comes to the application to CDs in generic formulations. The strong ability of CDs to enhance drug dissolution often results in CD-formulations failing in bioequivalence studies by outperforming the original medication. This decelerates the presence of CDs not only in original but also generic drug products [39].

CDs are sustainable excipients derived from starch through bacterial fermentation. They consist of D-glucopyranose monomers that are α -1,4-linked so that they form a cyclic structure. Due to the chair formation of the glucose units, the

CD molecules are shaped like truncated cones with a narrow and a wider edge. Here, primary hydroxyl (narrow edge) and secondary hydroxyl groups (wider edge) are located [40]. The inside of the central CD cavity is more lipophilic than their outer surface. This allows CDs to form ICs with a variety of drugs. In an IC, one (or rarely even more) drug molecule becomes incorporated in the central CD cavity [41]. This encapsulation occurs without the formation of covalent bonds. In aqueous solution, the API molecules that are included in the CD cavity are in equilibrium with the API molecules which are freely present [38]. In nearly all cases, ICF is performed with the aid of water or another solvent such as ethanol. However, there are reports that ICF with organic solvents yields inferior results to the use of water [42]. Carrier et al. reviewed the utilisation of CDs for enhancing oral bioavailability and investigated 28 different case studies. All presented ICs were prepared in an aqueous environment. Different ICF methods included freeze-drying, spray-drying, co-precipitation and grinding of a CD/API aqueous paste in a mortar [37]. Very often, ICs are proclaimed as solid systems or solid complexes. But, mostly this only refers to the final dosage form which was derived from an aqueous system of drug and CD [43,44]. A rare, truly solvent-free approach of creating ICs was attempted by Hassan et al. and Al-Marzouqi et al. who utilised supercritical carbon dioxide in a pressurised chamber to include ITR into β CD [45,46].

The driving forces for ICF have been extensively studied, however, to the best of the author's knowledge, only regarding ICF in solution. Nonetheless, it is still proclaimed that the complex mechanisms behind ICF are not fully understood. In 2002, Liu and Guo reviewed the literature about this issue and concluded that important driving forces for ICF in solution were electrostatic interactions, hydrophobic interactions, hydrogen bonding, charge-transfer interactions and Van-der-Waals forces. Moreover, they reviewed the release of cavity-bound high-energy water, release of conformational strain of the CD rings and the so-called "enthalpy-entropy compensation" [47]. With their findings, they continued the conclusion by Matsui et al. from 1985 who stated that the various intermolecular interactions act concurrently [48]. Although these results hold great value for the general understanding of CD chemistry, they do not fully apply for the investigated ICs in this work which were formed without further addition of solvents. As this manner of ICF by the combination of HME/HMG with CDs as matrix compo-

nents is a fairly new and innovative approach to create ICs, next to none research has been conducted in this field.

The present thesis concentrates on *in-vitro* evaluations of solid formulations intended for oral use. Consequently, understanding of the behaviour of a solid IC after oral administration is needed. Figure II.5. shows a simplified scheme of API absorption after intake of an IC. For the purpose of the scheme, it is not important how the IC is comprised. It could be any solid dosage form such as a capsule or a tablet.

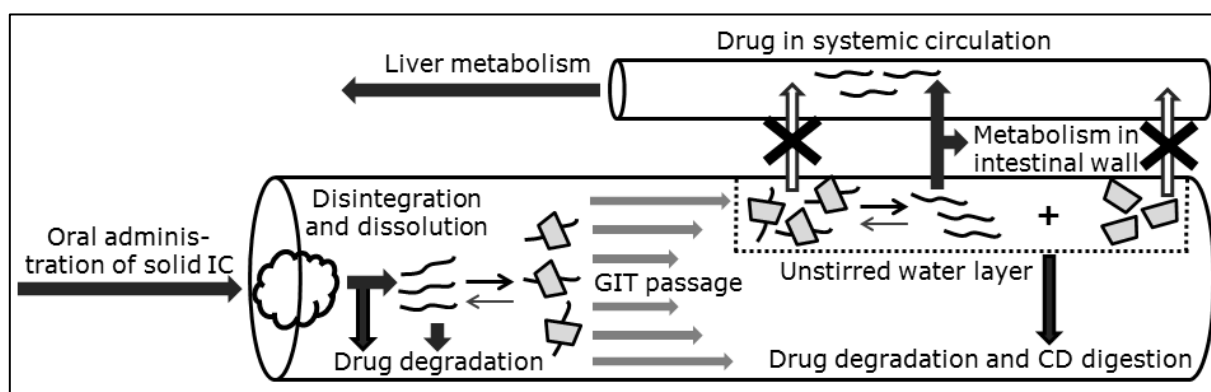


Figure II.5. - Scheme of drug absorption after oral administration of a solid IC, modified and combined from [17,40,41].

After intake, the dosage form has to disintegrate. The solid IC will most likely dissolve in the GIT fluids. There is a constant equilibrium between dissolved drug molecules and complex molecules. For simplification, the complex in Figure II.5. is depicted as the composition of one drug molecule and one CD molecule with the drug inhabiting the perfect centre of the cavity. In reality, the complex can also consist of a varying amount of CD and drug molecules or be a non-inclusion complex where the API can be located at the outer CD surface. Right after disintegration, the equilibrium will be switched to the side of the IC as it generally shows better aqueous solubility than the pure drug. The complex passes the GIT until it reaches the specified absorptive sites for the drug. Due to the high hydrophilicity and large size, CDs as well as ICs can only marginally pass biological membranes [38].

Most biological membranes exhibit an aqueous outer layer, also referred to as the unstirred water layer (UWL). The drug molecules need to diffuse through this barrier before they can further diffuse through the lipophilic membrane itself. Normally, CDs can only enhance the API absorption when the main hurdle of the

restricted bioavailability is the UWL and not the lipophilic membrane barrier. This also explains the fact that CDs only show little effect on the bioavailability of BCS class I and III drugs in contrast to BCS class II and IV [41,49]. In the scheme in Figure II.5. it is shown that the equilibrium in the UWL is switching to the free drug. This is simply caused by the fact that dissolved drug molecules further pass the intestinal wall which subsequently enhances the gradient of the equilibrium in the direction of the API. When formulating oral CD medications, care has to be taken in using an excess amount of CDs as this is known to rather decrease drug absorption in the GIT because not enough free drug molecules are able to pass the biological membrane [41].

Main driving forces for the exclusion of the drug from the IC have been described as dilution in the bodily fluids or competitive displacement (e.g. when substances in the GIT such as bile salts compete with the drug for the CD cavity). Additionally, drug-plasma binding, tissue uptake or CD elimination have also been postulated to be responsible for the rapid release of the API from the IC [49,50]. However, the latter three are most likely more dominant for parenteral IC application. Especially the dilution phenomenon is of great value in oral administration of solid CD formulations. If dilution occurs too early in the GIT, precipitation of the drug is possible. This is particularly the case if the drug:CD relationship in the formulation is non-linear [51]. Drug precipitation could further stall or decrease drug absorption as the drug molecules are not able to further reach their absorptive sites.

III. Material and Methods

III.1. Material

This section provides information about all investigated sample compounds. Details about the utilised analyser substances are located in the appendix (see section VII.2.).

III.1.1. Itraconazole

ITR is a triazole agent that inhibits the 14- α -demethylase, an enzyme that is found in fungal cells. It is responsible for converting lanosterol to ergosterol, a substance that is crucial for satisfactory function of the fungal cell membranes. Without functioning ergosterol synthesis, fungal cell proliferation is hindered. In addition to that, further mechanisms have been postulated about ITR's fungistatic - at high doses proclaimed fungicidal - effects. These are e.g. accumulation of intracellular hydrogen peroxide due to interactions with fungal cytochrome c oxidative and peroxidative enzymes, inhibition of purine uptake or interactions with membrane phospholipids. ITR is efficient against a broad spectrum of fungal pathogens (e.g. dermatophytes, dimorphic fungi, *Aspergilles spp.* and yeasts) and used in antifungal therapy since the 1980's [52,53]. Its high therapeutic efficacy is due to the lipophilic nature of the azole ring which is affiliated with enhanced tissue penetration, a longer serum half-life and improved interaction with the target enzymes [54]. Typical daily doses range from 50 - 400 mg dependent on the infested areas as well as on fungal species. Due to the risk of increased adverse effects like rare but severe hepatic toxicity at higher doses, if not necessary on medical grounds, 400 mg/d should not be exceeded [53,55].

Recently, ITR has been identified as a Hedgehog signalling pathway (Hh) inhibitor. Hh is suspected to support growth in different tumour species. *Ptch^{+/-}p53^{-/-}* mice that had allograft medulloblastomas treated with ITR showed suppression of tumour growth at serum levels that were comparable to patients undergoing antifungal therapy [56]. Searching for ITR as cancer treatment in the national database of the US government for clinical trials revealed that in the end of 2017, various clinical studies were recruiting or had already been finished, dealing with basal cell cancer, non-small cell lung cancer, oesophageal cancer, metastatic prostate cancer, metastatic breast cancer and others [57].

ITR is commercially available as oral capsules (see section III.1.2.) or in liquid form as oral and i.v. solution [58]. Figure III.1. shows ITR's chemical structure.

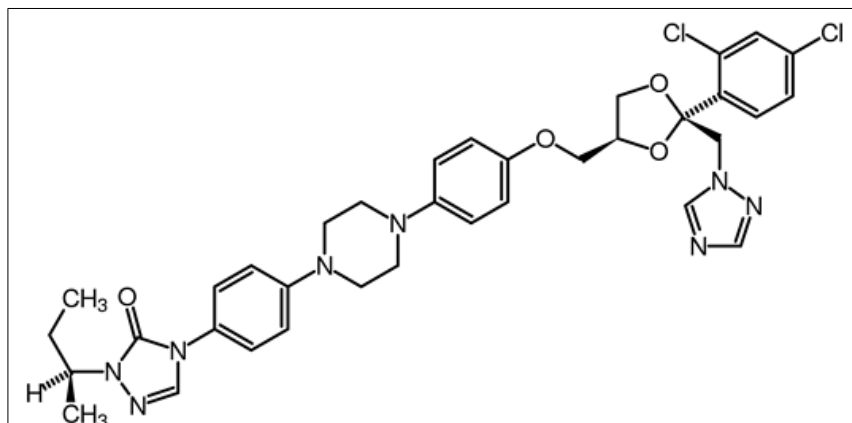


Figure III.1. - Chemical structure of ITR [59].

Important physico-chemical and pharmacokinetic characteristics are given in Table III.1.. As BCS class II compound with limited bioavailability, ITR is attractive for solubility enhancement research. The high T_m (see Table III.1.) and thermostability contribute to extensive research being conducted in the field of hot-melt processes [60–62]. Another research motif is the formation of ICs with CDs due to ITR's lipophilic nature and suitability as guest molecule [63–65].

Table III.1. - Physico-chemical properties of ITR [52].

Molecular weight	705.633 g/mol
Physical State	solid, white powder
Volume of distribution	796 ± 185 L
Plasma protein binding	99.8 %
Half life	21 h
Bioavailability	approximately 55 % when taken with full meal
Melting point	166.2 °C
Water solubility	practically insoluble, BCS class II
logP	5.66
pKa	3.70, weak base, ionised at low pH

Therefore, ITR was used as model BCS class II compound in this project. ITR batches ITRP12008 and ITRP13005 (Lee Pharma Ltd., India) were obtained via F. & A. Pharma-Handels-GmbH, Germany. x_{50} (average particle size) was determined by laser diffraction (see section III.2.2.7.) as 5.9 ± 0.1 µm.

III.1.2. Sempera[®]/Sporanox[®] Capsules

The German brand for the aforementioned ITR oral capsule formulation is Sempera[®], a product of Janssen-Cilag GmbH. Internationally, the formulation is often marketed as Sporanox[®] (Janssen Pharmaceuticals) [52]. In subsequent sections, Sempera[®] only refers to samples investigated in this project, whereas the term Sporanox[®] will be used affiliated to literature references. Yet, both formulations share nearly the same composition, as the only difference between them is the use of glucose syrup in Sempera[®] which is unlikely to have an influence on API dissolution. Therefore, the determined and literature related results will be correlated in this thesis.

The proposed manufacturing process of Sporanox[®] capsules is shown in Figure III.2.. The scheme is based on US Patents 5,633,015 and US 6,663,901 B1 that describe the production of the capsules [66,67]. First, a solution of methylene chloride and denaturated ethanol is prepared, ITR and hydroxypropyl methylcellulose (HPMC) 2910 (5 mPa · s) are added and dissolved completely. Neutral sugar spheres in the range of 600 - 700 µm are given into a fluidised bed granulator with Wurster bottom spray insert and coated with the ITR/HPMC 2910 solution at approximately 55 °C. After a short drying step (10 - 20 min) in the fluidised bed granulator, the coated pellets are transferred into a vacuum tumble drier for preferably 36 h at approximately 80 °C. The vacuum tumble drier is rotating at about 2 - 3 rpm. After a sieving step to separate agglomerated spheres, the pellets are given into a fluidised bed granulator with Wurster insert again and coated with a sealing solution of polyethylene glycol (PEG) 20000 in methylene chloride/denaturated ethanol at approximately 55 °C. After a 10 min drying step and cooling down of the pellets, they are removed from the fluidised bed granulator and automatically filled into hard gelatin capsules with a dose of 100 mg ITR [66].

The long vacuum drying step was later renewed and the possibility of drying under microwave conditions was introduced as the general limits for residual methylene chloride in dosage forms became stricter [67]. By applying this drying system, according to US 6,663,901 B1, drying time can be reduced to 1 h instead of 36 h.

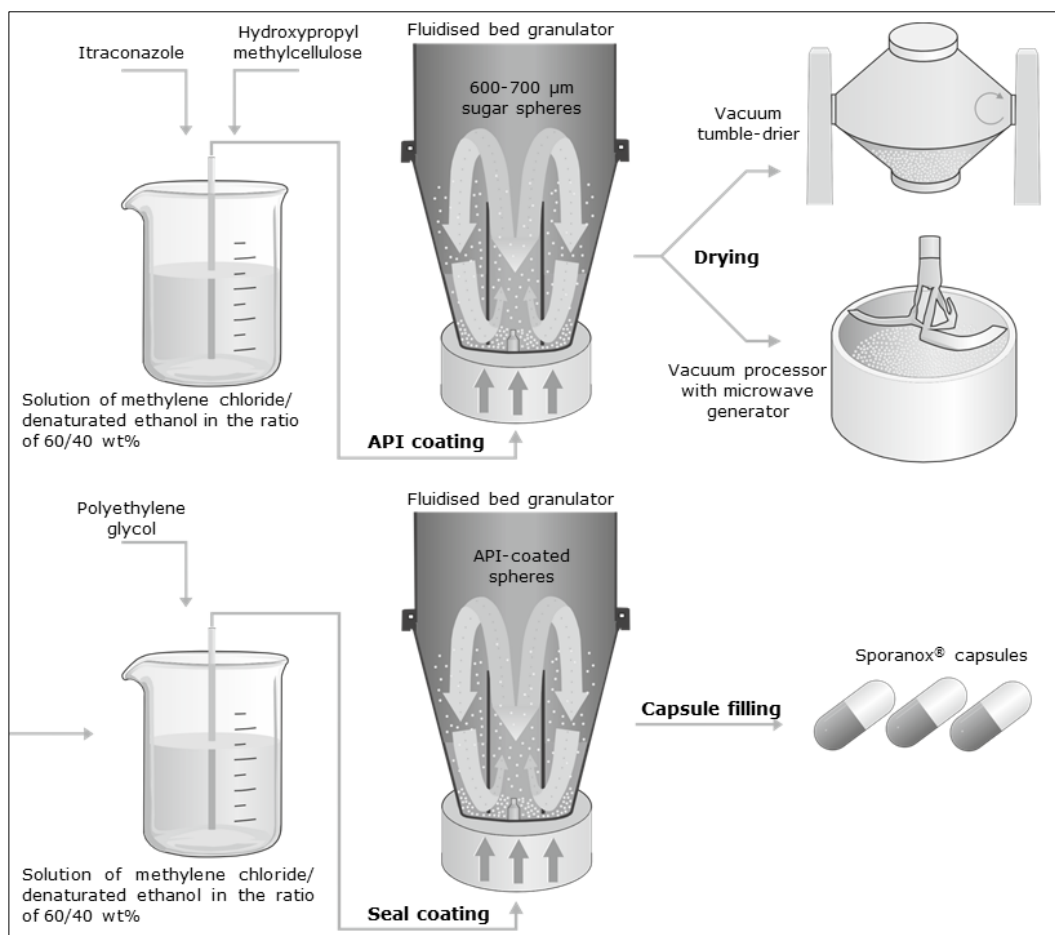


Figure III.2. - Manufacturing flow chart for Sporanox® capsules according to patents US 5,633,015 and US 6,663,901 B1 [66,67].

Even though the marketed formulation used in this project was the German product Sempera® which contains glucose syrup without un-disclosed information in which part of the process this excipient is employed, it can be assumed that the general manufacturing procedure will be closely related to the available, patented Sporanox® operation. Sempera® capsules used in this work (PZN 3853714; Batch FIL7Y00, FKL9F00) were acquired through a German pharmacy.

III.1.3. β -Cyclodextrin and Hydroxypropyl- β -Cyclodextrin

CDs are chemical entities that have been first reported by Villiers in 1891 and were characterised by Schardinger in the beginning of the 20th century during which period they were called "Schardinger dextrans". In the following decades, their chemical structure and other properties were extensively studied all around the globe [68]. They are cyclic oligosaccharides, in the case of β CD, consisting of seven α -(1,4)-linked D-glucopyranose units presenting the chair formation as shown in Figure III.3.. Also known "parent" CDs are α -cyclodextrin and γ -cyclodextrin which are composed of six and eight α -(1,4)-linked

D-glucopyranose units, respectively. CDs are gained in the bacterial fermentation of starch when certain enzymes, namely cyclomalto-dextrin glucanotransferases which can be found e.g. in strains of *B. macerans*, detach fragments of the starch polysaccharide helix and connect the two ends to a cyclic product. These natural enzymes yield mixtures of CDs that are challenging to separate and purify, e.g. by selective precipitation. The development of selective cyclomalto-dextrin glucanotransferases has significantly improved the manufacturing of CDs over the years and enabled their wide-spread use [68–70]. As presented in Figure III.3., the three-dimensional structure of β CD appears as a truncated, open cone. The reason is the chair conformation of the glucose units.

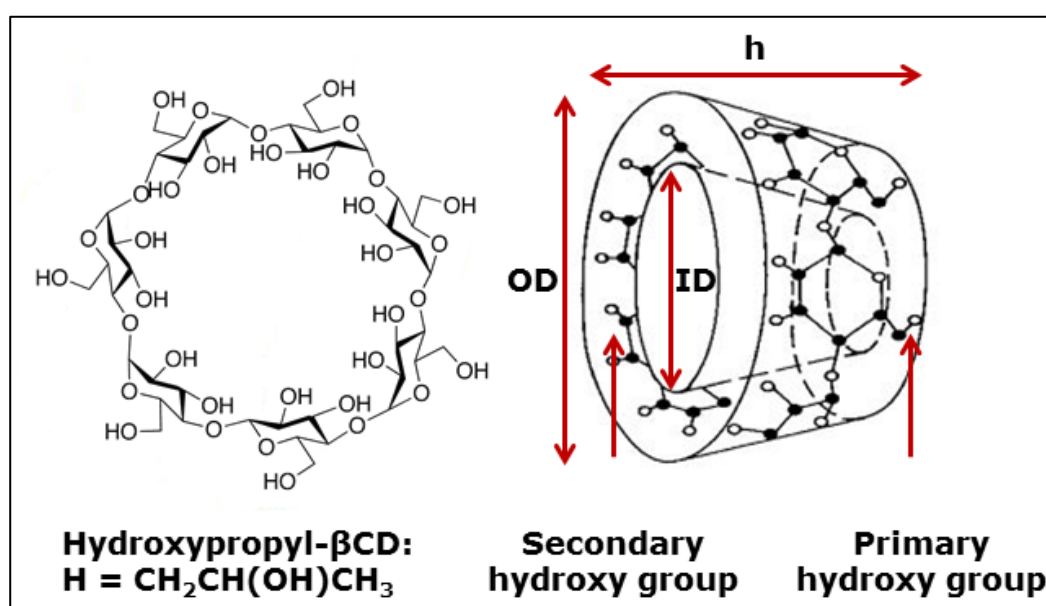


Figure III.3. - Chemical structure of β CD; ID = inner cavity diameter; OD = outer molecule diameter; h = height; for gaining hydroxypropyl- β CD, the visible H atoms might be etherified with hydroxypropyl groups in varying ratios from 0 - 3 per each glucose unit; adapted from [41,49].

Primary hydroxy groups of the molecule are located on the narrow end of the cone and secondary hydroxy groups on the wider edge. This phenomenon can also be seen for other CDs. Due to this, the surface of the CDs is strongly hydrophilic. The centre of the cone, the cavity, is more lipophilic because of the positioning of mostly skeletal carbons and oxygens from the ether groups [41,71]. From this structural particularity, positive properties of CDs arise. First of all, the cyclic structure causes a resistance to non-enzymatic hydrolysis and secondly, CDs exhibit the capability of creating non-covalent ICs with lipophilic substances such as APIs. These ICs oftentimes result in improved aqueous solubility and bioavailability of the drug as well as decreased volatility, less local irritation and

improved general stability [51,70]. This has caused CDs to be widely used in pharmaceutical applications, but also in the food and cosmetics industry where they can be employed to improve the product's shelf life or mask unwanted tastes and odours.

β CD is the most commonly applied CD due to its accessibility and low price (around 5 US\$/kg) [11,68]. Very often, it exhibits the highest attraction to different APIs for including them into the cavity which is shown by the highest average inclusion complex stability constant or complexation efficiency [49]. Nevertheless, there is a drawback in the application of β CD which is its aqueous solubility of approximately 18.4 ± 0.2 g/L at 25 °C [49]. Compared to APIs this appears genuinely high but when considering the water solubilities of α CD and γ CD (129.5 ± 0.7 g/L and 249.2 ± 0.2 g/L, respectively [49]), the limitation becomes obvious. This is supposed to be caused by very strong intramolecular hydrogen bonding in β CD and deems it unfit for parenteral administration [70,71].

The strategy to overcome this problem is the substitution of β CD. Even the addition of lipophilic moieties causes the new molecule to present a higher aqueous solubility by relaxing the intramolecular hydrogen bonds. This may also influence the toxicological profile and stability, possibly due to a decrease in crystallinity [11,70,72]. Substitution is generally possible at every terminal hydroxy function in the β CD molecule. One example for a frequently used β CD derivative is 2-hydroxypropyl- β -cyclodextrin (HP β CD) which presents favourable toxicological properties and can be administered parenterally. Doses of 8 g of HP β CD per day for two weeks were well tolerated [73]. Even though some minor organic histopathological and biochemical changes were observed mostly in animal toxicology studies, all were reversible and considered non-threatening for humans. In clinical investigations of the oral use in humans the main adverse effect reported was reversible diarrhoea [74]. β CD and HP β CD are both represented in the current Ph. Eur. [75,76] and β CD is included in the GRAS (generally regarded as safe)-list of the FDA. The maximum "acceptable oral daily intake" (ADI) of β CD is set to 5 mg/kg bw (body weight) by the Joint FAO (Food and Agriculture Organisation)/WHO (World Health Organisation) Committee of Food Additives (JECFA). This is not mainly due to CD-related health risks but by evaluation of toxic residual components from synthesis [70,77]. The oral "no observed adverse effect levels" (NOAEL) of β CD for adult humans was proposed 500 mg/day by the Eu-

ropean Medicines Agency (EMA) in 2014. However, in October 2017, the revision of the annex to the European Commission guideline on “Excipients in the labeling and package leaflet of medicinal products for human use” newly stated that “Based on animal studies and human experience, harmful effects of CDs are not to be expected at doses below 20 mg/kg bw per day.” [78,79].

HP β CD is the present CD in the marketed solution of Sporanox[®] where it is used to encapsulate ITR. In this FDA approved formulation, when high dose therapy is applied, up to 16 g of HP β CD are consumed daily [10]. After oral administration, the amount of absorbed β CD is considerably low because most of it passes stomach and small intestine intact and is then metabolised by bacteria in the colon. HP β CD in contrast is mostly excreted intact in the faeces as it is non-absorbable and non-metabolisable [73]. Table III.2. gives an overview of important characteristics of both β CD and HP β CD.

Table III.2. - Characteristics of the two applied CDs in this work, β CD and HP β CD, according to [41,49,77,80].

	β CD	HP β CD
Molecular weight, g/mol	1134.978	1399
Height, nm	0.78	not reported
Inner diameter, nm	0.62	(partially shielded) 0.62
Outer diameter, nm	1.54	not reported
Solubility in water, g/L at 25 °C	18.4 \pm 0.2	> 600
Melting range, °C	255 - 265	> 300 *
ADI level, mg/kg bw	5	no set limit
x_{50}, μm; see section III.2.2.7.	77.2 \pm 1.4	98.4 \pm 2.2
Molar degree of substitution	X	0.63**

* described as decomposition temperature, no melting range given, ** derived from the correlating Certificate of Analysis

As explained in section II.3., the use of CDs oftentimes improves the aqueous solubility and bioavailability of APIs. β CD presents the most favourable cavity size and often strongest IC stability constants. The high melting range of about 260 °C and thus, thermostability, generally qualify it for being employed in melt

processes. Additionally, the utilisation of β CD as sole matrix in the creation of a melt process has only been investigated very marginally. To the author's best knowledge, only one reference is available where HME with β CD was conducted. However, the focus of that work was on another CD derivative and the development of the process itself was not highlighted [81]. All of these argumentations give reason that β CD was investigated as first-choice matrix in this study. However, to examine an alternative, HP β CD was evaluated as it is already employed in marketed formulations with ITR. The used qualities of β CD (Kleptose[®]; Batch EE459) and HP β CD (Kleptose HPB[®]; Batch E0288) were kindly donated by Roquette Frères, France.

III.1.4. Soluplus[®]

Soluplus[®] (SOLU), a newly developed solubilising polymer especially designed to create solid solutions and dispersions by HME was launched by BASF SE, Germany in 2009. It has been used frequently in HME research ever since, particularly regarding formulations with BCS class II compounds due to their poor aqueous solubility [82,83]. Its structural formula is given in Figure III.4.. SOLU is a graft copolymer composed of polyvinyl caprolactam and polyvinyl acetate side chains attached to a polyethylene glycol backbone in the ratio of 57:30:13 [20]. It has a molecular weight of approximately 118 000 g/mol. SOLU shows excellent extrudability and has a T_g around 70 °C.

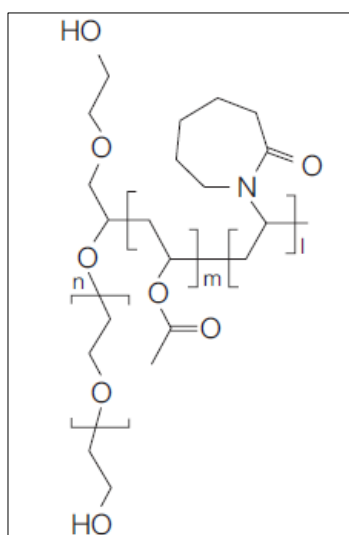


Figure III.4. - Chemical structure of Soluplus[®] [84].

Many APIs have plasticising effects on SOLU, enabling HME at lower temperatures than for the pure excipient (around 120 – 180 °C depending on screw configuration) [84]. No SOLU degradation has been reported for hot-melt processes

up to 220 °C [20]. Thus, SOLU can stand ITR T_m (around 167 °C) and is therefore often employed in ITR-HME research [85–87]. In this project, SOLU was used as an alternative matrix especially in regard to its solubilisation capability. x_{50} value was determined as described in section III.2.2.7. to be $303.1 \pm 5.2 \mu\text{m}$. SOLU (Batch 84414368EO) was kindly donated by BASF SE, Germany.

III.1.5. Polyethylene Glycol 6000

PEG 6000 consists of polyethylene oxide monomers connected via ether links. Its monomeric chemical structure is shown in Figure III.5.. The number 6000 stands for the average molecular weight in g/mol and corresponding to that, for the physical state of the substance.

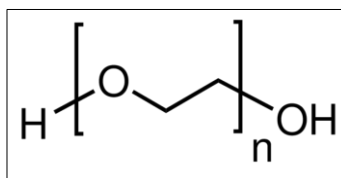


Figure III.5. - Chemical structure of PEG [88].

PEGs are viscous liquids with a molecular weight up to 600, semisolid up to 1000 g/mol and solid wax-like between 1000 and 20000 g/mol. They are pharmaceutically employed for many different applications, e.g. as solvents, ointment bases, plasticisers, lubricants or suppository bases [89]. There is a long history of research about solid dispersions and solutions with PEG 6000 studied as water-soluble matrix. Hereby, the focus is often based on the determination of the solubility enhancing properties of PEG 6000. Possible explanations include interactions of encapsulation, improvement of wettability and enhancing the dissolution rate by maintaining the reduced particle size of the API within the matrix [90–94].

In this project, PEG 6000 was examined as alternative matrix in binary formulations and furthermore as ternary additive to powder blends of β CD and ITR to investigate influences mostly regarding ITR dissolution rate. As previous experiments with the used mTSE system had shown, best content uniformity during feeding was acquired if the applied PEG 6000 by Clariant SE, Germany, was used as a milled fine powder (PF quality; Batch DEA4005506; 75 - 95 % < 90 μm [95]).

III.1.6. Xylitol

Xylitol is a sugar alcohol with five carbons. Industrially, it is manufactured by using a catalytic reduction process. By this hydrogenation, D-xylose, its corresponding sugar, is converted into the primary alcohol [96]. Xylitol can be used as a non-cariogenic sweetener [97] but is also investigated as crystalline matrix in HME to evaluate its potential for API dissolution enhancement [98]. The chemical composition of xylitol is given in Figure III.6.. It presents as a crystalline, white powder with an aqueous solubility of 664 g/L [97] and a reported T_m of about 91 °C [99]. Kaizawa et al. reported a decomposition temperature for xylitol of 200 °C [100]. This allows its utilisation in hot-melt processes up to that temperature.

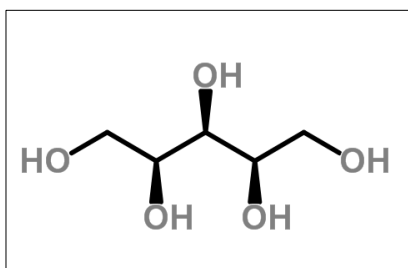


Figure III.6. - Chemical structure of xylitol [101].

In this project, xylitol (Xylisorb 90; Batch E270R; Roquette Frères) was mainly used as ternary additive in HMG formulations to assess the influence a combination of β CD and xylitol might have on ITR dissolution and possible ICF. x_{50} was determined according to section III.2.2.7. to be $149.9 \pm 4.7 \mu\text{m}$.

III.1.7. Hydroxypropyl Methylcellulose

HPMC is derived from purified pulp by caustic soda treatment and etherification with chloromethane and propylene oxide at high temperatures. Afterwards, the material is washed, dried and pulverised [102]. The result is a water-soluble, non-ionic cellulose ether. The chemical structure of HPMC is shown in Figure III.7.. The used HPMC quality (Metolose[®] 65SH) exhibited a substitution level of 1.8 regarding the average number of substituted hydroxy groups of each anhydrous monomeric glucose unit with a methoxy group and 0.15 regarding the average number of hydroxypropoxy groups added to each anhydrous glucose monomer which corresponds with the United States Pharmacopeia (USP) substitution 2906. A 2 % aqueous solution of the used HPMC material has a reported viscosity of 3000 - 5600 mPa · s at 20 °C [102].

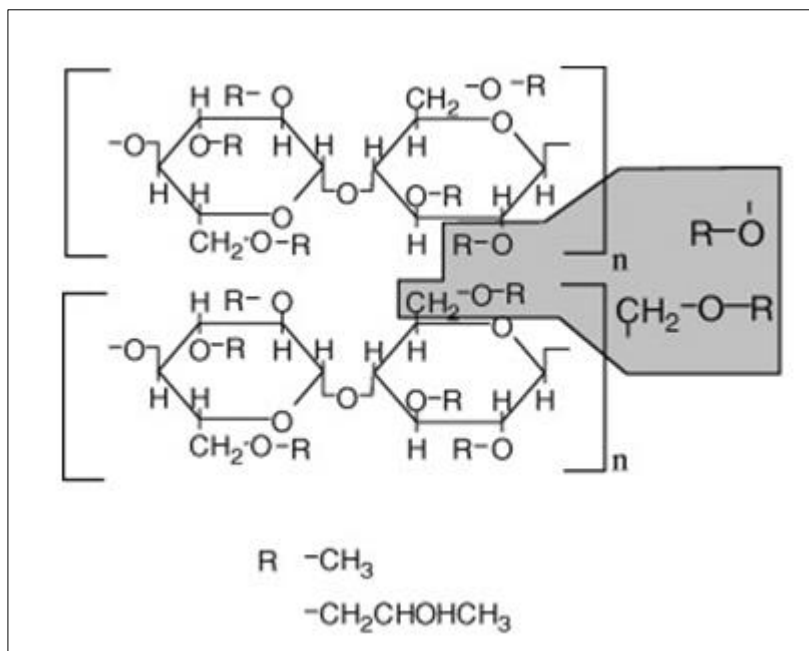


Figure III.7. - Chemical structure of Metolose® 65SH [103].

HPMC is a commonly used excipient in pharmaceutical formulations and is utilised for many different applications, such as hydrogel tableting matrix for sustained API release, coating of solid dosage forms, viscosity enhancer, stabiliser in suspensions or even capsule shell material due to not being of animal origin [104–107]. HPMC has a proclaimed melting range of 280 - 300 °C. Thus, it is often investigated as matrix in hot-melt processes [108,109]. Rambali et al. investigated a combination of HPMC and HP β CD in an HME process with ITR [110]. Apart from this, HPMC is the chosen polymer for the ITR solution that is spray-coated on the starter pellets for the marketed product Sporanox®. There is high scientific interest in the interaction of ITR and HPMC. Very often, third substances are added to further optimise these formulations. Rajarajan et al. examined a spray-drying procedure with HPMC, PEG and ITR [111]. The HPMC quality utilised in this work (Metolose® 65SH-4000; Lot 5095611; Shin-Etsu Chemical Company Ltd., Japan) has already been studied in hot-melt procedures [106]. The x_{50} value was determined according to section III.2.2.7. as $69.0 \pm 0.2 \mu\text{m}$.

In this project, HPMC was investigated as an alternative matrix in the binary hot-melt process. Also, ternary mixtures of HPMC, β CD and ITR were investigated to determine if the combination of the two glucose-based substances would further enhance properties of the developed formulation such as processability or ITR dissolution.

III.2. Methods

In the present chapter, the techniques used in this project are divided into preparative (see section III.2.1.) and analytical methods (see section III.2.2.).

III.2.1. Preparative Methods

In the context of this thesis, preparative methods describe all techniques that were used in the manufacturing of blends or samples.

III.2.1.1. Preparation of Powder Blends

As only one feeding station was used for all HMG and HME runs, the excipients had to be blended with the API prior to being filled into the feeding vessel. For all cases, a Turbula[®] shaker-mixer T2C (Willy A. Bachhofen AG, Switzerland) with a rotation speed of 42 rpm was employed. This blender is a three-dimensional free-fall mixer that uses translational, rotational and inversion forces. During mixing the powder constantly changes directions in a rhythmical pulsing motion [112]. The utilised plastic blending vessels were coated with Sprayflon Plus 3[®] (Saint-Gobain Performance Plastics Pampus GmbH, Germany), a pressurised gas polytetrafluoroethylene formulation, prior to weighing-in of powder, as previous studies had shown an anti-adhesive effect and improved content uniformity for powder blends during mixing and mTSE feeding.

For weighing-in of the substances, a double sandwich method was used where total excipient and API amounts were equally divided into three or two parts, respectively. About 10 - 20 % of the blending vessel's volume was filled. For all ternary mixtures the weighing-in protocol was ternary substance/excipient/API/excipient/API/excipient/ternary substance. Binary β CD/ITR blends for HMG and HME were prepared in singular ($n = 1$) and were composed as given in Table III.3.. Alternative HME or HMG mixtures were also singularly prepared and their respective compositions are given in the corresponding results sections.

Table III.3. - Composition of binary β CD/ITR powder mixtures.

	Stoichiometric Ratio	Weight Proportion
β CD	1	62 parts
ITR	1	38 parts

Standard blending time was set to 20 min. After that, the physical mixtures (PM) were spread upon a white paper (DIN A3) and divided into three parts, left side, middle and right side. Ten samples were drawn (three from the left and right side each and four from the middle) and evaluated for ITR content (see section III.2.2.3.). If content homogeneity did not deviate more than 5 %, PM was considered ready for further processing. If homogeneity was not met after 20 min of blending, a second blending step of 20 min was added. ITR content was evaluated again and if PM was still not in specification as mentioned above, it was discarded. Time between content evaluation and further processing was kept as short as possible to prevent segregation.

III.2.1.2. Kneading and Wet Granulation

For comparative purposes, ICs were prepared by the kneading method, also called "slurry" which is the preferred method of forming ICs with β CD [80]. The method used in this project was based on the proposed technique by the β CD's manufacturer [80] and slightly altered. Three parts of β CD were given into a mortar and manually mixed with one part of demineralised (dem.) water using a pestle until it reached a homogenous pasty state. If visual homogeneity was not reached by then, a few more droplets of dem. water were given into the mortar as generally suggested [80]. ITR was added gradually. If the mixture's viscosity did not allow the kneading process, dem. water was appended to the mixture at this stage again. The material was kneaded for 30 min and dried at 70 °C for 10 h in an oven (Mettler GmbH + Co. KG, Germany). The dried "slurry" was manually grinded in a mortar and sieved ($< 425 \mu\text{m}$) before analysis.

To investigate the influence of a combination of HMG and a kneading process, a wet granulation was conducted. The above-mentioned process was manually repeated in a stainless steel bowl. The granulation end-point was defined as a homogenous state when the newly built agglomerates would stick together after slight manual compression but disintegrate after release. After reaching the granulation end-point, the granulate was given through a 1 mm sieve and dried at 70 °C in an oven (Mettler GmbH + Co. KG). In previous experiments it was determined that feeding of the mTSE was only feasible at residual moisture of around 15 % and lower. Thus, drying was continued until this specification was met. The wet-granulate was then directly transferred into the hopper and hot-melt-granulated.

III.2.1.3. Hot-Melt Extrusion and Hot-Melt Granulation

All HMG and HME experiments were performed using the Pharma 11 Twin Screw Extruder (Thermo Fisher Scientific GmbH, Germany) which will be described in more detail in the subsequent sections.

III.2.1.3.1. Pharma 11 Twin Screw Extruder

An image of the Pharma 11 Twin Screw Extruder without its feeding unit is shown in Figure III.8.. The horizontal extruder barrel is divided into different parts. Firstly, the powder entry zone (funnel at the right side) which cannot be heated and is permanently water-cooled to prevent blockages. Second, seven separately controllable heating zones throughout the barrel that are connected to the water-cooling system and reach a maximum temperature of 280 °C. And lastly, the die at the left end of the extruder which is independently heated up to 280 °C but not cool-able.

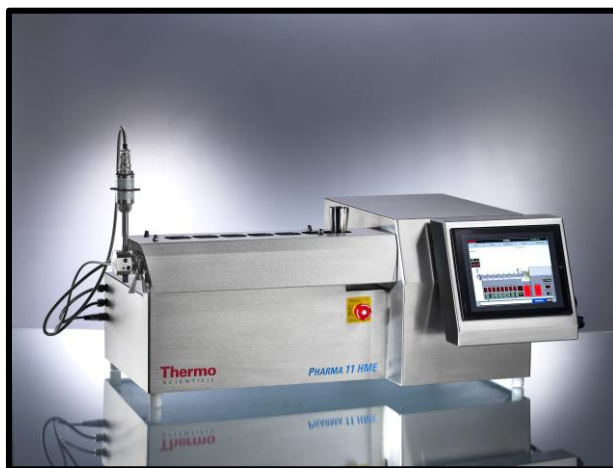


Figure III.8. - Set-up of the Pharma 11 Twin Screw Extruder without feeder; image used with copyright permission of Thermo Fisher Scientific.

The pressure control unit is connected to the nozzle head as well and can reach a maximum of 100 bar. The two screws are co-rotating within the barrel which allows sufficient mixing and inhabits a self-wiping aspect [27]. The ultimate screw speed is 1000 rpm. During the HMG/HME process, it is possible to monitor the screw torque to avoid motor damage. The highest tolerable torque is 12 Nm (6 Nm per screw). The higher the torque, the more energy is needed by the screws to mix the material and the more energy goes into the final extrudate. Thus, it holds importance in evaluating the HME/HMG procedure itself and will be taken into account for each HME/HMG process presented in this thesis.

In general, the upper barrel is completely closed and material within must follow the barrel down to the die before again coming into contact with air. As preliminary studies showed, the water from within the CD cavities started to evaporate at about 100 °C, vaporised and left through the feedstock access, causing fresh powder entering mTSE to become moist and obstruct the powder entry. Therefore it was necessary to use the Pharma 11 mTSE ventilation port system. Here, a special component with a hole in it was installed in the upper barrel directly next to the powder entrance so that the water vapour could exit there. The chosen feeding system is essential for the HME/HMG process as blend segregation and insufficient content uniformity can occur within the hopper. As pharmaceutical feedstock often lacks good flowability, many different hopper systems are available such as vessels with built-in rotating agitator paddles, side stuffers or with two transporting screws of varying dimensions for conveying specific materials [21].

There are two different main feeding categories recognised, gravimetric and volumetric feeding [113]. In gravimetric feeding a specified mass of excipient or mixture is fed into the extruder during a given time, e.g. 2 kg/h. These feeders have an installed scale that allows self-adjusting e.g. by adapting the rotation rate of the conveying screws to permanently stay within the appropriate feed rate limits. These feeders are mostly used industrially for pharmaceutical products as they allow more detailed oversight of the process. In volumetric feeding, the feeder set-up is the same with the exception of the built-in scale. The feed rate is often presented as a percentage of feeder capability, e.g. 50 % means that the conveying elements and agitator paddles are working at half of their maximum aptitude. This type of hopper has to be calibrated for each new feedstock as flowability will always differ for materials and freshly prepared PMs. Different filling levels are fed for a specified amount of time in a weighing vessel at full power. That way, it is possible to correlate the feeding capability to a throughput in kg/h [114]. Still, the process monitoring of volumetric feeding has drawbacks since it is much harder to detect changes in feed rate upon instant. To avoid segregation in PMs, it is possible to use two or more separate feeders, each only feeding one substance. By doing so, it is conceivable that excipients are added to the extrusion process at later process points, e.g. addition of thermosensitive APIs after the highest temperature has already passed.

Throughout this project, the Pharma 11 Volumetric Mini Twin Feeder (MT-S HYP, Brabender Technologie GmbH & Co. KG, Germany) was employed. This feeder has a stirring mixing wheel for destroying powder bridges and two conveying screws to ensure feedstock flow. It belongs to the category of starve-feeders which are most common when applying an mTSE as the formulation is given directly onto the rotating screws causing instant processing with the avoidance of material build-up in the powder entry zone [115]. A schematic view of the used hopper is shown in Figure III.9..

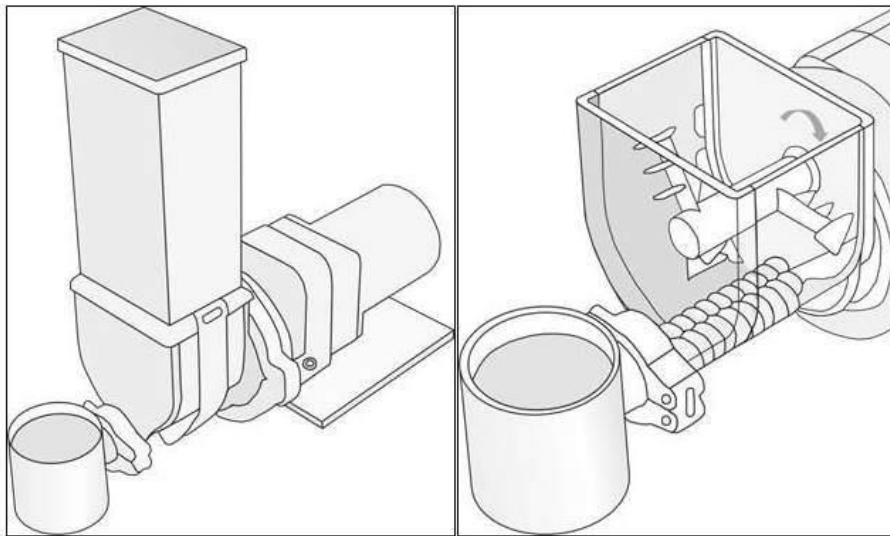


Figure III.9. - Outline of the used feeding system; the whole feeding unit (left) and inside view of the feeding vessel, showing two conveying screws and the agitator paddle wheel (right). Images are adapted from [114].

As it is critical to calibrate the feed rate when using this type of hopper, prior to each HMG/HME experiment, PMs to be processed were given into the feeder and after the conveying screws were completely filled, material was fed at 100 % feeding capability for 1 - 2 min, weighed and projected to the throughput in g/h. This was done three times each for low and high filling levels. The arithmetic mean of these six measurements was set as the maximum possible feeding rate (100 %). From this, the necessary feed rate in % was derived for the desired throughput in g/h. During HMG and HME, the amount of yielded product was weighed regularly to oversee the throughput and if necessary, the feed rate was adjusted. Moreover, powder samples were drawn periodically amidst feeding to analyse the API content with the aim to evaluate possible segregation within the feeder.

Also of importance for a successful HME/HMG process is the screw design as mechanical shear forces impact the material, especially in kneading zones. This

can influence the finished products [116]. For all experiments, the standard screw design was utilised as shown in Figure III.10.. The screw diameter (D) was 11 mm and length (L) 440 mm, resulting in a L/D ratio of 40 which is an important parameter for a possible up-scaling.

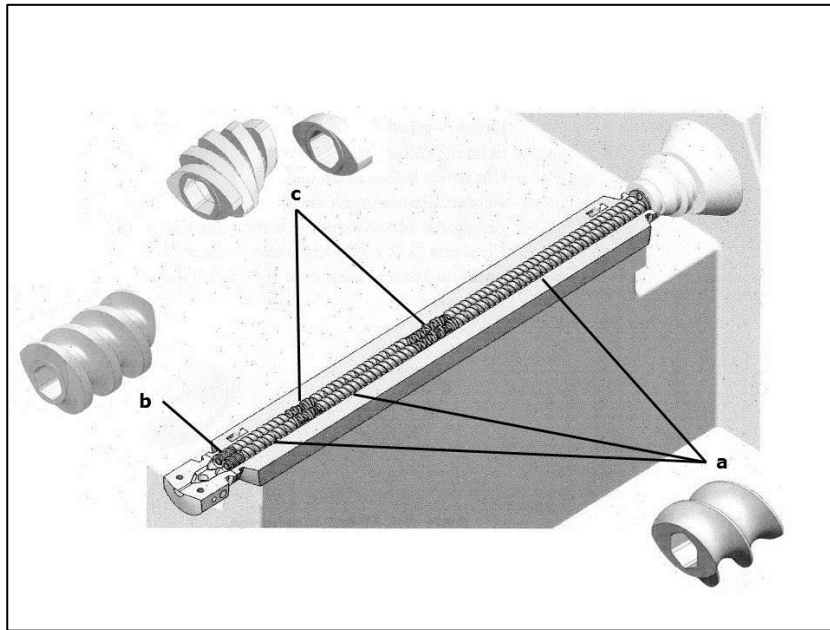


Figure III.10. - Applied standard screw design; a) forward conveying elements, b) discharge screw conveyors, c) kneading/mixing elements, on the right as a single element and on the left as a finished kneading/mixing zone block with its elements shifted between 30° and 60°, adapted from [117].

The most common screw element is the conveying element. The standard screw design only uses forward conveyors. The discharge screw conveyors are special elements. They are channel-specific (α and β for each screw respectively) as they need to build up the pressure when the material reaches the die. They do not necessarily have to be used when working without a die, but in this project, they were always kept at the end of the screws for comparative purposes. Kneading zones are where most mechanical shear forces are brought upon the material. They are arranged of single mixing elements which are shifted in their offset angle. The higher the offset angle, the smaller the conveying power of the element and the greater the mixing capability. A 90° offset angle is solely viable for mixing. In general, a kneading zone is composited in a way that the first elements are shifted by 30°, the middle elements by 60° and the last by 90° to maintain forward conveying together with strong mixing properties. The first kneading zone of the utilised standard screw design (c, right in Figure III.10.) consists of 12 single mixing elements, the first three shifted by 30°, the next five by 60° and the last four by 90°. For the second kneading zone (Figure III.10.,

c, left) three, three and four elements are shifted by 30°, 60° and 90° respectively [117]. The applied screw speeds are given in the corresponding results sections.

In HME processes, the die is a critical component as this is where the pressure builds up when the material is conveyed towards the narrowing structure. In this study, the standard Pharma 11 Twin Screw Extruder die (diameter 2 mm) was utilised next to a variable die (Thermo Fisher Scientific) with a flexible nozzle head that could be equipped with insets with varying diameter. The Thermo Fisher Scientific 3 mm inset and a self-built 6 mm inset were investigated. Furthermore, a 6 mm conical die was developed and tested in this work. The development of this die with a special inner structure will be presented in section IV.2.1.2..

When HMG was conducted, the die was removed completely from the mTSE and the material was allowed to fall freely from the extruder. By doing so, the material is only kneaded and mixed without the addition of high pressure [35]. To ensure a reproducible material exit, an in-house built granulation heel slide was applied to the end of the barrel (see Figure III.11.). After the extrudates/granules had left the die/granulation heel slide, they were air-cooled and stored in plastic containers until further processing.



Figure III.11. - Granulation heel slide attached to the end of the Pharma 11 Twin Screw Extruder barrel.

The utilised mTSE is structured in seven separately heatable zones plus - if applied - the heatable die. When creating temperature profiles, it is very important to avoid too large differences between neighbouring zones as temperature stabil-

ity might suffer. That is why usually the barrel temperatures rise from powder entry to the die. Sometimes it might be necessary to solely lower the temperature of the die if e.g. the extruded material is too liquid after having melted and thoroughly kneaded and would simply leak from the die. The temperature profiles used in this project are presented in the corresponding experimental sections as firstly, they were strongly dependent on the materials used and secondly, constitute an important factor in the process optimisation. Prior to further analysis, for comparative purposes, all HMG and HME samples were manually crushed and sieved ($< 425 \mu\text{m}$).

III.2.2. Analytical Methods

All techniques used in this work for characterising samples and products are summarised as analytical methods and described in the subsequent sections.

III.2.2.1. Phase Solubility Analyses and Data Interpretation

Phase solubility measurements (PSM) were first introduced to the scientific canon by Higuchi and Connors in 1965 [118]. Since then, this technique has often been employed as the foundation of CD inclusion research. The purpose of PSM is to determine the influence the CD has on the guest molecule (mostly APIs) in regard to its solubilisation. Furthermore, the stability constant and the complexation efficiency (CE) of the IC can be derived from this. Lastly, PSM can help to further understand the complex stoichiometry [71]. In PSM, an excess amount of drug is given into specified aqueous solutions of the CD in question (e.g. 0.001 mol/L, 0.002 mol/L, 0.003 mol/L). Solutions are then kept in motion (for example by shaking) for a certain amount of time at constant temperature until equilibrium is reached and later evaluated for dissolved API content.

CD concentration ($[\text{CD}]_t$) plotted against the dissolved API concentration (D_t) yields the phase solubility diagram (PSD) which classifies the type of IC into two categories A and B, with several subtypes respectively (see Figure III.12.). Category A is defined by an increased amount of dissolved drug the more CD is present in the solution. The profile of subtype A_N shows a negative deviation from linearity at higher $[\text{CD}]_t$, whereas subtype A_P then presents a positive deviation from linearity, indicating that CD is more effective at high $[\text{CD}]_t$. A_L type profiles show a linear enhancement of D_t and are reported as first order regarding CD. This means that one CD molecule complexes one or more molecules of

drug [71]. If the slope of the A_L type diagram is larger than unity, higher order ICs are assumed in respect to the drug.

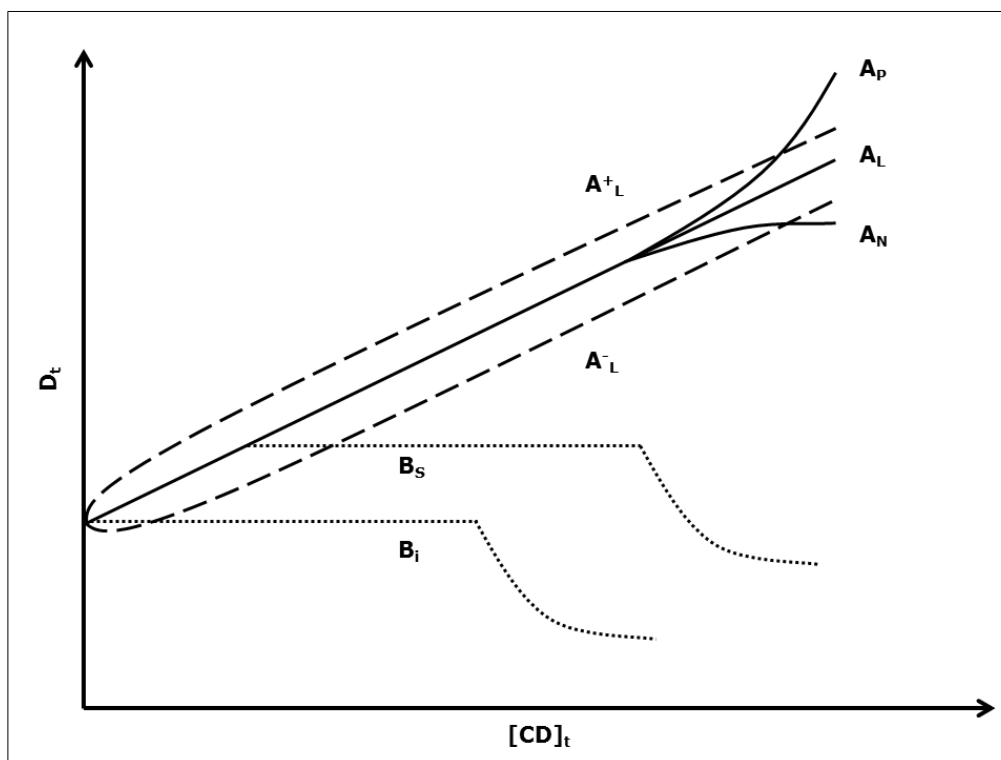


Figure III.12. - Model phase-solubility profiles of main categories A and B and their applicable subcategories; y-axis presents the concentration of dissolved drug, x-axis presents the concentration of the aqueous CD solution; adapted from [71,119].

Although this phenomenon can also occur if the PSD slope is less than one, in general, 1:1 ICs are considered as more common [119]. A_p systems are first-order complexes in regard to the drug. One drug molecule forms ICs with one or more CD molecules. The so-formed ICs have to be fitted to different mathematical models to evaluate the most probable complex stoichiometry. Explanations for A_N profiles include chaotropic or kosmotropic properties of the solubiliser, changed viscosity, surface tension or conductivity.

B type profiles are yielded when the formed IC shows limited aqueous solubility. B_s profiles become present when, at one point, D_t exceeds its maximum solubility. ICs begin to precipitate while remaining excess drug dissolves or becomes complexed. As long as precipitation, dissolution and complexation are in balance, a plateau is seen in the PSD. After all solid drug particles have been included, further precipitation decreases the amount of D_t . Profiles of subtype B_i show in general the same phenomena as B_s diagrams but as the ICs are very poorly soluble in water, the linear increase of dissolved drug at low $[CD]_t$ (B_s diagram)

does not occur [71]. As mentioned above, all of these generated phase-solubility profiles can be used to determine the stability constant (K) of the IC. Since the most common IC is of the stoichiometry 1:1, the stability constant $K_{1:1}$ is most often evaluated to gain information about the IC. As the plotting of D_t against $[CD]_t$ would reveal a straight line if 1:1 ICs were formed, according to Higuchi and Connors [118], $K_{1:1}$ can be determined by *equation 2*.

$$K_{1:1} = \frac{\text{Slope}}{D_0 (1-\text{Slope})} \quad \text{equation 2}$$

Here, Slope stands for the generated slope from the PSD and D_0 is the solubility of the drug without the presence of CD in the solution. Applying *equation 2* to the PSD, D_0 should be of the same value as the intercept of the linear equation (D_{int}) as the intercept per definition presents the D_t at zero $[CD]_t$. However, it is reported that especially for poorly water-soluble drugs (< 0.1 mM), such as ITR, there often is a deviation between D_0 and D_{int} ($D_0 > D_{int}$) that is not correlatable to any other drug property. These kinds of drugs often generate A^-_L type profiles as shown in Figure III.12., resulting in a too large value for $K_{1:1}$. In some cases, D_{int} and $K_{1:1}$ might become negative which is generally impossible. Postulated reasons for this include the physico-chemical non-ideality of water molecules, self-association of drug molecules and the fact that CDs also have the ability to form non-inclusion complexes or self-aggregate [119,120]. Charged CDs have been reported to result in PSD where $D_{int} > D_0$ which then causes $K_{1:1}$ to appear too small (A^+_L) [119].

All these occurrences give reason to suspect that $K_{1:1}$ actually rather is a combination of different stability constants of various reactions in the aqueous solution. To overcome this variability in the stability constant and gain a reliable variable for further conclusions, CE is of interest. By calculating CE, the molar ratio of CD and drug necessary to gain a 1:1 IC as well as the increase in formulation bulk can be assessed which is of great importance for a final dosage form [121]. CE can be derived without taking D_0 or D_{int} into account and is calculated according to *equation 3* where Slope describes the slope of the linear equation from the PSD [122].

$$CE = D_0 * K_{1:1} = \frac{\left[\frac{D}{CD}\right]}{[CD]} = \frac{\text{Slope}}{(1-\text{Slope})} \quad \text{equation 3}$$

From CE it is possible to calculate the drug : CD ratio by using the following *equation 4* [121].

$$D:CD = 1 : \left(1 + \frac{1}{CE}\right) \quad \text{equation 4}$$

The increase in formulation bulk (IFB) can be derived from *equation 5* where MW_{drug} and MW_{CD} mean the molecular weights of drug and CD [121]. Multiplying IFB with the drug dose per administration yields the new formulation bulk size.

$$IFB = \frac{MW_{CD}}{MW_{drug}} * \left(1 + \frac{1}{CE}\right) \quad \text{equation 5}$$

In this study, β CD solutions in dem. water and 0.1 N HCl besides HP β CD solutions in 0.1 N HCl in the range between approximately 0.001 M and 0.0018 M were spiked with an excess amount of ITR. They were agitated at ambient conditions until equilibrium was reached after seven days, filtered through 0.2 μ m filters (Chromafil[®] Extra PET-20/25, Macherey-Nagel GmbH & Co. KG, Germany) and analysed as described in section III.2.2.3.. Each measurement was conducted at least in triplicate and $K_{1:1}$, CE and IFB were derived from these analyses.

III.2.2.2. Thermal Analysis

Many important characteristics of solid samples can be determined by thermo-sensitive measurement techniques. By exposing the sample to constant or varying temperatures and tracking different measurands such as sample weight or heat flow against a reference, temperature or changes over time allow conclusions about different properties, like substance identity, crystallinity, thermal stability and water content [123,124] In this project, two of these techniques, differential scanning calorimetry (DSC) and thermal gravimetry (TGA), were employed.

III.2.2.2.1. Differential Scanning Calorimetry

DSC is the most common thermal technique due to its rapidity, uncomplicated sample preparation and the multitude of detectable events, such as melting, (re)crystallisation or T_g s. All these events can be evaluated quantitatively. The power compensation DSC which was applied during this work consists of two identical small furnaces that are separately heated, cooled or held isothermally according to the same associated measurement specification. The differences in the energy flow needed to keep both sample and reference at the same tempera-

ture is measured in mW or J/s. This energy variation plotted against either temperature or time yields the DSC curve [124]. Changes in the energy flow can be endothermic or exothermic depending on the occurring phase transitions in the sample, e.g. melting results in an endothermic peak, recrystallisation yields exothermic signals. Samples are weighed in sealed aluminium pans that can be closed air-tight or present a pierced lid to allow pressure compensation. This way, residual water can exit the pan during analysis. The reference usually consists of an empty aluminium pan. To avoid oxidation processes, the whole DSC apparatus is often flushed with nitrogen or helium gas [125].

Throughout this project, DSC measurements were used to gain insight into the thermal behaviour of the studied sample. Of utmost importance was the state of ITR regarding its amorphousness or possible ICF. The occurrence of a melting peak at the corresponding T_m of ITR (166.2 °C, see section III.1.1.) was always examined. DSC traces were also evaluated for any other appearing signal. DSC analyses were conducted using Perkin Elmer PYRIS™ Diamond DSC and DSC 7 (both Perkin Elmer Inc., US). Measurements were evaluated with PYRIS™ Software Version 9.0.2.0193 (Perkin Elmer Inc.). If not marked otherwise, the accurate sample amount equivalent to 1 - 2 mg of ITR was weighed in an aluminium pan and sealed with a pierced aluminium pan. The reference was prepared likewise with two empty aluminium pans. During analysis, the sample was flushed with 20 mL/min nitrogen gas.

The exact temperature range and heating rate are given collectively with the results shown in the corresponding sections. They were always individually chosen according to the properties to be examined, e.g. the investigation of the decomposition temperature called for higher maximum temperatures than the examination of loss of β CD cavity water or ITR T_m .

III.2.2.2.2. Thermal Gravimetry

TGA is a simple way of determining the water content of solids. Water can play an important role in recrystallisation processes. Additionally, the water content in melt-extrudates/melt-granules allows conclusions about the HME/HMG procedure. During the measurement, the sample is exposed to rising temperatures over time. Sample weight is monitored constantly and can be used to calculate the water loss during heating. This method yields results similar to those ob-

tained by Karl-Fischer titration and was therefore regarded as suitable for the desired purposes in this work [126].

A STA 6000 (Perkin Elmer Inc.) with ceramic pots and a constant flow of nitrogen (20 mL/min) was employed for all experiments and sample analysis was conducted with the PYRIS™ Software (Version 9.0.2.0193, Perkin Elmer Inc.). For each evaluation, 15 – 20 mg of sample were given into the ceramic pot, held at 35 °C for 2 min and then heated to 750 °C at 10 K/min. The percentage of weight loss between 50 and 150 °C displayed the water content of the measur- and as this allowed complete vaporisation of surface as well as β CD cavity water but sample degradation was avoided. Notwithstanding, some measurements, especially in the beginning of the experimental preformulation phase, were conducted using different parameters. In case of different settings, the used methodology is given together with the data shown.

III.2.2.3. Itraconazole Content Evaluation

Being the model API in this project, the development of a quantification method for ITR was necessary. This was firstly managed by using UV spectroscopy. But, the utilisation of additional substances, such as SOLU, made it impossible to use the method described in the following subsection. UV absorption interferences forced the development of a further method. Consequently, high performance liquid chromatography (HPLC) was selected.

III.2.2.3.1. UV-Spectroscopy

In 2011, Parikh et al. proposed a simple and reproducible UV-method with high recovery for ITR quantification at 262 nm where methanol was the only solvent employed. This method was also applicable for ITR quantification from a marketed formulation [127]. As a UV scan of ITR in methanol yielded an absorption maximum at 253 nm (Helios Omega, Thermo Fisher Scientific GmbH, Germany), this was subsequently chosen as the corresponding wavelength for all UV spectroscopy experiments. β CD did not show interference at this wavelength. ITR stock solutions in methanol (0.15 mg/mL) were prepared prior to each analysis, diluted with either methanol or 0.1 N HCl (only for dissolution testing) to gain a calibration curve in the appropriate range. Samples were diluted accordingly.

III.2.2.3.2. High Performance Liquid Chromatography

HPLC is a known technique for drug quantification that uses the hydrophilic/lipophilic interactions of the API with either the mobile phase or the stationary column. Depending on these interactions, the evaluated substance will elute earlier or later from the column and pass an appropriate detection system. By this, it is possible to analyse samples where different ingredients show UV absorption at the same wavelength which would not be possible by UV spectroscopy. Adapting the experimental set-up described by Trinadha Rao et al. [128], the used HPLC method is given in the appendix (see section VII.3.). Stock solutions were prepared as described in the previous subsection and diluted with mobile phase. For every analysis, a fresh calibration curve was prepared and analysed.

III.2.2.3.3. f_1 and f_2 -Concept

As stated, over the course of this study it was necessary to change the ITR quantification methodology from UV spectroscopy to HPLC. It had to be evaluated if measurements based on either UV spectroscopy or HPLC could be freely compared to each other and yielded the same results.

For that reason, the dissolution profile comparisons according to the FDA's guidance for industry were conducted in a modified way, namely by employing method A, the determination of the difference and similarity factors, f_1 and f_2 , respectively. This model independent approach results in two numbers describing the two products under investigation, in this varied case, the two quantification methods. f_1 means the percentage of differences between two dissolution profiles and f_2 concludes the percentage of similarity [129]. Mathematical operations for f_1 and f_2 are given in *equation 6* and *7*.

$$f_1 = \left\{ \frac{[\sum_{t=1}^n |R_t - T_t|]}{[\sum_{t=1}^n R_t]} \right\} * 100 \quad \text{equation 6}$$

$$f_2 = 50 * \log \left\{ \left[1 + \left(\frac{1}{n} \right) \sum_{t=1}^n (R_t - T_t)^2 \right]^{-0.5} * 100 \right\} \quad \text{equation 7}$$

n means the number of measuring time points, R_t stands for the amount of dissolution in per cent reached at a certain time point (t) for the reference formulation (in this case UV spectroscopy) and T_t the corresponding dissolution value for the HPLC quantification.

According to the FDA guideline, some specifications are recommended when applying f_1 and f_2 , such as are:

1. $n = 12$ for each R and T
2. same measuring time points as well as conditions for dissolution testing for R and T with at least three to four sampling times
3. only one sampling time point after 85 % of dissolution
4. up to 15 min of dissolution, variation coefficients below 20 %, after that below 10 %

Reaching f_1 below 15 % and f_2 above 50 % are the considered limits for regarding two dissolution profiles as similar. As dissolution of amorphous ITR (aITR) prepared by rapid cooling after melting did not show dissolution above 85 % after 4 h (see recommendation 3), it was used as suitable sample. 12 units of aITR underwent dissolution testing according to section III.2.2.9. and were analysed by HPLC and UV spectroscopy each. Dissolution curve is given in the appendix (see section VII.3.). Applying *equation 6* and *7* yielded a f_1 value of 1.91 % and a f_2 value of 95.92 % which also proved the similarity between the dissolution curves. Both results were strongly below and above the respective limits. Only recommendation 4 could not be met as the variation coefficient exceeded 20 % and 10 % respectively up to 60 min of dissolution but as this was true for both quantification methods, it could be disregarded. Even though the original f_1/f_2 -concept is not meant for these method-comparative purposes, it could still function as groundwork for the conclusion that it was possible to use either UV spectroscopy or HPLC in ITR quantification as they yielded the same results. Thus, in this thesis, results of both techniques were evaluated together without any further mention of the specified quantification method.

III.2.2.4. Quantification of Cyclodextrins

Quantification of β CD and HP β CD was conducted by HPLC adapted from the proposed method of the current Ph. Eur. for β CD [76]. Here, reverse phase HPLC is employed coupled with a refractive index (RI) detector as UV absorption spectra of CDs cannot be used for quantification due to lack of linearity. Both CDs could be investigated together. Stock solutions of either CD in bidistilled water were prepared prior to every analysis and further diluted with it for a calibration

curve. As HP β CD is specified by an average degree of substitution with methyl groups, it is not one defined substance. Therefore, HPLC chromatograms presented three HP β CD peaks (see Figure III.13.). Since every stock solution was prepared with the same raw material as had been used for HMG experiments, and integration of the third peak resulted in a linear calibration curve, quantification of HP β CD was deemed possible. Further details about the HPLC method are given in the appendix (see section VII.3.).

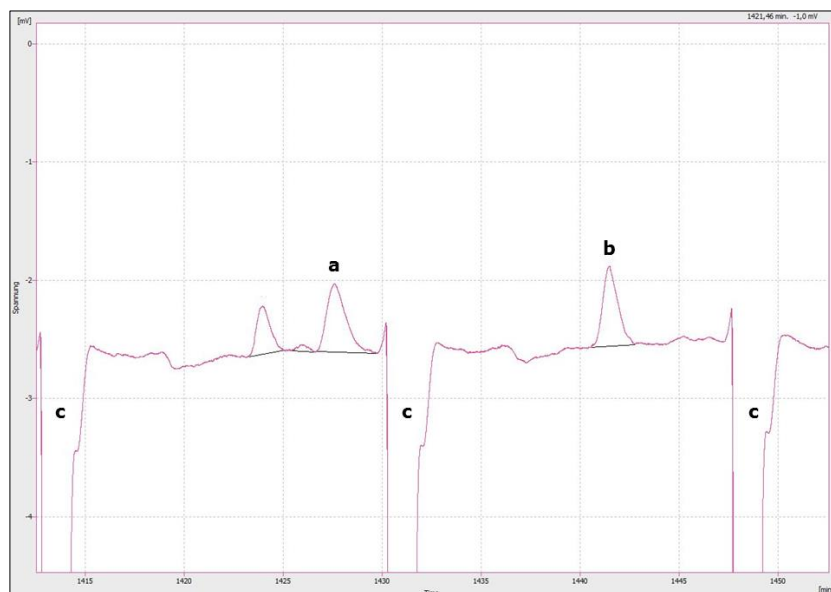


Figure III.13. - Model chromatogram taken from the Clarity™ software (DataApex, Czech Republic) where voltage in mV is plotted against the run time in min; a) HP β CD peak used for quantification, b) β CD peak used for quantification, c) injection signals.

III.2.2.5. X-ray Powder Diffraction

As of today, the gold standard in gaining valuable information about the crystal lattice of a molecule and its possible amorphousness is the x-ray powder diffraction (XRPD). Here, electrons derived at a cathode are accelerated by applying a voltage up to about 50 kV and move towards the anode. If a solid sample is brought into the electron's trajectory, the x-rays are scattered at the molecule's atoms according to Bragg's Law and are reflected at a specified angle. This way, characteristic diffraction rings can be detected. The intensity of this reflection plotted against the measuring angle 2θ results in the powder diffractogram which is specific for each pure substance and can be used for identification. Diffractograms of PMs are additions of the components and might show different patterns due to overlapping reflection angles. As amorphous powders lack long-range order, no x-ray diffraction can be detected, resulting in so-called "ha-

los (see Figure III.14.). Sometimes partially crystalline mixtures present a “halo” with some distinctive peaks [124].

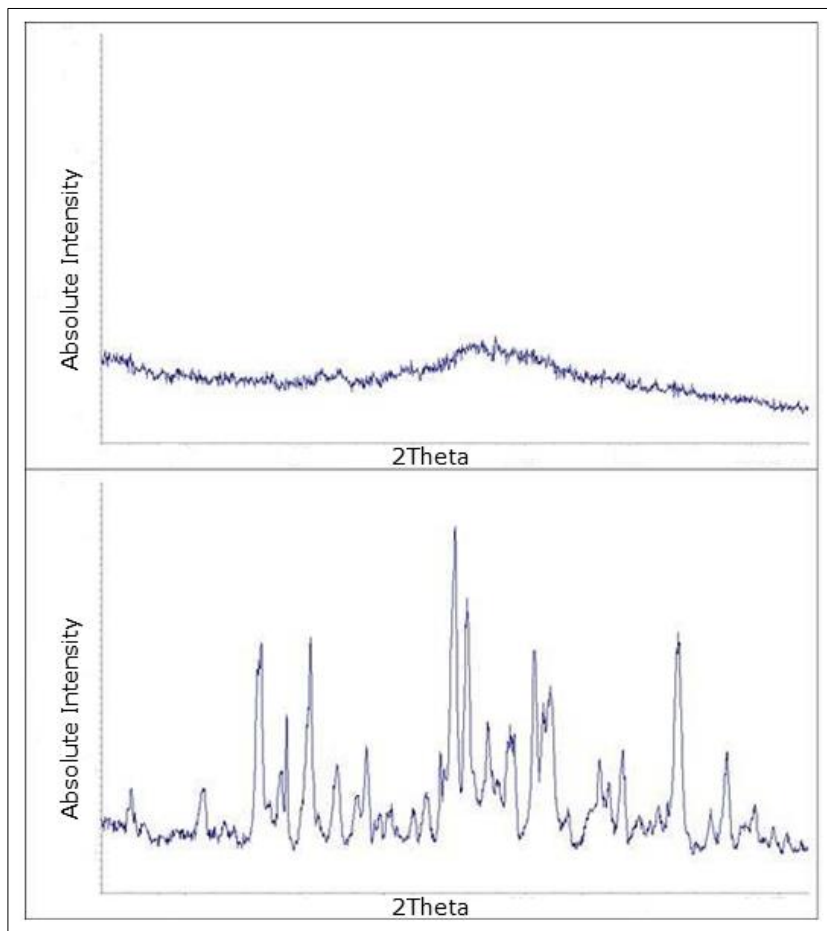


Figure III.14. - Exemplary diffractograms of a fully amorphous sample presenting a "halo", in this case a melt-extruded product (top) and a fully crystalline material, in this case a β CD/ITR powder blend (bottom).

In this study, XRPD was used to investigate the crystal status of PMs and HME/HMG products, especially regarding ITR. For a fully comprehensive picture, the obtained results were evaluated together with those conducted by DSC analysis. Due to costs and expenditure of time, single measurements were carried out using Stadi P (Stoe and Cie GmbH, Germany) with either IP-PSD (Stoe and Cie GmbH, resolution of $0.02^\circ 2\theta$) or MYTHEN 1K detector (DECTRIS AG, Switzerland, resolution of $0.009^\circ 2\theta$) and Cu- $K\alpha_1$ -radiation. Samples were fixated by Scotch[®] tape Magic[™] (3M Deutschland GmbH, Germany) as commercial glues necessary for acetate foils caused sample alteration. Samples were evaluated from $2 - 80^\circ 2\theta$ while being rotated at 40 kV and 30 mA. Due to technical issues, some samples were evaluated using a Stadi P (Stoe and Cie GmbH) with the following experimental set-up: PSD detector (Stoe and Cie GmbH, resolution of $0.06^\circ 2\theta$) measuring range from $5 - 50.98^\circ 2\theta$ at 20 kV and 5 mA.

III.2.2.6. Attenuated Total Reflectance Fourier-Transform-Infrared Spectroscopy Implementation and Data Evaluation

Attenuated total reflectance Fourier-transform infra-red spectroscopy (ATR-FT-IR) is a well-known technique for analysing solid samples [130]. A laser beam in the mid-infrared range ($4000 - 200 \text{ cm}^{-1}$) set on a molecule will result in the absorption of some frequencies depending on the nature of the molecule's atoms and their chemical environment such as covalent bonding. This absorption causes the IR-active molecular regions to vibrate in specified ways, e.g. symmetrical or asymmetrical deformation (δ_s, δ_{as}) and symmetrical and asymmetrical stretching vibrations (ν_s, ν_{as}). Generally, more energy is needed for the stimulation of stretching vibrations. Thus, above 1500 cm^{-1} , mostly stretching vibrations are detectable and deformation vibrations at lower wave numbers [131]. In organic molecules, many different atomic bonds are present which cause coupled vibrations that result in characteristic spectral patterns that are mostly used for the identification of substances [131]. By employing the ATR setup, no sample preparation is needed as the solid sample is firmly placed on the measuring device (e.g. a diamond or ZnSe crystal) and then analysed. Hereby, a laser beam that should be internally reflected by the crystal creates an evanescent wave that expands into the sample and is absorbed at the characteristic laser frequencies due to the chemical properties of the measurand. This causes an attenuated signal in the IR detector that can be used to generate a transmission spectrum [132].

ATR-FT-IR plays an important role in the detection of ICs. As a guest molecule enters the CD cavity, the corresponding functional groups will no longer have the same atomic environment as in a PM where both substance molecules, CD and guest, are merely blended together without much interaction. The comparison of IR-spectra of sole substances, their PM and suspected IC is therefore often used in proving the existing of the encapsulation. The effect that the inclusion will have on the absorption of infrared laser light is hard to predict and individual for each molecule. Changes in wave number to lower or lesser frequencies have been reported as well as the broadening/tightening of IR bands [133].

All measurements were conducted at least in triplicate using a Spectrum 100 (Perkin Elmer Inc.) with MIRacle ATR unit (Pike Technologies, US). Each spectrum was derived from 32 scans against the corrected background with

a resolution of 4 cm^{-1} over the range of $4000 - 550\text{ cm}^{-1}$. Spectra were then automatically baseline corrected and analysed for the existence of peaks (limit 0.5 % transmittance) by the Spectrum™ software (Version 6.3.4.0164, Perkin Elmer Inc.).

III.2.2.6.1. Data Evaluation for Inclusion Complex Detection

By employing ATR-FT-IR, differences in spectra were used to conclude interactions between the CD and the guest when comparing PM and processed samples. As variabilities detected differ from API to API [133], an analysis regimen had to be chosen for ITR before investigating HMG and HME samples. Thus, the molecular structure of ITR was evaluated to specify wave numbers that correlate to functional groups. However, as many specific atomic bonds such as C-H or C-N are present multiple times in the ITR molecule, their association to the respective functional groups had to be based on literature review, evaluation of neighbouring functional groups and the quantity of their appearance. Figure III.15. shows the constitutional structure of crystalline ITR with selected marked functional groups and their corresponding spectral band numbers chosen after evaluating the results of Kumar et al. [134], Nesseem [135], Al-Badr et al. [136] and the provided tables by R cker et al. [131].

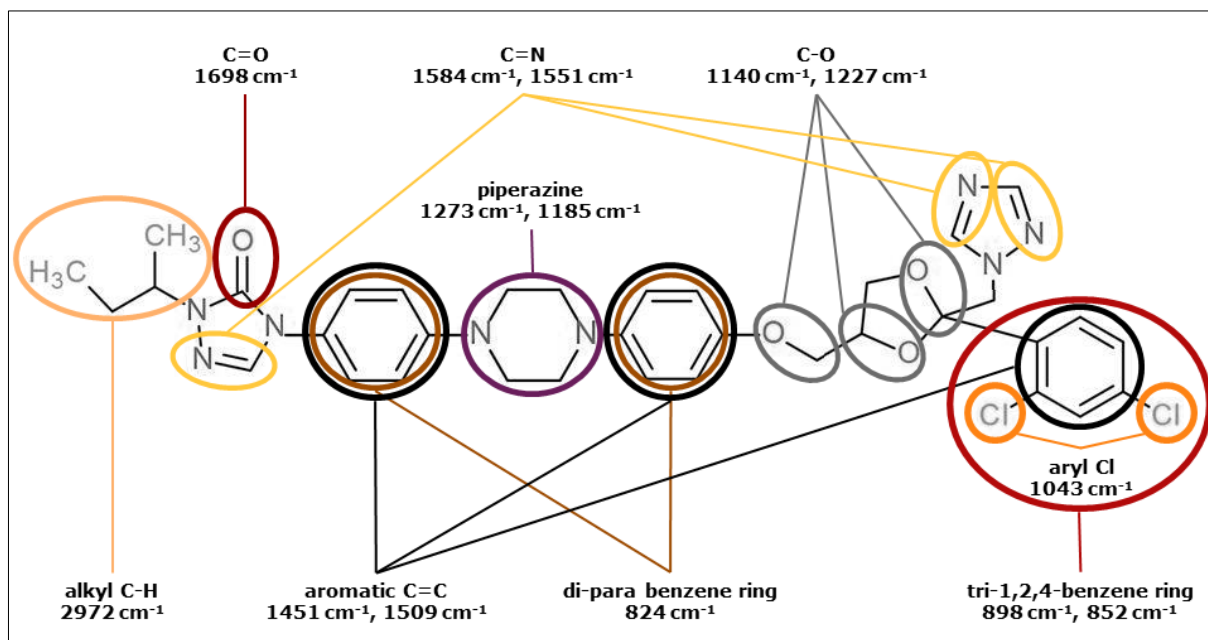


Figure III.15. - Chemical structure of ITR with corresponding wave numbers.

Especially the piperazine ring system, given its position in the middle of the molecule, was of interest regarding possible inclusion. As ATR-FT-IR bands were

complicated to determine with often arising C-H, C-C and C-N atomic bondings, ATR-FT-IR spectrum of pure piperazine was also evaluated to better correlate this functional ring within ITR [137]. Combining the allocations of the functional groups, first conclusions of which part of ITR (head (left) or tail (right) part) is entering the CD cavity during ICF could be drawn. It has to be remembered though that different ATR-FT-IR wave bands can overlap, particularly when ICF of less than 100 % is achieved in the investigated sample. Apart from this, it is important to recognise the existence of aITR in melt processed samples which can influence the ATR-FT-IR spectrum. aITR prepared by melting with successive rapid cooling was studied by ATR-FT-IR as positive control. Some peaks disappeared when comparing aITR to ITR (e.g. ~ 898 and 852 cm^{-1}) due to changes in the atomic structure caused by loss of crystal lattice. Those wave numbers were not further evaluated as any changes could solely be caused by amorphisation. To understand the spectral changes in more detail without subjectivity, twelve wave numbers originating from either ITR/aITR or β CD are given in Table III.4.. They had been identified as markers in evaluating possible ICF and were examined for shifts to higher or lower wave numbers or altogether disappearance.

Table III.4. - Identified marker wave numbers for examining ICF, derived from analyses of either ITR (aITR) or β CD [92]; n = 5; standard deviation (sd) = \pm .

Wave Number, cm^{-1}	Molecular Regions
1697.80 ± 0.23 (1698.87 ± 0.43)	C=O, ITR
1584.34 ± 0.17 (1585.57 ± 0.07)	C=N, ITR
1551.43 ± 0.15 (1552.49 ± 0.01)	C=N, ITR
1509.64 ± 0.29 (1510.59 ± 0.10)	aromatic C=C, ITR
1451.26 ± 0.12 (1450.87 ± 0.06)	aromatic C=C, ITR
1272.85 ± 0.45 (1271.56 ± 0.04)	piperazine, ITR
1227.32 ± 0.28 (1227.50 ± 0.14)	dioxolane, ITR
1185.03 ± 0.13 (1182.59 ± 0.18)	piperazine, ITR
1140.53 ± 0.11 (1137.71 ± 0.28)	C-O-C, ITR
1043.88 ± 0.50 (1040.81 ± 0.66)	aryl-Cl, ITR
1025.78 ± 1.03	C-O, β CD
824.10 ± 0.15 (823.81 ± 0.49)	di para benzene ring, ITR

Band intensity was not taken into account due to high variability and subsequently, insufficient explanatory grounds. The presented marker wave numbers were investigated for every sample analysed by ATR-FT-IR and always evaluated against a suitable control such as PM or PM with aITR (PMaITR). The detection of differences was used for concluding the possible existence of ICs. The detailed data evaluations are shown in the corresponding results sections.

III.2.2.7. Laser Diffraction

Particle size of raw materials and produced samples was determined by laser diffraction. Even though all self-processed samples were manually crushed and given through a 425 μm sieve prior to further analysis, the real mean particle size was still of interest. If differences in solving velocity become present in dissolution testing, the possibility of this effect being caused by a varying surface area of samples has to be taken into account. Raw material particle size can influence the blending procedure and therefore had to be evaluated as well.

During laser diffraction measurements, the analysed particles will flex the light of a helium-neon-laser. The angle and intensity observed by this diffraction can be reverse correlated to the particle size. As not all particles will be of exactly the same size, diffraction patterns will overlap and can be evaluated based on the Fraunhofer theory. Laser diffraction experiments were conducted using a HELOS system with a RODOS module (Sympathec GmbH, Germany) and evaluated with the Windox Software Version 5.4.2.2 (Sympathec GmbH). Each determination was carried out in triplicate with a dispersion pressure of 3 bar and lens R5 (measuring range 0.5 μm - 875 μm).

III.2.2.8. Scanning Electron Microscopy

In order to gain information about the visual appearance of raw materials and processed samples, in this project, the method of scanning electron microscopy (SEM) was chosen. This technique allows a higher magnification and resolution compared to light microscopy [124].

A bundled electron beam is induced by an electron gun, accelerated up to 30 kV and led through the objective lens towards the solid sample by a system of condenser lenses. Upon striking the sample, the electron beam enters and different interactions occur. Two of these are the most important, as they are detected in SEM. First, the low-energy secondary electrons which are emitted by atoms in

the sample after having been entered by the electron beam and second, the backscattering electrons which are reflected at the sample atom's surface and can have high energies. Also emitted from the sample are x-rays which might be used for identification in SEM devices with specific detection equipment. In general, signal converters and detectors such as scintillators are used for transforming the observed electrons into a microscopic image of the sample. Electroconductive samples are suited best for SEM measurements as for them the chance of disturbances caused by electric charging is minimised. Most pharmaceutical measurands are not electroconductive, hence they are often coated with a thin layer of metal [125]. The whole analysis is performed under vacuum conditions.

In this study, SEM images were generated using a Zeiss Ultra 55 Plus (Carl Zeiss NTS GmbH, Germany) applying a working voltage of 2 kV and utilising the SE-2 detector which visualises secondary electrons. Prior to analysis, samples were fixated on a sample holder by carbon stickers (Plano GmbH, Germany) and sputter coated with a Bal-Tec SCP 050 Sputter Coater (Leica Microsystems GmbH, Germany). This was conducted in an evacuated chamber at 50 mA for 65 s with the use of argon 5.0., resulting in a thin gold layer upon the sample ensuring electroconductivity in SEM characterisation.

III.2.2.9. Dissolution Testing

In formulation development and determining product characteristics on a lab scale, dissolution testing is one of the most important tools to obtain first insights into the drug's *in-vitro* behaviour [138]. Dissolution testing means to monitor the amount of dissolved API in a chosen medium over the course of a specified time. In the best case, these results then allow either the determination of an *in-vivo-in-vitro*-relationship (IVIVR) or in the best, but rarest case, an *in-vitro-in-vivo*-correlation (IVIVC) which may be used for regulatory or quality control purposes [139]. Different apparatuses can be used for dissolution testing and are, inter alia, presented in the Ph. Eur. [140].

The dissolution studies in this project were conducted with the Premiere 5100 (Distek Inc., US), using Apparatus 2, the Paddle Apparatus, which is commonly used for investigating solids. The dissolution vessels were brought to the predefined temperatures by heating jackets (see Figure III.16). Sampling was conducted with an automatic sampler model 2230 (Distek Inc., US) at given

time points. Each sampler featured a 0.45 μm filter (FIL045-DK, Quality Lab Accessories L.L.C., US) to avoid removal of solid particles from the dissolution vessel. Dissolution media was not replaced during these experiments. However, for some first dissolution trials, samples were drawn manually and the medium was replaced. Results of these preliminary tests will be labelled accordingly.

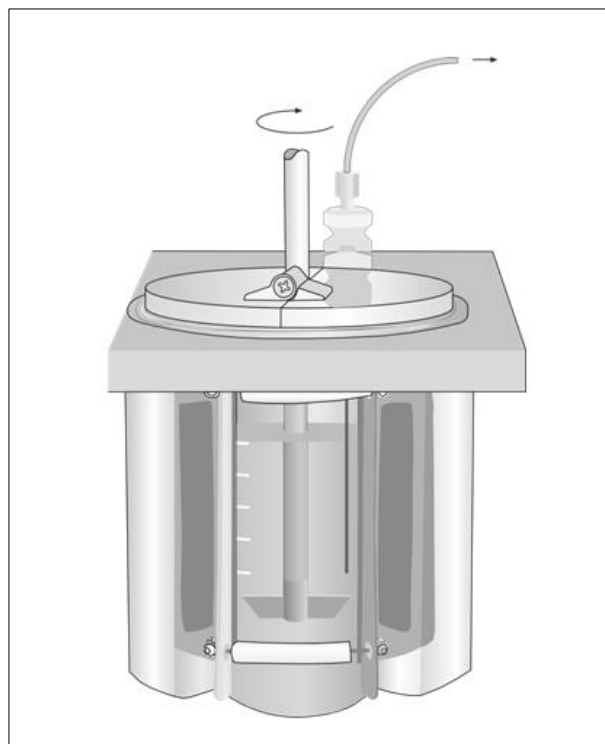


Figure III.16. - Exemplary dissolution vessel with heating jackets, rotating paddle as well as automatic sampling device.

Due to ITR being a weak base ($\text{p}K_a$ 3.7), acid conditions are often described as suitable dissolution media, most commonly 0.1 N HCl with specified variations to approximate gastric conditions [109,141]. Generally, in dissolution tests, sink conditions should be applied. This means that the volume of dissolution medium is at least three times larger than needed for a saturated solution of the investigated API. When working with poorly soluble BCS class II compounds it can be justifiable to employ non-sink conditions if the chosen dissolution method is discriminatory and reproducible [139]. Also, as stated above, a true IVIVC for BCS class II APIs, especially those designed for immediate release like ITR, is extremely rare so that the importance of *in-vitro* dissolution testing rather lies in evaluating stability or batch consistency [139]. Thus, a compromise between gastric resemblance and sink conditions was applied in this project. All dissolution parameters as well as the sampling time points are presented in Table III.5.. After dissolution testing was carried out, the samples were analysed for ITR content as

described in section III.2.2.3. within 48 hours. Sample stability for that time period had previously been ascertained.

Table III.5. - Dissolution testing parameters.

General dissolution settings	
Dissolution medium	<i>900 mL of 0.1 N HCl</i>
Medium temperature	<i>37 ± 0.25 °C</i>
Paddle rotation speed	<i>100 rpm</i>
Analysis time	<i>4 h</i>
API analysis amount	<i>equivalent to 100 mg ITR, given directly into the dissolution vessel</i>
General sampling settings	
Sample amount	<i>5 mL</i>
Sampling velocity	<i>10 mL/min</i>
Sampling time points	<i>2, 5, 10, 15, 30, 45, 60, 90, 120, 150, 180, 210, 240 min</i>

III.2.2.10. Storage Stability

For evaluating the HMG products' qualities against the marketed counterpart and alternative formulation approaches, they underwent stability testing over six months. This stability study was based on the suggestions of the ICH Guideline Q1A (R2) [142] at 25 °C/ambient humidity and 40 °C/75 %RH (accelerated study) (Climate chamber SB 111³⁰⁰, Weiss Klimatechnik GmbH, Germany). After HMG, the products were manually crushed in a mortar, given through a 425 µm sieve and separated into four customary plastic containers. Two were closed with a cap with a built-in drying agent (Gerresheimer AG, Germany), whereas the remaining two containers were left open to investigate the influence of the ambient moisture. For each sample and storage condition, a closed and an open canister were deposited.

The samples were investigated according to the experimental plan given in Table III.6.. All analytical methods were performed as reported in the associated sections. Due to time-consuming and partially costly analyses, DSC experiments, XRPD analysis, SEM imaging and TGA testing were carried out as single determinations, content evaluations were conducted at least in triplicate, ATR-FT-IR

spectra were recorded at least in triplicate, and dissolution testing was carried out at least in duplicate for the investigated samples.

Table III.6. - Analytical protocol for stability testing.

Production	2 Weeks	1 Month	3 Months	6 Months
<i>DSC</i>	<i>DSC</i>	<i>DSC</i>	<i>DSC</i>	<i>DSC</i>
<i>TGA</i>	<i>TGA</i>	<i>TGA</i>	<i>TGA</i>	<i>TGA</i>
<i>βCD content</i>	<i>βCD content</i>	<i>βCD content</i>	<i>βCD content</i>	<i>βCD content</i>
<i>ITR content</i>	<i>ITR content</i>	<i>ITR content</i>	<i>ITR content</i>	<i>ITR content</i>
<i>Dissolution</i>	<i>Dissolution</i>	<i>Dissolution</i>	<i>Dissolution</i>	<i>Dissolution</i>
<i>ATR-FT-IR</i>	<i>ATR-FT-IR</i>	<i>ATR-FT-IR</i>	<i>ATR-FT-IR</i>	<i>ATR-FT-IR</i>
<i>SEM</i>	X	X	X	<i>SEM</i>
<i>XRPD</i>	X	X	X	X

IV. Results and Discussion

The results obtained in the course of this project will be presented and discussed in the subsequent sections in a chronological order following the development and optimisation of a hot-melt formulation consisting of β CD and ITR.

IV.1. Phase Solubility Measurements Results

As described in section III.2.2.1., PSM are frequently used as groundwork when investigating ICs with APIs and their possibly increased aqueous solubility, especially for the determination of complex stoichiometry and stability constants. All these information were of interest for the development of a binary formulation. A deeper knowledge about how simple the IC is formed in regard to how many CD molecules are necessary to encapsulate one ITR molecule is very important as it strongly influences the increase in formulation bulk. There are several literature references about PSM with ITR and β CD in different aqueous media. But, as these results were not always in perfect agreement, it was decided to not solely rely on those suggestions, but to self-conduct PSM.

In the first experiments, ITR PSM were conducted for solutions of β CD in dem. water in the range between approximately 0.001 - 0.017 M. Higher β CD concentrations could not be evaluated. Because of the moderate water solubility of β CD itself, solutions up from 0.017 M were only preparable by ultrasonification. These solutions were not stable as precipitation of β CD crystals occurred within the seven day experiment time. Thus, they had to be excluded from data assessment. As all dissolution experiments were carried out in 0.1 N HCl, PSM were also conducted in this medium in the same concentration range. The utilised CD in the marketed ITR oral solution Sporanox[®] is HP β CD [10]. Due to this application it was expected that HP β CD would be able to substantially reach ITR solubilisation. This outlined HP β CD as an alternative matrix in the hot-melt process. Thus, the PSD for HP β CD and its corresponding IC constants were analysed.

IV.1.1. Evaluation of Phase Solubility Diagrams and Discussion

Results of the PSM studies are shown in Figure IV.1.. Obviously, PSD of β CD in dem. water resulted in very low amounts of dissolved ITR. A magnification of the PSD was necessary to examine if ITR concentration changed at all with rising β CD concentrations.

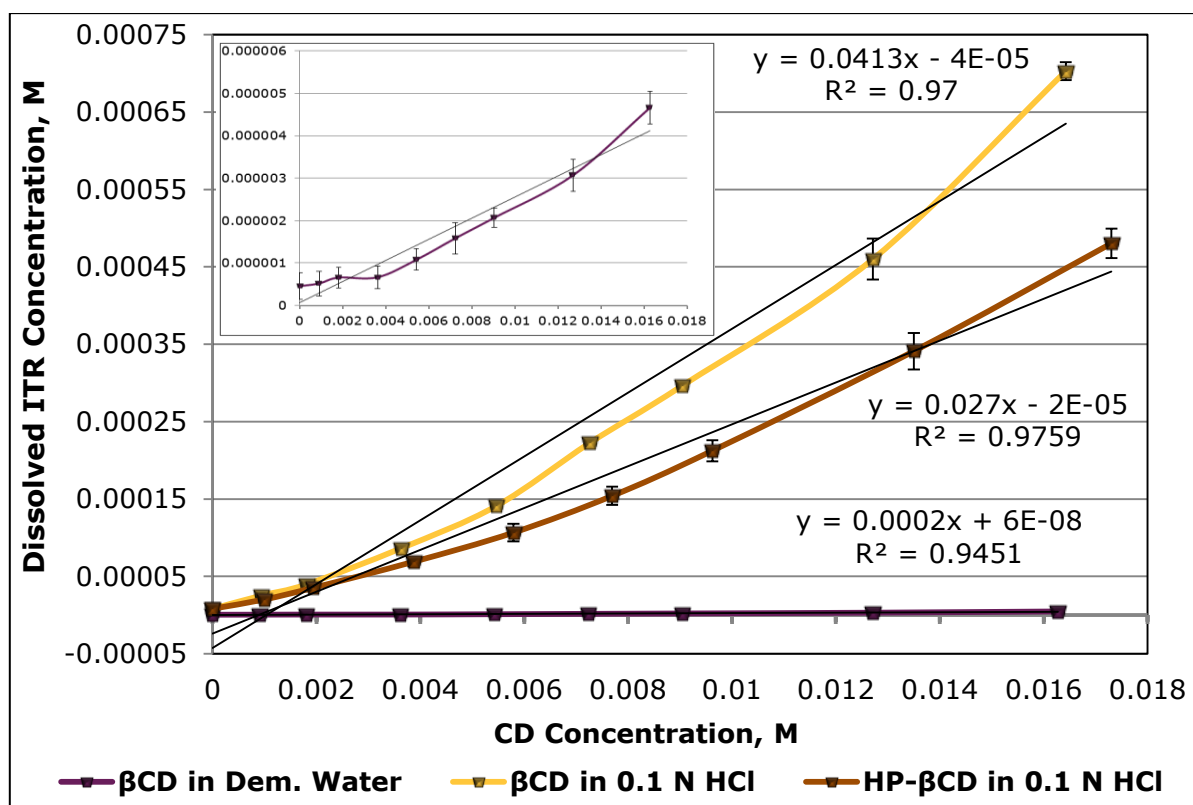


Figure IV.1. - PSD of ITR in β CD in dem. water, β CD in 0.1 N HCl and in HP β CD in 0.1 N HCl; $n = 3$; linear equations and correlation coefficient (R^2) are given next to the respective solubility profile; inserted graph in the upper left corner shows PSD of ITR in β CD in dem. water with adjusted y-axis; $n = 8$; error bars = sd.

Consequently, PSD of HP β CD was not determined in dem. water, but only in 0.1 N HCl. PSD of both CDs in 0.1 N HCl presented strong ITR solubility enhancements. Loftsson et al. determined $K_{1:1}$ for 28 different drugs. The lowest correlation coefficient for which they assumed complex stoichiometry of 1:1 was 0.967 for ergotamine with HP β CD [119]. Taking this into account, at least for the PSD in 0.1 N HCl, nearly linear relationships between ITR and β CD could be confirmed as shown by the correlation coefficients of 0.9700, and 0.9759 for β CD in 0.1 N HCl and HP β CD in 0.1 N HCl. Furthermore, the slopes of all regression lines were lower than unity which suggested ICs in the stoichiometric ratio of 1:1. Consequently, at least for the PSD in 0.1 N HCl, ICs consisting of one ITR molecule and one CD molecule could be assumed [71]. This is the most common type of IC [119]. Furthermore, evaluating the curve progression, A_L -type diagrams, more precisely, A_L^- -type diagrams, could be recognised.

PSM in dem. water showed a lesser correlation coefficient of 0.9451. The diagram might have also been interpreted as A_P -type, meaning that the solubility enhancing properties of β CD became more pronounced at higher CD concentra-

tions. But as the quantified amounts of ITR were very low and always presented a quite high sd, this conclusion could not be regarded as substantial as for the other two analyses in 0.1 N HCl. This held particularly true because this experiment was carried out eightfold without a distinctive result. Additionally, the occurrence of A_L -type diagrams for all three PSD was supported by the fact that the correlation coefficients rose to 0.9896, 0.9912 and 0.9853 for β CD and HP β CD in 0.1 N HCl and β CD in dem. water when excluding the first three determined ITR concentrations at 0 M, 0.001 M and 0.002 M of the respective CD.

Gökbulut et al. characterised the PSD of ITR and β CD in buffer solution pH 1.2 as B_S -types [143]. However, they tested β CD concentrations up to 100 mM which strongly exceeded C_S of β CD (around 18 mM). As reported, β CD precipitation could have likely occurred at these high concentrations which would have caused false results. Yet, the interpretation of A_L -type diagrams was in good agreement with the conclusions drawn by Alanazi et al. and Kumari et al. [144,145]. Alanazi et al. tested β CD concentrations up to 0.016 M in dem. water and 0.1 N HCl while Kumari et al. studied β CD in concentrations up to 0.015 M in dem. water. They obtained similar PSD as shown in this project. For the PSD of ITR with HP β CD, literature results seemed to be compliant about the existence of A_P -type diagrams as reported by Peeters et al. and Alanazi et al. [145,146]. Peeters et al. investigated HP β CD concentrations up to 40 wt/v % (around 0.29 M) at pH 2 and concluded ICs in the ratio of 1:2 ITR:HP β CD. Alanazi et al. evaluated concentrations up to 0.04 M in 0.1 N HCl, also assuming higher order complexes. Even though Shah et al. reported A_P -type diagrams of HP β CD and ITR in phosphate buffer pH 6.8, the experimental results shown rather suggested A_L -type diagrams, because the correlation coefficient nearly reached unity (0.9912) for the concentration range up to 15 mM [147]. Although different media were used and the absolute amount of dissolved ITR differed extensively from the determination in this project, the general influence CDs seem to have on ITR was still complementary with literature results. For both PSM in 0.1 N HCl, D_0 of ITR ($8.174 \times 10^{-6} \pm 5.286 \times 10^{-7}$ M) was clearly diverged from D_{int} which should have been the same value. D_{int} yielded negative results by the linear regression which is implausible. As previously reported, this is often observed for APIs with very low aqueous solubility such as ITR. Most of the time, it is not possible to determine the exact complex stoichiometry as many different effects overlap in solution and the system is constantly changing and interacting. Not only do CDs

form ICs, non-inclusion complexes are possible as well which might further enhance the API's solubility or solubility rate. Recently, the IC stability constant $K_{1:1}$ is often understood as an interplay of many different stability constants in the solution such as dissociation and association constants, equilibrium between complexed and non-complexed API to only name a few [121]. For the purpose of this thesis, two important denouements needed to be taken from PSM. First of all, it was clearly shown that ITR solubility could be improved by using CDs. Secondly, it was necessary to evaluate if either β CD or HP β CD presented stronger ITR encapsulation under the same experimental conditions. From the shown PSD results, a complex with the stoichiometric ratio of 1:1 was supposed for all further calculations.

The stability constant ($K_{1:1}$) for both y-axes intercepts (D_0 and D_{int}), complexation efficiency (CE), drug to CD ratio (D:CD), the increase in formulation bulk (IFB) as well as the resulting formulation bulk for the three PSD were calculated according to *equation 2-5* using D_0 , D_{int} and the slope from the linear regression. Results are presented in Table IV.1..

Table IV.1. - ITR solubility without CD (D_0), ITR solubility at the PSD intercept (D_{int}), slope of regression line, IC stability constant ($K_{1:1}$) calculated with either D_0 or D_{int} , complexation efficiency (CE), drug to CD ratio (D:CD) increase in formulation bulk (IFB) and formulation bulk (IFB · 100 mg single dose of ITR) given for all three PSM and rounded to three significant decimals.

	β CD in dem. water	β CD in 0.1 N HCl	HP β CD in 0.1 N HCl
D_0 , M	$4.560 \times 10^{-7} \pm 3.092 \times 10^{-7}$	$8.174 \times 10^{-6} \pm 5.286 \times 10^{-7}$	
D_{int} , M	5.697×10^{-8}	-4.243×10^{-5}	-2.381×10^{-5}
Slope	0.000250	0.0413	0.0270
$K_{1:1} D_0$, M ⁻¹	548.228	5265.113	3398.739
$K_{1:1} D_{int}$, M ⁻¹	4388.601	-1014.409	-1166.864
CE	0.000250	0.0430	0.0278
D:CD	0.000250 → ~ 1 : 4001	0.0413 → ~ 1 : 24	0.0270 → ~ 1 : 37
IFB	6435.320	38.981	73.345
Formulation bulk*, mg	643532	3898.1	7334.5

*assuming a single dose of 100 mg ITR

As all PSD depicted the mean value of at least three experiments and all IC constants were derived from there, no sd could be enumerated for these terms. Clearly, the medium in which PSM had been conducted had a strong influence on the obtained characteristic parameters for the IC. Comparing the results of β CD in dem. water and in 0.1 N HCl, $K_{1:1}$ calculated with D_0 increased 9.60-fold when using 0.1 N HCl. This might have been related to the enhancement of D_0 itself (17.93-fold increase) due to the ionisation of the drug in the acid milieu. An increase in solubilisation properties of the CD with improved solubility of the API itself has been reported before and is in good agreement with the literature [122,146,148]. The medium-dependency demonstrates a challenge when interpreting PSM results and using them for formulation development. After oral administration of a drug formulation with CDs, the medium (i.e. the gastric environment) will always differ, even for the same person. Therefore, the capability of the CD to include the API may be different upon every administration. This in itself supports the idea of a drug formulation which already entails ICs.

D_{int} gave negative values for both PSD in 0.1 N HCl which resulted in negative $K_{1:1}$ values. This is genuinely impossible. Alanazi et al. investigated $K_{1:1}$ in 0.1 N HCl for β CD and HP β CD at different temperatures [145]. Since PSM in this project were conducted at room temperature, their reported values for 25 °C were regarded as most comparable. With $K_{1:1}$ of 5923.2 M⁻¹ for β CD and 2953.6 M⁻¹ for HP β CD, those results came close to the ones attained in this study (5265.113 M⁻¹ and 3398.739 M⁻¹, respectively). Assuming 1:1 complexation, Peeters et al. calculated $K_{1:1}$ for HP β CD at pH 2 of 5280 M⁻¹ after six days. This was higher than 3398.739 M⁻¹ but probably merely caused by the different experimental design [146]. Kumari et al. analysed β CD in dem. water at 37 °C and obtained a $K_{1:1}$ value of 177.0 M⁻¹ [144]. This was smaller than 548.228 M⁻¹ as obtained here, however expectable, as higher temperatures increase Brownian motion, causing the IC to become less stable.

Generally, $K_{1:1}$ strongly depends on the drug solubility and is therefore often very inaccurate and yields differing results. The more precise expression for IC interpretation is CE. The higher the efficiency of the CD to include the API, statistically less CD molecules are necessary until an IC is formed [121]. Upon comparing CE of all three PSM, it seemed that β CD had shown the highest potential for ICF. Just by changing the experimental medium from dem. water to

0.1 N HCl, CE had increased 172-fold. The CE of β CD in 0.1 N HCl was also about 1.55 times higher than for HP β CD. The $K_{1:1}$ values obtained with D_0 were in agreement with this as they followed the same order. It appeared that the stability and likelihood of ICF between CD and ITR rose from β CD in dem. water < HP β CD in 0.1 N HCl < β CD in 0.1 N HCl. The D:CD ratio (see Table IV.1.) also clearly showed the high influence of the medium, as in dem. water, only every 4001th molecule of CD resulted in a 1:1 IC. HP β CD in 0.1 N HCl statistically needed at least 37 CD molecules for the encapsulation of one ITR molecule and β CD in 0.1 N HCl still 24 molecules. Compared to 4001, this number appeared small but the formulation bulk would have still increased 38.981-fold which would have resulted in a single dose of nearly 4 g per administration. This was unacceptable for many reasons; mainly because the amount of orally taken β CD would have exceeded the proposed maximum of 20 mg/kg bw by far (see section III.1.3.).

The marketed oral solution Sporanox[®] which has a pH of approximately 2 contains 400 mg/mL of HP β CD in contrast to 10 mg/mL of ITR. This results in a D:CD ratio of 0.014 M : 0.286 M or rather 1 molecule of ITR to around 20 molecules of HP β CD. This is less than the determined 37 CD molecules but this is likely caused by the addition of other excipients such as propylene glycol [10] which might interfere with the CE or further enhance the API's solubility.

IV.1.2. Concluding Remarks about Phase Solubility Measurements

As PSM results showed, ICF took place in both dem. water and 0.1 N HCl between β CD and ITR resulting in improved drug solubility. Complex stoichiometry of 1:1 could be assumed from the gained PSD. Resulting from this, all future PM and formulations were prepared striving this ratio to avoid excess use of CDs and evaluate the possibility of 100 % encapsulation. PSM results displayed that the determined CE was very low, clearly stating that for spontaneous ICF, the equilibrium would call for an extreme overabundance of CD. This would subsequently result in an intolerable increase in formulation bulk when trying to acquire therapeutic ITR doses of 50 - 400 mg. Therefore, it was not possible to solely rely on voluntary ICF. PSM outcome also showed higher attraction between β CD and ITR compared to HP β CD which further supported β CD being the preferred choice as extrudate matrix. An oral liquid formulation containing HP β CD is on the market, but high dose therapy causes patients to take about 20 mL of the solution twice

daily which results in a HP β CD intake of 16 g. Even though this is considered innocuous, it might be non-ideal for patient adherence due to the large amounts that have to be consumed, especially since it should be taken 10 mL at a time and swished extensively in the mouth before swallowing. Also, the oral solution of Sporanox[®] is marketed in 150 mL amber glass bottles. With a recommended dose, e.g. for oropharyngeal candidiasis, of 20 mL per day for up to two weeks, one unit would not be enough, causing higher expenses [10].

Taking all these results into account, the development of a binary hot-melt process for β CD and ITR could be the resolve to overcome the low CE by using the mTSE to force the API into the β CD cavity. This could successively lead to an innovative solid formulation containing preformulated ICs. The accompanying amorphisation of ITR might influence ICF favourably or further improve product characteristics such as ITR dissolution.

IV.2. Development of Binary Hot-Melt Process

As described in section I.2., the aim of this thesis was to develop a binary melt process for PM of β CD and ITR resulting in ICF within the mTSE and showing sufficient product qualities. PSM results (see section IV.1.) showed that β CD indeed encapsulated ITR and improved its aqueous solubility which qualified it as matrix candidate for the hot-melt process.

IV.2.1. Binary Hot-Melt Extrusion Process

The most common application when utilising mTSE is HME (see section II.2.1.). The investigation of β CD as sole matrix during a hot-melt process has only been carried out marginally before. Subsequently, nearly no literature references were available for the planning of the HME process. For that reason, first approaches were taken to develop and optimise this procedure. The results are shown in the subsequent segments. To generate valuable information about the two components of the desired melt-extrudate, they were physico-chemically characterised, both individually and as PM which was prepared according to section III.2.1.1..

IV.2.1.1. Physico-Chemical Characterisation of Raw Material and Powder Blend

To develop a hot-melt process, it is necessary to gain an understanding about the properties of the involved goods. Even though the absolute thermal stress on

the material is sometimes lower than expected due to the short residence time in the barrel, it is still important to investigate the degradation behaviour of the applied substances. Temperatures above the degradation point (T_d) are not feasible. The determination of ITR T_m was also of importance, as, depending on the operating temperatures, amorphisation of the API remained a possibility. Figure IV.2. shows XRPD diffractograms of β CD, ITR and PM.

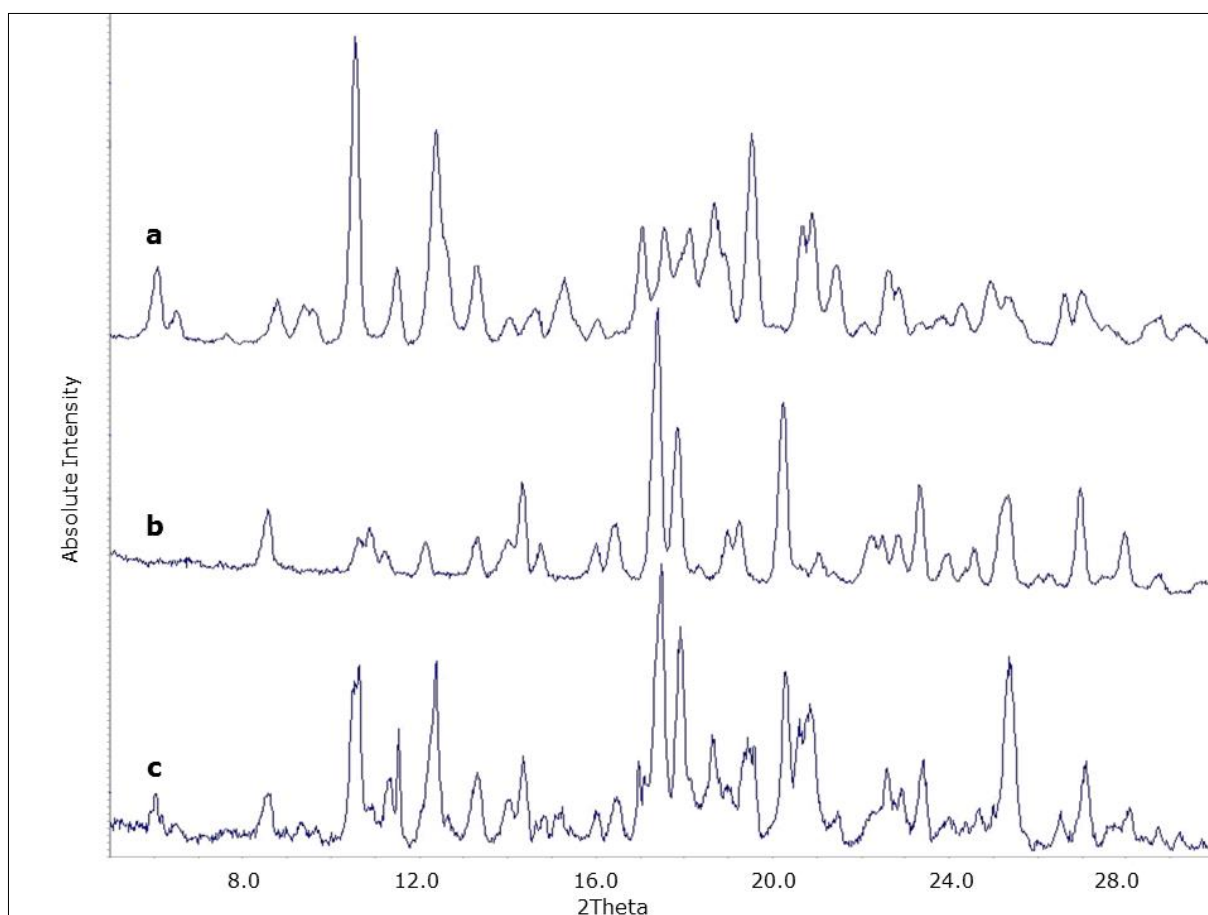


Figure IV.2. - XRPD diffractograms of a) β CD, b) ITR and c) PM.

Both mixture components were fully crystalline as they gave strong defined peaks. The PM diffractogram appeared to be the addition of the other two diffractograms. In some 2θ regions where both pure components presented signals, peaks now seemed to overlap, e.g. around $20^\circ 2\theta$. With ITR being fully crystalline in PM, a distinct T_m peak had to be expected in the DSC trace. Results of DSC measurements of ITR, β CD and PM are shown in Figure IV.3.. The curve of pure ITR exhibited a melting signal at 166.73°C which was in good agreement with the literature reference of 166.2°C (see section III.1.1.). No sign of degradation was detectable for ITR between T_m and 300°C . The trace of β CD showed a broad peak at 119.09°C which corresponded to the cavity water loss.

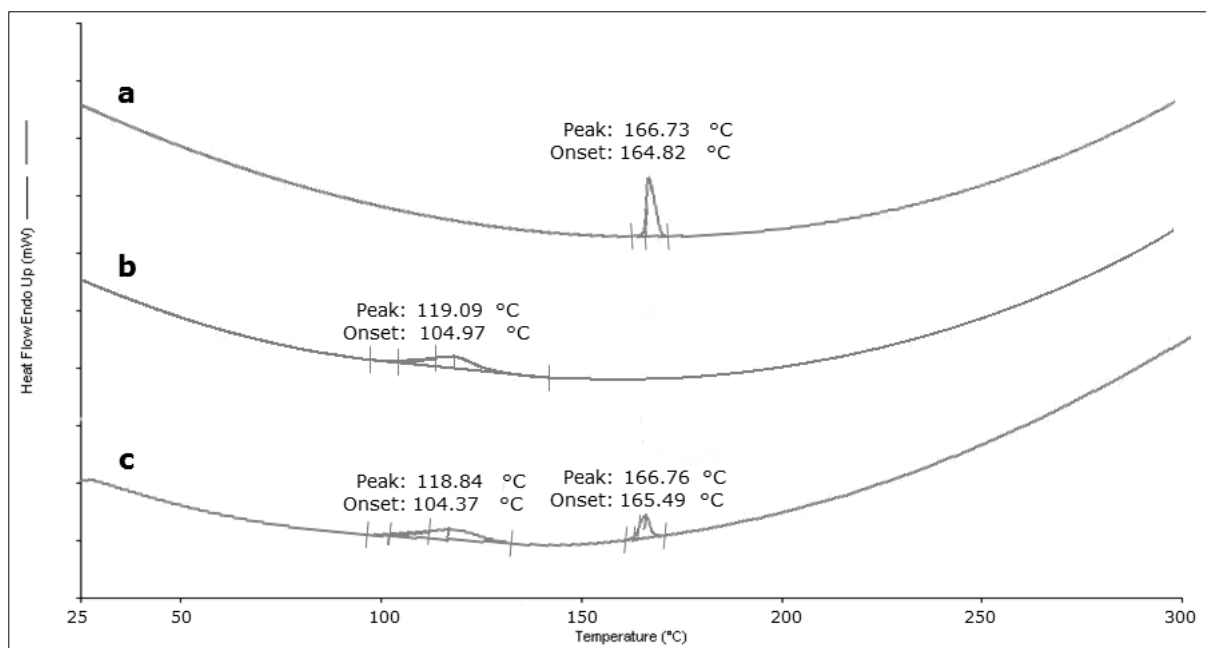


Figure IV.3. - DSC curves of a) ITR, b) β CD and c) PM; analysis conducted from 25 - 300 °C; ITR and β CD heating rate 10 K/min; PM heating rate 20 K/min.

No further signal could be observed, neither of melting (see section III.1.3., 255 - 265 °C) nor deterioration. This was in compliance with β CD's thermo-analytical behaviour as described by Giordano et al. [149]. DSC results of PM seemed to be the sum of the components as seen in XRPD. Both events, β CD water loss and T_m of ITR, were observed. Heating up to 300 °C revealed no degradation. Consequently, TGA experiments were carried out to further investigate this. In TGA, the maximum temperature can be higher than in DSC and it is more sensitive to weight loss corresponding with deterioration. The resulting TGA curve of PM is shown in Figure IV.4.. The stretch between 50 °C and 150 °C represented the water content of the sample. Following the water loss, the sample gave a weight plateau during which the temperature rose further until two turning points became detectable at 320.26 °C and 360.31 °C, serving as the T_d of the two mixture components. TGA experiments of pure ITR and β CD (data not shown) led to the conclusion that the first event at 320.36 °C belonged to β CD and 360.31 °C to ITR.

Taking all data from XRPD, DSC and TGA into account, it could be concluded that no degradation seemed to have occurred at the applicable temperatures of the mTSE (< 280 °C), at least if no mechanical stress was acting on the material. ITR T_m was detected around 167 °C. Process temperatures slightly below and above this limit may very well lead to amorphisation of the API. As amorphisation

can lead to additionally improved aqueous solubility of ITR, the first HME runs were carried out around T_m of ITR.

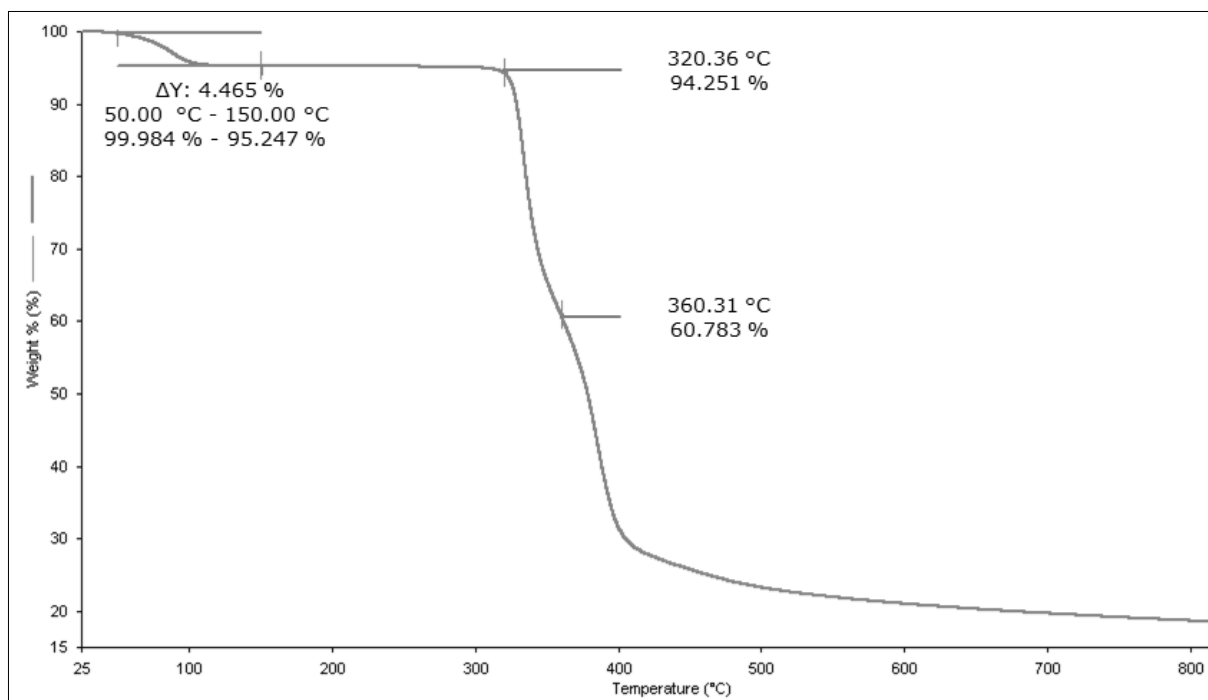


Figure IV.4. - TGA results of PM; analysis conducted from 25 - 850 °C; heating rate 20 K/min.

IV.2.1.2. Preliminary Hot-Melt Extrusion Trials and Optimisations

Results from section IV.2.1.1. were taken to establish the basic framework of the HME process. Screw design was utilised according to section III.2.1.3. without variations, while different die arrangements were investigated. The die is the part of the mTSE where most pressure builds up and where product shape is determined. In common polymer HME, this typically results in an infinite homogeneous extrudate strand drooling from mTSE that can then be pulled with uniform velocity towards further downstream equipment. By doing so, die swelling (swelling of the extrudate strand after exiting the die due to molecular relaxation of the polymer matrix) can be avoided and the molecular orientation of the polymer can be controlled [115]. Since β CD does not possess these thermoplastic properties, it was not expected to yield a potentially never-ending fully deformable extrudate strand. Thus, it was important to not only investigate the suitable temperature profile for the HME process combined with monitoring the throughput and torque, but also to evaluate the influence of different die structures on the product. Principally, due to lowering the mechanical stress on the extrudate as well as for safety reasons, the lowest applicable temperature should be chosen

for an HME process. Therefore, not only product qualities were taken into account for the preliminary HME runs but also the lowest feasible temperature for the different die arrangements.

IV.2.1.2.1. Different Die Arrangements: 2 mm Standard Die

PM was given into the hopper and average throughput of PM was determined as presented in section III.2.1.3.. The standard die of the Pharma 11 TSE has a 2 mm diameter and allows separate heating up to 280 °C which is functionalised by a die heater. Due to the space-saving design and since uniform heating is crucial, no direct cooling aid is applied. It can only be air-cooled. A frontal image of the standard die is presented on the left in Figure IV.5.. In TSEs, the die usually connects to the barrel with an 8-O transition after which the material is led into the flow channel [115]. This can be seen in the cross section view of the standard die (see on the right in Figure IV.5.).

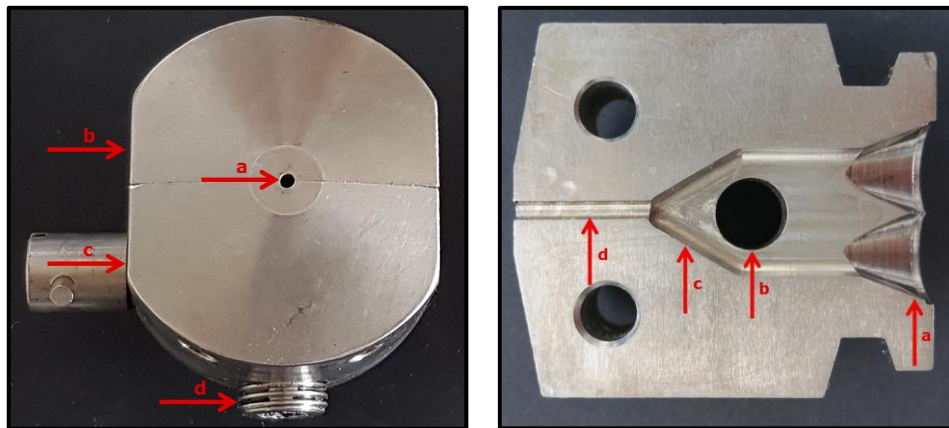


Figure IV.5. - Left: frontal view of standard 2 mm die; a) die opening, 2 mm in diameter, b) adapter for die heater, c) adapter for temperature control, d) adapter for pressure control; Right: Cross section image of standard 2 mm die; a) 8-O transition, b) measuring point for pressure control, c) strict narrowing inner structure, d) flow channel 2 mm in diameter.

Two different HME temperature profiles (see Table IV.2.) were investigated, both nearly reaching the maximum mTSE temperature of 280 °C. HME Trial 1 was implemented with a screw speed (ScS) of 100 rpm whereas the higher temperature in HME Trial 2 allowed a faster ScS of 225 rpm. Torque and die pressure varied during the HME run and are given as average values during stable sample collection. $T_{\text{Extrudate}}$ is the temperature that was measured directly at the die and was slightly above the set die temperature for both HME runs (+4 °C in Trial 1 and +6 °C in Trial 2). This is a common phenomenon as the high energy input causes the extrudate to heat up.

Table IV.2. - mTSE parameters for HME Trials with 2 mm standard die, torque and die pressure are given as average values monitored during sampling.

HME Trial	Z1, °C	Z2, °C	Z3, °C	Z4, °C	Z5, °C	Z6, °C	Z7, °C	Die, °C	ScS, rpm
1	95	120	160	170	190	210	250	270	100
2	120	160	200	245	265	270	270	275	225
HME Trial	Throughput, %		Torque, %		Die Pressure, bar			T _{Extrudate} , °C	
1	15		25		9			274	
2	25		21		4			281	

The average pressure at the die when material was flowing out was quite low with 9 bar and 4 bar but this parameter strongly varied within both HME runs. In some cases, material got stuck in the die, causing the momentary pressure to rise above 100 bar which resulted in mTSE emergency shut-down. While applying the standard die, only very short partial extrudate strands could be acquired and most of the extrudate was strongly deteriorated (see Figure IV.6.). Extrudate pieces exhibited the phenomenon of "shark skin" which is defined as a "rough, wavy appearance of the extrudate" [115].



Figure IV.6. - Deteriorated extrudate strand coming out of the 2 mm standard die during an HME run.

The average throughput is given in Table IV.2. as 15 % and 25 % for HME Trial 1 and 2, respectively. Even though the throughput capacity was correlated to an amount of PM in g/h, this correlation did not longer hold true during the HME runs. This was caused by the instability of the operating pressure, the resulting process interruptions and the fact that the extrudate strands were not continuously leaving mTSE. Consequently, it was not possible to determine the exact material throughput for HME Trial 1 and 2. Nevertheless, it can be noted

that the lowest applicable temperature for applying the 2 mm die was around 270 - 275 °C to acquire any kind of product. This temperature was considerably close to the possible maximum of the apparatus. After conducting experiments with the 2 mm standard die, a material sample was extracted out of it. The extricated specimen is shown in Figure IV.7. in the position from where it was taken.

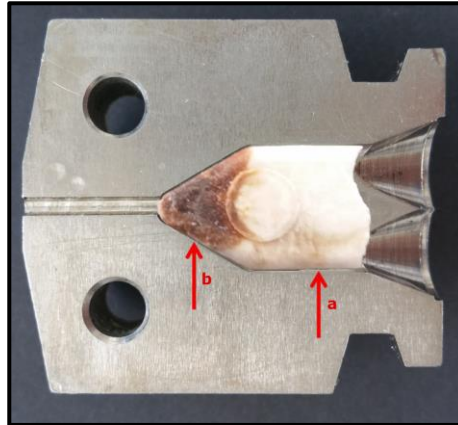


Figure IV.7. - Cross section view of standard 2 mm die with extracted extrusion sample positioned inside; a) undegraded material right after barrel exit, b) origin of deteriorated product at steep narrowing within die.

The extruded material appeared white-greyish intact after leaving the barrel and when entering the 8-O transition zone. At the stricture before penetrating the 2 mm flow channel, degradation was visible and seemed to originate from there. It appeared that product congestion had occurred before the flow channel. High shear and mechanical forces impacted on the partially molten mixture when arriving at this narrowing point. The material was rapidly conveyed towards the die and due to the missing thermoplastic behaviour of β CD, it could not follow the path down towards the flow channel but rather caused a blockage which then resulted in product deterioration.

IV.2.1.2.2. Different Die Arrangements: 3 mm and 6 mm Variable Systems

To overcome the problem of product congestion at the narrowing within the die, a variable die system was tested. Here, the general inner structure was similar to the 2 mm standard die but different insets could be used that presented wider flow channels. A 3 mm and a 6 mm inset were studied to evaluate differences to the standard die. Different temperature profiles with die temperatures between 200 - 280 °C were examined without reaching a completely stable process for both die insets. On the left in Figure IV.8., a typical result if applying the 3 mm inset is shown, while on the right, a typical result of the 6 mm inset can be seen.

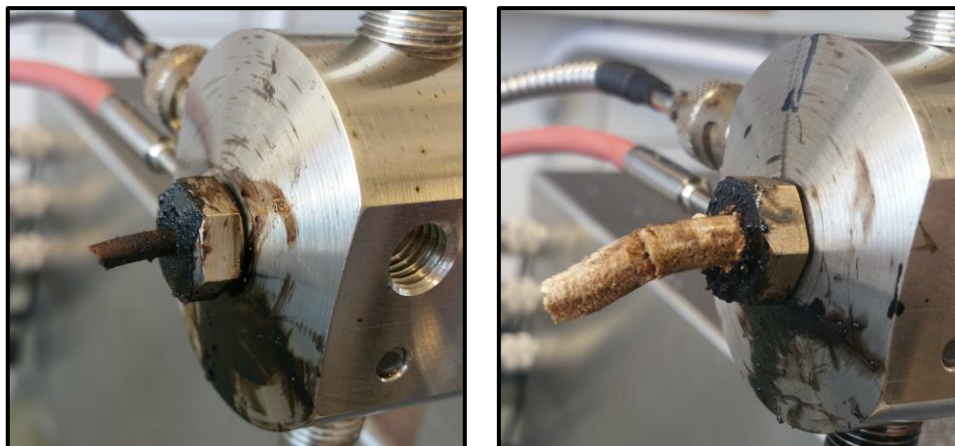


Figure IV.8. - Left: extrudate strand coming out of the variable die with 3 mm die inset; Right: extrudate strand coming out of the variable die with 6 mm die inset.

Even though short extrudate strand-like pieces could leave the die due to the larger opening, product degradation still occurred. Again, “shark skin” was observed. Pressure was unstable, causing the mTSE to shut down at some points and the lowest applicable die temperature was around 270 °C which was nearly as high as for the 2 mm standard die. This might have also been explained by the similar inner structure of the die. As the variable nozzle head is not severable in two parts as the standard die, it was not possible to retrieve a sample from within. To examine an even wider flow channel and subsequently, a less steep narrowing inside the die, a 6 mm inset was built and attached to the die head as can be seen on the right in Figure IV.8.. Short extrudate strands could leave mTSE in partially undegraded shape. Comparing the product to the extrudate from the variable 3 mm inset, it appeared distinguishably lighter in colour, especially in the extrudate core. The degraded surface of these strands might have been the cause of product deterioration or product residue that became previously stuck on the die caused by material from mTSE filling phase. The first specimen to enter always exhibits a longer residence time within the barrel. The extrudate surface occurred smoother than before. Upon using the 6 mm inset, the die pressure was considerably lower but yet unstable as material flow was not continuous. However, the mTSE did not shut down. The lowest applicable temperature was 200 °C which was a considerate decrease compared to the other investigated die arrangements. Nevertheless, degradation due to product congestion could not be completely excluded and the extrudate strand was not drooling from the die without interruptions.

To conclude, experiments with the described die arrangements showed that β CD as an oligosaccharide and lacking thermoplastic properties was only partially

susceptible to the appropriate deformation at the die, even when mixed with fully molten ITR. Even though partial extrudate strands could be obtained, this was not of importance as the instability of the process necessitated the need for a different die system without steep narrow inner structures. The development of this original die is presented subsequently.

IV.2.1.2.3. Development of 6 mm Conical Die and Utilisation

Because the 6 mm inset had yielded the only HME product that appeared rather intact than deteriorated, this diameter was also chosen for the new die arrangement. Figure IV.9. presents a frontal image of the self-developed die. As the variable 6 mm die had demonstrated irregular extrudate exit, the opening of the flow channel was slightly widened. Die heater and temperature control were incorporated in the die head. In regard to product congestion caused by the steep angle in the standard die head (see Figure IV.7.) the new die should not present any harsh stricture. Hence, a conical structure was selected.

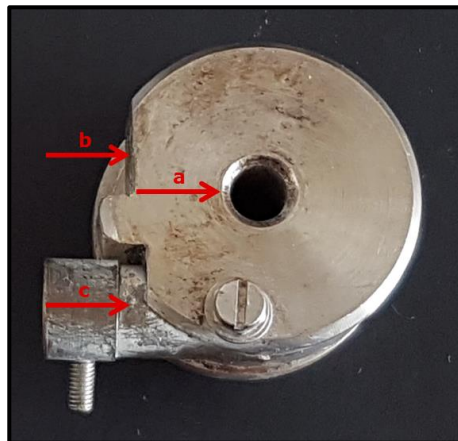


Figure IV.9. - Frontal view of self-built 6 mm conical die; a) die orifice with 6 mm diameter and widened opening for easier extrudate exit, b) adapter for die heater, c) adapter for temperature control.

Figure IV.10. displays the rear view of the built 6 mm die. Due to the large opening at the die entry, it was not possible to apply the usual 8-O transition. The opening was tapering concentrically towards the 6 mm orifice and the die head did not harbour a flow channel of measurable length as visible in Figure IV.5. (right). Since the inner cone took up most of the inner die space and due to enabling sufficient heating properties, it was not possible to enlarge the die in a way that the pressure control was applicable. Thus, no die pressure was measurable when applying this die arrangement.

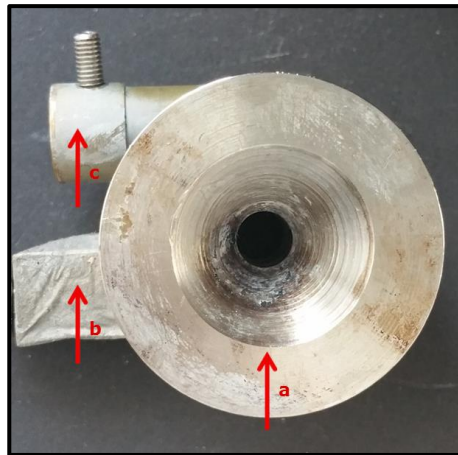


Figure IV.10. - Rear view image of 6 mm conical die; a) conical inner ring-structure, b) attached die heater, c) adapter for temperature control.

The first HME experiments utilising the 6 mm conical die showed the necessity to install the ventilation port into the system directly after the powder feed (see section III.2.1.3) because water evaporated continuously in the barrel, causing material to get stuck in the powder entry. This caused the torque to vary and the temperature in Zone 1 to destabilise as it became higher due to the water vapour. Upon attaching the die to mTSE and starting the HME process, the first material exiting during the filling phase came out degraded, but after the process was stabilised, longer white-greyish extrudate strands could be obtained than before. Table IV.3. exhibits the parameters chosen for Trial 3 and 4. The throughput of 40 % was correlated to 200.6 g/h and could not be increased further because the ventilation port became blocked. Torques between 35 and 39 % were considerably higher than for the 2 mm standard die but not distressing for a stable HME process where 60 - 80 % is often common. A ScS of 250 rpm was examined but the screws started screeching. This is a sign for lack of lubrication within the barrel. Thus, 225 rpm was chosen as maximum ScS.

Table IV.3. - Parameters of HME runs with 6 mm conical die attached to mTSE.

HME Trial	Z1, °C	Z2, °C	Z3, °C	Z4, °C	Z5, °C	Z6, °C	Z7, °C	Die, °C	ScS, rpm
3	75	130	170	200	240	260	260	260	225
4	98	130	170	200	200	220	220	225	225
HME Trial	Throughput, %		Torque, %		Die Pressure, bar			T _{Extrudate} , °C	
3	40		35		X			X	
4	40		39		X			X	

The die pressure and $T_{\text{Extrudate}}$ which are monitored by the pressure sensor could not be measured with the conical 6 mm die. Because mostly black degraded product was acquired from Trial 3, operating temperatures were lowered. Even though it was possible to gain extrudate strands with die temperatures as low as 200 °C, the parameters presented for Trial 4 yielded a more continuous process, probably due to a lower melt viscosity at the die temperature of 225 °C. As shown in Figure IV.11., the extrudate surface appeared smoother than for the 6 mm variable inset though there was still minor roughness observable. The extrudate strand could leave mTSE continuously but no infinite strand was created. This caused irregular fragments of the strand to break off due to the brittle un-thermoplastic behaviour of β CD.

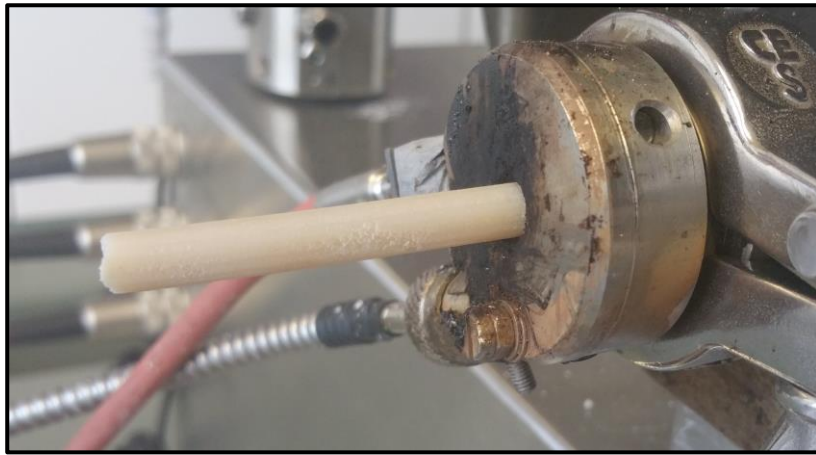


Figure IV.11. - Intact extrudate strand coming out of the 6 mm conical die during HME Trial 4.

Through applying the self-developed 6 mm conical die, it was possible to achieve an applicable operating temperature as low as for the 6 mm variable inset, of about 200 °C. The procedure appeared to be stable at 225 °C die temperature judging from torque monitoring, though this could not be fully confirmed due to the missing pressure data. Nevertheless, the conical die was the only die arrangement feasible for constant visually completely undegraded extrudate strand production and was therefore utilised for all following HME experiments.

IV.2.1.3. Characterisation of Extrudates for Content Evaluation and Amorphousness

Of all presented HME runs, Trial 4 was regarded as the most promising HME profile as it was the only one yielding fully white-greyish extrudates. It was not considered necessary to investigate degraded samples. Therefore, only samples

from Trial 4 were examined for ITR and β CD content, as well as for ITR amorphisation by DSC analysis. Determined contents were $98.04 \pm 0.10 \%$ and $102.85 \pm 2.22 \%$ for β CD and ITR, respectively. The analysis was carried out in triplicate. This supported the hypothesis after visual inspection of the extrudate strands that no product degradation had occurred.

DSC results of HME Trial 4 are shown in Figure IV.12.. When evaluating the DSC trace as presented by the software (large DSC curve in Figure IV.12.), the sample appeared fully amorphous as no distinct T_m of ITR could be detected. Only upon further magnification of the DSC curve (see a and b in Figure IV.12.) small signals at $163.57 \text{ }^\circ\text{C}$ (0.1530 J/g) corresponding to the melting of crystalline ITR and T_g of aITR at approximately $60 \text{ }^\circ\text{C}$ were identified. Additionally, a very small broad exothermic signal slightly above $110 \text{ }^\circ\text{C}$ became visible in this magnification. This exothermic broad peak had previously been reported in the literature as so-called "cold crystallisation" of ITR during DSC analysis [150]. This phenomenon describes the recrystallisation of ITR while being heated during the experiment.

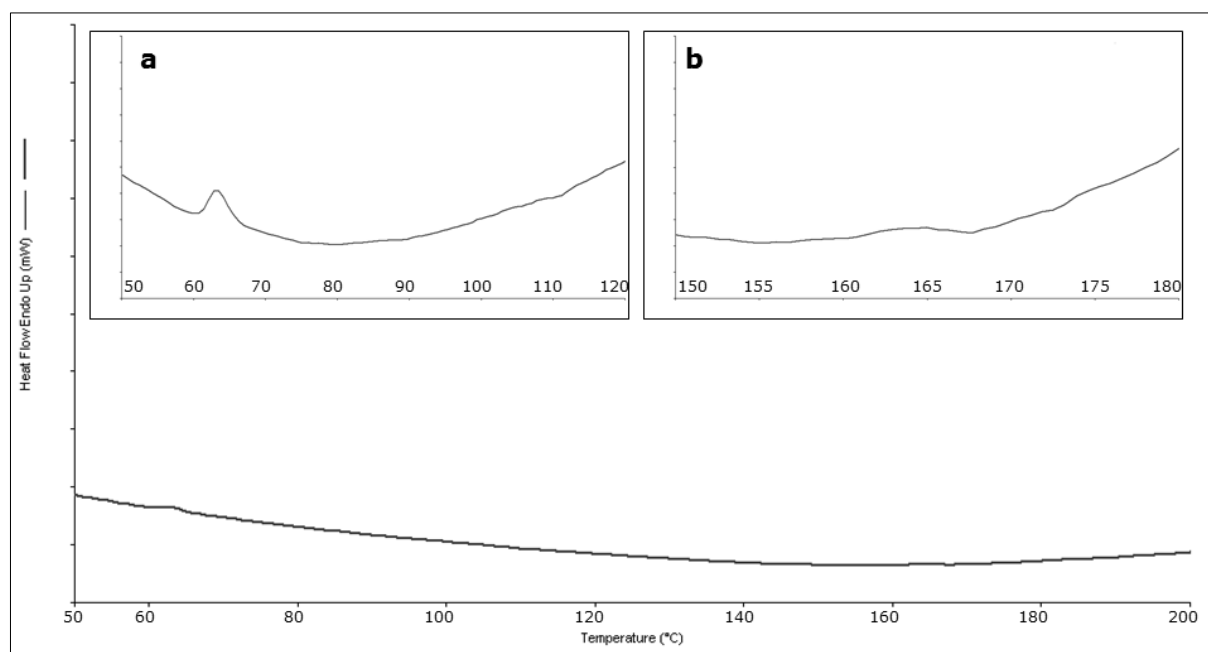


Figure IV.12. - Excerpt from DSC trace of HME Trial 4 sample; analysis conducted from $30 - 300 \text{ }^\circ\text{C}$; heating rate 20 K/min , $\Delta Y: 50 \text{ mW}$; a) excerpt from $50 - 120 \text{ }^\circ\text{C}$, $\Delta Y = 1 \text{ mW}$, b) excerpt from $150 - 180 \text{ }^\circ\text{C}$, $\Delta Y = 1 \text{ mW}$.

For technical reasons, XRPD analysis of this sample was not possible. Thus, after the examination of DSC results, two possible hypotheses were set. Firstly, not all ITR was either amorphous after HME or recrystallised between manufacture and DSC measurement (approximately one day at ambient storage conditions),

resulting in the very small T_m signal of ITR. Secondly, ITR was fully amorphous in the sample but recrystallised upon heating during the DSC analysis.

IV.2.1.4. Concluding Remarks about the Hot-Melt Extrusion Process

Considering the results presented in the previous section, it can be concluded that it was possible to develop a stable HME procedure resulting in undegraded product that appeared at least partially amorphous. However, the production of extrudate strands was not continuous as for a typical HME process. During mTSE operating, no die pressure could be monitored with the self-developed conical 6 mm die system. This aggravated the feasibility of the process. An alternative to the more common HME practice is the HMG procedure, where the mTSE is operated without a die. As particularly the die arrangement was identified as the crucial parameter responsible for product deterioration, this was a promising approach for an alternative hot-melt procedure.

Consequently, a binary HMG process was developed and results are given in the following section. Moreover, HME Trial 4 was further characterised regarding ITR solubility and dissolution as well as compared to the novel HMG operation.

IV.2.2. Binary Hot-Melt-Granulation Process

Deviating from HME where the material left mTSE through the die, in HMG processes, the die was switched to the granulation heel slide, allowing the melt-granulated material to gently slide out of the mTSE. HME Trial 4 was previously identified as the most stable HME procedure, yielding undegraded extrudate strands. Thus, parameters used for Trial 4 served as foundation for the development of the HMG process as this would allow substantial statements regarding the comparison of the two hot-melt operations.

IV.2.2.1. Hot-Melt Granulation Parameters

The chosen parameters for the HMG process are presented in Table IV.4.. The throughput of 40 % correlated to 200.6 g/h as it was the case for HME Trial 4. The only difference apart from the removal of the die was the ScS of 150 rpm which could not be further enhanced as the screws started shrieking and the risk of barrel scratch marks became too high. Consequently, the presented parameters are the closest possible towards HME Trial 4.

Table IV.4. - Parameters for the chosen HMG procedure.

HMG Trial	Z1, °C	Z2, °C	Z3, °C	Z4, °C	Z5, °C	Z6, °C	Z7, °C	Die, °C	ScS, rpm
1	100	130	170	200	200	220	220	X	150
HMG Trial	Throughput, %		Torque, %		Die Pressure, bar			T _{Extrudate} , °C	
1	40		20		X			X	

The average torque of 20 % was considerably lower than for HME Trial 4 (39 %). The torque was more stable during HMG Trial 1. This was most likely attributed to the missing die as material could leave mTSE without hindrance and without any component causing constrictions. The final product appeared as white-greyish pasty granules that seemed partially molten as is shown in Figure IV.13..

**Figure IV.13. - Collection of HMG sample with the granulation heel slide.**

Since β CD does not melt at the applied temperatures but ITR does, it is most likely that the molten ITR caused the pasty appearance and granulation-like procedure within mTSE. Thus, the agglomerated granules appeared larger in size. However, the granules were not evenly distributed regarding their particle size, as this varied strongly during product collection which is why it was so important to crush and sieve all samples prior to further testing (see section III.2.1.3.).

IV.2.2.2. Characterisation of Hot-Melt-Granules

HMG Trial 1 was investigated for ITR and β CD content in triplicate. The determined amounts of 97.83 ± 0.31 % and 102.34 ± 3.51 % for β CD and ITR respectively agreed well and showed that no product degradation had occurred as

the intact white-greyish appearance of the granules had suggested. DSC measurements were also performed and results are shown in Figure IV.14..

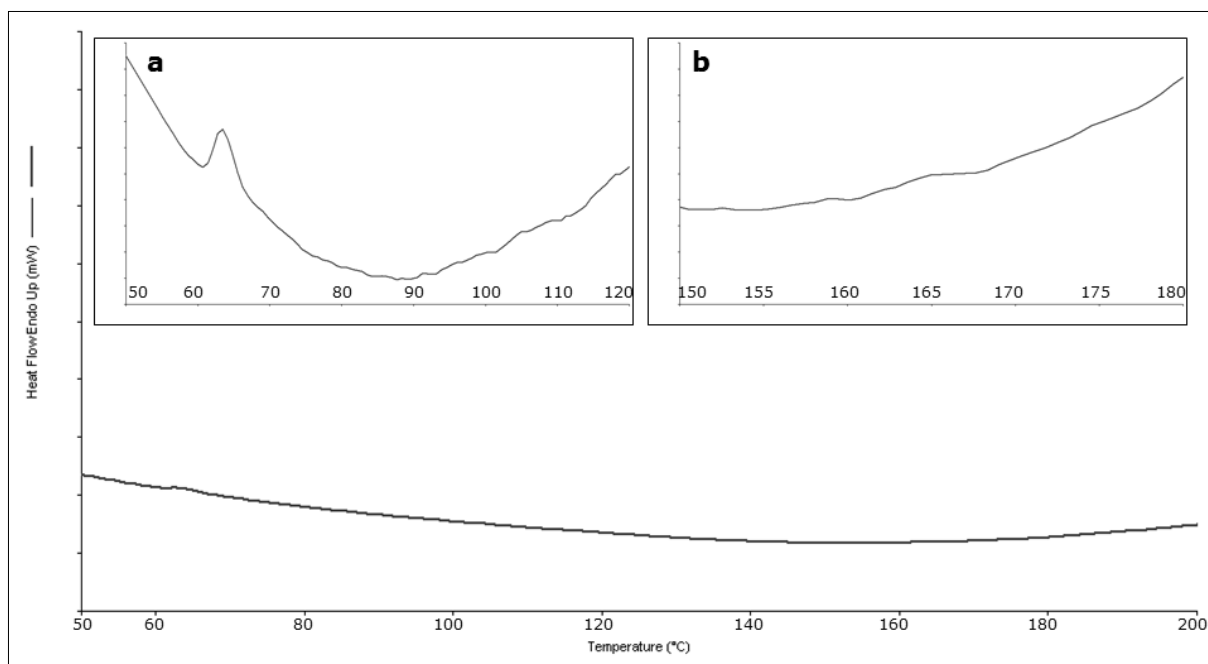


Figure IV.14. - Excerpt of DSC trace of HMG Trial 1; analysis conducted from 30 - 300 °C; heating rate 20 K/min, ΔY : 50 mW; a) excerpt from 50 - 120 °C, $\Delta Y = 1$ mW, b) excerpt from 150 - 180 °C, $\Delta Y = 1$ mW.

Upon first inspection of the DSC trace no melting peak of ITR was detectable and amorphousness of sample seemed likely but by magnifying the DSC curve (b in Figure IV.14.) a small endothermic signal correlatable to ITR melting became observable at 164.94 °C (0.1375 J/g). Moreover, T_g of ITR slightly above 60 °C was observed, as well as the very small signal ascribed to "cold crystallisation" of ITR (a in Figure IV.14.). Accordingly, either ITR only partially melted during HMG process, it recrystallised between manufacturing and DSC analysis (approximately one day at ambient conditions) or ITR was fully amorphous after HMG and recrystallised during DSC analysis. XRPD measurements of this sample could not be conducted due to technical reasons.

IV.2.3. Closing Remarks about the Hot-Melt-Granulation Procedure

Summarising the results presented in the previous section it can be stated that it was possible to create a stable HMG process by switching the die to the granulation heel slide and maintaining the same temperature profile which was presented for the most successful HME run (HME Trial 4, see section IV.2.). Merely ScS had to be reduced from 225 rpm to 150 rpm to avoid damaging mTSE. Samples collected showed no product degradation whereas ITR appeared to be

at least partially amorphous in the DSC measurements. At this point, two different hot-melt procedures were available for the processing of PM of β CD and ITR. Comparative approaches were necessary to choose the most sufficient operation for achieving improved ITR dissolution and possibly ICF.

IV.3. Comparative Evaluation of Hot-Melt Extrusion and Hot-Melt Granulation Procedures

A more detailed comparison between HME and HMG was carried out that utilised further analysis tools and investigated the possibility of ICF within mTSE as this was defined as an important quality parameter. By this, it was attempted to examine the possible superiority of one process over the other.

IV.3.1. Physico-Chemical Comparison of Melt Extrudate and Granules

Comparing the physico-chemical results of HMG Trial 1 and HME Trial 4, no differences stood out. Content evaluation studies disclosed no ITR degradation (102.85 ± 2.22 % for HME Trial 4, 102.34 ± 3.51 % for HMG Trial 1) and β CD (98.04 ± 0.10 % for HME Trial 4, 97.83 ± 0.31 % for HMG Trial 1). Both DSC traces gave small endothermic peaks at 163.57 °C and 164.94 °C for HME Trial 4 and HMG Trial 1, respectively, after magnification. By that, a broad signal ascribed to "cold crystallisation" of ITR was also observed. Generally, the T_m of ITR in PM occurred at approximately $166 - 167$ °C which was higher than T_m s presented for HME and HMG samples. It had yet to be determined whether the detected T_m was corresponding to partial crystallinity of the product or caused by recrystallisation during DSC analysis. Figure IV.15. shows SEM images of both HMG and HME surfaces prior to crushing. No visual differences were observed.

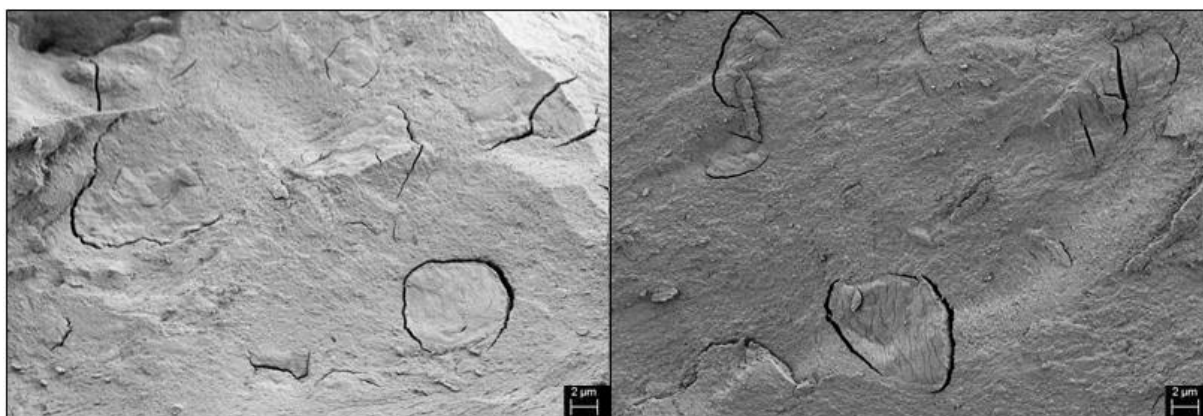


Figure IV.15. - SEM visualisation of HMG (left side) and HME extrudate strand in cross section (right side); bar = 2 μ m.

IV.3.2. Solubility Measurements and Itraconazole Dissolution

Of utmost importance for the finished hot-melt product was the solubility or dissolution rate enhancement of ITR. For a first impression, an excess amount of HME Trial 4 and HMG Trial 1 was each weighed in brown glasses and 50 mL of dem. water was added. Samples were stirred at room temperature for 24 h before ITR and β CD contents were evaluated. These measurements were conducted in duplicate and results are shown in Figure IV.16.. PM served as control and was treated the same way. No enhancement of aqueous solubility of β CD was detected for any hot-melt treatment. Whereas PM reached β CD solution of 6.80 ± 0.01 mg/mL, HMG Trial 1 and HME Trial 4 presented dissolved β CD in the amounts of 6.72 ± 0.08 mg/mL and 6.75 ± 0.02 mg/mL, respectively. On the one hand, this was expected as both hot-melt procedures were carried out below the reported melting range of β CD, so no amorphisation of the oligosaccharide should have taken place [80]. Additionally, as described in section III.1.3., the limited aqueous solubility of β CD is hypothesised to be caused by intramolecular hydrogen bonds due to the ring-structure. As no degradation was detected for the samples, the same solubility-limiting structural qualities should have been intact as reflected by similar solubility.

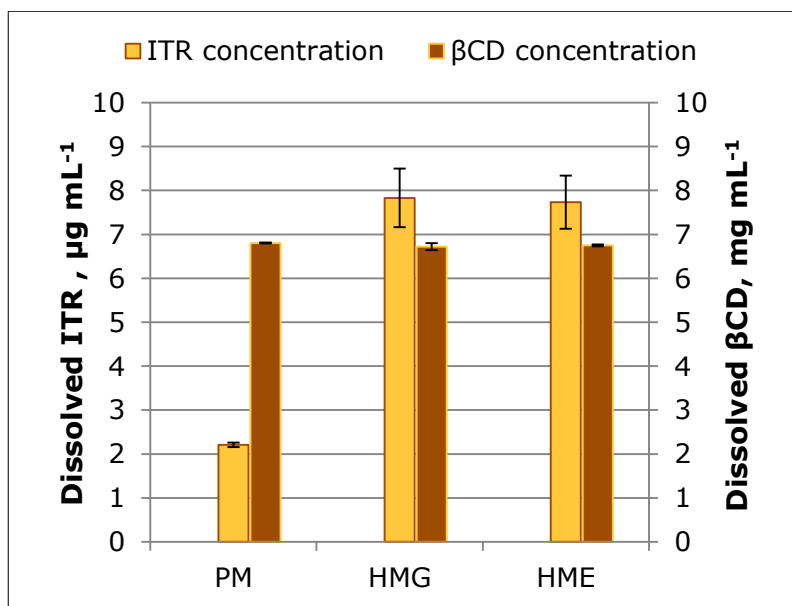


Figure IV.16. - Results of solubility analysis of PM, HMG and HME after 24 h, n = 2, error bars = min/max.

Substantial differences became observable in the amount of dissolved ITR. PM reached ITR solubility of 2.21 ± 0.05 μ g/mL while HMG Trial 1 and HME Trial 4 showed extended amounts of dissolved ITR of 7.83 ± 0.67 μ g/mL and

$7.73 \pm 0.60 \mu\text{g/mL}$. This constituted an increase of approximately 250 % for both hot-melt procedures. This solubility enhancement might have been attributed to ITR amorphousness or ICF during HME/HMG. Here, no substantial difference was found between HMG Trial 1 and HME Trial 4.

ITR dissolution was also investigated. The same amount of dissolved ITR after 24 h might have hinted at identical improvement in absolute solubility but it did not indicate which of the two hot-melt procedures gave the faster ITR dissolution rate. This is of importance for a novel formulation. The medium had to be switched to 0.1 N HCl as preliminary experiments failed to deliver quantifiable amounts in the beginning of the analysis, especially for PM. Thus, results were not comparable to the absolute amounts of dissolved ITR acquired by the solubility testing shown in Figure IV.16.. PM was chosen as negative control. Furthermore, aITR was investigated as well as PMAITR to evaluate the possibility of dissolution rate enhancement caused solely by ITR amorphisation. Dissolution testing with pure crystalline ITR was carried out but yielded un-evaluable results possibly due to ITR particles passing the installed filter system and distorting content evaluation. Sample amount was the equivalent to 100 mg of ITR. Results of dissolution testing are given in Figure IV.17..

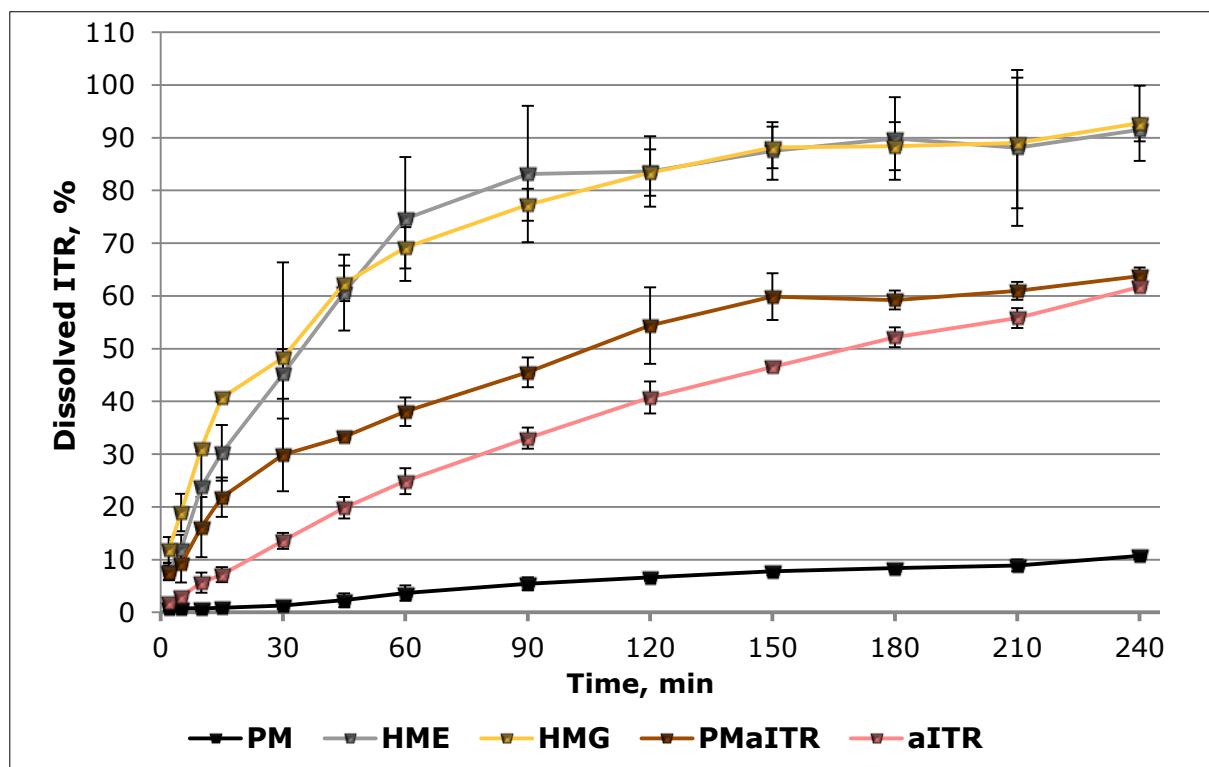


Figure IV.17. - Dissolution results of PM*, PMAITR, aITR, HMG* and HME* in 0.1 N HCl over 4 h; n = 3; error bars = sd; *)dissolution medium replaced.

PM reached ITR dissolution of 10.32 ± 0.76 % after 4 h. Upon inspecting the dissolution curve, a slight increase starting approximately at 30 min became apparent. This rise could be attributed to ICF in aqueous medium. As results of PSM had shown (see section IV.1.), the presence of β CD increased ITR solubility in 0.1 N HCl. This definitely occurred within the dissolution vessel as well. As longer experiment times were not evaluated, it remained a possibility that PM could have reached higher absolute ITR dissolution levels then. However, in regard to a later immediate release formulation, longer experimental times would not hold that much realistic value. Even though it was not possible to investigate pure crystalline ITR, it could be assumed that its dissolution profile would not have exceeded that of PM. Pure aITR showed an almost zero-order-like dissolution profile with a constantly rising amount of dissolved API and reached dissolution of 61.71 ± 0.67 % after 4 h. This strongly underlined the effect of API amorphisation and proved to be a dissolution enhancement of 576.80 % compared to PM. This phenomenon was in general agreement with the literature [151]. Kumar et al. stated that dissolution of aITR prepared by melt quenching reached comparable results in 0.1 N HCl. After 2 h, approximately 30 $\mu\text{g/mL}$ were dissolved at only 50 rpm paddle rotation speed versus approximately 45 $\mu\text{g/mL}$ with the faster 100 rpm rotating set-up used in this project. They also observed a similar zero-order-type curve [151].

Comparing PMAITR to PM, the ICF period between 30 - 120 min was observed as well. PMAITR reached dissolution of 63.76 ± 1.65 % after 4 h which was very similar to pure aITR. Although PMAITR and aITR reached nearly the same dissolution after 4 h, PMAITR clearly showed a faster dissolution rate which might have hinted at the fact that either small amounts of ICs were present in the mixture or that due to the generally better dissolving properties of aITR, it had experienced faster ICF in the dissolution medium. The dissolution curve of PMAITR was always above aITR. Both HME and HMG samples reached nearly complete dissolution (91.48 ± 2.16 % and 92.75 ± 7.15 %). Both dissolution curves were not substantially different, especially since the error bars overlapped for most of the sampling time points. Nevertheless, upon inspecting the first 30 min, HMG seemed to have achieved faster dissolution. At 15 min of investigation, HMG and HME gave ITR dissolution levels of 40.68 ± 0.73 % and 30.26 ± 5.27 % respectively. After 60 min, though, ITR dissolution of HME slightly outperformed HMG until both nearly delivered the same dissolution levels from 2 h on. Generally, variations were much higher for HME than HMG as sd for nine out of thirteen sampling points was

above 5 %, whereas this was only the case for three sampling points of HMG. This might have indicated less ICF during HME procedure or inhomogeneous dispersion thereof within the sample. Apart from this high variance, both hot-melt procedures had resulted in products that showed strongly improved ITR dissolution compared to PM (898.74 % increase for HMG after 4 h and 786.43 % increase for HME) and to PMaITR (45.46 % increase for HMG and 43.48 % for HME). Although dissolution medium was replaced for HMG and HME, results were still comparable as later dissolution analyses of hot-melt processed samples did not show tremendous changes upon not replacing the dissolution medium. In regard to PM, dissolution was lower without replacing dissolution medium (see section IV.4.2.). As all later dissolution studies were carried out without media replacement, PM results obtained in section IV.4.2. were used as appropriate reference values.

IV.3.3. Inclusion Complex Detection in Melt Extrudates and Granules

As shown in previous sections, both HMG and HME were manageable processes that yielded products with similar physico-chemical properties and dissolution over 4 h. However, they additionally had to be evaluated for possible ICF. The subsequent section gives insights into the analysis thereof by ATR-FT-IR. By evaluating these results together with the dissolution results, it could be attempted to choose the optimal processing strategy between HME Trial 4 and HMG Trial 1.

IV.3.3.1. ATR-FT-IR Results and Discussion

In section III.2.2.6. it was explained that ATR-FT-IR measurements are an easy opportunity for evaluating ICF in solid samples. In Figure IV.18., exemplary ATR FT-IR spectra of aITR, crystalline ITR, PMaITR as well as HMG Trial 1 (HMG) and HME Trial 4 (HME) are presented. These samples were evaluated according to the identified marker wave numbers as given in section III.2.2.6.. During these first experiments, ITR, aITR, PM and PMaITR were investigated separately to determine the suitable negative control for the melt processed samples. Already by visual inspection it was obvious that aITR and ITR generated different spectra, as did their corresponding PMs. Accordingly, PMaITR was used as reference for HMG and HME samples and PM for crystalline material. On first macroscopic review of the ATR-FT-IR spectra, HME and HMG appeared almost the same. Detailed results of the detected peaks are given in Table IV.5.. After evaluating HMG and HME wave bands it could be concluded that they were nearly

identical. Of special importance was the comparison between PM and PMAITR as it became apparent that aITR interacted stronger with β CD after mere blending compared to the crystalline blend.

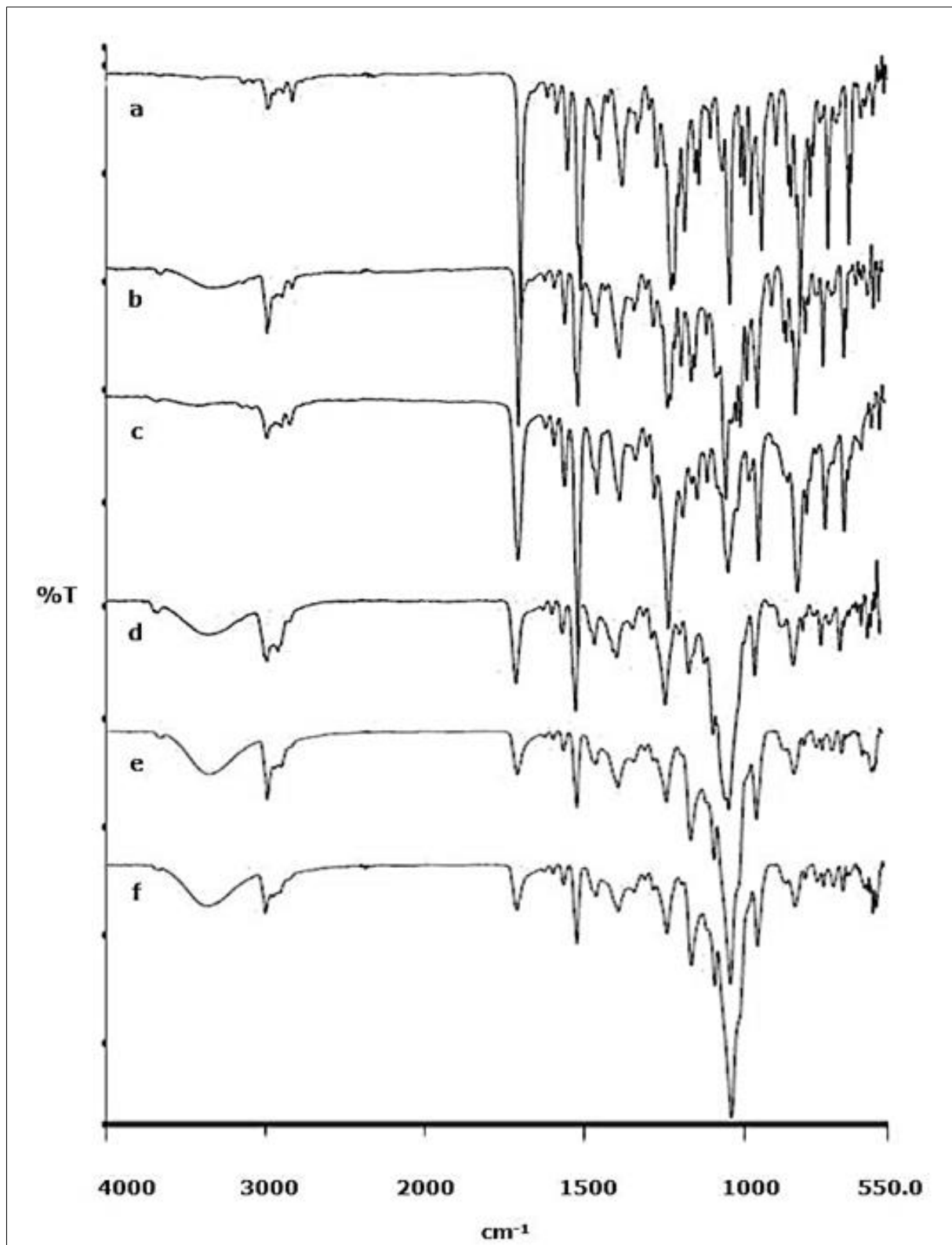


Figure IV.18. - Archetypal ATR-FT-IR spectra of a) ITR, b) PM, c) aITR, d) PMAITR, e) HME and f) HMG.

Table IV.5. - ATR-FT-IR results of HME and HMG evaluated by comparison with reference wave numbers; sd = \pm ; n = 3; *n = 5; if wave number markers were not detected in every single analysis, the percentage of their occurrence is given in brackets below.

	ITR* aITR*	PM* PMaITR*	HME	HMG
Wave Numbers, cm ⁻¹	1697.80 \pm 0.23 1698.87 \pm 0.43	1697.60 \pm 0.15 1698.89 \pm 0.33	1699.63 \pm 0.95	1699.59 \pm 0.27
	1584.34 \pm 0.17 1585.57 \pm 0.07	1584.60 \pm 0.25 (80 %) 1585.76 \pm 0 (20 %)	1585.94 \pm 0.09	1585.90 \pm 0 (33.33 %)
	1551.43 \pm 0.15 1552.49 \pm 0.01	1551.18 \pm 0.13 1552.74 \pm 0.27	1552.96 \pm 0.25	1552.75 \pm 0.30
	1509.64 \pm 0.29 1510.59 \pm 0.10	1509.80 \pm 0.23 1511.07 \pm 0.34	1511.28 \pm 0.22	1511.11 \pm 0.05
	1451.26 \pm 0.12 1450.87 \pm 0.06	1451.20 \pm 0.16 (80 %) 1451.08 \pm 0.21	1451.89 \pm 0.27	1451.72 \pm 0.07
	1272.85 \pm 0.45 1271.56 \pm 0.04	1270.96 \pm 0.98 (80 %) X	X	X
	1227.32 \pm 0.28 1227.50 \pm 0.14	1227.41 \pm 0.59 1228.55 \pm 0.62	1228.76 \pm 0.28	1228.52 \pm 0.13
	1185.03 \pm 0.13 1182.59 \pm 0.18	1184.44 \pm 0.52 X	X	X
	1140.53 \pm 0.11 1137.71 \pm 0.28	1140.58 \pm 0 (20 %) X	X	X
	X	1072.64 \pm 0.06 (40 %) 1077.55 \pm 0.36 (40 %)	1078.32 \pm 0.11	1078.35 \pm 0.03
	1043.88 \pm 0.50 1040.81 \pm 0.66	1043.15 \pm 0.11 1042.58 \pm 0.95 (40 %)	X	X
	X	X 1028.45 \pm 1.81 (60 %)	1026.80 \pm 0.09	1026.41 \pm 0.24
	824.10 \pm 0.15 823.81 \pm 0.49	823.82 \pm 0.09 824.74 \pm 0.72	826.14 \pm 0.26	826.68 \pm 0.29

Some spectral bands altogether disappeared for PMaITR (e.g. around 1270 cm⁻¹ and 1185 cm⁻¹) whereas others were not detected in all measurements (e.g. around 1042 cm⁻¹). This suggested interactions between the two substances and was more pronounced than for PM where only occasional missing events (e.g. around 1270 cm⁻¹ and 1140 cm⁻¹) were observed. This made the analysis of HME and HMG samples more challenging as the disappearance of spectral bands around 1270 cm⁻¹, 1185 cm⁻¹ and 1140 cm⁻¹ could not be ascribed to ICF completely. Only the peak around 1040 cm⁻¹ was never detected for the melt processed samples whereas partially observed for PMaITR which indicated

further interactions. This was backed up by the event around 1078 cm^{-1} . As this signal was attributed to β CD and had only been partially detected for PM and PMaITR, it suggested enhanced interactions, such as hydrogen bonds possibly caused by ICF. The same was hypothesised for the wave band around 1026 cm^{-1} which also originated from β CD. It appeared sheltered from the laser beam in PM and only partially detectable for PMaITR. The peak around 824 cm^{-1} had shifted to slightly higher wave numbers (around 826 cm^{-1}) for HME and HMG which proposed interactions between the two substances in the formulations. This shift was less pronounced for PMaITR. Concerning the vanished wave bands, it appeared likely that parts of ITR became sheltered from the laser beam. Many wave numbers had not changed substantially, especially above 1300 cm^{-1} which indicated not too many interactions in that spectral region.

When correlating the detected events with the functional molecular groups as presented in Figure III.15., results suggested that most changes occurred in the region of the tri-1,2,4-benzene ring system with the two aryl-Cl groups, as the Cl peak at 1043 cm^{-1} had disappeared completely for HME and HMG. The slightest shifts were seen for the corresponding aromatic C=C bonding wave numbers around 1451 cm^{-1} and 1509 cm^{-1} but this might have been caused by overlapping results from the two di-para benzene rings or partial ICF in the samples. The two piperazine markers around 1273 cm^{-1} and 1185 cm^{-1} disappeared as well which advocated inclusion of that molecular part. No changes were detectable for 1584 cm^{-1} and 1551 cm^{-1} , wave bands correlated to C=N bonding. As these bonds exist multiple times in the ITR molecule, this could have also been caused by partial ICF and overlapping of both the triazole and the triazolone rings. As no considerable change was seen for the wave band around 1699 cm^{-1} for any sample, it was concluded that the ring system hosting the ketone group was not involved in ICF. This backed up the suggestion of overlapping results for the C=N bonds. The wave bands associated with ether groups around 1140 cm^{-1} and 1227 cm^{-1} also disappeared and slightly increased, respectively, for each HME, HMG and PMaITR. This underlined the theory that at least the right "tail part" of ITR (as shown in Figure III.15.) took part in ICF, most probably up to the piperazine system. Concerning the di-para benzene rings, it was not possible to establish if both of them became included due to overlapping peaks. The inclusion of the triazole function was in agreement with the literature as Peeters et al. reported. They investigated a theoretical molecular mechanics framework of the β CD/ITR IC

which showed that in a 1:1 stoichiometric ratio, an interaction with this functional group was energetically favourable and the most stable possibility. Only for higher order ICs, the other part of ITR, namely the 2-butyl group, the piperazine and the 1,4-diaminophenyl ring next to the triazolone interacted as well in the IC [146].

Recapping these outcomes, ATR-FT-IR appeared suitable to give results about interactions and even ICF between ITR and β CD. This technique further allowed suggestions regarding the functional groups involved. However, some signals were not detected in every conducted measurement. As each sample analysed by ATR-FT-IR was newly prepared, it was possible that the amount of IC positioned on the measuring crystal had varied. Also, interactions were already seen for PMs, especially with aITR. That raised the question if mere blending would yield the same amount of IC as processing PM in the mTSE. Secondly, as intensity of ATR-FT-IR spectra varied and the limit of peak detection was set to 0.5 % transmission in the current experimental setup, the results had to be interpreted mostly in a relative manner. Consequently, it became apparent that solely trusting ATR-FT-IR determinations might not always capture the whole picture of possible ICF. Therefore, for the final detection of ICs, the dissolution results were also taken into account. Only the connection between changes in the ATR-FT-IR spectrum together with enhanced dissolution compared to the respective reference (PM or PMAITR) could enable the assured conclusion of ICF. The improved ITR dissolution after 4 h of HMG and HME compared to PMAITR (increase of 45.46 % and 43.48 %, respectively) clearly supported the theory that although interactions were observed in ATR-FT-IR spectra of the PMs, sufficient ICF needed a manufacturing procedure that further forced the API into the CD cavity.

IV.3.4. Concluding Remarks and Decision for Hot-Melt Procedure Gold Standard

Both hot-melt processes were feasible and operable. However, some differences were found regarding the simplicity of the process and the resulting product. As presented in section IV.2.1., particularly the die utilisation proved to be the biggest challenge during process development. The 6 mm conical die did not allow pressure monitoring which could be a safety risk even during a stable process. Figure IV.19. shows the photography of an extrudate strand from HME Trial 4. Although results of content evaluation proved that no deterioration had taken place, the surface of the extrudate strand exhibited darker, brown-ish

areas. During HME procedure, it was visible that this was caused by product residue at the die from hot-melt extruded material of the filling phase of the mTSE. Nonetheless, this contamination would not be acceptable when thinking about a later formulation.

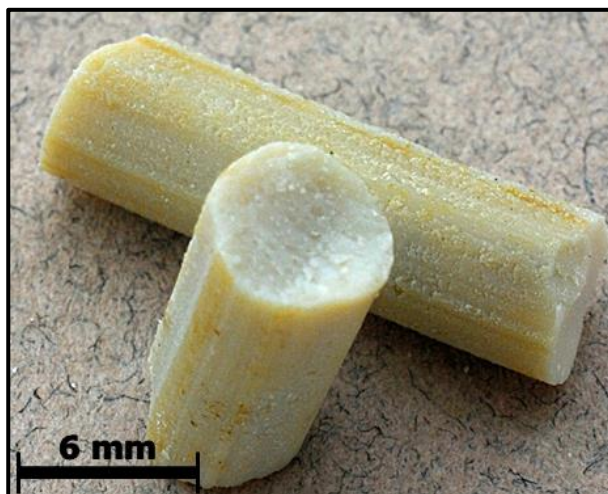


Figure IV.19. - Image of extrudate strand acquired with 6 mm conical die.

Keeping in mind the results presented from physico-chemical analysis as well as from dissolution and solubility testing, no difference was found that suggested superiority of the HME sample over the HMG sample. The maximum dissolved amount of ITR (see Figure IV.16.) was higher for HMG Trial 1, albeit only to a very low extent of 0.10 $\mu\text{g}/\text{mL}$. Additionally, ITR dissolution appeared generally more stable with smaller variations compared to HME Trial 4. These results after 4 h did not propose dominance of one sample over the other. Moreover, the presented results for IC detection by ATR-FT-IR did not reveal representative differences between the samples. By evaluating ATR-FT-IR spectra in correspondence with the dissolution profiles against PMAITR, nearly the same increase in ITR dissolution was seen as well as nearly identical peak patterns at the same wave number markers. Lastly, taking into account that the mTSE process for HMG was easier stabilised and simpler to control due to the missing die, it had to be concluded that the gold standard to be further used in this study was the HMG procedure. Thus, all following results of hot-melt processes were prepared by HMG.

IV.4. Hot-Melt Granulation Process Optimisation

HMG was chosen as the most suitable hot-melt process while simultaneously delivering ICF and sufficient product properties. However, the developed HMG procedure was chosen in regard to HME Trial 4. The optimal hot-melt process

presents a compromise between the lowest applicable temperature while maintaining desired product qualities. For this reason, a granulation concept was investigated wherein different temperature profiles were analysed for their processability as well as product characteristics.

IV.4.1. Experimental Set-Up and Processability

Five different temperature profiles were tested. Parameters are shown in Table IV.6.. HMG Trial A corresponded with HMG Trial 1 described in previous sections and was processed at the highest temperatures with a maximum of 220 °C. From HMG Trial B to D, temperatures were further lowered. HMG Trial B was melt-granulated slightly above T_m of ITR, HMG Trial C slightly below and HMG Trial D at a maximum of only 100 °C. Another temperature profile, HMG Trial E, was investigated at a temperature of 50 °C throughout the whole barrel but no sample could be drawn. The screws started screeching and damage to the barrel became likely which necessitated stopping the procedure.

Table IV.6. - Different HMG temperature profiles and processing parameters.

HMG Trial	Z1, °C	Z2, °C	Z3, °C	Z4, °C	Z5, °C	Z6, °C	Z7, °C	ScS, rpm	Throughput, g/h	Torque, %
A	100	130	170	200	200	220	220	150	200.6	10
B	100	130	170	180	180	180	180	150	184.6	14
C	100	130	150	150	150	150	150	150	207.2	6
D	50	80	100	100	100	100	100	150	200.0	16
E*	50	50	50	50	50	50	50	150	X	X

*process not feasible due to screeching of mTSE screws

An average throughput of 200.6 g/h was aimed at, as this had been chosen during the development of the HMG procedure, but, due to the volumetric feeding system (see section III.2.1.3.), this was not always possible. During product collection, the actual throughput was calculated every few minutes and the feeder adjusted accordingly. The throughput presented in Table IV.6. constitutes the average derived from these calculations. While HMG Trials A and B resulted in melt-granules of equal appearance, HMG Trials C and D yielded more powder-like products. These HMG runs were carried out below ITR T_m . Therefore no molten material was present in the barrel which induced pasty properties of the finished product. Nevertheless, both processes were stable during mTSE operating, only

nearing the end of sample collection for HMG Trial D, the screws began to screech.

IV.4.2. Physico-Chemical Characterisation of HMG Trial A - D

All samples derived from the different HMG temperature profiles and PM were analysed for their physico-chemical properties. Figure IV.20. shows SEM images of PM and the four HMG Trial runs. The granulated specimen were manually crushed and sieved through 425 μm prior to this visualisation.

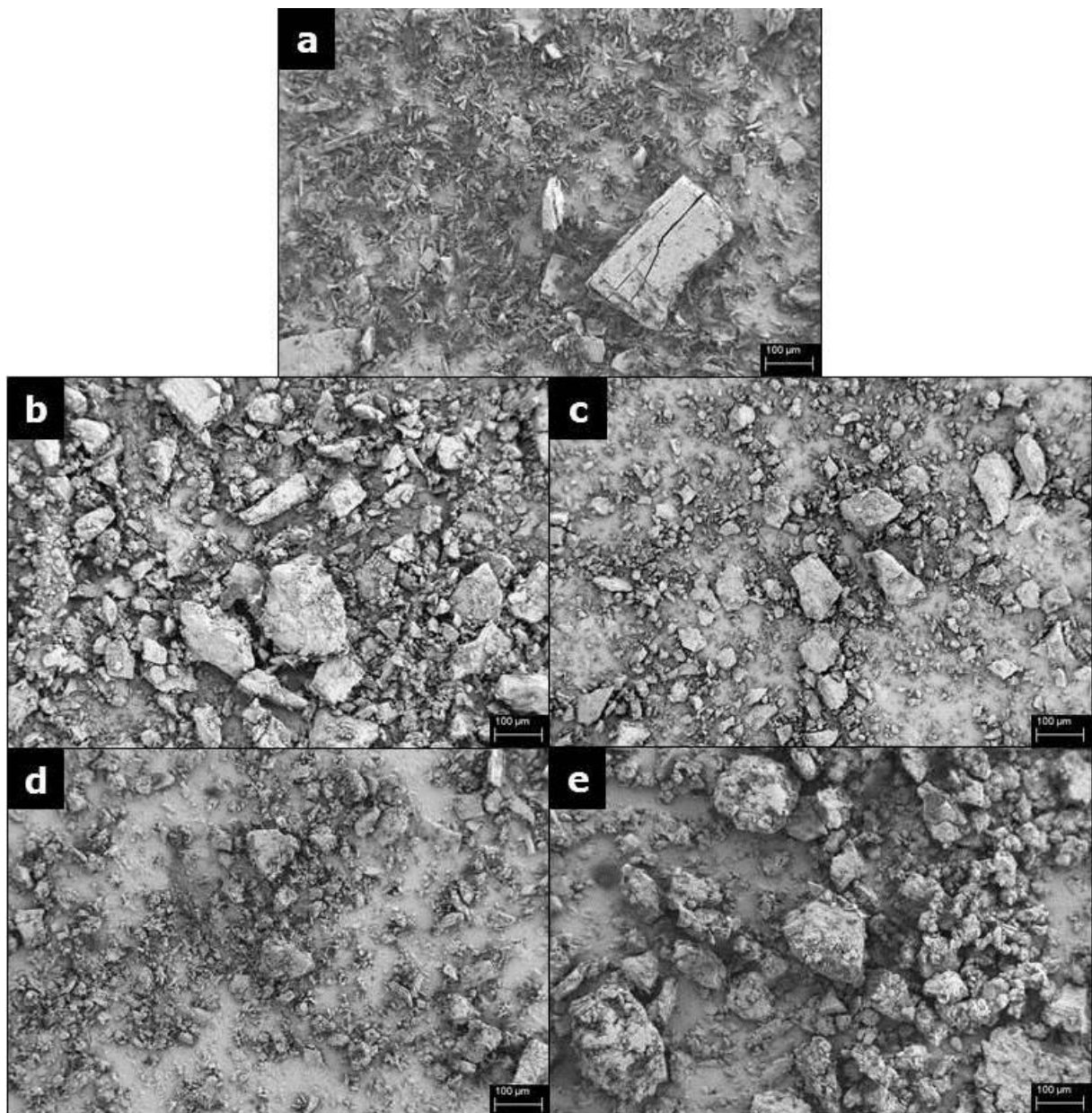


Figure IV.20. - SEM images of a) PM, b) HMG Trial A, c) HMG Trial B, d) HMG Trial C, e) HMG Trial D; bar = 100 μm .

Observing PM (a in Figure IV.20.), smaller needle-like particles were visible as well as larger particles. Concluding from the particle size measurements reported

in the corresponding material sections, the smaller particles could be ascribed to ITR and the larger particles to β CD. Comparing HMG Trial A and B (b and c in Figure IV.20.), particles appeared almost identical. Although in the chosen image, HMG Trial A seemed to show larger particle sizes, this did not hold true when examining the results of laser diffraction measurements as presented in Table IV.7..

Table IV.7. - Results of particle size measurements for PM, HMG Trial A, B, C and D conducted directly after manufacturing; n = 3; \pm = sd.

	PM	HMG Trial A	HMG Trial B	HMG Trial C	HMG Trial D
x_{50} , μm	15.1 ± 0.2	96.4 ± 10.7	116.3 ± 24.4	16.6 ± 0.4	41.9 ± 0.8

HMG Trial B exhibited slightly larger particles with a x_{50} of $116.3 \pm 24.4 \mu\text{m}$ as opposed to $96.4 \pm 10.7 \mu\text{m}$ for HMG Trial A. Investigating the HMG runs below ITR T_m (d and e in Figure IV.20. for HMG Trial C and D) the particle surfaces appeared somewhat rougher than for HMG Trial A and B. This might have been due to no melted component having been present during processing. For HMG Trial A and B, liquefied, molten ITR served as a kind of "binder" in the granulation process and was kneaded into the β CD matrix. This could have caused the particle surfaces to appear slightly smoother. In the SEM image, HMG Trial D seemed to consist of larger particles than HMG Trial C. This held true when examining the laser diffraction results as x_{50} of $41.9 \pm 0.8 \mu\text{m}$ was more than twice the size of $16.6 \pm 0.4 \mu\text{m}$ for HMG Trial C. Particles of HMG Trial D appeared similar to the particles of HMG Trial A and B. On first inspection, it seemed as if ITR was forced into the β CD cavity with less single ITR particles present. In contrast, HMG Trial C looked more like PM (x_{50} of $15.1 \pm 0.2 \mu\text{m}$). Nevertheless, it has to be stated that HMG Trial C and D were more powder-like and although they were sieved through $425 \mu\text{m}$, both samples passed the sieve mostly without any need for grinding. HMG Trial A and B presented larger particles than HMG Trial C and D, explained by the "binding" ability of the molten ITR.

Figure IV.21. displays DSC traces of all four HMG Trials and PM. For PM, an endothermic signal was visible slightly above $100 \text{ }^\circ\text{C}$ corresponding to the evaporation of β CD cavity water. Moreover, T_m of ITR could be detected (see Table IV.8.). The corresponding signal to cavity water loss was also detectable for HMG Trial C and D, however not as distinctively.

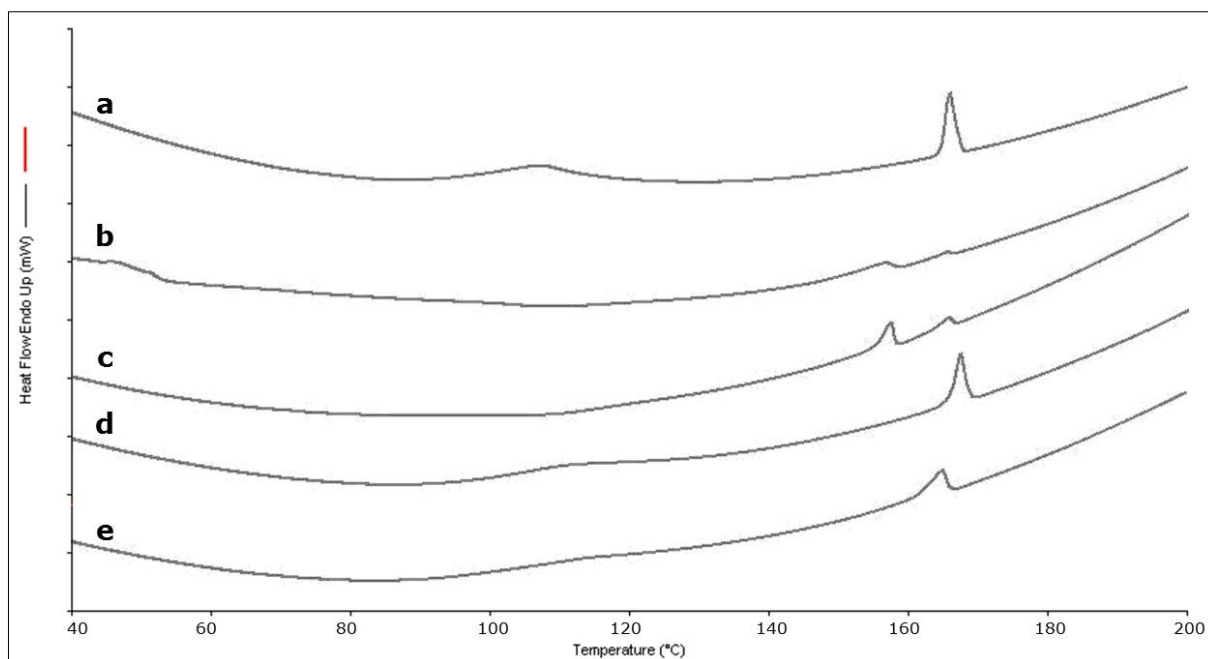


Figure IV.21. - Excerpts from DSC curves of a) PM, b) HMG Trial A, c) HMG Trial B, d) HMG Trial C, e) HMG Trial D, measured from 30 - 200 °C after 2 min holding period at 30 °C; heating rate 3 K/min.

This was in good agreement with the results of the TGA study which showed water contents of 4.887 % and 4.846 % for HMG Trial C and D, respectively. These values were only slightly smaller than for PM (5.717 %). Even though HMG Trial C was processed well above 100 °C, the rapid conveying of the material through the barrel apparently hindered vaporisation of most of the present water. ITR T_m of HMG Trial C was approximately 1 °C higher than for PM, whereas HMG Trial D showed a marginal shift to a lower temperature (164.96 °C) as well as broadening of the peak. This might have been indicative of an IC although not in a substantial portion. HMG Trial A and B lacked any distinctive signal corresponding to water loss which was supported by evaluating their residual water contents of 1.893 % and 2.335 %. Due to processing at such high temperatures (≥ 180 °C), most water of PM had evaporated as had been observed during HMG (vapour formation).

Table IV.8. - Signals correlated to melting of ITR examined in the DSC traces of PM, HMG Trial A, B, C and D.

	PM	HMG Trial A		HMG Trial B		HMG Trial C	HMG Trial D
ITR signal, °C							
Onset	164.79	151.58	163.47	155.25	163.89	165.98	161.70
Peak	166.08	156.51	165.48	157.39	165.70	167.45	164.96

Interestingly though, two endothermic signals were observed correlating to ITR melting (see results shown in Table IV.8.). Apart from the typical T_m of ITR at about 166 °C, another peak was detected at around 157 °C. This agreed with a polymorph described in the literature [150,152,153]. It seemed as if ITR had re-crystallised after HMG procedure. Since Zhang et al. described this polymorph, also called Form II, as having the fastest crystallisation velocity of all recognised ITR crystal forms, this might have backed up this hypothesis. The second T_m might have been caused by either ITR changing from Form II to the more stable Form I, or by crystalline material left in the sample after melt processing. However, as previously mentioned, ITR can show a special behaviour during melting called "cold crystallisation". Moreover, ITR forms thermotropic mesophases. Figure IV.22. presents a magnification of the DSC traces of HMG Trial A and B in the range of 50 - 120 °C. Especially by carefully inspecting the trace of HMG Trial B (b in Figure IV.22.), two very small signals just above 70 °C and between 80 and 90 °C became visible. These have been described by Six et al. as monotropic mesophases [154].

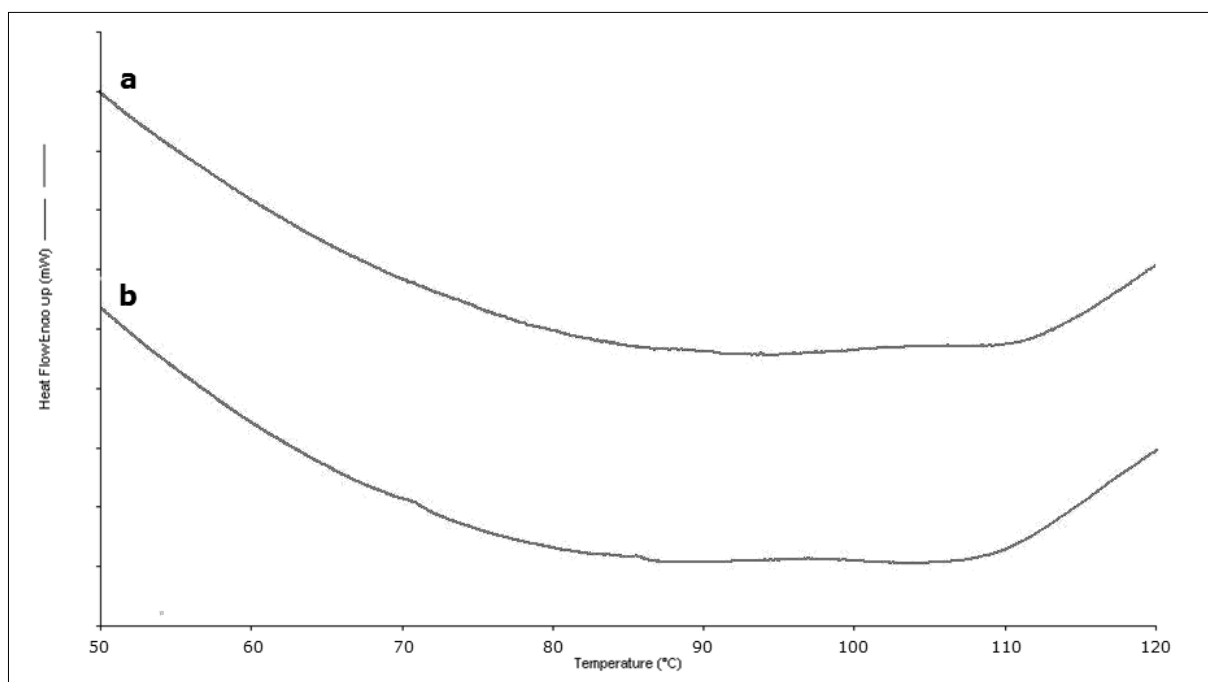


Figure IV.22. - Magnified DSC traces of a) HMG Trial A and b) HMG Trial B; measured from 30 - 200 °C after 2 min holding period at 30 °C; heating rate 3 K/min.

In another publication, Six et al. investigated ITR extrudates in a polymer matrix and not only observed the two endothermic signals of the mesophases but also reported "cold crystallisation" of ITR above 100 °C and two ITR melting endotherms

corresponding to the polymorph and the more stable form. They concluded that upon DSC analysis, recrystallisation had occurred and the recrystallised polymorph then further recrystallised into Form I during the measurement. This last recrystallisation was not observed in the DSC trace due to overlapping with T_m . They also found this to be correlatable to high amounts of ITR in their solid dispersions [150]. These results agreed with the findings of Janssens et al. who investigated solid dispersions with ITR and Kollicoat IR[®]. Up from 40 % of ITR in the solid dispersions, they also observed "cold crystallisation" and two T_m s of the polymorphic Form II as well as the stable Form I [155]. In Figure IV.22., at approximately 110 °C, an exothermic broad signal could be detected that might have been correlating to "cold crystallisation". Since the endothermic signal of water loss was nearly at the same point, the exothermic and endothermic reactions might have overlapped, causing decreasing observabilities. Lastly, the polymorphic T_m was not previously detected for the first HMG and HME runs but as those had been investigated by higher DSC heating rates, this could have been ascribed to this. It had yet to be determined if ITR was fully amorphous in the samples after melt processing or if the changes regarding the crystallinity appeared during DSC analysis.

Thus, XRPD measurements were conducted and results are given in Figure IV.23.. It appeared that both HMG Trial A and B were partially amorphous as the peak pattern was not as tidy and strict as for PM. However, some peaks could be detected. It was mentioned before that β CD did not melt upon heating. Subsequently, it stayed in its crystalline form. When evaluating the XRPD diffractograms of the pure substances, ITR and β CD, many peaks showed the same diffraction angle and overlapped. Thus, for PM, it was not always possible to ascribe a peak to either substance. There is a patent available regarding the polymorphic Form II where a distinctive IR spectrum and XRPD diffractogram are published [153]. When comparing the results obtained in this project to the identified marker diffraction angles of the polymorphic Form II as described there ($7.3^\circ 2\theta$, $19.9^\circ 2\theta$, $21.9^\circ 2\theta$, $26.1^\circ 2\theta$ and $32.2^\circ 2\theta$), none of these signals could be detected. This was also in agreement with the results of ATR-FT-IR analysis (see Table IV. 9.). Specific wave numbers were identified for the polymorph and none of those were seen. Observed shifts regarding possible ICF were not in accordance with the defined polymorph. Many signals ascribed to the polymorph had already vanished in PMaITR and were also not observable in HMG Trial A and B (e.g. 1585 cm^{-1} , 1275 cm^{-1} , 1191 cm^{-1} , 1137 cm^{-1} and 1043 cm^{-1}).

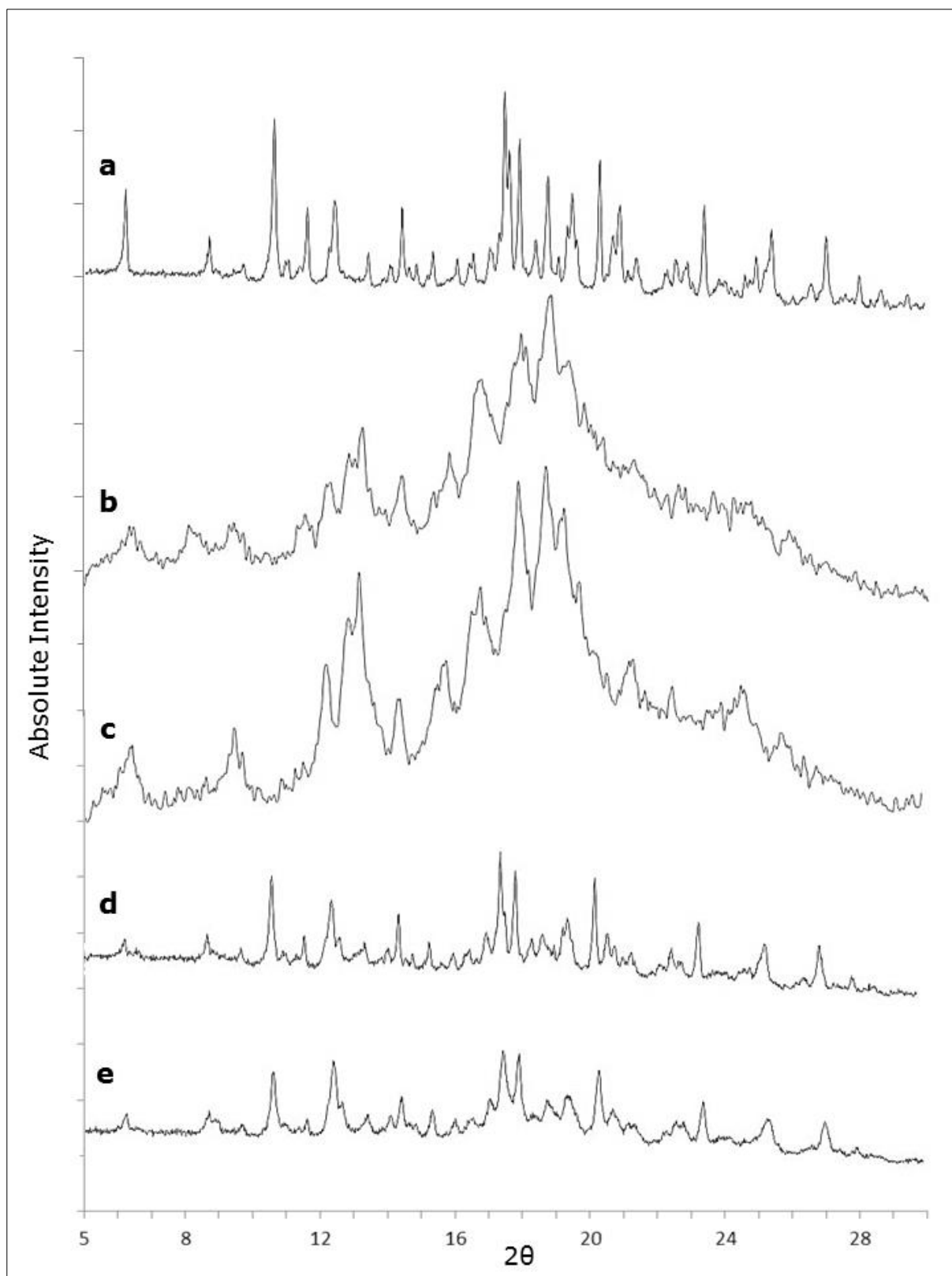


Figure IV.23. - Excerpts from XRPD diffractograms of a) PM, b) HMG Trial A, c) HMG Trial B, d) HMG Trial C and e) HMG Trial D; measurement conducted from 5 - 50 ° 2θ .

Taking all these results as well as the literature into account, it seemed appropriate to conclude that even though partial crystallinity of ITR could not be excluded with certainty (see XRPD results), the presence of the polymorphic

Form II was most likely only caused by recrystallisation during DSC analysis as no other analysis technique showed results that proved the existence of it in the solid form. Regarding the XRPD results of the two HMG samples processed below ITR T_m , HMG Trial C and D (d and e in Figure IV.23.), it seemed apparent that the distinctive peak pattern could still be observed for both of them, as they were fully crystalline. However, the intensity of the detected diffraction angles had decreased compared to PM which might have been indicative of ICF. In this regard, following the results of SEM imaging and particle size determination, it appeared that HMG Trial D seemed to stronger interact with β CD.

Lastly, content analysis was carried out. Results are shown in Figure IV.24.. No degradation was detected for either ITR or β CD. No degradation products were observed. ITR and β CD contents of HMG Trial A, B, C, D and PM were 97.59 ± 0.11 % and 105.21 ± 0.37 %, 93.00 ± 2.34 % and 93.70 ± 1.93 %, 97.67 ± 1.18 % and 98.45 ± 0.94 %, 100.93 ± 2.53 % and 97.44 ± 4.22 % as well as 100.86 ± 2.69 % and 94.06 ± 5.14 %, respectively. As later results of HMG Trial B stability data (see section IV.10.) suggested, the determined ITR value of 93.00 % might have been too low.

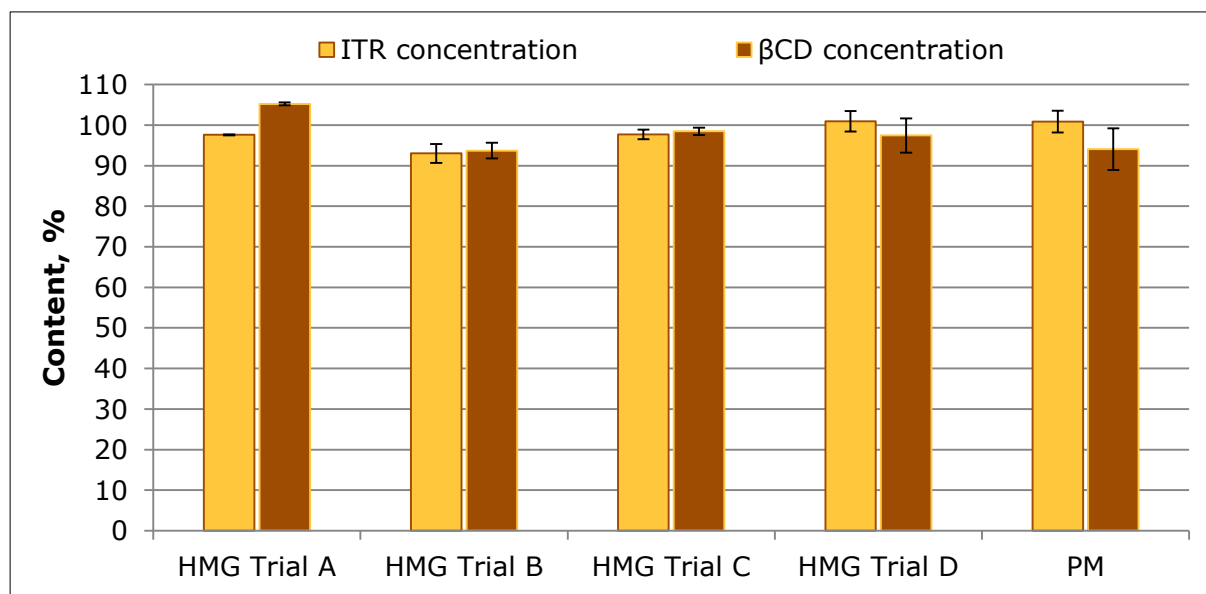


Figure IV.24. - Content evaluation of different HMG samples and PM; n = 3; error bars = sd.

Reviewing the general physico-chemical characterisation, the HMG runs could be divided into two categories, the specimen prepared above ITR T_m and the samples prepared below. Evaluating HMG Trial A and B, no differences were detected in the presented methods so far, whereas for the fully crystalline samples HMG Trial C and D, variabilities were found, regarding particle size, intensity in

XRPD and the broadened ITR T_m for HMG Trial D. All these results hinted at the possibility that HMG Trial D might show superior dissolution properties due to higher ICF compared to HMG Trial C.

IV.4.3. Dissolution Testing and Inclusion Complex Formation Evaluation of HMG Trial A - D

To gain further insights into possible ICF during HMG, dissolution testing was carried out and results for HMG Trial A, B, C and D and PM are shown in Figure IV.25..

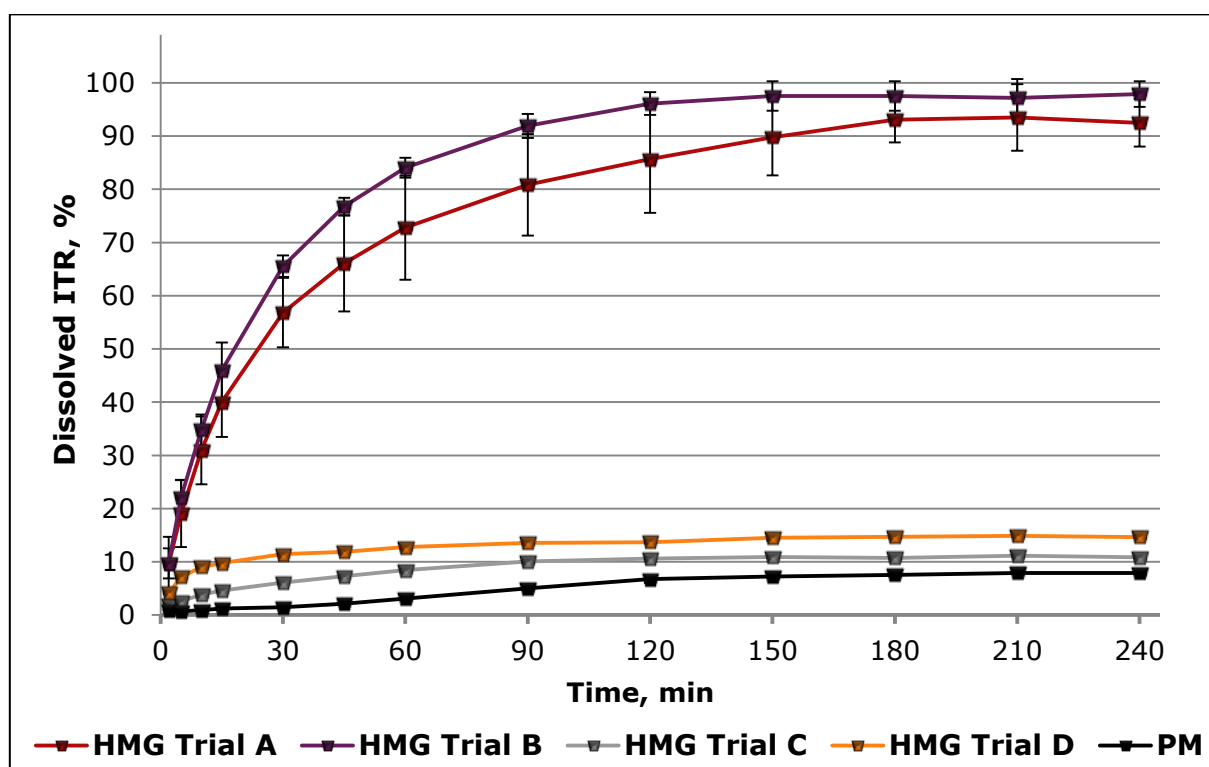


Figure IV.25. - Dissolution results of HMG Trial A, B, C, D and PM; n = 2; error bars = min/max.

After 4 h, HMG Trial A and B reached ITR dissolution of 92.49 ± 4.48 % and 97.89 ± 2.39 %, respectively. HMG Trial C and D showed ITR dissolution of 10.84 ± 0.07 % and 14.67 ± 0.12 %, whereas PM gave 7.89 ± 0.16 %. This was 18.58 % less as seen for PM in section IV.3.2. (10.32 ± 0.76 %) and was caused by the fact that the dissolution medium was not replaced in this analysis. As reported, HMG Trial A and B were produced above T_m of ITR which led to at least partially amorphous API in the samples. As described in section IV.3.2., PMaITR had already presented improved ITR dissolution of 63.76 ± 1.65 % after 4 h. Thus, it was plausible that ITR dissolution of HMG Trial A and B exceeded the fully crystalline samples by far. Consequently, it was most suitable to evaluate the

samples according to their processing regimen of either above ITR T_m or below. Only by this it was possible to distinguish if improved dissolution was caused by ICF. HMG Trial B reached highest and also fastest ITR dissolution. The average curve was always slightly above HMG Trial A. However, as deviations for both samples were quite high (e.g. after 15 min 6.56 % and 5.23 % for HMG Trial A and HMG Trial B, respectively), this could not be viewed as significant at this point. However, the maximum and minimum values varied far more for HMG Trial A. Compared to PMAITR, HMG Trial A reached improved dissolution of 45.06 %, whereas HMG Trial B reached an enhancement of 53.53 % after 4 h. Both dissolution curves of HMG Trial A and B showed nearly the same kinetics with fast ITR dissolution during the beginning of the experiment, resulting in a plateau phase up from approximately 120 min. The fast dissolution at the outset of the experiment indicated ICF during HMG as the dissolution curve of pure aITR and PMAITR (see section IV.3.2.) did not give this steep beginning of the curves. Moreover, the dissolution profile of aITR appeared rather zero-order like throughout the analysis while PMAITR only showed this behaviour in the beginning. Then, PMAITR started to reach a plateau after approximately 150 min.

These results proved that HMG procedure above ITR T_m had definitely altered HMG Trial A and B in a way that further improved ITR dissolution rate which could most likely be ascribed to ICF. Nonetheless, ICF during dissolution testing also occurred simultaneously, as generally, 100 % ICF after processing the material is improbable. Although HMG Trial B was processed at colder temperatures, the dissolution and dissolution rate appeared higher than for HMG Trial A. Table IV.7. showed that HMG Trial B presented a larger x_{50} value than HMG Trial A which constituted that improved dissolution velocity was not caused by larger surface area of the material. As presented in Table IV.6., the average torque during processing was slightly higher with 14 % compared to 10 %. This might have been an explanation for greater ICF in this sample as a higher torque correlates with higher energy input in the sample due to rising shear forces. Apart from that, in general the melt viscosity is higher with lowered temperatures. Consequently, more shear forces might have generated improved kneading and mixing abilities within mTSE, forcing a larger amount of ITR into the β CD cavities for HMG Trial B. Albeit the differences in dissolution between HMG Trial A and HMG Trial B were not extensive, the high absolute dissolution in general as well as the lower temperature profile for HMG Trial B deemed it the favourable HMG process.

For a more comprehensive understanding, the dissolution results of HMG Trial C and D and PM are shown in Figure IV.26. in magnification. Upon first inspection of the three curves, it became obvious that PM showed a different dissolution profile than the two processed samples. PM dissolution started slowly and experienced a rise between 30 - 120 min ($1.45 \pm 0.02 \%$ - $6.74 \pm 0.67 \%$). This hinted at ICF within the dissolution vessel. After 120 min, the ITR content nearly stayed on a plateau and reached $7.89 \pm 0.16 \%$ after 4 h.

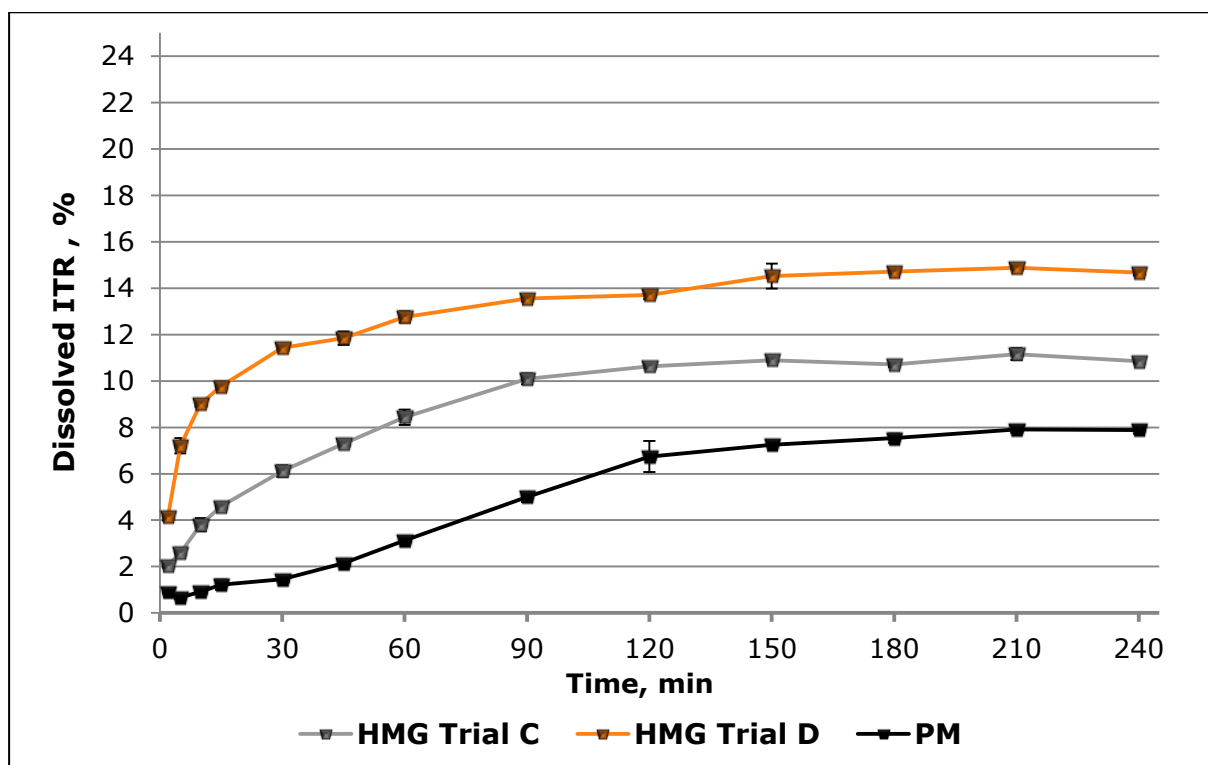


Figure IV.26. - Close up view of the dissolution results of HMG Trial C, D and PM; n = 2; error bars = min/max.

HMG Trial C and HMG Trial D exhibited different dissolution profiles. From the beginning onwards, for HMG Trial C, the dissolved amount of ITR was always above PM. Although there was a similar rise between 15 - 120 min which was most likely attributed to ICF in the liquid media, surely, mTSE processing had increased ITR dissolution. With $10.84 \pm 0.07 \%$ after 4 h, the final dissolution was enhanced by 37.39 %. Examining the dissolution profile of HMG Trial D, the curve presented even further improved dissolution and dissolution rate. It started above the other samples. Kinetic-wise the dissolution profile appeared more as shown for HMG Trial A and B, only on a smaller scale. The slow rise shown for HMG Trial C and PM was not certainly detected for HMG Trial D. Nonetheless, at 30 - 120 min, small dissolution increase ($11.43 \pm 0.12 \%$ - $13.71 \pm 0.19 \%$) was seen. After 4 h, HMG Trial D reached ITR dissolution of $14.67 \pm 0.12 \%$ which

was an increase of 85.93 % compared to PM. Thus, the outcome suspected in the previous section held true for the fully crystalline samples. As also shown for HMG Trial A and B, although HMG Trial D was processed at lower temperatures, the torque during HMG had been higher (16 % in respect to 6 % for HMG Trial C). This might have caused higher shear forces resulting in improved mixing and kneading during HMG. Again, particle size measurements excluded faster dissolution due to larger surface area (see Table IV.7.). Despite the fact that the absolute ITR dissolution was not largely improved by processing crystalline material, the highest relative enhancement of all samples was seen for HMG Trial D. To completely evaluate possible ICF, ATR-FT-IR results were also taken into account (see Table IV.9.).

Particularly for HMG Trial C, no substantial changes became apparent in the ATR-FT-IR spectrum compared to PM. Partial ICF was most likely, as it appeared that non-included ITR was overlapping IC signals. The detected wave numbers for HMG Trial C were very similar to PM throughout the whole spectrum. Evaluating HMG Trial A and B, the previously detected changes for partial amorphous content also became apparent. The peak at 1042.58 cm^{-1} detected for PMaITR had completely disappeared. As HMG Trial D had shown the highest relative improvement in dissolution most likely caused by ICF, the largest spectral changes were suspected for this sample. This suspicion held true upon inspecting ATR-FT-IR results, especially by comparing the detected wave numbers to PM or HMG Trial C. Overall, the results of HMG Trial D appeared more distinct and less challenging to interpret as shown for the partially amorphous samples. Some peaks (around 1585 cm^{-1} , 1271 cm^{-1} , and 1184 cm^{-1}) had disappeared altogether and the signal around 1027 cm^{-1} had previously only been reported for at least partially amorphous samples. The signal at 1077.45 cm^{-1} had shifted to a higher wave number compared to the other crystalline samples that gave a wave band at approximately 1073 cm^{-1} . The signal at 1462.05 cm^{-1} presented a shift of over 10 cm^{-1} in contrast to all other samples. As HMG Trial D showed the largest relative dissolution enhancement, it might have been possible that this sample exhibited lowest amount of remaining, non-included ITR, causing overlapping signals. Thus, in the other samples, this shift in wave number might have been masked.

It was shown again that the sole examination of ATR-FT-IR spectra did not give sufficient results for proving ICF. Even though for HMG Trial D, changes were de-

tected that could not be explained by amorphisation, it has to be acknowledged that these changes largely appeared in regions that became affected by amorphisation. Therefore, these results stressed the limited informative value for melt processed samples with amorphous content. IC detection for HMG Trial A and B only by ATR-FT-IR was not possible. However, the determination of spectral changes could help to further explain dissolution results.

Table IV.9. - ATR-FT-IR results of HMG Trial A, B, C and D; evaluated by comparison with reference wave numbers; sd = \pm ; n = 3; *n = 5; if wave number markers were not detected in every single analysis, the percentage of their occurrence is given in brackets below.

	PM* PMaITR*	HMG Trial A	HMG Trial B	HMG Trial C	HMG Trial D
Wave Numbers, cm ⁻¹	1697.60 \pm 0.15 1698.89 \pm 0.33	1698.40 \pm 0.08	1698.63 \pm 0.23	1697.93 \pm 0.02	1698.26 \pm 0.04
	1584.60 \pm 0.25 (80 %) 1585.76 \pm 0 (20 %)	X	X	1584.72 \pm 0 (66.67 %)	X
	1551.18 \pm 0.13 1552.74 \pm 0.27	1552.73 \pm 0.10	1552.69 \pm 0.21 (66.67 %)	1551.38 \pm 0.05	1551.57 \pm 0.08
	1509.80 \pm 0.23 1511.07 \pm 0.34	1510.50 \pm 0.20	1510.75 \pm 0.25	1510.16 \pm 0.06	1510.50 \pm 0.04
	1451.20 \pm 0.16 (80 %) 1451.08 \pm 0.21	1451.44 \pm 0.22	1451.51 \pm 0.21 (66.67 %)	1451.44 \pm 0.01	1462.05 \pm 0.10
	1270.96 \pm 0.98 (80 %) X	X	X	1270.34 \pm 0.07 (66.67 %)	X
	1227.41 \pm 0.59 1228.55 \pm 0.62	1228.35 \pm 0.41	1229.45 \pm 0.55	1227.98 \pm 0.27	1229.38 \pm 0.14
	1184.44 \pm 0.52 X	X	X	1184.53 \pm 0.29	X
	1140.58 \pm 0 (20 %) X	X	X	X	X
	1072.64 \pm 0.06 (40 %) 1077.55 \pm 0.36 (40 %)	1078.43 \pm 0.06	1078.32 \pm 0.29	1072.92 \pm 0.18 (66.67 %)	1077.45 \pm 0.11
	1043.15 \pm 0.11 1042.58 \pm 0.95 (40 %) X	X	X	1043.13 \pm 0.09	1042.05 \pm 0 (66.67 %)
	1028.45 \pm 1.81 (60 %)	1026.06 \pm 0.58	1025.93 \pm 0.63	X	1027.84 \pm 0.25 (66.67 %)
	823.82 \pm 0.09 824.74 \pm 0.72	824.93 \pm 0.45	825.01 \pm 0.69	824.00 \pm 0.03	824.11 \pm 0.02

IV.4.4. Concluding Remarks about HMG Trial A - D

The previous section showed the physico-chemical analyses of different HMG runs as well as evaluations of possible ICF and ITR dissolution. As stated, the most suitable HMG temperature profile was supposed to be chosen. Although the largest relative improvement in dissolution was gained for a fully crystalline sample (HMG Trial D), it was shown that the combination of amorphisation and ICF during HMG resulted in the highest absolute ITR dissolution (see Figure IV.25.). Both at least partially amorphous samples yielded ITR dissolution above 90 %. Since the lowest applicable temperatures should always be chosen during melt processes, it was concluded that the most promising temperature profile for HMG was HMG Trial B, where PM was processed above T_m of ITR. Consequently, all alternative formulation approaches from here on that were processed with the mTSE were operated at this temperature profile. The scientific value of the greatest relative improved dissolution (HMG Trial D) will be taken up again in section V. for the overall discussion and scientific perspective of this work.

IV.5. Investigating Hot-Melt-Granulation against Physical Inclusion Complex Formation Methods

For comparative reasons, the developed HMG procedures were evaluated against a kneading process (KN) as well as a melt processed wet granulation (WG). KN was chosen as it is the traditional method of creating ICs. Since HMG with temperatures above ITR T_m had shown to enhance ITR dissolution after 4 h but yet had reached maximum dissolution after 2 h, it was hypothesised that a combination of WG and HMG might further improve the dissolution rate. Even though KN and the melt processed WG were different regarding their fabrication, they were evaluated together in the following subchapter as they shared manufacturing steps that utilised physical modification to improve ICF.

IV.5.1. Kneading Process and Wet Granulation Processability

KN and WG were produced according to section III.2.1.2.. KN was further characterised without alterations, whereas WG was dried to residual moisture of 13.30 % and then given into the hopper. As reported, HMG Trial B had shown favourable characteristics coinciding with the lowest processing temperatures. Thus, WG was hot-melt granulated using these parameters. Processing features of HMG Trial WG are given in Table IV.10..

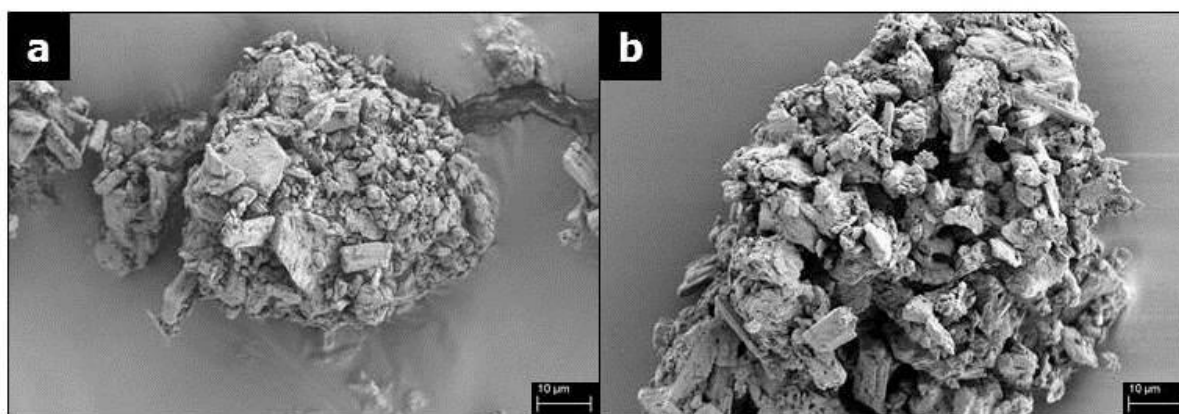
Table IV.10. - HMG processing details for HMG Trial WG.

HMG Trial	Z1, °C	Z2, °C	Z3, °C	Z4, °C	Z5, °C	Z6, °C	Z7, °C	ScS, rpm	Throughput, g/h	Torque, %
WG	100	130	170	180	180	180	180	150	187.1	13

WG exhibited best flowability of all samples processed by mTSE with a calibrated maximum throughput of 1268.7 g/h. During the mTSE filling phase, it became apparent that the residence time was much shorter than for the other HMG runs, although the later average throughput was kept below the desired value of 200.6 g/h and ScS constant at 150 rpm. A large part of WG was lost as reject during this starting period. Whereas the process itself was stable, the yielded product appeared different from the reference HMG Trial B which had emerged as partially molten granules. However, for HMG Trial WG, next to no molten ITR was visible. The difference in appearance between the raw WG and the melt-granulated product was less pronounced compared to the reference. Moreover, the observed water loss by vaporisation through the ventilation port was also to a lesser extent. The torque was well in range with the HMG runs presented in the previous chapter with 13 %. The general processability of WG could be regarded as acceptable. No deteriorated material was observed during the process, not even in the mTSE filling phase, most probably caused by the shorter residence time. Both, KN and HMG Trial WG, were manually crushed and sieved through 425 µm. But, for both of the samples crushing was mostly not necessary for passing the sieve.

IV.5.2. Physico-Chemical Characterisation of KN and HMG Trial WG

Both samples were characterised regarding their physico-chemical properties. SEM images of KN and HMG Trial WG are shown in Figure IV.27..

**Figure IV.27. - SEM images of a) KN and b) HMG Trial WG; bar = 10 µm.**

Upon this magnification, the samples appeared very similar. For both portrayed granules, it was clearly visible that they were composed of different materials. Some of the larger β CD particles were visually observable in the agglomerates. Also, ITR particles could be visibly identified. Especially for HMG Trial WG, some needle-shaped ITR crystals were seen which hinted at partial crystallinity of the sample. However, areas that seemed to consist of molten ITR were also detected. With lesser magnification, KN and HMG Trial WG particles appeared identical, only differing in particle size as KN particles were smaller. These results were backed up by laser diffraction analyses which resulted in x_{50} values of $12.5 \pm 0.2 \mu\text{m}$ and $48.5 \pm 3.2 \mu\text{m}$ for KN and HMG Trial WG, respectively.

DSC traces of KN and HMG Trial WG are presented in Figure IV.28.. DSC events correlating to ITR are given in Table IV.11.. KN displayed an endothermic signal slightly above 100 °C corresponding to water loss, and ITR T_m at 164.93 °C. This result was slightly below that of PM (see Table IV.8.), indicating ICF during kneading. The DSC curve of HMG Trial WG seemed to show only one T_m corresponding to ITR but when magnified (data not shown), a very small melting endotherm became detectable at 157.06 °C. This signal most likely belonged to the polymorph Form II. Due to the diminutiveness of the melting signal, no exothermic signal of the previously described "cold crystallisation" could be detected around 110 °C.

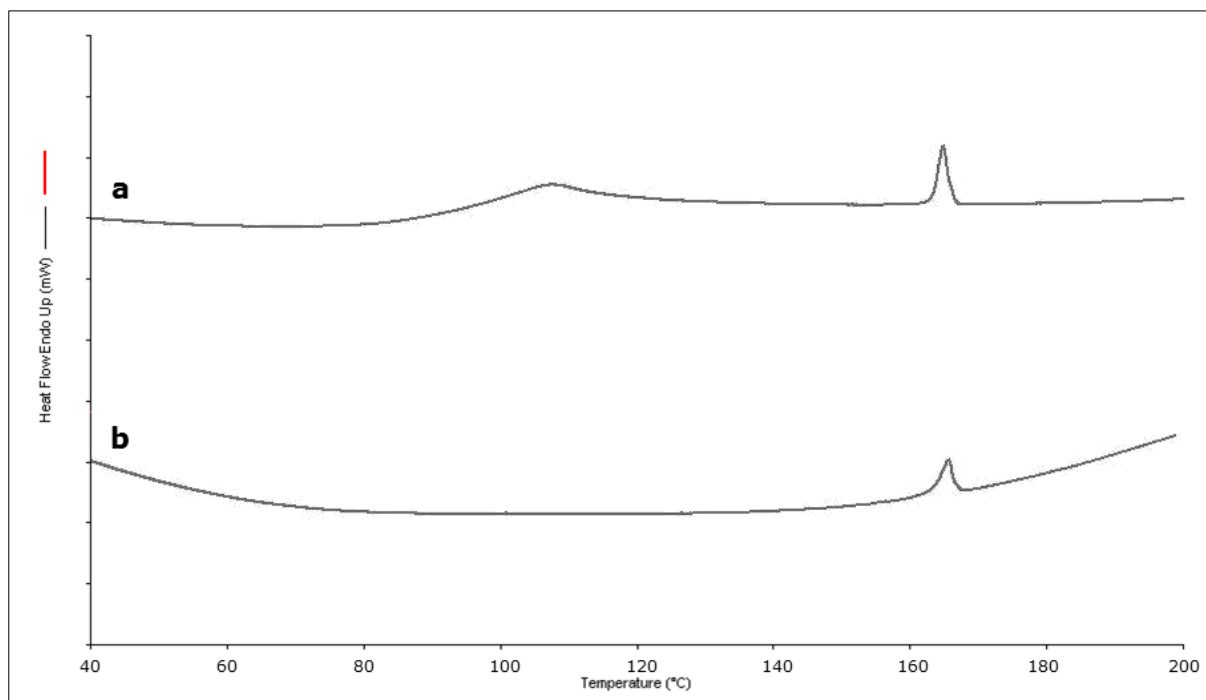
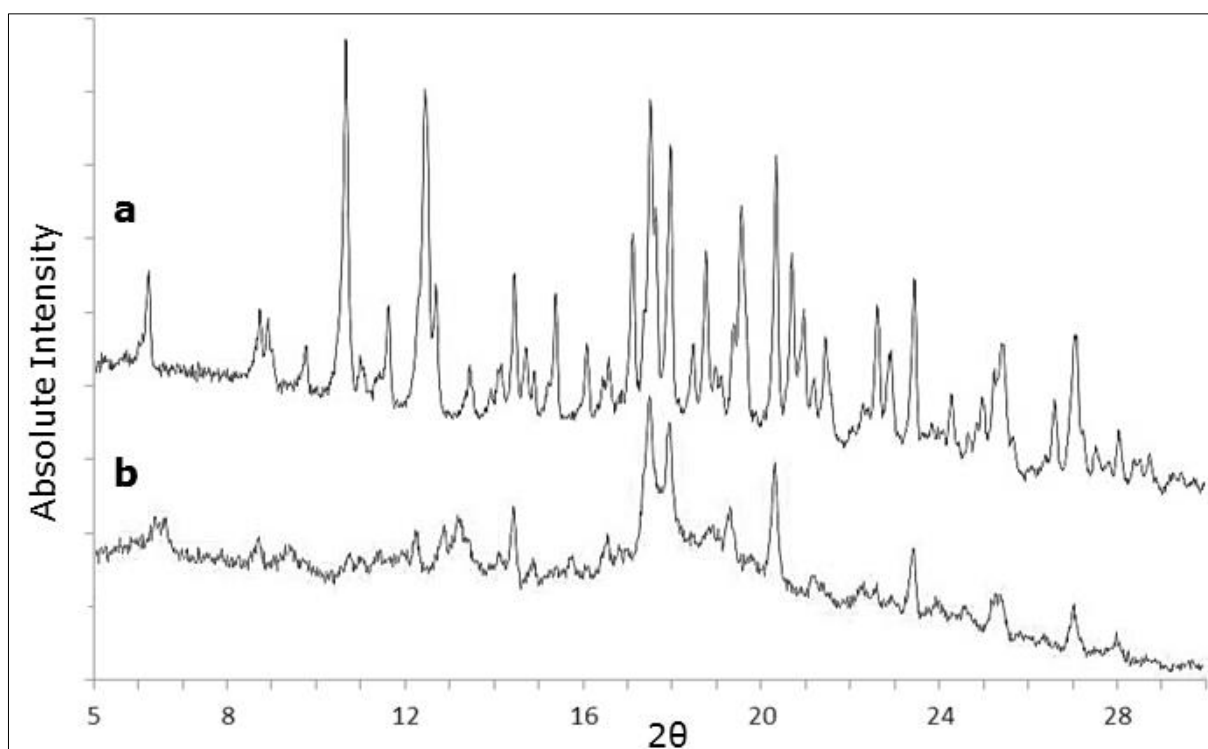


Figure IV.28. – Excerpts of DSC traces of a) KN and b) HMG Trial WG; analysis conducted from 30 - 200 °C after 2 min holding period at 30 °C; heating rate 3 K/min.

Table IV.11. - DSC signals correlating to ITR melting for KN and HMG Trial WG.

	KN	HMG Trial WG	
ITR signal, °C			
Onset	163.46	155.85	164.35
Peak	164.93	157.06	166.65

Due to lack of polymorphic signals in XRPD or ATR-FT-IR analyses, it was concluded that material within HMG Trial WG was most likely negligibly amorphous and mostly crystalline. This hypothesis was based on the T_m at 166.65 °C. The exhibited ITR T_m was slightly higher compared to KN which indicated less ICF. The observation that HMG Trial WG showed shorter HMG residence time and appeared different from other HMG runs was reflected in this DSC result and the subsequent crystallinity. Succeeding production, a water content of 2.133 % was determined for HMG Trial WG. This was only inconsiderably below the value determined for HMG Trial B (2.335 %), so the observation that less water had evaporated during HMG did not hold true. Nonetheless, it might have been possible that the energy during HMG was sufficient for water removal but, due to the fast conveying within the barrel, was not enough to completely melt the API. XRPD results of KN and HMG Trial WG are presented in Figure IV.29.. KN appeared completely crystalline with distinct peaks that could mostly be correlated to either ITR or β CD.

**Figure IV.29. - Excerpts of XRPD diffractograms of a) KN and b) HMG Trial WG.**

This had been somewhat expected as no processing steps had been conducted that would have changed ITR crystallinity. It has been reported that ICF in crystalline samples can cause changes in peak intensity, disappearance or shift of XRPD signals or in some cases, results in new peaks. Very often, studied samples have been exposed to techniques that could have altered API crystallinity. Then, XRPD results are without value in making distinct conclusions (see Figure IV.23. and XRPD evaluation of HMG Trial A and B) [133,156]. In the here presented case, XRPD diffractogram of KN gave the same diffraction pattern as PM. As ICF during kneading most probably did not take place quantitatively, there was the possibility that un-included ITR signals overlapped possible changes caused by the IC. Otherwise, XRPD results did not support ICF in KN. The XRPD pattern of HMG Trial WG supported the DSC results. Though most peaks had dropped in their absolute intensity, there still was a pattern observable that hinted at partial ITR crystallinity. Especially the peaks at $8.69^{\circ} 2\theta$, $12.29^{\circ} 2\theta$, $17.54^{\circ} 2\theta$, $17.99^{\circ} 2\theta$ and $20.36^{\circ} 2\theta$ could be correlated to crystalline ITR.

ITR and β CD content were evaluated. Results are given in Figure IV.30.. No product degradation was visible during HMG. These results were backed up by the content analyses. KN exhibited respective ITR and β CD contents of $98.78 \pm 0.38 \%$ and $97.13 \pm 1.25 \%$. ITR content in HMG Trial WG was $97.48 \pm 1.51 \%$ and β CD $102.91 \pm 0.63 \%$. Deviating from all other samples, longer ultrasonification times had been necessary for HMG Trial WG samples to dissolve.

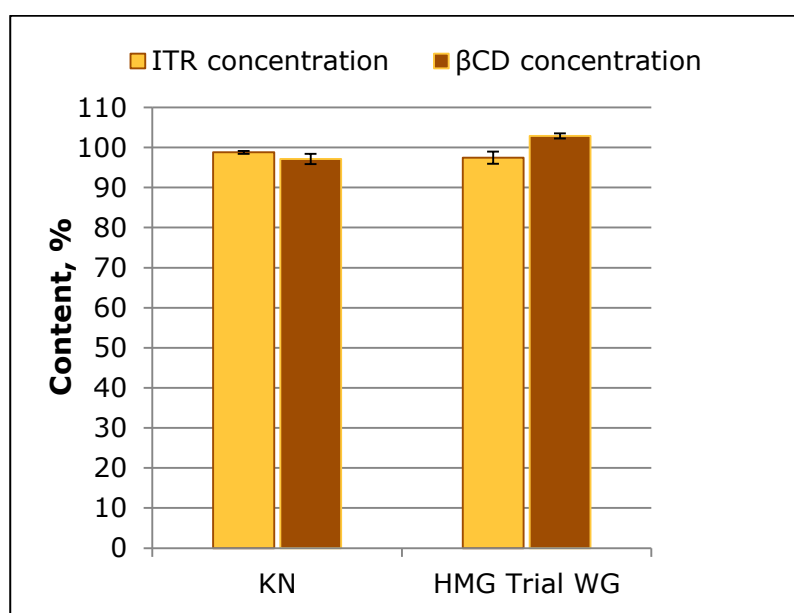


Figure IV.30. - Content evaluation of KN and HMG Trial WG; n = 3; error bars = sd.

Comparing these two samples with the melt processed specimen presented previously, it seemed as if HMG Trial WG lacked amorphousness compared to reference HMG Trial B. This would most likely decrease ITR dissolution. Solely by investigating physico-chemical characteristics of KN, the only detectable change compared to PM was that ITR T_m had shifted to a slightly lower temperature.

IV.5.3. Dissolution Testing and Inclusion Complex Formation Evaluation of KN and HMG Trial WG

To further examine possible ICF, dissolution experiments of KN and HMG Trial WG were carried out. Dissolution curves are shown in Figure IV.31.. Although HMG Trial WG had been melt processed above ITR T_m , partial crystallinity of ITR was detected in DSC.

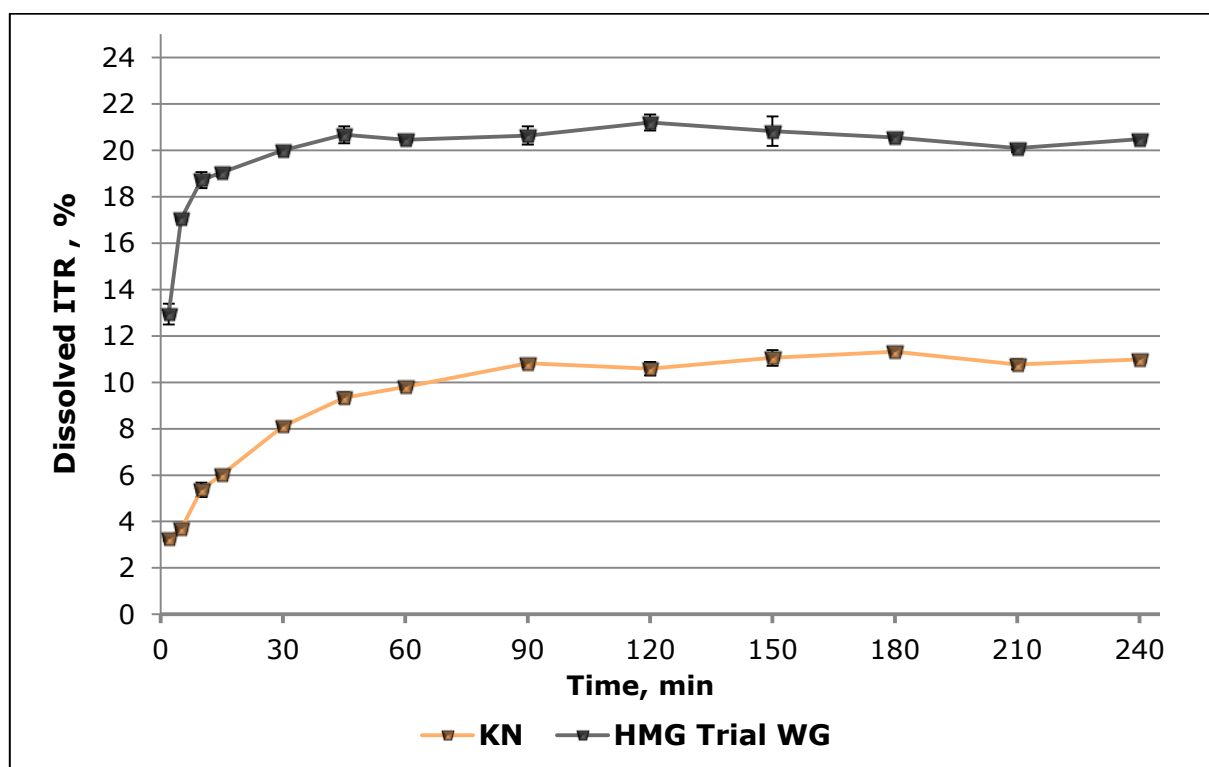


Figure IV.31. - Dissolution results of KN and HMG Trial WG; $n = 2$; error bars = min/max.

The assumption of a decrease in dissolution caused by this held true. After 4 h, HMG Trial WG reached 20.47 ± 0.08 % ITR dissolution which was only 20.91 % of the reference sample's result (97.89 % for HMG Trial B). No relative difference in absolute dissolution could be calculated as none of the two chosen references was appropriate. PM could not be used due to a ITR in the sample, PMaITR could not be used since most ITR appeared crystalline. KN showed dissolution of

10.99 ± 0.08 % after 4 h. With this, it was nearly on the same level as HMG Trial C (10.84 %). Compared to PM, this was an increase in ITR dissolution of 39.29 %. This was most likely caused by ICF. The curvature of KN also hinted at ICF, as the previously described slow rise between 30 - 120 min for PM was not as pronounced for this sample. The plateau phase of KN was already reached after approximately 75 min. The dissolution profile of HMG Trial WG partially resembled the dissolution curve of HMG Trial D (see Figure IV.25.), but presented a higher absolute amount of dissolved ITR as well as the complete lack of rising caused by ICF in the liquid medium. The plateau phase was reached after 30 min. Taking into account the observation during content analysis and the fact that after dissolution testing, large fragments of white sample were swirling in the dissolution medium, it was possible that the dissolution result of HMG Trial WG was solely built on aITR dissolving whereas the crystalline granules did not dissolve at all. Without sufficient solvation of β CD, ICF within the dissolution vessel was hindered.

To further characterise possible ICF, ATR-FT-IR experiments were carried out. The detected marker wave numbers for KN and HMG Trial WG are given in Table IV.12.. For KN, only one marker wave number directly hinted at ICF, the signal at 1075.09 cm^{-1} . This meant a shift from 1072.64 cm^{-1} as seen for PM. However, this wave number was only detected during one experiment run. As opposed to HMG Trial D (see Table IV.9.) where numerous signals had disappeared without ITR amorphisation, these peaks were still observed for KN (e.g. 1584.79 cm^{-1} and 1185.07 cm^{-1}). It appeared that only partial ICF had occurred during kneading and caused overlapping ATR-FT-IR results. The detected wave numbers for HMG Trial WG also differed strongly from the reference HMG Trial B (see Table IV.9.). The disappeared signals around 1140 cm^{-1} and 1043 cm^{-1} might have been connected to ITR amorphisation, however, those two signals had also not been observed in every analysis run of PM and PMaITR. Other markers, e.g. at 1585.30 cm^{-1} and 1185.11 cm^{-1} were detected in every measurement of HMG Trial WG. The shift of the peak around 1072 cm^{-1} to 1078.04 cm^{-1} might have either indicated amorphisation or ICs in the sample. Generally, the results of HMG Trial WG strongly suggested that most ITR was crystalline. Otherwise the spectral signals were inconclusive and did not allow any distinct conclusion or support of dissolution results. Combining dissolution and ATR-FT-IR results, it seemed fairly certain that ICF had occurred for KN,

however only partially. The existence of ICs within HMG Trial WG could not be proven or concluded as the dissolution stayed well below the reference range of aITR. Therefore, it was not possible to ascribe the change in dissolution to either amorphous content or ICF.

Table IV.12. - ATR-FT-IR results of KN and HMG Trial WG, evaluated by comparison with reference wave numbers; sd is given as \pm , $n = 3$, * $n = 5$; if wave number markers were not detected in every single analysis, the percentage of their occurrence is given in brackets below.

	PM* PMaITR*	KN	HMG Trial WG
Wave Numbers, cm^{-1}	1697.60 \pm 0.15 1698.89 \pm 0.33	1698.12 \pm 0.14	1698.11 \pm 0.14
	1584.60 \pm 0.25 (80 %) 1585.76 \pm 0 (20 %)	1584.79 \pm 0.10	1585.30 \pm 0.11
	1551.18 \pm 0.13 1552.74 \pm 0.27	1551.51 \pm 0.14	1551.65 \pm 0.08
	1509.80 \pm 0.23 1511.07 \pm 0.34	1510.31 \pm 0.13	1510.55 \pm 0.21
	1451.20 \pm 0.16 (80 %) 1451.08 \pm 0.21	1451.34 \pm 0.12	1451.19 \pm 0.09
	1270.96 \pm 0.98 (80 %) X	1272.61 \pm 0.16	1272.51 \pm 0.14
	1227.41 \pm 0.59 1228.55 \pm 0.62	1227.48 \pm 0.09	1227.77 \pm 0.12
	1184.44 \pm 0.52 X	1185.07 \pm 0.05	1185.11 \pm 0.06
	1140.58 \pm 0 (20 %) X	1141.16 \pm 0 (33.33 %)	X
	1072.64 \pm 0.06 (40 %) 1077.55 \pm 0.36 (40 %)	1075.09 \pm 0 (33.33 %)	1078.04 \pm 0.17
	1043.15 \pm 0.11 1042.58 \pm 0.95 (40 %) X	1042.81 \pm 0.10	X
	1028.45 \pm 1.81 (60 %)	X	1026.38 \pm 0.21
	823.82 \pm 0.09 824.74 \pm 0.72	824.04 \pm 0.04	824.12 \pm 0.11

IV.5.4. Concluding Remarks about KN and HMG Trial WG

This chapter presented two approaches of physically creating ICs and the comparison against reference samples. For KN, it was concluded that manual kneading had resulted in only partial ICF. Dissolution after 4 h was increased by

39.29 %. Comparing this with HMG Trial C, nearly the same dissolution results were achievable without the addition of water during the continuous HMG process. This was an advantage over KN, particularly when taking into account that HMG Trial D (see previous chapter) had reached even higher final ITR dissolution after being processed at lower temperatures. The crystalline HMG samples appeared superior to the traditional ICF method.

The hypothesis that a combination of WG and HMG processed above T_m of ITR might further enhance dissolution rate or product properties had to be rejected. The tremendously improved flowability properties of WG had negatively influenced HMG procedure. Even though a short residence time is favourable for melt processes as the material is only exposed to high temperatures for a very short time, it needs to be long enough to allow complete melting and mixing within the barrel. This had apparently not been the case for HMG Trial WG. The obtained results of physico-chemical and dissolution analyses were difficult to evaluate as the degree of ICF could not be determined and thus, the degree of aITR's influence. Overall, it was concluded that both physical methods, KN and HMG Trial WG were inferior to the reference sample HMG Trial B. Furthermore, KN was also inferior to HMG Trial C and D. The combination of WG and HMG was discarded as ineffective.

IV.6. Examination of the Influence of Hydroxypropyl- β -Cyclodextrin on Product Quality

As described in section IV.1., PSM showed improved ITR solubility with HP β CD. Apart from this, HP β CD is used in the marketed oral solution Sporanox[®] (see section III.1.3.). Thus, HP β CD was investigated as matrix in HMG to evaluate possible advantages and disadvantages over β CD. For comparative reasons, the stoichiometry of 1:1 was kept which meant a smaller mass fraction of ITR in the blend compared to β CD.

IV.6.1. Hot-Melt Granulation Process

Since operating parameters of HMG Trial B were selected as favourable (see section IV.4.), these parameters were used for PM of HP β CD and ITR. They are given in Table IV.13.. The procedure was stable as had been seen for PMs with β CD.

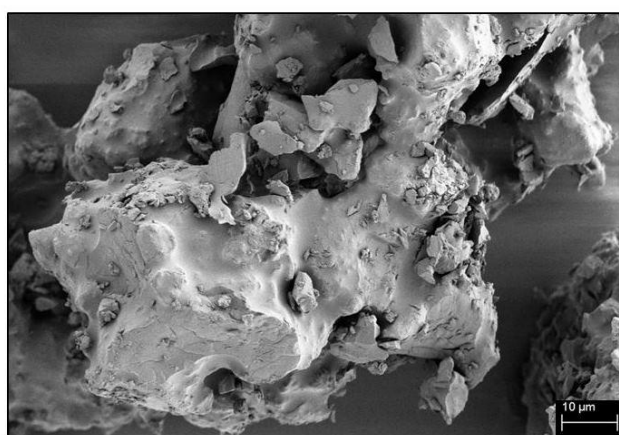
Table IV.13. - HMG processing parameters for HMG Trial HP.

HMG Trial	Z1, °C	Z2, °C	Z3, °C	Z4, °C	Z5, °C	Z6, °C	Z7, °C	ScS, rpm	Throughput, g/h	Torque, %
HP	100	130	170	180	180	180	180	150	214.6	23

However, this PM appeared dustier during handling which was not a desired quality. The average throughput was kept at 214.6 g/h with a torque of about 23 % which was substantially higher as for the reference sample HMG Trial B (14 %). The yielded product looked the same as the other HMG samples processed above ITR T_m . Seemingly intact CD particles were agglomerated by molten ITR that had solidified. The material passing mTSE during the filling phase exited degraded. After a stable process was reached, the product appeared completely intact without visible deterioration. Even though the torque was considerably higher than observed before, the screws did not screech and the whole operation could be described as successful. No differences were seen compared to using β CD as matrix regarding the behaviour within mTSE.

IV.6.2. Physico-Chemical Characterisation of HMG Trial HP

HMG Trial HP was analysed in view of its physico-chemical properties. Figure IV.32. shows a magnified SEM image of the sample. Differently sized agglomerates were present, but commonly appeared like the one displayed in the picture. The molten surface was plainly visible. Still, not all particles of one agglomerate were covered by molten material. The solidified melt seemed "bumpy". This might have been explained by the fact that HP β CD did not melt during HMG and thus, these particles did not change regarding roughness or general composure during processing.

**Figure IV.32. - SEM image of HMG Trial HP shortly after production; bar = 10 µm.**

The x_{50} value of the sample after manual crushing was determined to be $66.8 \pm 2.1 \mu\text{m}$. This was only 57.44 % of the reference sample HMG Trial B ($116.3 \pm 24.4 \mu\text{m}$) and could indicate a faster dissolution rate due to a larger surface area.

Figure IV.33. and Table IV.14. display the DSC results of HMG Trial HP. Comparing the curve with the DSC trace of the reference sample HMG Trial B (see Figure IV.21.), they appeared similar. Again, there was a second, colder T_m of ITR, in this case at $158.41 \text{ }^\circ\text{C}$, corresponding to the previously reported polymorph. The second melting endotherm of ITR occurred at $166.97 \text{ }^\circ\text{C}$.

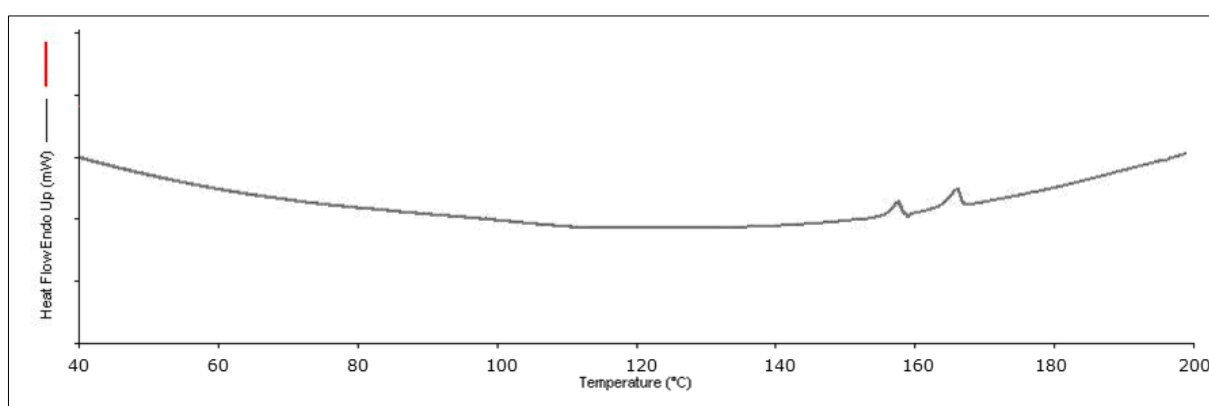


Figure IV.33. – Excerpt from DSC curve of HMG Trial HP; analysis conducted from 30 - 200 °C after 2 min holding period at 30 °C; heating rate 3 K/min.

Upon magnifying the DSC trace as shown for HMG Trial A and B (see Figure IV.22.; data for HMG Trial HP not shown), the “cold crystallisation” of ITR as well as the endothermic signals correlating to ITR mesophases became detectable. This characteristic was a property that all samples processed above T_m of ITR had in common except the previously presented HMG Trial WG. Same as for the other HMG samples, no further sign of the polymorph was detected for HMG Trial HP in any further analysis which is why it was concluded that the polymorph had formed during the DSC experiment and was not present in the solid sample.

Table IV.14. - DSC signals correlating to melting of ITR for HMG Trial HP.

	HMG Trial HP	
ITR signal, °C		
Onset	156.70	164.79
Peak	158.41	166.97

The second T_m at $166.97 \text{ }^\circ\text{C}$ might have been caused by partially crystalline ITR within the sample or by recrystallisation during the DSC measurement. To further

study these possibilities, XRPD diffractograms of the sample and pure HP β CD were obtained. They are given in Figure IV.34.. The diffractogram of HP β CD did not show any peak pattern in contrast to β CD. This was probably caused by the irregular substitution of the glucose units with the hydroxypropyl groups and corresponded to literature results [157]. The XRPD diffractogram of HMG Trial HP suggested the sample to be amorphous. No peaks of ITR were visible for the sample. This supported the theory regarding “cold crystallisation” of the polymorph during DSC analysis. Moreover, it suggested that both detected T_m s of ITR in the DSC were caused by recrystallisation processes during the analysis.

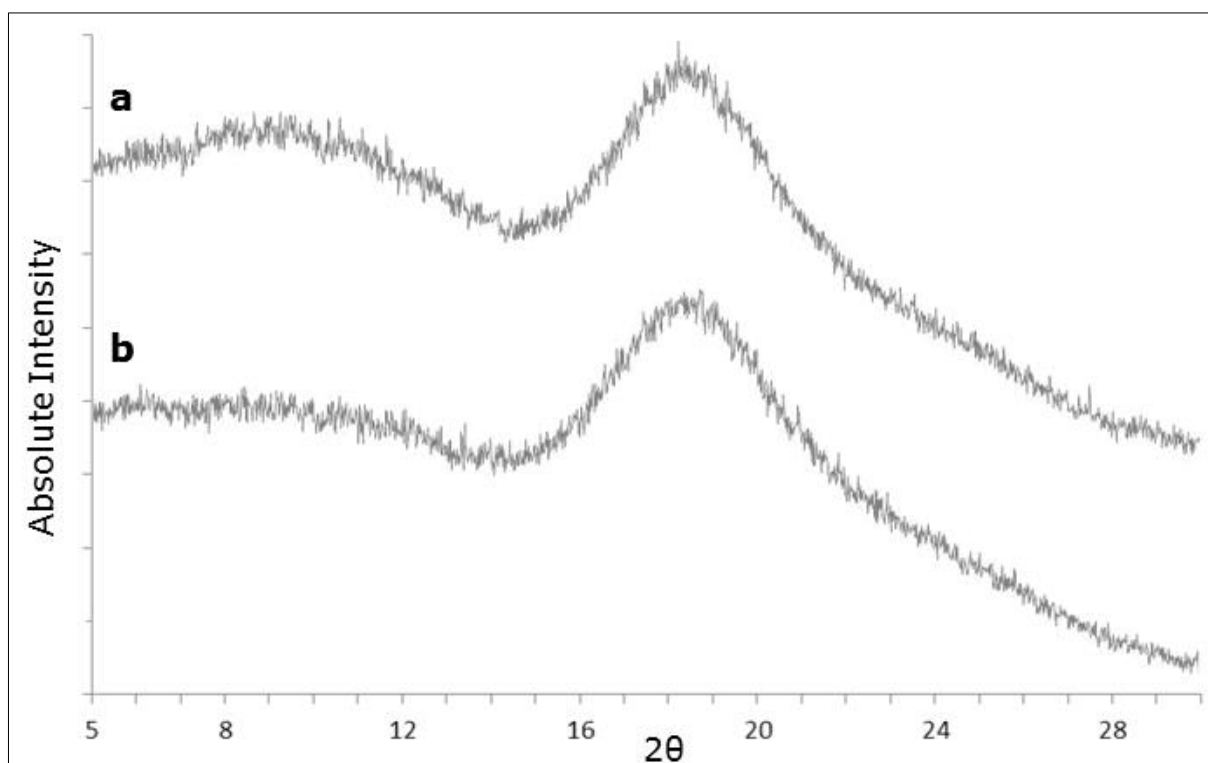


Figure IV.34. - Excerpts from XRPD diffractograms; a) pure HP β CD and b) HMG Trial HP.

Nevertheless, as XRPD has a limit in detecting crystallinity, the possibility of at least minimal ITR crystallinity could not be excluded. Anyhow, the XRPD analysis of HMG Trial HP showed the least traces of crystalline ITR of all investigated samples. It seemed that HP β CD was better suited as matrix in keeping ITR amorphous, also during the analysis. This might again have been caused by the substitutional pattern, as this might have hindered ITR from redefining its long-range crystal order. Content evaluation was carried out in triplicate for each ITR and HP β CD. No product degradation was visible. This was mirrored in the analysis results with an ITR content of $100.20 \pm 1.39 \%$ and HP β CD content of $102.49 \pm 2.62 \%$.

The physico-chemical examination of the sample showed parallels to the reference sample HMG Trial B but also highlighted one possibly important difference, the ability of HP β CD to maintain aITR and prevent recrystallisation directly after production. These results hinted at the possibility of improved dissolution compared to the reference. However, as was presented in section IV.1., unmodified β CD had shown a higher CE with ITR compared to HP β CD. Thus, any changes in dissolution of the CD derivative might solely be caused by higher aITR content and not due to more extensive ICF within mTSE.

IV.6.3. Dissolution Testing and Inclusion Complex Formation Evaluation of HMG Trial HP

The dissolution of HMG Trial HP was investigated over 4 h and results are shown in Figure IV.35.. As the physico-chemical examination had shown, the sample appeared fully amorphous which is why the negative control for dissolution testing had to be PMAITR (63.76 % after 4 h; see section IV.3.2.).

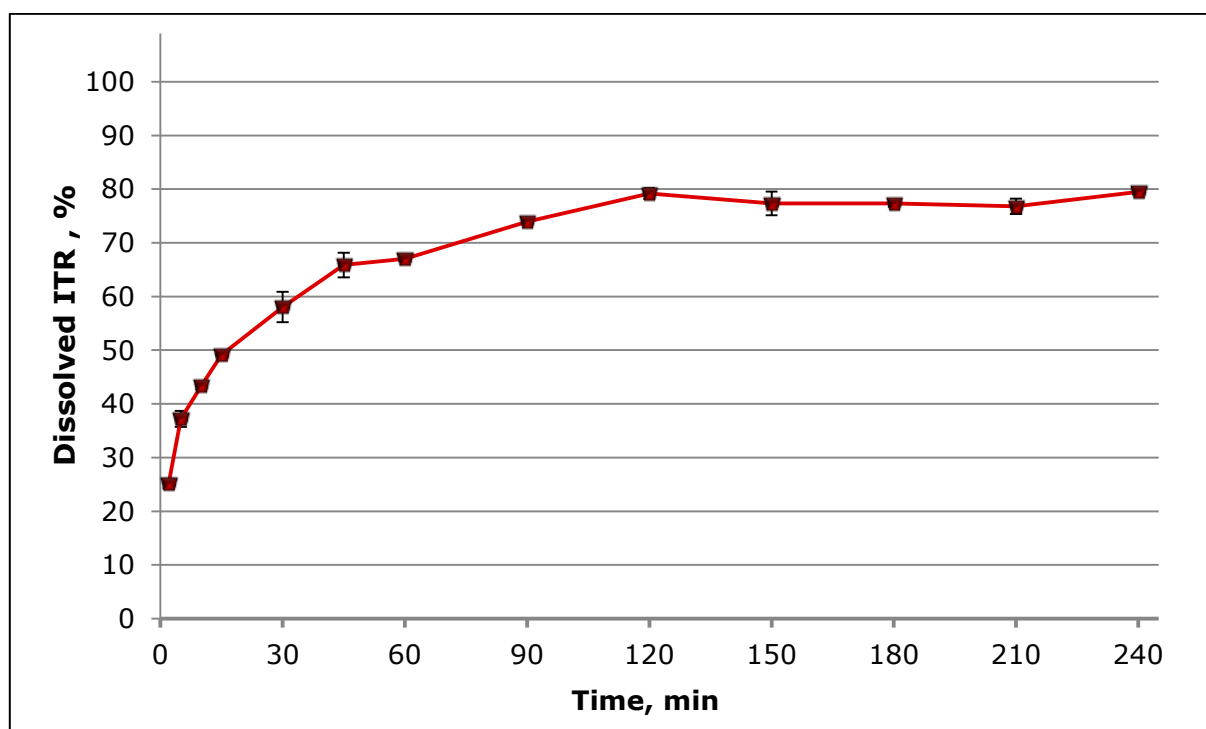


Figure IV.35. - Dissolution results of HMG Trial HP; n = 2; error bars = min/max.

HMG Trial HP reached ITR dissolution of 79.50 ± 0.42 % after 4 h. This was an enhancement of 24.69 % compared to PMAITR but a reduction of 18.79 % compared to HMG Trial B (97.89 ± 2.39 % after 4 h; see section IV.4.3.). The dissolution profile started higher than for HMG Trial B (37.19 ± 1.48 % after 5 min for HMG Trial HP compared to 22.15 ± 3.22 % after 5 min for HMG Trial B). This

could have been related to a burst effect of aITR on the granules' surface (see Figure IV.32.) or to the fast dissolution rate of formed ICs. Another possibility could be the larger surface area of the smaller particles as shown in the x_{50} determination. After 45 min, HMG Trial B dissolution exceeded HMG Trial HP. Same as for the reference sample, there was a long rise between 30 - 120 min that most probably was caused by ICF in the dissolution vessel. After that, comparable to HMG Trial B as well, a plateau was reached. Dissolution of HMG Trial B rose 61.33 % between 30 - 120 min. Dissolution of HMG Trial HP on the other hand, only 35.52 %. As it was shown that β CD gave a higher CE for ITR, this discrepancy could possibly at least in part be ascribed to more extensive ICF during analysis. However, the investigation of PMaITR had shown an increase of only 38.23 % in the same time period which was well below 61.33 % of HMG Trial B. This overrode the theory that most of the aforementioned discrepancy was caused by ICF during the dissolution testing. Therefore, the higher result of HMG Trial B must have been either caused by more aITR or more ICs in the sample compared to HMG Trial HP. As DSC and XRPD analyses had shown, more aITR was most probably not the case. Thus, higher ICF during HMG of HMG Trial B was the most presumable explanation. Consequently, it could be stated that contradicting the assumption based on the results of the physico-chemical analysis, HMG Trial HP did not show superior dissolution compared to the reference sample in view of the full experiment. Its dissolution rate was faster during the first 30 min, but it was not possible to ascribe this to ICF due to the smaller particle size.

As the dissolution results allowed speculations regarding ICF in HMG Trial HP, ATR-FT-IR results were evaluated. Marker wave numbers of the samples compared to PMaITR and pure HP β CD are given in Table IV.15.. Nothing really stood out. As already seen for the other samples containing aITR, some signals of ITR had disappeared (e.g. around 1585 cm^{-1} and 1043 cm^{-1}). Still, it is noteworthy that PM of HP β CD and ITR was not evaluated and the chosen reference PMaITR only contained β CD. In Table IV.15., it can be seen that HP β CD only presented two wave bands in the regions of the marker wave numbers. Most of the selected markers were attributed to ITR anyway. Still, it was possible that detected changes for HMG Trial HP might have only been typical results for a PM of ITR and HP β CD. However, the general results of HMG Trial HP were very compliant with PMaITR. Since the presence of aITR in the samples generally interfered with a clear evaluation of possible ICs, using PMaITR as reference was considered ac-

ceptable. Accordingly, the only strong indicator that there were in fact ICs within HMG Trial HP was the improved dissolution compared to pure aITR.

Table IV.15. - ATR-FT-IR results of HMG Trial HP, evaluated by comparison with reference wave numbers; sd = \pm ; n = 3; *n = 5; if wave number markers were not detected in every single analysis, the percentage of their occurrence is given in brackets below.

	PM* PMaITR*	HPβCD	HMG Trial HP
Wave Numbers, cm⁻¹	1697.60 \pm 0.15 1698.89 \pm 0.33	X	1700.24 \pm 0.72
	1584.60 \pm 0.25 (80 %) 1585.76 \pm 0 (20 %)	X	X
	1551.18 \pm 0.13 1552.74 \pm 0.27	X	1552.78 \pm 0.08 (66.67 %)
	1509.80 \pm 0.23 1511.07 \pm 0.34	X	1511.03 \pm 0.06
	1451.20 \pm 0.16 (80 %) 1451.08 \pm 0.21	X	1450.96 \pm 0 (33.33 %)
	1270.96 \pm 0.98 (80 %) X	X	X
	1227.41 \pm 0.59 1228.55 \pm 0.62	X	1228.55 \pm 0.22
	1184.44 \pm 0.52 X	X	X
	1140.58 \pm 0 (20 %) X	X	1152.14 \pm 0.63
	1072.64 \pm 0.06 (40 %) 1077.55 \pm 0.36 (40 %)	1080.27 \pm 0 (33.33 %)	1079.87 \pm 0.01 (66.67 %)
	1043.15 \pm 0.11 1042.58 \pm 0.95 (40 %) X	X	X
	1028.45 \pm 1.81 (60 %)	1025.27 \pm 0.10	1028.20 \pm 0.77
	823.82 \pm 0.09 824.74 \pm 0.72	X	826.26 \pm 1.11

IV.6.4. Concluding Remarks about HMG Trial HP

The present chapter showed the investigation and interpretation of the melt processed sample HMG Trial HP. By these experiments, the suitability of a modified CD matrix was investigated compared to unmodified β CD. To reach a distinct conclusion from the presented data was challenging as HMG Trial HP did show positive properties. The ability to keep ITR amorphous after production had not

been as distinctively shown for β CD. The HMG procedure was stable. However, dissolution results were somewhat surprising with average ITR dissolution after 4 h of 18.79 % less than for the reference HMG Trial B. It was not distinguishable to what extent aITR and ICs influenced dissolution. But, when comparing the data to pure aITR or PMaITR, it seemed apparent that ICF had occurred during HMG for HMG Trial HP, however, not to the extent as for HMG Trial B. Within the first 30 min, HMG Trial HP showed superior dissolution, but it was also possible that this had been caused by a larger surface area. Nonetheless, the sample was subjected to stability experiments. Even so, at this point, a definite superiority of the CD derivative over the unmodified CD could not be ascertained.

IV.7. Influence of a Polymer Matrix in Hot-Melt Granulation

Usually, hot-melt procedures are operated using a polymer matrix due to thermoplastic properties of these substances (see section II.2.2.). Thus, HMG with a polymer was carried out for comparative reasons. SOLU (see section III.1.4.) was chosen as matrix. Since ICF could not occur during HMG with ITR and this substance, ATR-FT-IR results were used to examine the amorphous character of ITR and possible interactions with SOLU. Thus, in the present chapter, these results were integrated in the physico-chemical characterisation.

IV.7.1. Hot-Melt-Granulation Process Parameters and Processability

SOLU was especially developed for HME procedures. It shows excellent thermoplastic behaviour and is known to result in stable extrudate strands with a variety of different die structures. However, in this project, it served as an alternative matrix for the developed HMG process and was supposed to be processed as similar as possible to the reference sample HMG Trial B. That is why the utilisation of a die was waived. To keep the ratio of the PM comparable to the reference HMG Trial, a drug load of an approximate mass fraction of 38 % was chosen for the PM with SOLU and ITR. The investigated HMG process parameters are given in Table IV.16.. The flowability of PM with SOLU and ITR was very low with a maximum of 178.8 g/h in the hopper. This made it impossible to calibrate the desired feeding capacity of 200.6 g/h. During HMG, the feeder was set to 100 % throughout the whole procedure.

Table IV.16. - HMG processing parameters for HMG Trial SOLU.

HMG Trial	Z1, °C	Z2, °C	Z3, °C	Z4, °C	Z5, °C	Z6, °C	Z7, °C	ScS, rpm	Throughput, g/h	Torque, %
SOLU	100	130	170	180	180	180	180	150	max. 178.8	33

Figure IV.36. shows a picture of the product sampling of HMG Trial SOLU. Since no die was present to force material into a specific form, the pasty yield trooped up at the die position and could not pass the granulation heel slide. It was necessary to manually pull the product from the mTSE. Upon this, thin strands resulted. The thickness of these strands was dependent on the dragging force. During HME, it is important to obtain an extrudate strand with defined diameter and in regular shape. In the present HMG procedure, however, it was not feasible to deem this a priority. Even though the shown process did not really qualify as HMG, it was labelled accordingly as HMG Trial SOLU since the processing parameters were those of the previous HMGs. As it was impractical to keep the strand-pulling 100 % accurate during HMG, it was not possible to calculate the average throughput by measuring the yielded product over a defined time period. The process itself was stable with a torque of 33 %. This was a higher value than for the partially molten HMG runs, yet an anticipated result. The polymeric elasticity necessitates the higher shear energy not only for mixing and kneading but also for conveying the material along the barrel.

**Figure IV.36. - Product sampling during HMG process of HMG Trial SOLU.**

The obtained strands were greyish-brown in colour which raised the question of possible ITR degradation. Since SOLU is theoretically stable at the applied temperatures (see section III.1.4.) and particularly designed for mTSE operation and forming translucent extrudate strands, it was excluded that the change in colour

was caused by this component. The amorphisation of ITR had previously shown that the white-greyish powder morphed into a brown-greyish liquid and then after solidification and grinding, appeared in this colour-range without showing any signs of degradation in the HPLC. Therefore, it was most likely that this was causing the appearance of the strands. This was further elaborated in regard to the content analysis. More force was necessary for the manual grinding of this polymer sample as the obtained strands were quite stable.

IV.7.2. Physico-Chemical Characterisation of HMG Trial SOLU

Same as for all other HMG runs, HMG Trial SOLU was investigated for its physico-chemical properties. Figure IV.37. shows a SEM image of the sample. Smooth areas were visible as well as agglomerates. However, it could not be determined whether ITR was only dispersed in SOLU or if it was at least partially or fully dissolved in the polymer.

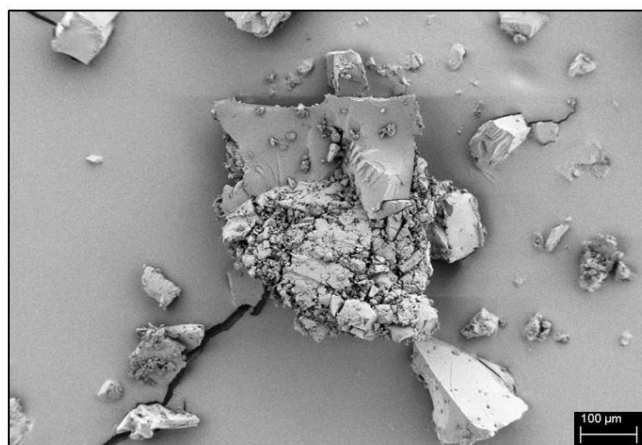


Figure IV.37. - SEM image of HMG Trial SOLU; bar = 100 μm.

The manual grinding yielded particles of different sizes. The determined x_{50} value was $190.1 \pm 18.2 \mu\text{m}$. This was the highest of all samples with an increase of 63.46 % compared to the largest sample so far (HMG Trial B). Furthermore, sd was quite high, undermining the fact that manual grinding of the material resulted in an uneven particle size distribution. To investigate the amorphousness of ITR, DSC and XRPD analysis were carried out. The DSC trace is shown in Figure IV.38.. No T_m of crystalline ITR was visible. Upon magnifying the DSC curve (data not shown), a very small, broad signal corresponding to the T_g became visible around 60 - 70 °C. This one signal might have hinted at the presence of a solid solution where ITR was completely dissolved in SOLU.

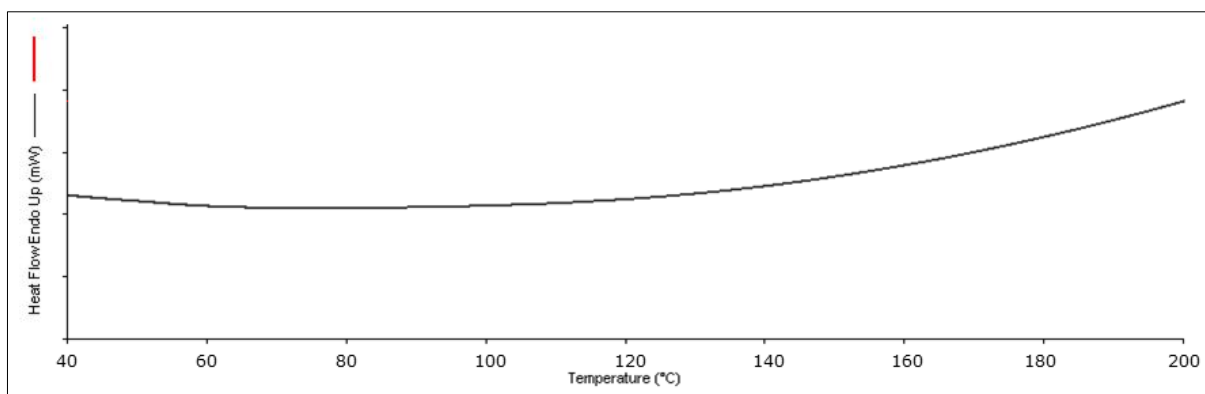


Figure IV.38. - Excerpt from DSC trace of HMG Trial SOLU; analysis conducted from 30 - 200 °C after 2 min holding period at 30 °C; heating rate of 3 K/min.

However, it was also a possibility that separate T_g s of ITR and SOLU had overlapped in the broad signal. This has previously been reported in the literature. Singh et al. found that the compression of a ITR/SOLU extrudate could cause phase separation which resulted in broadened T_g signals that appeared bimodal and overlapping when evaluating the derivative reversing heat flow [158]. In contrast to the DSC results shown for all other samples processed above ITR T_m (HMG Trial, A, B, WG and HP), no melting endotherm of ITR was detected for HMG Trial SOLU. The phenomenon of “cold crystallisation” was also not visible here, regardless of the DSC trace magnification. It was probable that the polymer matrix inhibited recrystallisation of ITR altogether and kept it stable in its amorphous state. The very low water content of the sample (0.395 %) might have been a supporting factor in this, since the presence of water often promotes recrystallisation.

The drug load of this sample was approximately 38 %. It is known that SOLU/ITR systems with high drug load can behave differently from systems with less ITR. Singh et al. studied extrudates with a 50 : 50 ratio of drug : polymer. They observed a melting endotherm of ITR at approximately 159 °C which they attributed to small crystalline regions in their sample. However, when investigating a DSC signal at approximately 110 °C which is in this thesis described as “cold crystallisation”, they experienced the same challenges as presented previously in section IV.4.2.. The very small signal was hard to regard as either endo- or exothermic depending on the baseline slope. Yet, they conducted high temperature XRPD measurements and proved the peak to be an exothermic crystallisation signal [158]. These results further supported the previously described ITR behaviour during DSC. Zhang et al. also observed a small ITR T_m in ITR/SOLU

extrudates which only appeared for the sample with 60 % drug load although no diffraction pattern was detectable in XRPD. However, they did not further characterise this occurrence in relation to “cold crystallisation” and concluded that ITR was partially crystalline in the extrudate but below the XRPD detection limit. For extrudates with a 40 % drug load, they did not observe any melting endotherms in DSC [62]. Taking all these literature results into account and comparing them to the results obtained in this work, it was concluded that given the drug load of 38 %, the SOLU matrix kept ITR immobile and hindered its recrystallisation. Nonetheless, it could not be determined if HMG Trial SOLU was in fact, a solid solution or a dispersion, whereby generally, the latter would have been much more likely. DSC results were also in agreement with the XRPD diffractogram (see Figure IV.39.). No diffraction pattern could be seen throughout the whole measurement range, only a halo was visible for both, pure SOLU (data not shown) and HMG Trial SOLU.

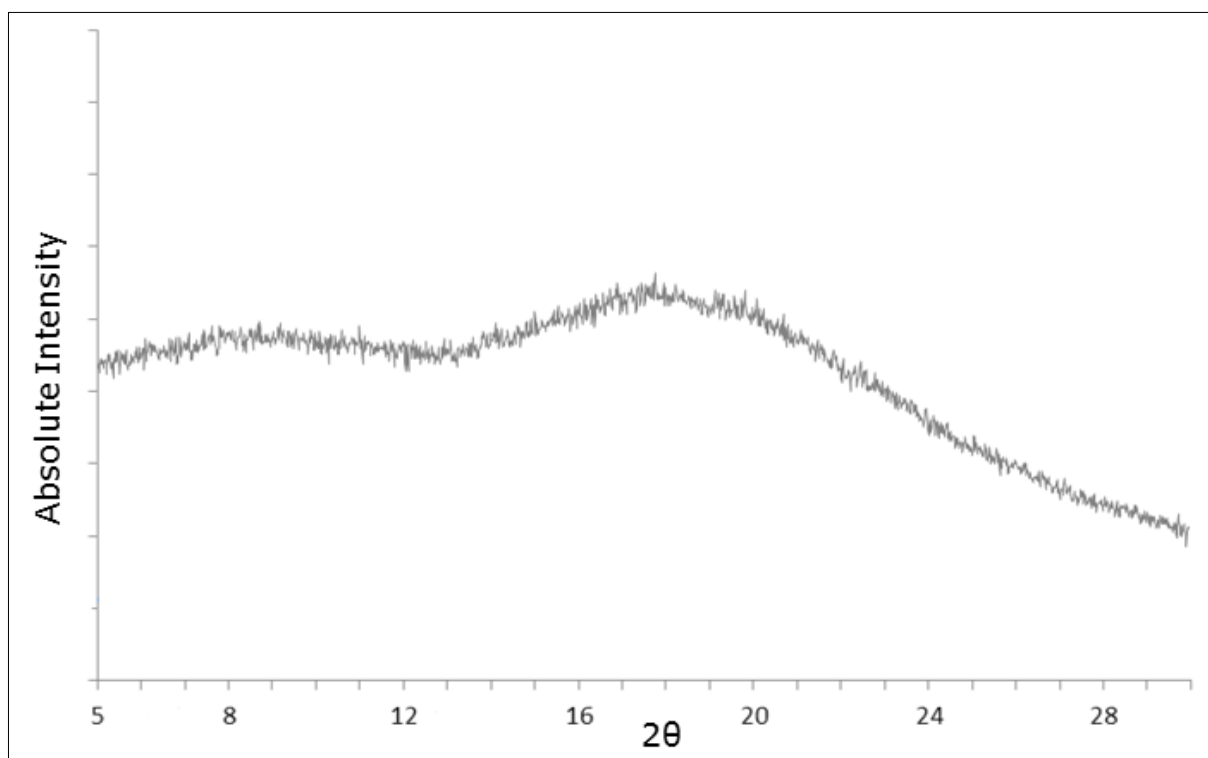


Figure IV.39. - Excerpt from XRPD diffractogram of HMG Trial SOLU.

For further characterisation of the interactions between SOLU and ITR, ATR-FT-IR measurements were conducted. Exemplary ATR-FT-IR spectra of pure SOLU, PM of SOLU and ITR as well as HMG Trial SOLU are presented in Figure IV.40.. Interactions between the polymer and the API were clearly visible. The signals

belonging to pure SOLU seemed more dominant in the melt processed sample in contrast to PM. This was strongly pronounced for the peak around 1634 cm^{-1} .

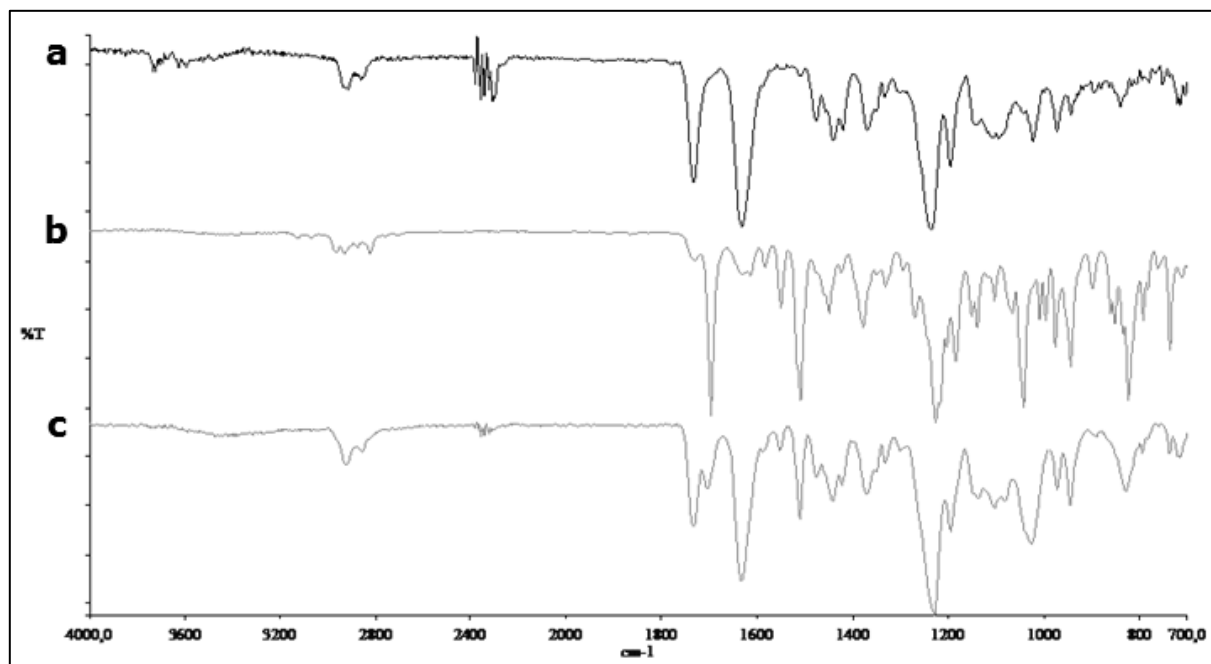


Figure IV.40. - Excerpts from ATR-FT-IR spectra of a) pure SOLU, b) PM of SOLU and ITR, c) HMG Trial SOLU.

The signal around 1705 cm^{-1} , corresponding to the ketone group of ITR, was shown as a strong peak for PM with the SOLU peak around 1735 cm^{-1} presenting only as a shoulder. This was reversed for HMG Trial SOLU with the peak around 1705 cm^{-1} being the shoulder of the more intense peak around 1735 cm^{-1} . Reasons for this behaviour could be found in the organised structure of the melt processed sample where there was a stable matrix surrounding and immobilising ITR or by the fact that aITR was present after HMG. Yet, the possibility that the analysed sample of HMG Trial SOLU consisted of a SOLU-rich phase could not be discarded. Singh et al. observed similar SOLU-rich regions during their analyses [158]. To exclude the possibility of ITR degradation being the cause for the colour change in the HMG product, content analysis was carried out in triplicate. The content of HMG Trial SOLU was $96.04 \pm 2.02\%$. The fed mixture showed an average ITR content of $97.51 \pm 5.58\%$ for ten samples drawn during the HMG procedure. This large sd could be ascribed to the poor flowability of the mixture which had supported segregation. Especially during the beginning of HMG procedure, the feedstock content was the lowest (87.92%) and then rose over time. Taking these feeder results into account, it was concluded that no product degradation seemed to have occurred for HMG Trial SOLU.

IV.7.3. Dissolution Results of HMG Trial SOLU

The solubilising property of SOLU is often exploited when applying SOLU as matrix in hot-melt processes. Figure IV.41. shows the results of the dissolution testing of HMG Trial SOLU which obviously showed the highest dissolution rate of all samples presented so far.

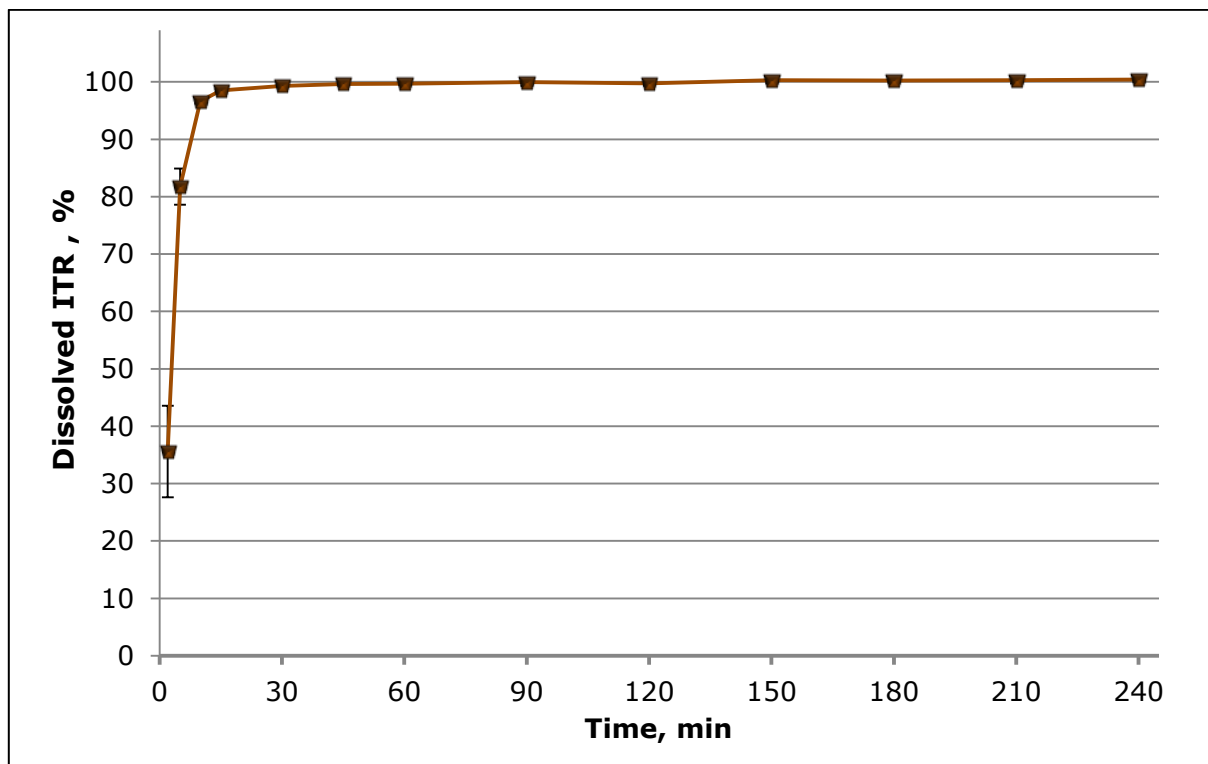


Figure IV.41. - Dissolution results of HMG Trial SOLU; n = 6; error bars = sd.

After 10 min, ITR dissolution had already reached 96.92 ± 0.38 %. After that point, the amount of ITR stayed on the same level until the end of the experiment (100.44 ± 0.41 %). In contrast to all other dissolution analyses, the dissolution medium became cloudy quite fast and stayed that way throughout testing. This was ascribed to SOLU forming solubilising micelles. The high sd for the first sampling point after 2 min (7.99 %) could be explained by the fact that prior to the analysis, all samples were manually given into the appropriate dissolution vessels as fast as possible before the autosampler was started. That way, there was a time inaccuracy of about 15 s between the investigated samples. Apparently, this short time frame had a large impact on the solubilisation velocity of SOLU. The absolute amount of dissolved ITR after 4 h was only 2.60 % higher compared to the reference sample HMG Trial B (97.89 %). Nevertheless, the dissolution rate of HMG Trial SOLU exceeded any other sample by far. These obtained dissolution results were well in line with other reports of SOLU and ITR.

Zhong et al. reported 98 % of dissolution for their ITR/SOLU tablet system in HCl pH 1.2, whereas Zhang et al. observed dissolution between 80 - 90 % for their ITR/SOLU extrudate with 40 % drug load in simulated gastric fluid without pepsin. It is noteworthy that the paddle rotation speed was 75 rpm in both of these references in contrast to 100 rpm used here [62,86].

IV.7.4. Concluding Remarks about HMG Trial SOLU

This chapter gave insights into the HMG production of a polymer-based sample and its characterisation. As section IV.7.1. highlighted, SOLU is not explicitly an excipient usable in HMG but rather appropriate for HME where the elastic material is forced through a die. The process itself was stable, yet it was constantly necessary to pull the product strands from the mTSE. Even though this could industrially be managed by employing a conveyor belt, the collecting of material directly at the end of the screws would hardly be manageable in a reproducible manner. The need for a die when working with SOLU became apparent.

Compared to all other samples described so far, the flowability of the SOLU PM was by far the worst, making it impossible to reach the desired throughput. The variability in feeding was resembled in the content of the produced sample. It is advisable to use separate feeding stations when processing ITR and SOLU. Thus, only speaking for the process itself, HMG Trial SOLU was inferior to the reference sample HMG Trial B. However, when interpreting the results of the physico-chemical analysis and especially from dissolution testing, it was clearly shown that the polymer managed to keep amorphous ITR stable at this given drug load. Additionally, it reached nearly quantitative dissolution only after 10 min. This was a definite acceleration compared to HMG Trial B (beginning of the plateau phase approximately at 120 min). In this regard, there was a very strong superiority of HMG Trial SOLU. The sample underwent stability testing to examine this effect over time. The scientific relevance of these results will be evaluated in the overall conclusion of this project (see section V.), not only because there are many literature references available for ITR/SOLU formulations but also regarding the likelihood of a SOLU-based formulation being used in a marketed product as this - to the best of the author's knowledge - has not been accessible up to date.

IV.8. Comparison of Hot-Melt Granulation Procedure against the Marketed Formulation

The marketed formulation, Sempera[®] capsules (see section III.1.2) (SEMP), was investigated as comparison against the reference sample HMG Trial B. Due to the nature of the marketed product (coated sugar spheres) only chosen technologies were carried out for sample characterisation. The most vital experiment for the comparison with HMG Trial B was the dissolution analysis.

IV.8.1. Physico-Chemical Characterisation of SEMP and Pellet Dissolution

Since SEMP consists of sugar beads filled in hard gelatin capsules, the pellets were emptied from the capsule container for all analyses to increase comparability to the reference. That way, the gelatin capsule could not interfere, especially during dissolution testing. Weighing of the capsule content gave an average filling mass of 464 mg per capsule, corresponding to the declared ITR content of 100 mg. This was a drug load of 21.55 %. Figure IV.42. shows a SEM picture of a SEMP pellet. The PEG seal coating was visible on the pellet surface. Most of the coating appeared intact. Upon strong magnification, very small ruptures became visible. Generally, the surface of the pellet appeared smooth. Based on this image, the analysed pellet had a diameter of about 968 μm which was in the range described in the corresponding patents (see section III.1.2.).



Figure IV.42. - SEM image of SEMP pellet; bar = 100 μm .

The small tears in the seal coating should not have influenced product quality as it had to be assumed that the ITR/HPMC coating of the spheres should have been intact. This had to be suspected because SEMP is a marketed formulation

with a validated shelf life and the investigated sample shown in Figure IV.42. was emptied from a recently obtained hard gelatin capsule. Results of DSC analysis of SEMP are given in Figure IV.43. and Table IV.17..

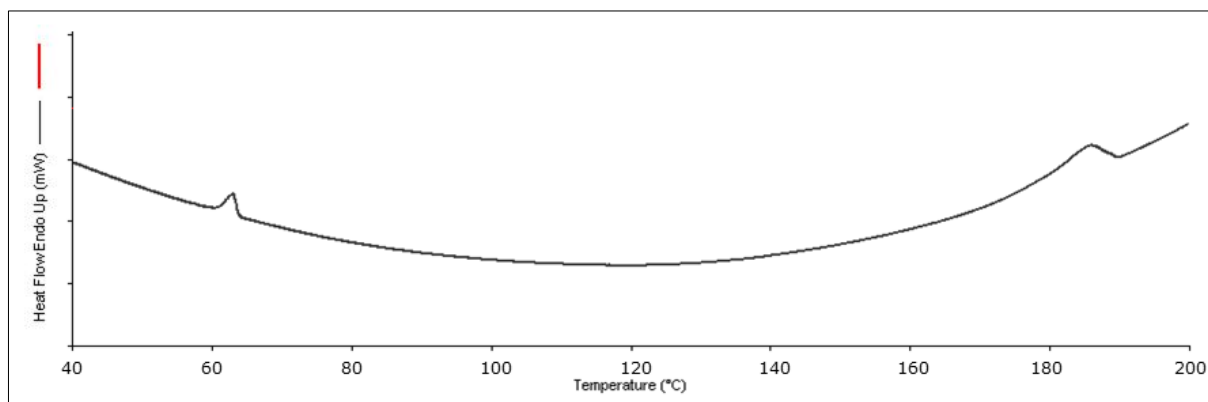


Figure IV.43. - Excerpt from DSC trace of SEMP; analysis conducted from 30 - 200 °C after 2 min holding period at 30 °C; heating rate 3K/min.

Two endothermic signals were visible at 62.97 °C and 185.62 °C. The first peak corresponded to T_m of the PEG seal coating. Unfortunately, this signal would most likely have concealed T_g of aITR. The signal at 185.62 °C was ascribed by Kapsi et al. to T_m of crystalline ITR dispersed in the HPMC coating [159]. However, it seemed more likely that this endothermic event corresponded to T_m of the sucrose spheres. The defined T_m of sucrose is given in the literature as 185.5 °C [160]. This fit the DSC results perfectly and was more probable than a shift in T_m for ITR of about 20 °C which – to the best of the author’s knowledge – has not been reported regardless of the excipients used. The width of the sucrose melting peak was obtained by manual integration which caused an inaccuracy. It could not be excluded that the sucrose peak might have masked an earlier melting of ITR around its usual T_m , but again, it seemed unlikely due to the large difference in temperature.

Table IV.17. - DSC signals detected for SEMP.

	SEMP	
Signal, °C		
Onset	60.75	179.07
Peak	62.97	185.62

Concluding these findings, no T_m distinctively corresponding to ITR was observed regardless of the magnification of the DSC trace. No sign of “cold crystallisation” was visible. It seemed that the HPMC film matrix kept immobilised ITR in its amorphous state and hindered recrystallisation.

Figure IV.44. presents the results of the dissolution testing of SEMP. The dissolution profile obtained showed dissolution of 98.49 ± 4.29 % after 4 h which corresponded to the full ITR amount in the sample. The curve progression during the first 30 min could be explained by the SEMP formulation.

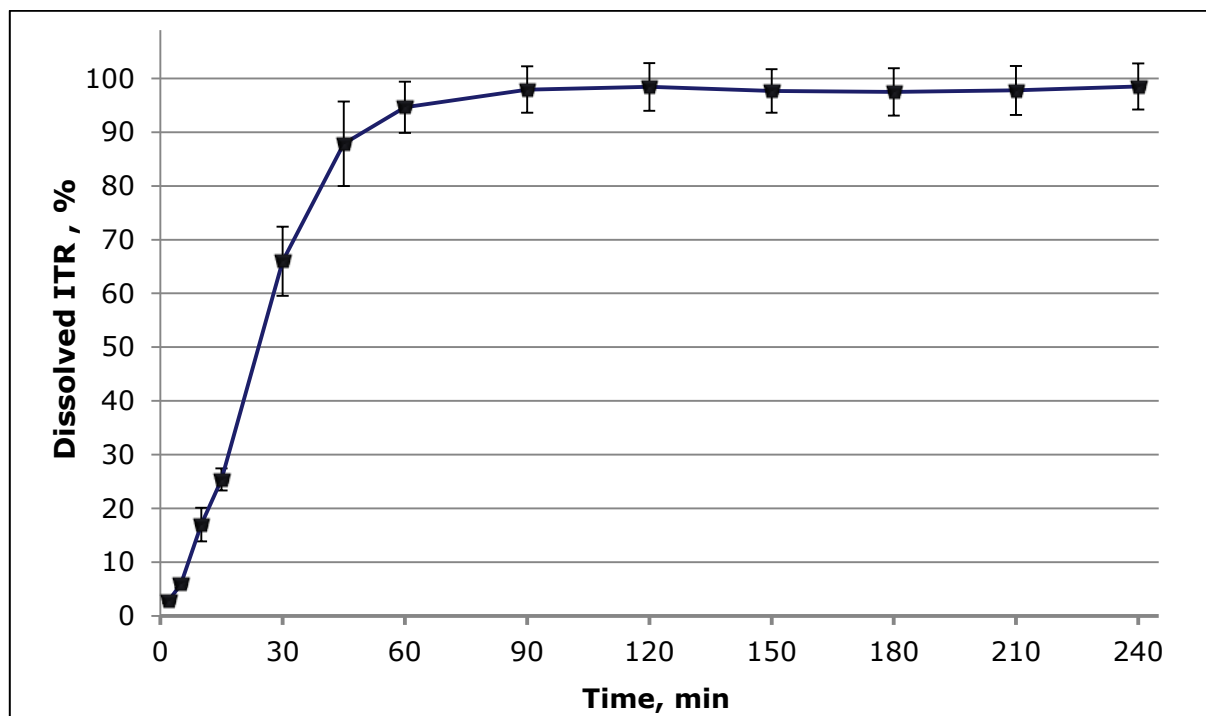


Figure IV.44. - Dissolution profile of SEM; n = 6; error bars = sd.

In the beginning, there was a lag time of about 5 min at which point the detected ITR content was 5.90 ± 0.72 %, corresponding to the dissolving of the PEG seal coating. After 10 min, 17.01 ± 3.13 % of ITR were dissolved, indicating that the HPMC/ITR coating began to dissolve. The curve now showed a steep rise and reached dissolution of 94.63 ± 4.74 % after 60 min. Here, the rest of the wetted ITR in the HPMC film matrix dissolved. From 60 min on, the dissolution profile reached a plateau and fluctuated around 97 - 99 % for the rest of the experiment. This was in excellent agreement with the literature. Kapsi et al. investigated Sporanox[®] dissolution in 900 mL simulated gastric fluid at pH 1.4 with the paddle apparatus at 100 rpm and observed about 15 % of dissolution after 10 min and about 70 % after 30 min (compared to 66.00 ± 6.42 % for SEMP). After 60 min, about 90 % of ITR was dissolved in their analysis [159]. Sarnes et al. investigated Sporanox[®] dissolution over 60 min under the same conditions as shown in this work. They also experienced a lag time which they explained with the time necessary for the PEG seal coating to dissolve [161]. The curvature of their investigated sample was similar to SEMP. However, they reached 100 % of

dissolution at 30 min and 120 % after 60 min which raised questions about quantification method or if their investigated sample might have contained more than 100 mg of ITR. Comparing SEMP dissolution with the reference sample HMG Trial B, it could be stated that the cumulative amount of dissolved ITR after 4 h was on the same level (98.49 ± 4.29 % vs. 97.89 ± 2.39 %). The beginning of the dissolution differed. The dissolved amounts of ITR for HMG Trial B against SEMP during the first 60 min of the experiment are shown in Table IV.18..

Table IV.18. - Amount of dissolved ITR during dissolution testing for HMG Trial B (n = 2; error bars = min/max) and SEMP (n = 6; error bars = sd).

Sampling point, min	Dissolved ITR of HMG Trial B, %	Dissolved ITR of SEMP, %
2	9.72 ± 2.85	2.83 ± 0.44
5	22.15 ± 3.22	5.90 ± 0.72
10	34.78 ± 2.90	17.01 ± 3.13
15	45.96 ± 5.23	25.39 ± 2.03
30	65.55 ± 2.01	66.00 ± 6.42
45	76.75 ± 1.67	87.85 ± 7.88
60	91.90 ± 2.24	94.63 ± 4.74

HMG Trial B showed faster dissolution until 30 min. At this time, both formulations showed average dissolution of about 65 %. Relatively seen, HMG Trial B exhibited 81.02 % more dissolution than SEMP after 15 min which could be of therapeutic value. SEMP reached the plateau phase faster than HMG Trial B.

IV.8.2. Concluding Remarks about SEMP

This chapter presented the evaluation of the marketed formulation SEMP and the comparison against reference sample HMG Trial B. The dissolution results of SEMP were as anticipated and showed quantitative ITR dissolution within 60 min. This was expected from a marketed formulation. The dissolution profile could be explained by the specially formulated sugar spheres. HMG Trial B showed superior dissolution during the first 15 min of the experiment. Remembering the proclaimed rapid absorption of ITR from the GIT this could be of therapeutic interest. Apart from this, it can be said that SEMP is a complex pharmaceutical product which is produced in various manufacturing steps that include the use of organic solvents (see section III.1.2.). This was not the case for HMG Trial B that

combined the mixing of the excipients with the continuous HMG process plus crushing and sieving. All of these processes could be combined with the right equipment. Additionally, the drug load of SEMP was approximately 22 % compared to HMG Trial B with about 38 % which was 73 % higher. Nevertheless, dissolution properties of SEMP were satisfactory and the DSC analyses did not show signs of crystalline ITR. Therefore, SEMP was subjected to testing of storage stability and will be taken up again in section V. for the overall discussion and de-nouement of this work.

IV.9. Ternary Additives as Possible Dissolution Enhancers

CDs do not show good thermoplastic behaviour which complicates their processing within mTSE. Thus, most research conducted in the field of hot-melt processes with CDs utilises ternary additives in the formulations such as polymers to increase the operability and to potentially further increase drug bioavailability and/or dissolution [63,87]. Section IV.7. clearly showed the fastest dissolution rate for HMG Trial SOLU, judging from the beginning of the plateau phase in the dissolution profile. Although HMG Trial B, the HMG sample with the most sufficient product properties, showed nearly quantitative ITR dissolution after 4 h, it was still to be determined if a ternary additive could further enhance the dissolution rate within the first 30 min to a level comparable to SEMP and HMG Trial SOLU.

The subsequent chapter highlights the influence of ternary additives on HMG samples. In that regard, the sugar alcohol xylitol was employed to investigate the phenomenon of API displacement from the CD cavity. HMG formulations containing different ratios of xylitol were investigated. Secondly, two typical HME/HMG polymers, PEG 6000 and HPMC 4000 were used and evaluated in binary and ternary form. Due to technical issues as well as time constraints, not all of the samples of the following case studies could be evaluated by XRPD, SEM and for their β CD content. Thus, these experimental results were omitted in the following chapter, even if they were carried out. By this, the same argumentative basis could be applied to all investigated specimen. Foundation of the HMG process were the parameters of the reference sample HMG Trial B.

IV.9.1. Case Study Polyethylene Glycol 6000

Due to its frequency of occurrence in research about hot-melt processes with ITR, PEG 6000 was chosen to be investigated in one binary and two ternary formulations with ITR and β CD.

IV.9.1.1. Preparation and Behaviour During Hot-Melt-Granulation of Polyethylene Glycol 6000 Blends

Three different PMs were prepared. Firstly, a binary mixture of ITR and PEG 6000 with a drug content of about 38 % in mass corresponding to the binary formulations with β CD and ITR (HMG Trial PEG), and secondly, two ternary mixtures. These contained mass fractions of 10 % and 20 % PEG 6000 (HMG Trial PEG10 and PEG20), referring to the overall mixture, e.g. PM in the stoichiometric ratio of 1:1 of ITR and β CD was prepared, resembling mass fractions of 80 % or 90 % and was then added up to 100 % with PEG 6000. That way, HMG Trial PEG10 and PEG20 showed ideal drug content of 33.54 % and 30.52 %, respectively. HMG parameters of all three HMG runs of this case study are shown in Table IV.19..

Table IV.19. - HMG parameters of the case study with PEG 6000.

HMG Trial	Z1, °C	Z2, °C	Z3, °C	Z4, °C	Z5, °C	Z6, °C	Z7, °C	ScS, rpm	Throughput, g/h	Torque, %
PEG	100	130	170	180	180	180	180	150	169.9	3
PEG 10	100	130	170	180	180	180	180	150	90.0	8.5
PEG 20	100	130	170	180	180	180	180	150	213.3	13

The PMs did not show similar flowability compared to the binary ITR/ β CD mixture. The maximum average throughput during calibration of PEG was 299 g/h, for PEG10 311 g/h and 324 g/h for PEG20. Interestingly, HMG Trial PEG10 showed the lowest actual HMG throughput by far with only 90 g/h. Only HMG Trial PEG20 could be produced with a throughput above 200.6 g/h which was the target (see section IV.4.). PEG 6000 melts at about 60 °C, so during the production of HMG Trial PEG, the whole mixture was liquefied, dripped from mTSE and hardened in the steel bowl where samples were collected. This did not meet the general definition of HMG. However the sample was referred to as HMG Trial PEG. The low melt viscosity explained the very low torque of 3 %. Up-

on leaving mTSE, the product was bubbling as if water vaporisation had not been possible through the ventilation port. Otherwise, the process was stable. HMG Trial PEG10 and PEG20 exhibited higher torques due to β CD in the mixture which increased the formulation's viscosity. Both of these HMG runs appeared slightly inhomogeneous upon leaving mTSE with product that appeared either as binary ITR/ β CD granules or seemed liquefied due to higher percentage of PEG 6000. The ventilation port got stuck a few times during the procedure which forced the water to exit the barrel at the granulation heel slide. Nevertheless, the general processes of the ternary mixtures were stable.

IV.9.1.2. Physico-Chemical Characterisation of HMG Trial PEG, PEG10 and PEG20

The samples in this case study were evaluated for ITR crystallinity by DSC analysis. Moreover, particle size distribution and ITR content were examined. x_{50} values of the three different HMG runs after crushing and sieving are given in Table IV.20..

Table IV.20. - Results of particle size measurements for the case study PEG; n = 3; \pm represents sd.

	HMG Trial PEG	HMG Trial PEG10	HMG Trial PEG20
x_{50} , μm	161.8 \pm 28.6	175.4 \pm 13.0	176.1 \pm 23.1

Compared to all other previous HMG runs, the PEG 6000 samples showed higher x_{50} values. This could influence ITR dissolution by decreasing the dissolution rate. Additionally, sd was quite high for all three HMG runs. Manual crushing and sieving did not yield particles of a precise size. However, comparing HMG Trial PEG, PEG10 and PEG20 amongst each other, no substantial difference was detected. Thus, differences in dissolution between these three could not be ascribed to differences in particle size.

Results of the DSC analysis are shown in Figure IV.45. and Table IV.21.. PEG 6000 has a defined T_m of approximately 60 °C. This endothermic signal was visible for all three samples. The most pronounced peak was shown for the binary HMG run due to the high PEG 6000 content. All melting signals of PEG 6000 did not appear like one distinctive peak. HMG Trial PEG10 seemed to present two overlapping signals and HMG Trial PEG and PEG20 exhibited shoulders to the peaks. There were two different explanations for this. Firstly, it is known that

PEG 6000 crystallises by forming lamellae that either have their chains folded once or twice or are fully extended.

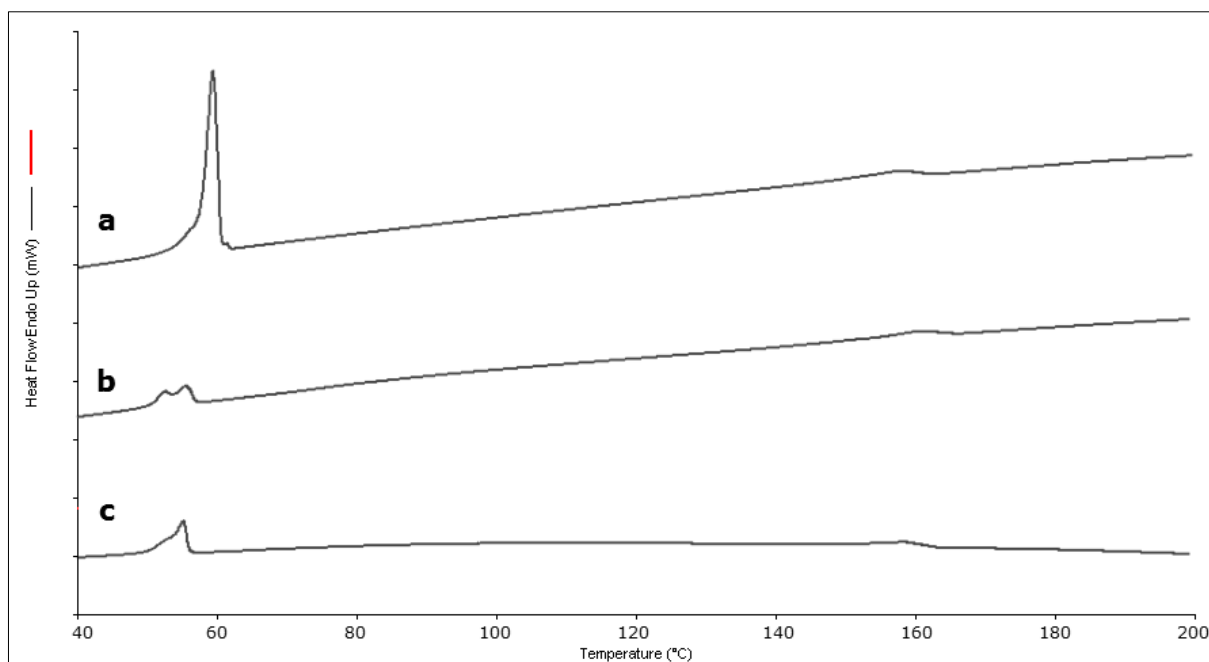


Figure IV.45. - Excerpts from DSC traces of a) HMG Trial PEG, b) HMG Trial PEG10, c) HMG Trial PEG20; analysis conducted from 30 - 200 °C after 2 min holding period at 30 °C; heating rate 3 K/min.

Consequently, when melting semi-crystalline PEG 6000, the different folding modifications can exhibit different T_m s. Wang et al. reported endothermic peaks at 56 °C, 59 °C and 63 °C corresponding to that [162]. This hypothesis might explain why HMG Trial PEG10 showed the most unpronounced T_m . Having the lowest PEG 6000 content, it could have been possible that the least amount of PEG 6000 had recrystallised after HMG, giving way to higher amounts of semi-crystalline lamellae in the system. This explanation also accounted for the results of HMG Trial PEG. Due to the large PEG 6000 content and the lack of a third component that might have hindered recrystallisation, T_m around 60 °C seemed the most distinct.

Table IV.21. - DSC signals corresponding to ITR melting for the case study PEG.

	HMG Trial PEG	HMG Trial PEG10	HMG Trial PEG20
ITR signal, °C			
Onset	151.85	154.41	150.64
Peak	155.71	160.13	157.92

Nevertheless, the second possibility could have been that ITR T_g which also lies around 60 °C overlapped with PEG 6000 melting and caused the peak shoulders. Wang et al. found that at drug loads of 40 % ITR in solid dispersions with

PEG 6000, only one melting peak for PEG 6000 was detectable. This was explained by ITR's ability to influence the folding properties of PEG 6000 [162]. All three PEG 6000 samples exhibited broad melting endotherms corresponding to ITR. From the detected temperatures, this should have been the earlier mentioned polymorph. Upon magnifying the DSC traces, no signals corresponding to "cold crystallisation" or liquid mesophases of ITR were observed. Despite that, it has been reported that ITR shows this phenomenon in PEG 6000 at higher concentrations [162]. Probably it was the case that the "cold crystallisation" signals were too small to be detected by the utilised DSC method. No ITR T_m around 164 - 167 °C was detected which would have suggested stable crystalline ITR in Form I. Unfortunately, XRPD analysis could not be conducted to further investigate the possible ITR crystallinity in the HMG samples with PEG 6000.

When working with ternary PMs, segregation of the components is always an important issue. That is why Figure IV.46. not only shows the determined ITR contents of HMG Trial PEG, PEG10 and PEG20, but also the average ITR contents during mTSE feeding. That way, variations in final content may be explained.

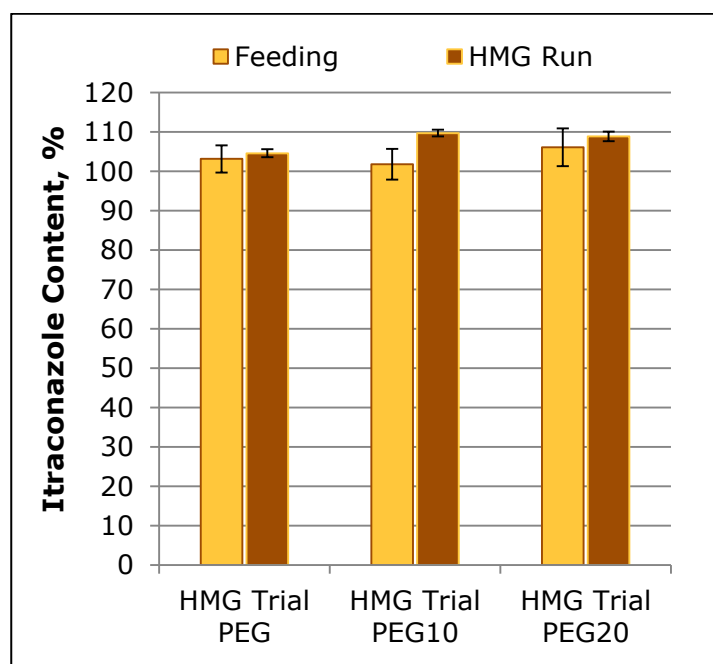


Figure IV.46. - ITR content of HMG Trial PEG, PEG10 and PEG20 during feeding (n = 10) and of the HMG yield (n = 3); error bars = sd.

For all three samples no ITR degradation was detectable. ITR content of HMG Trial PEG, PEG10 and PEG20 was 104.56 ± 1.02 %, 109.69 ± 0.85 % and 108.83 ± 0.83 %, respectively. ITR content was implausibly high for all three samples. At this point, ITR contents during feeding had to be evaluated. For

HMG Trial PEG, the average content of fed ITR was 103.12 ± 3.48 %. For HMG Trial PEG10 and PEG20 it was 101.77 ± 3.93 % and 106.07 ± 4.83 %. All three HMG runs showed high variations during feeding, especially considering that this value was derived from ten samples throughout the whole HMG process. For all PMs, the average ITR content was above 100 %. It seemed that particularly during the filling phase, PEG 6000 had segregated from the mixtures and had been hot-melt granulated predominantly. That way, upon product collecting, too much of PEG 6000 had already been processed. This was in agreement with the observations described in section IV.9.1.1.. The lowest variation was shown for the binary formulation which could be expected. Nonetheless, obviously, it is advised to use separate feeding stations for co-processing these two substances.

IV.9.1.3. Dissolution Results and Inclusion Complex Formation Evaluation of HMG Trial PEG, PEG10 and PEG20

Dissolution results of HMG Trial PEG, PEG10 and PEG20 are given in Figure IV.47.. Interestingly, even though all of these samples were processed above T_m of ITR, the reached dissolution was well beyond the level of aITR. The only sample to reach dissolution this low after the same heat treatment had been HMG Trial WG (see section IV.5.).

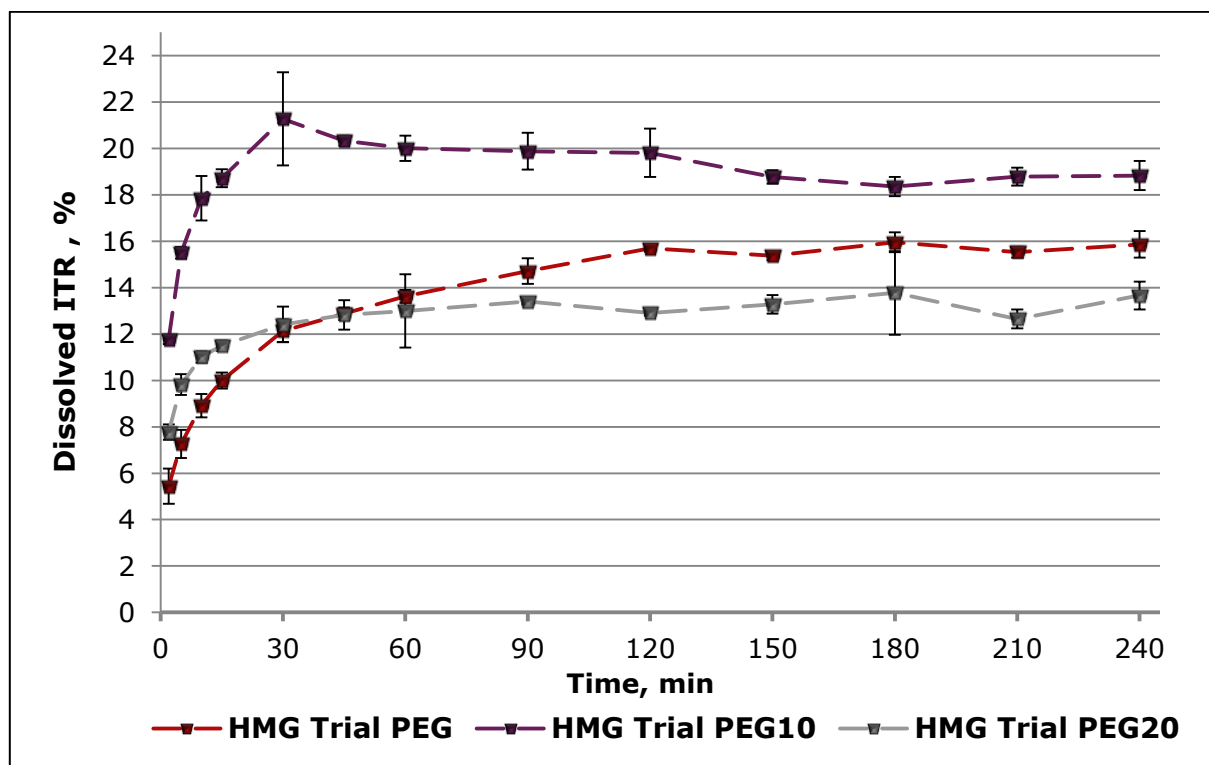


Figure IV.47. - Dissolution results of the case study PEG; n = 3; error bars = sd.

In the previous subsection, it was not possible to determine whether ITR was completely amorphous in these PEG 6000 systems. The dissolution results now indicated that this was not the case (maximum dissolution of 18.82 ± 0.63 % after 4 h for HMG Trial PEG10). This was only 19.23 % of the reference amount by sample HMG Trial B. It appeared as if PEG 6000 had not improved ITR dissolution at all, but rather supported the production of inhomogeneous melt-granules. During the beginning of dissolution, HMG Trial PEG gave the lowest amount of dissolved ITR (10.00 ± 0.34 % after 15 min). This could be explained by the fact that the other two samples contained β CD which most likely had resulted in some ICF during HMG. From 30 min on, the binary formulation HMG Trial PEG showed a higher dissolution rate than HMG Trial PEG20 which had already reached a plateau. HMG Trial PEG exhibited a slow rise between 30 - 120 min from where on its ITR dissolution fluctuated around 15.50 % before finishing at 15.86 ± 0.58 % after 4 h. This low rise in curvature could have been caused by ITR diffusion out of the crystalline PEG 6000 matrix.

Interestingly, the highest dissolution and dissolution rate were shown by HMG Trial PEG10 that had combined β CD and the lowest amount of PEG 6000. Compared to HMG Trial PEG (13.66 ± 0.59 % after 4 h), HMG Trial PEG10 showed 37.78 % enhanced ITR dissolution. Nevertheless, the presence of PEG 6000 during HMG did not present the desired effects. Janssens et al. made similar experiences for polymeric mixtures of PVPVA 64 and PEG 6000. They found that the addition of PEG 6000 to mixtures with 20 % ITR did not show any enhancing effect during dissolution testing. They only detected dissolution improvement for solid dispersions containing at least 40 % of ITR [163].

The presented dissolution results showed that PEG 6000 was not helpful in keeping ITR amorphous as well as in improving the dissolution and solubility rate. Still, the absolute dissolution and the fast dissolution rates for both samples containing β CD showed the likelihood of ICF during HMG. Thus, ATR-FT-IR results were evaluated for further indications of this. It has to be stated however, that the addition of a third component to the mixture aggravated the interpretation of these data even further. Results of the ATR-FT-IR investigation are given in Table IV.22..

Table IV.22. - ATR-FT-IR results of the case study PEG 6000, evaluated by comparison with reference wave numbers; sd = as \pm ; n = 3; *n = 5; if wave number markers were not detected in every single analysis, the percentage of their occurrence is given in brackets below.

	PM* PMaITR*	Pure PEG 6000	HMG Trial PEG	HMG Trial PEG10	HMG Trial PEG20
Wave Numbers, cm ⁻¹	1697.60 \pm 0.15 1698.89 \pm 0.33	X	1698.03 \pm 0.20	1698.78 \pm 0.13 (66.67 %)	1698.72 \pm 0.03 (66.67 %)
	1584.60 \pm 0.25 (80 %) 1585.76 \pm 0 (20 %)	X	X	X	X
	1551.18 \pm 0.13 1552.74 \pm 0.27	X	1551.99 \pm 0.11	X	X
	1509.80 \pm 0.23 1511.07 \pm 0.34	X	1510.73 \pm 0.20	1511.37 \pm 0.01	1511.11 \pm 0.05 (66.67 %)
	1451.20 \pm 0.16 (80 %) 1451.08 \pm 0.21	1466.71 \pm 0.03	1466.60 \pm 0.06	1466.20 \pm 0 (33.33 %)	X
	1270.96 \pm 0.98 (80 %) X	1279.53 \pm 0.11	1278.89 \pm 0.11	1277.94 \pm 0 (33.33 %)	X
	1227.41 \pm 0.59 1228.55 \pm 0.62	1241.31 \pm 0.10	1240.71 \pm 0.08	1230.91 \pm 2.14 (66.67 %)	1229.21 \pm 0.03
	1184.44 \pm 0.52 X	X	1184.84 \pm 0 (33.33 %)	X	X
	1140.58 \pm 0 (20 %) X	1147.40 \pm 0.14	1147.90 \pm 0.06	1149.28 \pm 0.39 (66.67 %)	1149.97 \pm 0 (33.33 %)
	1072.64 \pm 0.06 (40 %) 1077.55 \pm 0.36 (40 %)	1060.21 \pm 0.04	1060.69 \pm 0.07	X	1073.66 \pm 6.47
	1043.15 \pm 0.11 1042.58 \pm 0.95 (40 %) X	X	X	X	1043.19 \pm 0 (33.33 %)
	1028.45 \pm 1.81 (60 %)	X	X	1025.50 \pm 0.50	1027.82 \pm 0 (33.33 %)
	823.82 \pm 0.09 824.74 \pm 0.72	X	825.44 \pm 0.06 (66.67 %)	X	X

Pure PEG 6000 showed wave bands in regions that overlapped with chosen marker wave bands, such as around 1466 cm⁻¹, 1279 cm⁻¹, 1241 cm⁻¹ or 1060 cm⁻¹. Comparing the results of pure PEG 6000 with HMG Trial PEG, no substantial shifts in the given wave numbers were seen. This hinted at low interactions between the polymer and ITR. As the DSC analyses had already shown, PEG 6000 and ITR did not form a solid solution. Consequently, this was expected. This lack of interaction with APIs has been reported for PEG 6000 with other drugs as well, such as indomethacin or zolpidem [91,164].

It was hard to determine if ITR was amorphous in the samples due to marker wave numbers such as 1270 cm^{-1} and 1140 cm^{-1} overlapping with pure PEG 6000 signals. Taking a look at HMG Trial PEG10 and PEG20, it was interesting that the signal around 1698 cm^{-1} was not detected in all single measurements. This hinted at PEG 6000 chains shielding the ketone group. Apart from this, it was intriguing that there were differences observed between these two samples. No peak was observed for HMG Trial PEG10 around 1072 cm^{-1} in contrast to HMG Trial PEG20. Still, the high sd ($1073.66 \pm 6.47\text{ cm}^{-1}$) showed that no distinct wave band had been detected. Rather, either a peak around 1060 cm^{-1} originating from PEG 6000 or the ITR peak around 1077 cm^{-1} were observed. Both samples lacked the signal around 825 cm^{-1} . This had not been seen for any previously studied sample. Probably, PEG 6000 chains shielded this functional group from the laser beam as well. Generally, ATR-FT-IR results failed to determine ICF because of the various possible interferences that prevented a profound statement.

IV.9.1.4. Outcome of Case Study Polyethylene Glycol 6000

After close investigation of the samples it can be stated that PEG 6000 did not positively influence the developed HMG formulation. The solubility rate and absolute ITR dissolution were not substantially enhanced, neither by the binary nor the ternary formulations. PEG 6000 failed to keep ITR amorphous. Processing with the mTSE was mostly stable, however, it was shown that the PMs had segregated in the feeder.

IV.9.2. Case Study Hydroxypropyl Methylcellulose

As reported in section III.1.2., Sporanox[®] capsules are coated with a HPMC 2910/ITR solution. Therefore, much research has been conducted examining ITR together with HPMC 2910 [60,108,109,165]. In this project, another common quality of HPMC, HPMC 4000, was investigated as possible ternary additive during HMG. HPMC 4000 can be used as matrix component e.g. in tablets for sustained release due to its swelling in water. Furthermore, it can be utilised as seal coating for IR tablets. Thus, the addition of mass fractions of 10 % and 20 % of HPMC 4000 (HMG Trial HPMC10 and HPMC20) to the ITR/ β CD blend was examined. For comparative purposes, a binary formulation of HPMC 4000 and ITR was also hot-melt granulated (HMG Trial HPMC). Foundation of the HMG process was again the reference sample HMG Trial B.

IV.9.2.1. Preparation and Behaviour During Hot-Melt Granulation of Hydroxypropyl Methylcellulose Blends

Same as for the case study with PEG 6000, three different powder blends were prepared. Firstly, a binary formulation of HPMC 4000 and ITR with a drug load of approximately 38 %. Secondly, mass fractions of 10 % and 20 % of HPMC 4000 were added to a binary blend of ITR and β CD, resulting in theoretical drug loads of 34.47% and 30.55 %. HMG parameters of all three HMG runs of this case study are given in Table IV.23..

Table IV.23. - HMG parameters of the case study with HPMC.

HMG Trial	Z1, °C	Z2, °C	Z3, °C	Z4, °C	Z5, °C	Z6, °C	Z7, °C	ScS, rpm	Throughput, g/h	Torque, %
HPMC	100	130	170	180	180	180	180	150	200.7	9
HPMC 10	100	130	170	180	180	180	180	150	165.2	6
HPMC 20	100	130	170	180	180	180	180	150	234.7	13

Flowability of all three blends was sufficient compared to PM of ITR and β CD. This resulted in generally satisfactory throughputs. However, HMG Trial HPMC10 showed the lowest average of the three mixtures with 165.2 g/h. During HMG of the binary formulation, the screws were screeching. HPMC 4000 was neither melted nor had become more elastic at the operating temperatures. The yielded product appeared similar to binary ITR/ β CD granules. HMG Trial HPMC10 seemed inhomogeneous during HMG. While in the beginning, the product was powder-like, in the end it looked more like the binary product, partially molten granules. This was in agreement with the lower throughput that could have also indicated segregation of PM. Screw screeching was not as pronounced for this sample. This was also the case for HMG Trial HPMC20 which exhibited the highest torque during HMG. During this HMG run, the ventilation port got stuck a few times during operating. Otherwise the process was stable. Generally, it was possible to melt-granulate the binary and ternary formulations with HPMC 4000. Nevertheless, screeching of the screws indicated that the molten ITR's lubricating effect was not as sufficient as had been observed for the binary reference formulation, HMG Trial B.

IV.9.2.2. Physico-Chemical Characterisation of HMG Trial HPMC, HPMC10 and HPMC20

The three HPMC formulations were investigated for their physico-chemical properties. Table IV.24. presents the mean x_{50} values for HMG Trial HPMC, HPMC10 and HPMC20. The binary HPMC 4000 formulation showed the largest x_{50} with $162.2 \pm 1.1 \mu\text{m}$. This could potentially slow down ITR dissolution rate. The x_{50} value of HMG Trial HPMC10 showed quite high sd of $8.00 \mu\text{m}$. This could have indicated inhomogeneities in the product.

Table IV.24. - Results of particle size analysis for case study HPMC 4000; n = 3; \pm = sd.

	HMG Trial HPMC	HMG Trial HPMC10	HMG Trial HPMC20
x_{50} , μm	162.2 ± 1.1	137.0 ± 8.00	91.1 ± 4.3

To investigate the possible amorphousness of ITR, DSC measurements were carried out. The DSC traces of the three samples are given in Figure IV.48., the DSC signals corresponding to melting of ITR in Table IV.25.. All three HPMC samples showed two T_m of ITR, corresponding to the most stable crystalline form and the defined polymorph. Upon magnifying the DSC traces (data not shown), signs of "cold crystallisation" became visible slightly above $100 \text{ }^\circ\text{C}$ as well as endothermic signs of the liquid mesophases of ITR around $70 \text{ }^\circ\text{C}$ and between $80 - 90 \text{ }^\circ\text{C}$.

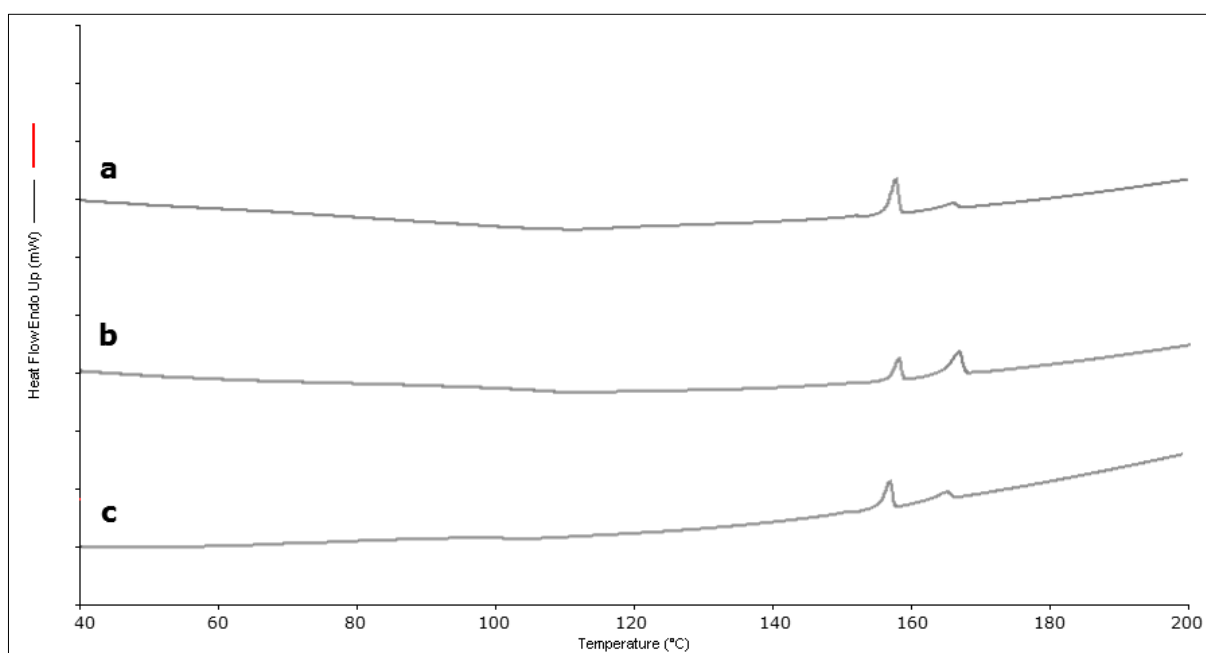
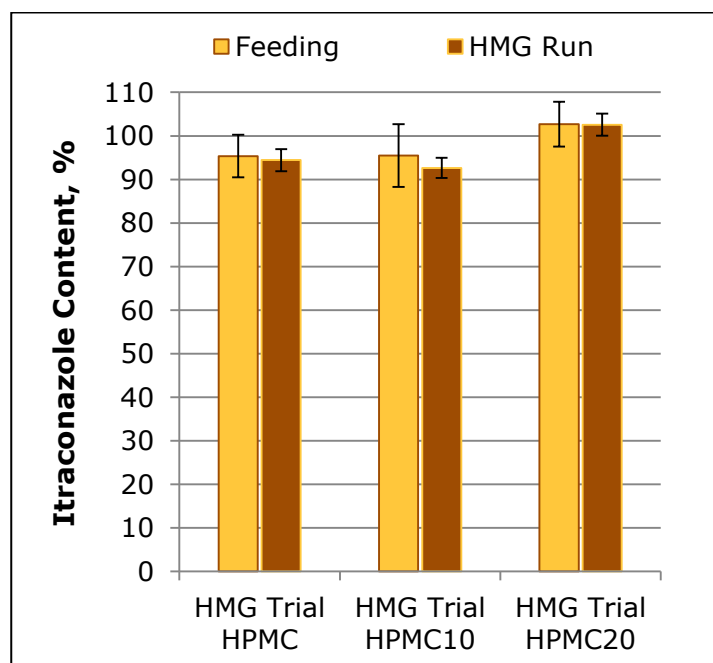


Figure IV.48. - Excerpts from DSC traces of a) HMG Trial HPMC, b) HMG Trial HPMC10, c) HMG Trial HPMC20, analysis conducted from $30 - 200 \text{ }^\circ\text{C}$ after 2 min holding period at $30 \text{ }^\circ\text{C}$; heating rate 3 K/min .

Table IV.25. - DSC signals corresponding to ITR melting of case study HPMC.

	HMG Trial HPMC		HMG Trial HPMC10		HMG Trial HPMC20	
ITR signal, °C						
Onset	155.02	161.75	155.31	162.74	154.61	161.21
Peak	156.49	164.54	156.50	164.10	156.13	164.23

Interestingly, right before the first ITR T_m , there was a very small third event in the DSC trace. For the binary formulation this third event happened at 150.74 °C. However, the distinction was hard if this event really was endo- or exothermic as the signal grew out of the rising slope of the DSC trace and then fell slightly down again before giving rise to T_m around 155 °C. It seemed to be the same difficulty as was previously reported for the characterisation of “cold crystallisation”. The detected liquid mesophases proved the presence of glassy ITR in the samples. Otherwise, the presence of crystalline ITR could not be excluded completely. This had to be suspected especially for HMG Trial HPMC10, since the peak area at 164.10 °C was distinctively larger than for the other two samples. Figure IV.49. shows the analysed ITR content of all three HPMC 4000 samples after HMG and also during mTSE feeding to investigate possible segregation of the PMs. No ITR degradation was observed.

**Figure IV.49. - ITR content of HMG Trial HPMC, HPMC10 and HPMC20 during mTSE feeding (n = 10) and of the melt-granulated yield (n = 3); error bars = sd.**

ITR content of HMG Trial HPMC, HPMC10 and HPMC20 was 94.44 ± 2.53 %, 92.64 ± 2.33 % and 102.57 ± 2.51 %, respectively. Taking into account the ITR content during feeding, the reason for these values became obvious. All three

HPMC samples exhibited sd above 4.8 % during feeding (95.35 ± 4.88 % for HMG Trial HPMC, 95.46 ± 7.19 % for HMG Trial HPMC10 and 102.68 ± 5.16 % for HMG Trial HPMC20). This again stressed the need for utilising at least a second feeding station. HMG Trial HPMC10 which had appeared most inhomogeneous during HMG exhibited the largest sd during feeding. These results agreed with each other. The too high content of HMG Trial HPMC20 could also be explained by investigating the feeding content. Segregation of HPMC 4000 or β CD seemed to have occurred during the filling phase.

IV.9.2.3. Dissolution Results and Inclusion Complex Formation Evaluation of HMG Trial HPMC, HPMC10 and HPMC20

Of utmost interest were the dissolution results of all three HPMC samples which are given in Figure IV.50.. All three HPMC samples reached quantitative ITR dissolution after 4 h. 97.83 ± 6.37 % ITR dissolution was shown for HMG Trial HPMC. HMG Trial HPMC10 and HPMC20 achieved 104.87 ± 0.60 % and 97.92 ± 4.74 %, respectively.

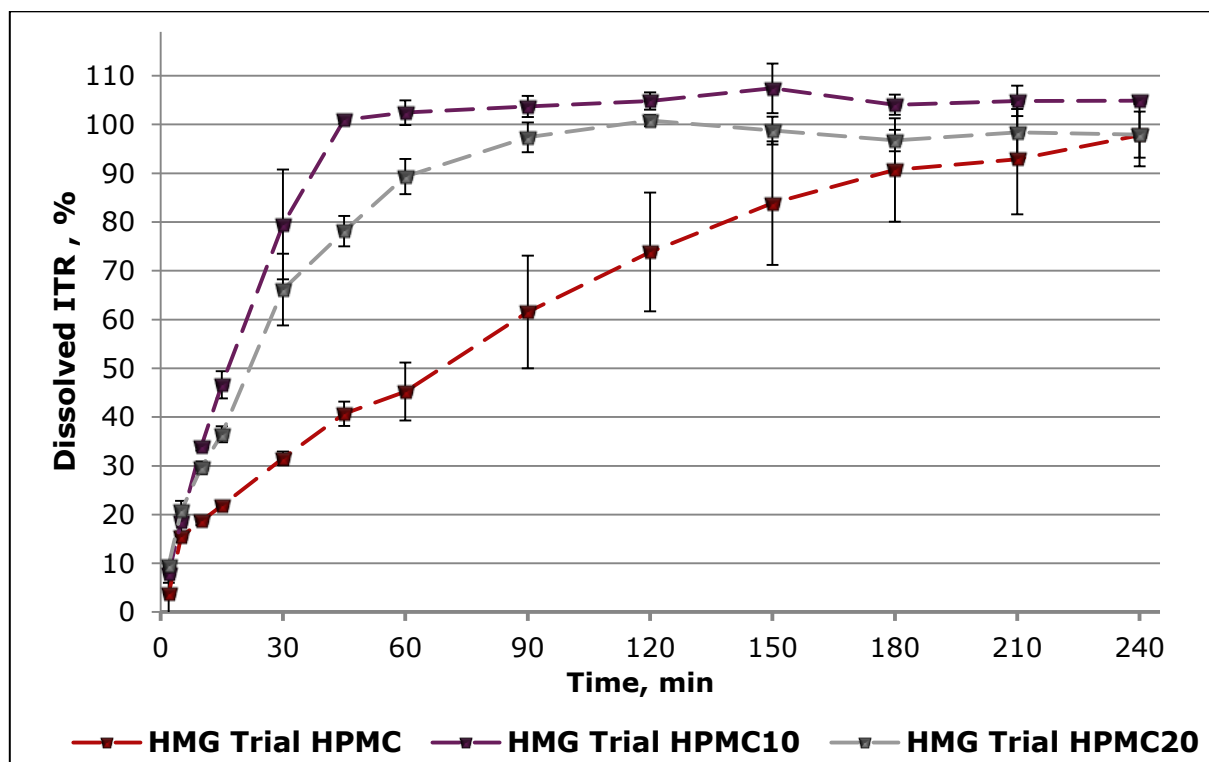


Figure IV.50. - Dissolution results of case study HPMC 4000; n = 3; error bars = sd.

The fact that HMG Trial HPMC10 showed ITR dissolution above 100 % up from 60 min could be explained by the high sd in the content analysis. It might have been that the studied samples were not completely homogenous. This most likely

also explained the high variations for the binary system. When it came to the amount of dissolved ITR of all samples, it seemed that ITR was mostly amorphous in all systems. Interestingly, different curve progressions were observed for the three samples. HMG Trial HPMC showed a near zero-order like dissolution profile. The amount of dissolved ITR rose slowly. This was in agreement with HPMC 4000 being a swelling matrix and sustaining ITR dissolution. ITR had to diffuse through the swollen layer before dissolving in the dissolution medium. HPMC 4000 might have also slightly increased the viscosity of the dissolution medium. Of further importance were the dissolution profiles of the ternary systems as both of them showed substantially faster ITR dissolution rates. HMG Trial HPMC20 reached a plateau after 90 min with ITR dissolution of $97.37 \pm 3.06 \%$. HMG Trial HPMC10 showed the fastest ITR dissolution rate. Here, the plateau phase already began at 45 min ($100.96 \pm 0.82 \%$). This could be explained by the facts that HMG Trial HPMC20 with the higher HPMC 4000 content formed a larger diffusion layer and/or further increased viscosity. The latter, however, was less likely, as Loftsson et al. reported only a negligible increase in viscosity for an aqueous solution of 0.05 wt/v % HPMC 4000 at room temperature [166]. The HPMC 4000 concentration of HMG Trial HPMC20 in the dissolution vessel was 0.0074 wt/v % at maximum. HMG Trial HPMC20 presented a slow rise in the dissolution curve between 30 - 90 min (from $66.14 \pm 7.33 \%$ to $97.37 \pm 3.06 \%$). During this time period, ICs were forming in the dissolution vessel. This slow rise was not observed for HMG Trial HPMC10. Here, the increase of the dissolution curve was steeper.

Comparing all these dissolution results to the reference sample HMG Trial B, it became obvious that all dissolution curves gave nearly the same endpoint after 4 h ($97.89 \pm 2.39 \%$ for HMG Trial B). The curve progressions, however, were different. The binary HPMC 4000 formulation showed the slowest dissolution rate. During the first 15 min, HMG Trial HPMC10 and HPMC20 stayed on the same level as HMG Trial B but after that, they both showed superior dissolution rates. HMG Trial B had reached the dissolution plateau of $96.11 \pm 2.14 \%$ after 120 min. This time was reduced by 62.5 % and 25 % by HMG Trial HPMC10 and HPMC20, respectively. This might hold therapeutic value and showed that the addition of HPMC 4000 to a binary mixture of β CD and ITR increased the *in-vitro* dissolution rate. Nevertheless, these results also indicated that the addition of too much HPMC 4000 delayed the dissolution. Rambali et al. also found that the

addition of a low viscosity HPMC to a mixture of ITR and HP β CD significantly increased ITR solubility after HME. They reported the highest solubility for a HPMC:HP β CD:ITR system in the ratio of 17:60:23 [110].

ATR-FT-IR analysis was used to determine ICF in the case study samples. Results are shown in Table IV.26.. Regarding the marker wave numbers, pure HPMC 4000 only presented one wave band interfering around 1054 cm^{-1} .

Table IV.26. - ATR-FT-IR results of the case study HPMC, evaluated by comparison with reference wave numbers; sd = \pm , n = 3, *n = 5; if wave number markers were not detected in every single analysis, the percentage of their occurrence is given in brackets below.

	PM* PMaITR*	Pure HPMC 4000	HMG Trial HPMC	HMG Trial HPMC10	HMG Trial HPMC20
Wave Numbers, cm^{-1}	1697.60 \pm 0.15 1698.89 \pm 0.33	X	1699.72 \pm 0.22	1699.37 \pm 0.37	1699.52 \pm 0.38
	1584.60 \pm 0.25 (80 %) 1585.76 \pm 0 (20 %)	X	1585.70 \pm 0.05	1585.43 \pm 0.03 (66.67 %)	1585.50 \pm 0.18
	1551.18 \pm 0.13 1552.74 \pm 0.27	X	1552.57 \pm 0.06	1552.41 \pm 0.06	1552.40 \pm 0.05
	1509.80 \pm 0.23 1511.07 \pm 0.34	X	1510.86 \pm 0.02	1510.88 \pm 0.13	1510.93 \pm 0.16
	1451.20 \pm 0.16 (80 %) 1451.08 \pm 0.21	X	1451.13 \pm 0.07	1450.85 \pm 0.25	1451.04 \pm 0.07
	1270.96 \pm 0.98 (80 %) X	X	1271.80 \pm 0.02 (66.67 %)	1271.73 \pm 0.10 (66.67 %)	X
	1227.41 \pm 0.59 1228.55 \pm 0.62	X	1228.23 \pm 0.09	1228.44 \pm 0.17	1228.74 \pm 0.04
	1184.44 \pm 0.52 X	X	1183.68 \pm 0.11	1184.58 \pm 0 (33.33 %)	X
	1140.58 \pm 0 (20 %) X	X	1137.79 \pm 0.25 (66.67 %)	1152.44 \pm 0.22	1152.44 \pm 0.12
	1072.64 \pm 0.06 (40 %) 1077.55 \pm 0.36 (40 %)	X	X	1077.53 \pm 0.16	1077.19 \pm 0.06
	1043.15 \pm 0.11 1042.58 \pm 0.95 (40 %) X	1054.23 \pm 0.72	1042.10 \pm 0.54	X	X
	1028.45 \pm 1.81 (60 %)	X	X	1026.35 \pm 0.70	1027.40 \pm 0.16
	823.82 \pm 0.09 824.74 \pm 0.72	X	825.03 \pm 0.17	825.18 \pm 0.22	825.48 \pm 0.17

However, interpretation of the melt processed specimen was challenging as many signals that had previously disappeared after HMG above ITR T_m were de-

tected, such as around 1585 cm^{-1} or 1184 cm^{-1} . The peak around 1699 cm^{-1} was observed in every sample containing ITR. The results indicated that ITR was present in both, crystalline and amorphous form. A shift from around 1072 cm^{-1} to 1077 cm^{-1} was observed for HMG Trial HPMC10 and HPMC20. The wave band around 1271 cm^{-1} was not observed in every ATR-FT-IR run of HMG Trial HPMC and HPMC10 and not at all for HPMC20. Both samples containing β CD exhibited the wave band around 1027 cm^{-1} which showed interactions between ITR and β CD. Nevertheless, due to the partial presence of aITR and the addition of a third component, these results could not be utilised for clearly detecting ICs. The fast dissolution rates, however, strongly supported ICF during HMG. Still, it was not possible to determine if the faster dissolution rates were caused by improved ICF due to the HPMC 4000 presence, more stabilised glassy ITR in the samples or by additional mechanisms of the polymer.

IV.9.2.4. Outcome of Case Study Hydroxypropyl Methylcellulose

The second case study clearly showed that the dissolution rate of ITR could be increased by adding HPMC 4000. The binary HPMC 4000 formulation showed sustained dissolution as had been expected. The addition of 10 % HPMC 4000 in mass showed more satisfactory results than a mass fraction of 20 % of HPMC 4000. The processing of the PMs was not ideal at the chosen temperature range. Additionally, feeding of the three-component systems should rather be conducted with separate hoppers.

IV.9.3. Case Study Xylitol

Lastly, xylitol was investigated as ternary additive. It is known that different substances in the intestinal fluids can theoretically displace APIs from the CD cavity by becoming guest molecules themselves. This has e.g. been investigated *in-vitro* for ICs of ITR and HP β CD by Stappaerts et al. [167]. As a small, hydrophilic molecule, it should be theoretically possible for xylitol to get included in the β CD cavity. Apart from this, xylitol has previously been investigated regarding its potential for improving dissolution rates. These two circumstances made it an interesting third component in this case study. Again, basis for the HMG procedure was the temperature profile of the reference sample HMG Trial B.

IV.9.3.1. Preparation and Behaviour During Hot-Melt Granulation of Xylitol Blends

Same as for the other two case studies, PMs were prepared. The binary formulation of xylitol and ITR showed a drug load of approximately 38 % , the blend with 10 % in mass of xylitol 35.11 % and the blend with 20 % in mass of xylitol 30.82 %. HMG parameters for the three samples are given in Table IV.27..

Table IV.27. - HMG parameters of the case study with xylitol.

HMG Trial	Z1, °C	Z2, °C	Z3, °C	Z4, °C	Z5, °C	Z6, °C	Z7, °C	ScS, rpm	Throughput, g/h	Torque, %
XYL	100	130	170	180	180	180	180	150	214.1	4
XYL10	100	130	170	180	180	180	180	150	178.6	18
XYL20	100	130	170	180	180	180	180	150	191.6	11.5

All three mixtures showed sufficient flowability in the feeder. However, tendency to segregate was already visually observed. HMG of the binary formulation was generally stable with a very low torque of 4 %. As xylitol melts slightly above 90 °C, both components should have been completely molten. Still, the product appeared inhomogeneous as it was partially liquid and partially pasty. This could have related to possible segregation of PM and to very short residence time of the material in the barrel so that the substances could not fully melt.

HMG of the two ternary systems was very similar. Both products seemed segregated. Especially for HMG Trial XYL20, colour changes were observed during HMG. As previously reported, aITR was slightly brown-greyish in colour. During sample collection of HMG Trial XYL20, the product at the beginning appeared whiter. After a while, the melt-granules seemed to contain more aITR judged by a slight darkening in colour. Water vaporisation through the ventilation port was not working sufficiently for HMG Trial XYL10 where steam evaporated through the mTSE exit. The products of the ternary formulations appeared almost chewing-gum like at some points (see Figure IV.51.). This elastic property could be ascribed to xylitol and most likely presented itself in inhomogeneous granule parts consisting of too much xylitol.



Figure IV.51. - Image of the HMG procedure of HMG Trial XYL20; granulation heel slide was removed for better visualisation.

IV.9.3.2. Physico-Chemical Characterisation of HMG Trial XYL, XYL10 and XYL20

All samples of the xylitol case study were physico-chemically analysed. Particle size measurements were carried out to exclude possible changes in the dissolution rate being caused by larger surface areas. Results are shown in Table IV.28..

Table IV.28. - Results of the particle size measurements of the case study with xylitol; n = 3; \pm = sd.

	HMG Trial XYL	HMG Trial XYL10	HMG Trial XYL20
x_{50} , μm	154.7 ± 16.3	164.1 ± 2.4	149.8 ± 4.0

No substantial difference could be observed for the three samples as all showed x_{50} values well above 100 μm . HMG Trial XYL10 exhibited the largest particles. The binary formulation showed the largest sd with 16.3 μm . This could be related to the suspected inhomogeneity. No large differences in dissolution rate should have been expected judging from these results. To determine the possible crystallinity of the samples, DSC measurements were conducted. Results are given in Figure IV.52. and Table IV.29.. Upon inspecting the DSC traces, a clear difference was detectable between the binary formulation and the two ternary systems. There was a distinct peak at 91.53 $^{\circ}\text{C}$ corresponding to T_m of xylitol. The sugar alcohol had recrystallised after HMG. The ternary systems did not show this signal which indicated that xylitol had stayed amorphous. The incorporation in the βCD matrix seemed to have hindered recrystallisation. Two T_m s corresponding to ITR were observed for all samples. Upon magnifying the DSC traces (data not shown), two endothermic signals correlating to the ITR mesophases became visible between 70 - 80 $^{\circ}\text{C}$ and between 80 - 90 $^{\circ}\text{C}$ for HMG Trial XYL10 and XYL20.

HMG Trial XYL only showed one endothermic event between 70 - 80 °C. The second endothermic event was most likely overlapping with T_m of xylitol.

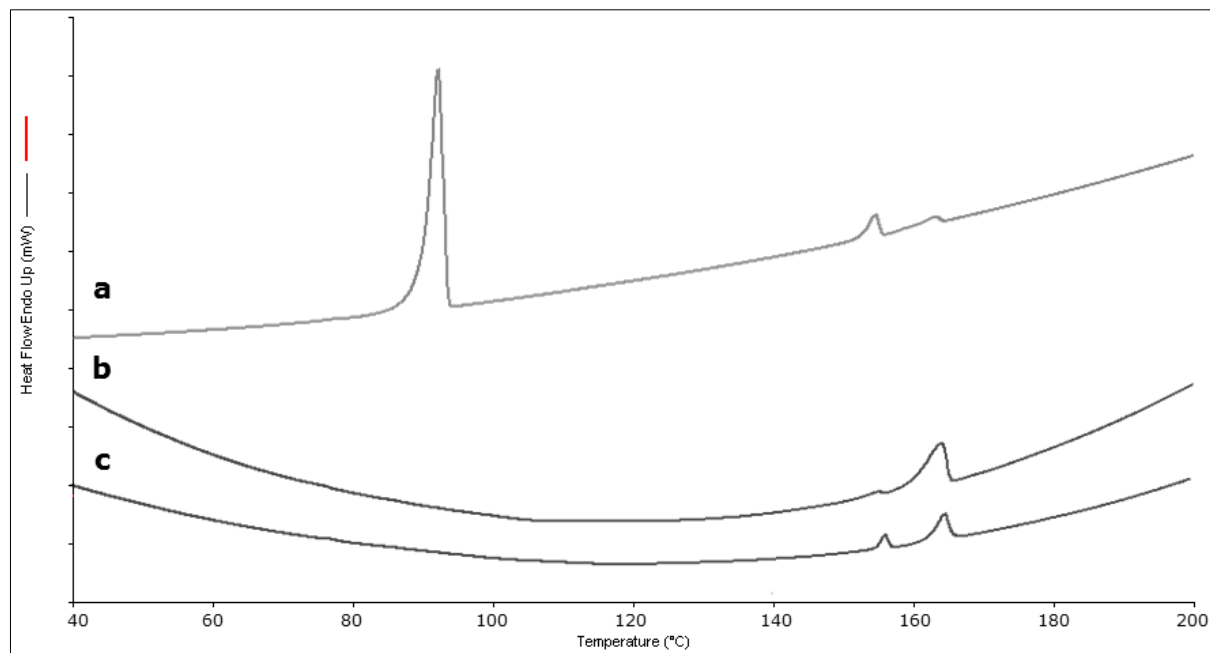


Figure IV.52. - Excerpts from DSC curves of a) HMG Trial XYL, b) HMG Trial XYL10, c) HMG Trial XYL20; analyses conducted from 30 - 200 °C after 2 min holding period at 30 °C; heating rate 3 K/min.

DSC curves of HMG Trial XYL10 and XYL20 showed signs of “cold crystallisation” around 110 °C. This was not observed for the binary system. For HMG Trial XYL10 and XYL20, the second ITR T_m was 25.20-fold and 2.95-fold larger area-wise than the first peak around 155 °C. In contrast, for the binary system, the peak at 153.24 °C was 2.44-fold larger than the second event. Even though it was previously reported that different recrystallisation events could possibly happen during heating of glassy ITR, it still seemed unlikely that most of the polymorphic ITR had directly recrystallised. Rather, it had to be assumed that ITR was partially crystalline in the ternary systems. As xylitol in these formulations was kept amorphous, it was possible that β CD could not hinder further recrystallisation of the API.

Table IV.29. - DSC signals corresponding to ITR melting for case study xylitol.

	HMG Trial XYL		HMG Trial XYL10		HMG Trial XYL20	
ITR signal, °C						
Onset	151.36	158.75	152.16	159.95	155.29	162.68
Peak	153.24	161.59	154.73	164.07	156.41	164.92

Since PMs appeared segregated during HMG, ITR content evaluation of the finished products as well as of the fed PM was carried out. Results are presented in Figure IV.53.. As already seen in DSC results, the binary formulation stood out again. Segregation of the PM was clearly proven with an average fed ITR content of 79.60 ± 14.91 %. It has to be added that during blending of the binary PM, it was already visually observable that ITR was strongly attached to the blending vessel which corresponded well with the fact that apparently, a large amount of ITR had been lost before PM had been filled into the hopper.

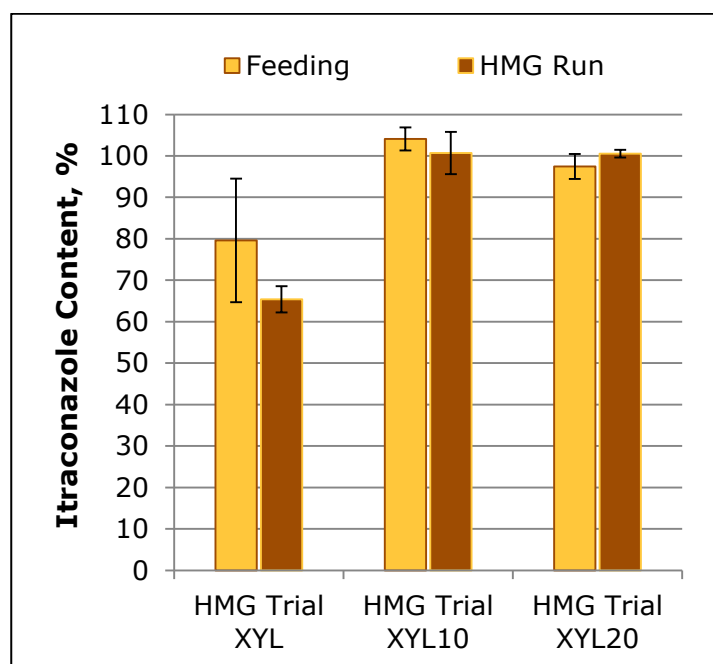


Figure IV.53. - ITR content of HMG Trial XYL, XYL10 and XYL20 during mTSE feeding (n = 10) and of the yielded products (n = 3); error bars = sd.

Inspecting the individual results, a trend became visible. At HMG beginning, the lowest ITR amounts were fed. The highest ITR content was determined for the last inspected sample. Xylitol segregated from PM and was melt-granulated predominantly. This varying feeding led to ITR content of 65.40 ± 3.15 % for the finished product. This might explain the DSC results of the binary formulation. If less ITR was present, the amount of crystalline ITR would be smaller. Additionally, xylitol might have been able to keep ITR amorphous at this low content. The average ITR content during feeding was 104.08 ± 2.78 % and 97.46 ± 3.00 % for HMG Trial XYL10 and HMG Trial XYL20, respectively. This resulted in contents of 100.72 ± 5.11 % and 100.56 ± 0.92 % for the respective products. The same observation already made for the other two case studies applied again, it definitely had to be advised to use separate feeders.

IV.9.3.3. Dissolution Results and Inclusion Complex Formation Evaluation of HMG Trial XYL, XYL10, XYL20

Dissolution testing was carried out for the three xylitol formulations. Results are given in Figure IV.54.. The content analysis of HMG Trial XYL had shown high variations coupled with a very low ITR content. This resulted in high deviations determined for the ITR dissolution experiments.

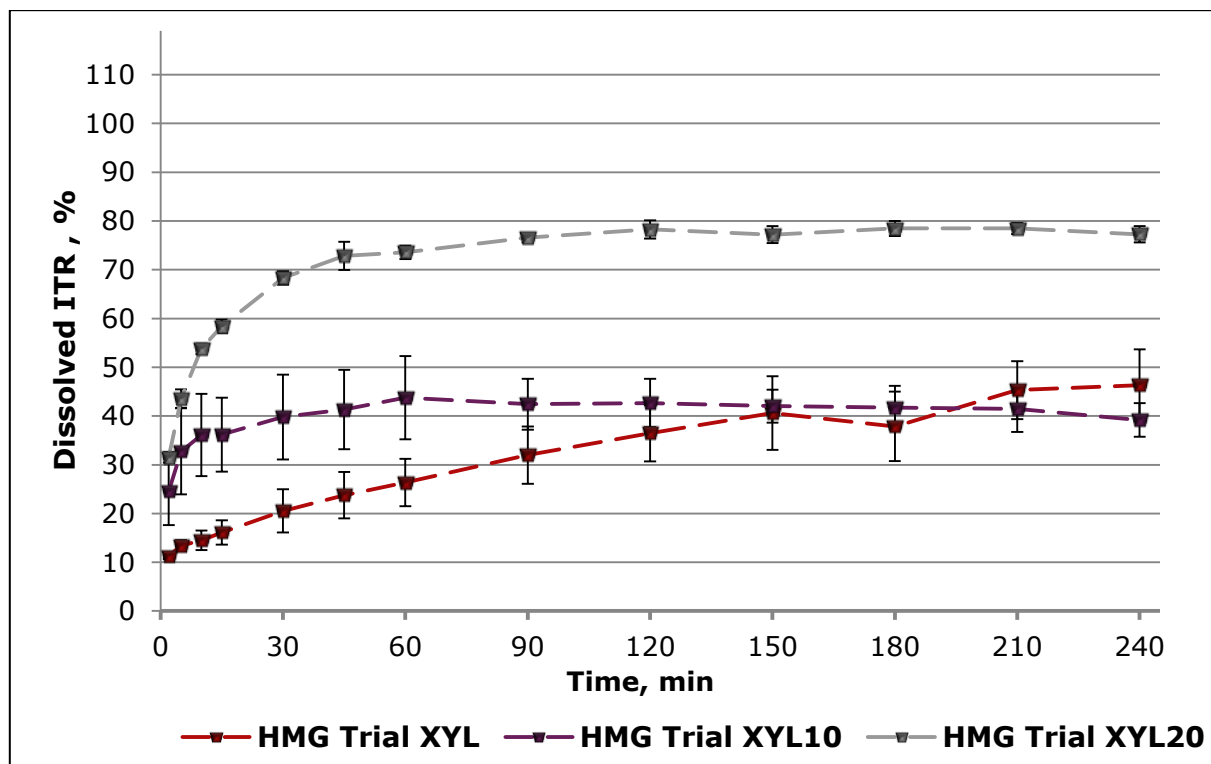


Figure IV.54. - Dissolution results for the case study xylitol; n = 3; error bars = sd.

HMG Trial XYL reached about 46.33 ± 7.35 % ITR dissolution after 4 h. The curve progression showed a long rise. It appeared as if ITR was amorphous. However, xylitol did not influence the dissolution rate positively. Comparing HMG Trial XYL10 and XYL20, the suspected results of the DSC analysis were confirmed. HMG Trial XYL10 reached ITR dissolution of 39.18 ± 3.43 % after 4 h. This plateau was already reached after 30 min. ICF in the dissolution vessel did not seem to occur. The high variations of HMG Trial XYL10 could be correlated to the high determined variation in the content analysis (5.11 %; see Figure IV.53.). This low dissolution and fast reached plateau supported the presence of at least partially crystalline ITR. Three individual samples of HMG Trial XYL10 were investigated. By inspecting these dissolution curves closely, it became apparent that the determined ITR content at the end of the experiment was always

lower than the detected maximum (49.06 % \rightarrow 40.44 %, 48.37 % \rightarrow 41.81 %, 38.33 % \rightarrow 35.30 %). This upheld the theory of competition for the β CD cavity. ITR could precipitate when dissolved xylitol displaced it from the cavity. Interestingly, this phenomenon was not seen for HMG Trial XYL20. This sample showed highest ITR dissolution. After 4 h, 77.26 ± 1.68 % of ITR had dissolved. This was more than was experienced for aITR (61.71 ± 0.67 %, see section IV.3.) and strongly indicated ICF during HMG. The plateau phase of the dissolution was reached after 45 min which was faster than for the reference sample HMG Trial B. However, the final ITR dissolution was 21.07 % less than for the reference. An explanation for this might have been partially crystalline ITR or insufficient ICF in the sample due to the presence of xylitol.

To gain deeper understanding in possible ICF, ATR-FT-IR measurements were conducted. The obtained results are given in Table IV.30.. Pure xylitol did show wave bands interfering with the marker peaks, such as around 1279 cm^{-1} . Judging from the ATR-FT-IR results, it seemed as if HMG Trial XYL10 would have contained more aITR than crystalline. Most of the previously defined wave bands that disappeared upon amorphisation were not observed for HMG Trial XYL10, but in contrast, detected for HMG Trial XYL20. However, it could not be determined how much of this was influenced by the presence of xylitol. Xylitol in the β CD cavity could e.g. have negated the shielding ability for the functional groups of ITR. HMG Trial XYL20 showed the highest wave number around 1077.68 cm^{-1} . This signal had previously been put in connection with ICF. HMG Trial XYL20 also presented a signal at 1153.80 cm^{-1} which had not been reported before. The signal around 825 cm^{-1} was not observed for HMG Trial XYL10, probably due to shielding by the xylitol molecules. Moreover, the signal around 1700 cm^{-1} was only detected once. This also supported xylitol lowering the interactions between ITR and β CD. Generally, the ATR-FT-IR results pointed out differences between the samples, but a distinct determination of ICF was not possible with the interfering third component.

Table IV.30. - ATR-FT-IR results of the case study xylitol, evaluated by comparison with reference wave numbers; sd = \pm , n = 3, *n = 5; if wave number markers were not detected in every single analysis, the percentage of their occurrence is given in brackets below.

	PM* PM aITR*	Pure Xylitol	HMG Trial XYL	HMG Trial XYL10	HMG Trial XYL20
Wave Numbers, cm ⁻¹	1697.60 \pm 0.15 1698.89 \pm 0.33	X	1700.00 \pm 1.50	1700.48 \pm 0 (33.33 %)	1699.35 \pm 0.31
	1584.60 \pm 0.25 (80 %) 1585.76 \pm 0 (20 %)	X	1585.58 \pm 0.10 (66.67 %)	X	1585.76 \pm 0.09
	1551.18 \pm 0.13 1552.74 \pm 0.27	X	1552.34 \pm 0.11	X	1552.53 \pm 0.08
	1509.80 \pm 0.23 1511.07 \pm 0.34	X	1510.79 \pm 0.11	1511.53 \pm 0 (33.33 %)	1511.08 \pm 0.11
	1451.20 \pm 0.16 (80 %) 1451.08 \pm 0.21	X	1450.63 \pm 0.06	X	1450.90 \pm 0.01
	1270.96 \pm 0.98 (80 %) X	1279.27 \pm 0.32	1276.91 \pm 0 (33.33 %)	X	1271.64 \pm 0.09
	1227.41 \pm 0.59 1228.55 \pm 0.62	1230.13 \pm 0 (33.33 %)	1229.16 \pm 0.19	1229.46 \pm 0.16	1228.34 \pm 0.17
	1184.44 \pm 0.52 X	X	X	X	1183.01 \pm 0.32
	1140.58 \pm 0 (20 %) X	1124.37 \pm 0.88	1123.84 \pm 0.11	X	1153.80 \pm 0.06
	1072.64 \pm 0.06 (40 %) 1077.55 \pm 0.36 (40 %)	1087.15 \pm 1.03 1065.32 \pm 1.07	1065.90 \pm 0.09	1075.77 \pm 0.19 1066.10 \pm 0.04	1077.68 \pm 0.12
	1043.15 \pm 0.11 1042.58 \pm 0.95 (40 %) X	X	1057.64 \pm 0 (33.33 %)	1055.07 \pm 3.07	X
	1028.45 \pm 1.81 (60 %)	1027.64 \pm 0 (33.33 %)	1027.93 \pm 0.01	1027.88 \pm 0.03	1025.25 \pm 0.09
	823.82 \pm 0.09 824.74 \pm 0.72	X	825.33 \pm 0.27	X	825.19 \pm 0.05

IV.9.3.4. Outcome of Case Study Xylitol

This third case study again showed that segregation was a valid problem, not only when operating with ternary PMs. Xylitol failed to further enhance ITR dissolution or solubility rate compared to the reference sample HMG Trial B. Additionally, for the addition of 10 % xylitol in mass, indications for cavity competition and displacement as well as ITR precipitation were observed.

IV.9.4. Concluding Remarks About the Addition of Ternary Additives

Three different case studies were presented that dealt with the addition of hydrophilic polymers and a sugar alcohol to the binary ITR/ β CD formulation. Generally, it could be concluded that the detection of ICs in these ternary samples was more challenging, if not impossible. Due to interferences, ATR-FT-IR results were not useful in determining ICF. Solely the dissolution results could be interpreted for this. Furthermore, here it was questionable which amount of dissolved ITR could be ascribed to ICs, aITR and then, the addition of the third substance. The satisfactory dissolution results for the addition of 10 % and 20 % in mass of HPMC 4000 could also be explained by HPMC 4000 improving the wettability of ITR or maintaining more stable aITR.

Apart from this, it is also reported that water-soluble polymers tend to form complexes with drugs themselves in aqueous solution [168]. Savolainen et al. found that the addition of HPMC to an oral glibenclamide formulation made it possible to reduce the necessary amount of CD due to synergistic effects. They further reported that the addition of HPMC did not change the PSM results regarding the proposed complex stoichiometry [169]. Nevertheless, the addition of polymers can positively influence the IC stability constant and CE [166]. All the polymeric mechanisms of interaction such as electrostatic bonds, Van-der-Waals forces or hydrogen bonds work together with the mechanisms influencing the inclusion complexation of the API. The determined drug solubility then shows the outcome of these synergistic couplings. As the results of the HPMC 4000 case study clearly showed, this synergism had occurred and optimised ITR dissolution and dissolution rate. It may be fair to say that the exact determination of ICs was not of that much interest when discussing these ternary formulations and their properties as a whole.

To conclude, two of the presented case studies failed to yield sufficient results, namely the case study PEG 6000 and the case study xylitol. Apart from the segregation of the PMs, the produced samples presented high amounts of crystalline ITR. The case study HPMC 4000, however, showed positive results. The dissolution rates of the two ternary formulations were superior compared to the reference sample HMG Trial B. Thus, this formulation approach will be taken up again in the overall discussion in section V..

IV.10. Storage Stability

All results presented so far were gained shortly after production of the corresponding samples. For a complete interpretation of the different formulation approaches, it was also important to investigate their stability over a longer time period. Thus, a stability study was conducted at 25 °C/ambient humidity and 40 °C/75 % RH over the course of six months.

IV.10.1. Chosen Samples

All presented formulations in sections IV.4., IV.5., IV.6., IV.7. and IV.8. were investigated for their storage stability. However, the main objective of this work was to determine the most favourable formulation approach which of course included sufficient ITR dissolution. Therefore, only the results of the following chosen samples will be presented in this chapter:

1. HMG Trial A
2. HMG Trial B
3. HMG Trial HP
4. HMG Trial SOLU
5. SEMP

IV.10.2. Stability over Six Months

The samples first exposed to the different conditions of the stability study (HMG Trial A and HMG Trial B) for six months did not show any substantial changes at 25 °C/ ambient humidity, regardless if they had been stored in closed or open containers (data not shown). Consequently, samples produced and stored at a later time were only analysed for their behaviour under the elevated conditions 40 °C/75 % RH. The corresponding results are presented in the following subsections. All shown results were conducted for samples stored at 40 °C/75 % RH and thus, are only divided into "open" and "closed", corresponding to the used PE container, either with cap or without.

IV.10.2.1. Changes in Physico-Chemical Properties

The samples undergoing the stability study were investigated for their visual appearance by SEM. No differences were observed for HMG Trial A, HMG Trial B, HMG Trial HP and HMG Trial SOLU (data not shown). Figure IV.55. shows SEM images of SEMP. a and b show a SEMP pellet at the beginning of the stability study and a close-up of its surface, respectively. c and d were taken after six months of storage in the open container.

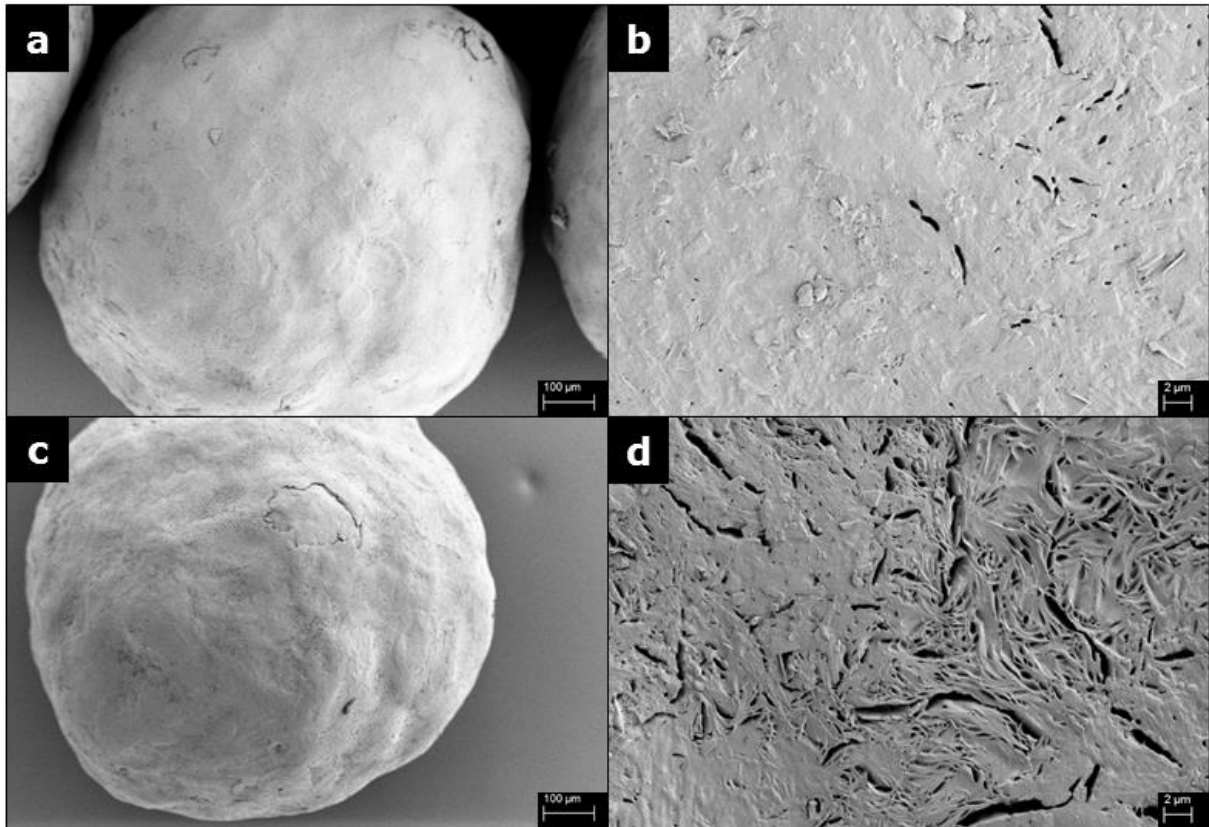


Figure IV.55. - SEM images of SEMP; a) pellet at the start of stability study, b) close up of pellet surface at start of stability study, c) pellet stored in open container at end of stability study, d) close up of pellet surface stored in open container at the end of stability study; left bars = 100 µm; right bars = 2 µm.

In c, there was a circular area visible where the seal coating seemed to be torn whereas d showed a close-up of the seal coating surface. These results indicated that the PEG coating had become disrupted during storage and became more porous. This could have been due to more molecular mobility in the polymer chains at 40 °C. The images suggested alterations during storage of SEMP, however, they could not display if the ITR coating had also become damaged. It has to be added that not all pellets under the microscope showed the same lacerations as shown in image c. Still, the torn surface was exhibited by more pellets than observed at the beginning of the stability study. Additionally, it was visually possible to detect colour changes of the pellets. After six months of storage, a substantial amount of them had turned slightly yellow.

Also of interest was the water content of the samples. Although formulations are usually packaged in a way that protects them from a humid environment as much as necessary, a less hygroscopic product might reduce costs for packaging material. Additionally, the formulation might still be efficacious even after wrong storage by the patient, e.g. after being kept out in the open in the bathroom. Re-

sults of the water content analysis of all investigated samples over the whole storage time are given in Figure IV.56.. The investigated four samples exhibited two different behaviours.

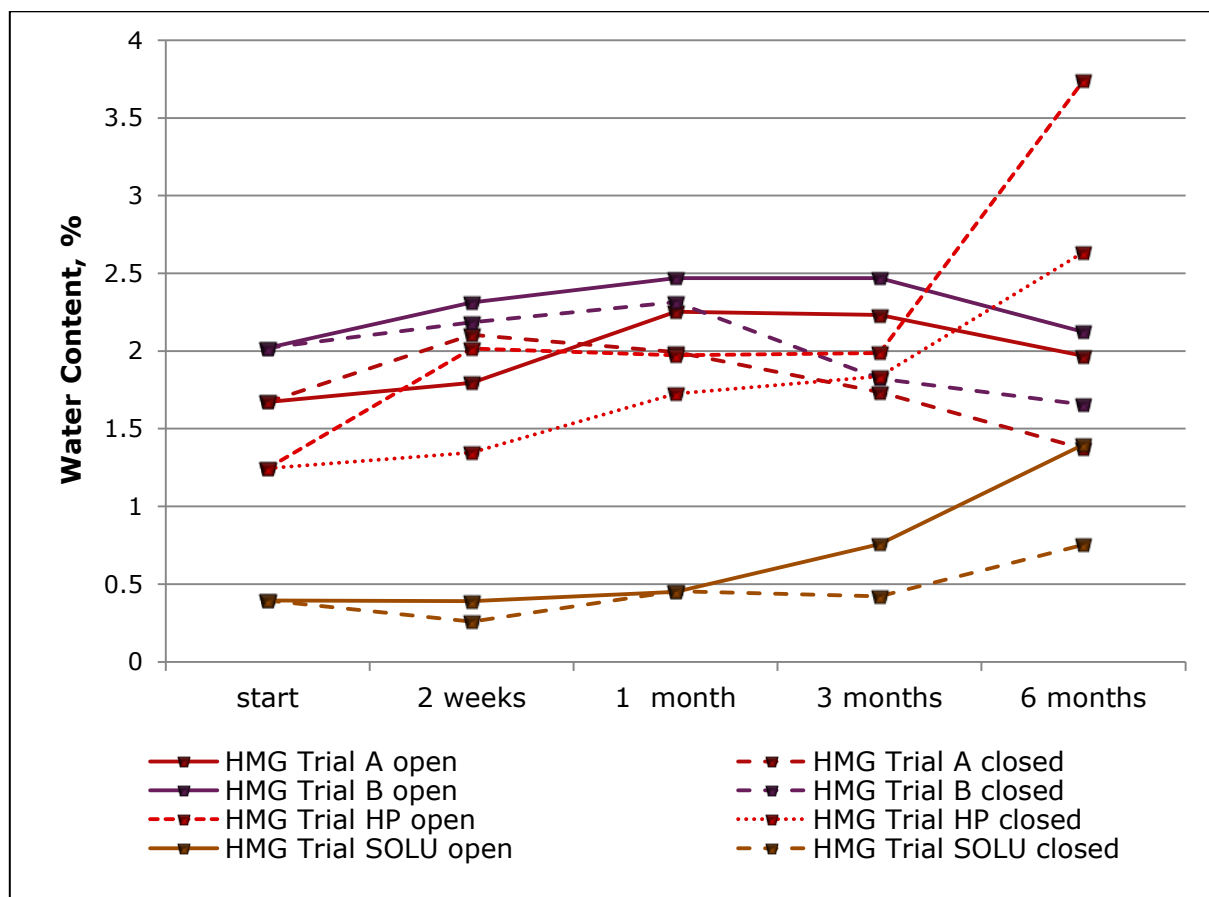


Figure IV.56. - Results of water content analyses during the stability study.

HMG Trial HP and HMG Trial SOLU adsorbed water during storage. As could be expected, this adsorption was more pronounced for the samples in open containers. The water content of HMG Trial SOLU rose by 254.18 % and 90.89 % in the open and closed container over six months, respectively. The highest water content was observed for HMG Trial HP. Here, the increase in adsorbed water was 200.48 % and 111.73 %, respectively. This might have induced further recrystallisation of ITR. HMG Trial A and B, however, showed only a slow rise up to one month of storage and then, the water content decreased again. In the case of the two samples in closed containers, the water content even fell below the value at the beginning of the stability study (-17.99 % for HMG Trial A and -18.07 % for HMG Trial B). This was interesting for a few reasons. First of all, CDs are postulated to be non-hygroscopic in general, the parent β CD more so than the derivative HB β CD [170]. These results agreed well with that. Also, it had to be taken into account that usually in CDs, water is situated in the cavity.

These water molecules are exchanged with the API during ICF. Usually cavity water is not volatile. The fact that HMG Trial A and B exhibited water loss after three months indicated that the rest of the previous cavity water left in the samples after HMG was not situated within the cavity. This further supported the presence of ICs. At the maximum of the respective curves for HMG Trial A and B, they showed increases of 34.61 % and 22.28 % in open containers and 25.82 % and 14.60 % in closed containers.

As the results of the water content have shown, indicators were present regarding recrystallisation of ITR. Therefore, DSC measurements were conducted at all time points of the stability study. For reasons of clarity, the following figures presenting these results only show the respective DSC trace at the beginning of the stability study (a) as well as the DSC curves after six months of storage in open (b) and closed (c) PE bottles. Figure IV.57. gives the DSC results of HMG Trial A. Regarding the melting of ITR and the presence of a signal corresponding to "cold crystallisation", the sample appeared stable over the whole six months.

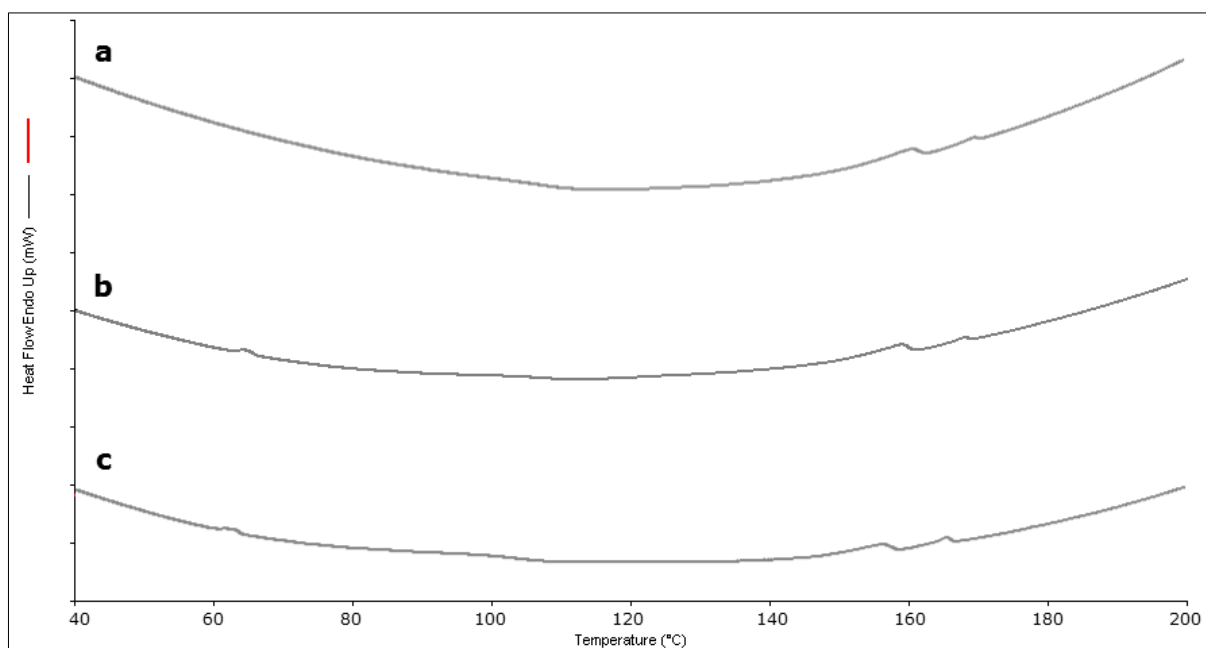


Figure IV.57. - Excerpts from DSC traces of HMG Trial A during the stability study; a) start, b) 6 months in open container, c) 6 months in closed container, analyses conducted from 30 - 200 °C after 2 min holding period at 30 °C; heating rate 3 K/min.

Only one observation was made concerning T_g of ITR around 60 °C. This signal was more pronounced after six months of storage both in open and closed containers. This was not surprising, as it is known that amorphous substances often exhibit enthalpy relaxation peaks in the region of T_g when stored at temperatures

close to T_g due to higher molecular mobility [171]. The same was observed for HMG Trial B. These results are given in Figure IV.58.. There were always two distinct peaks corresponding to ITR melting, as well as "cold crystallisation" visible in the DSC traces. The only difference to the beginning of the stability study was the more pronounced endothermic signal around T_g of ITR due to enthalpy relaxation.

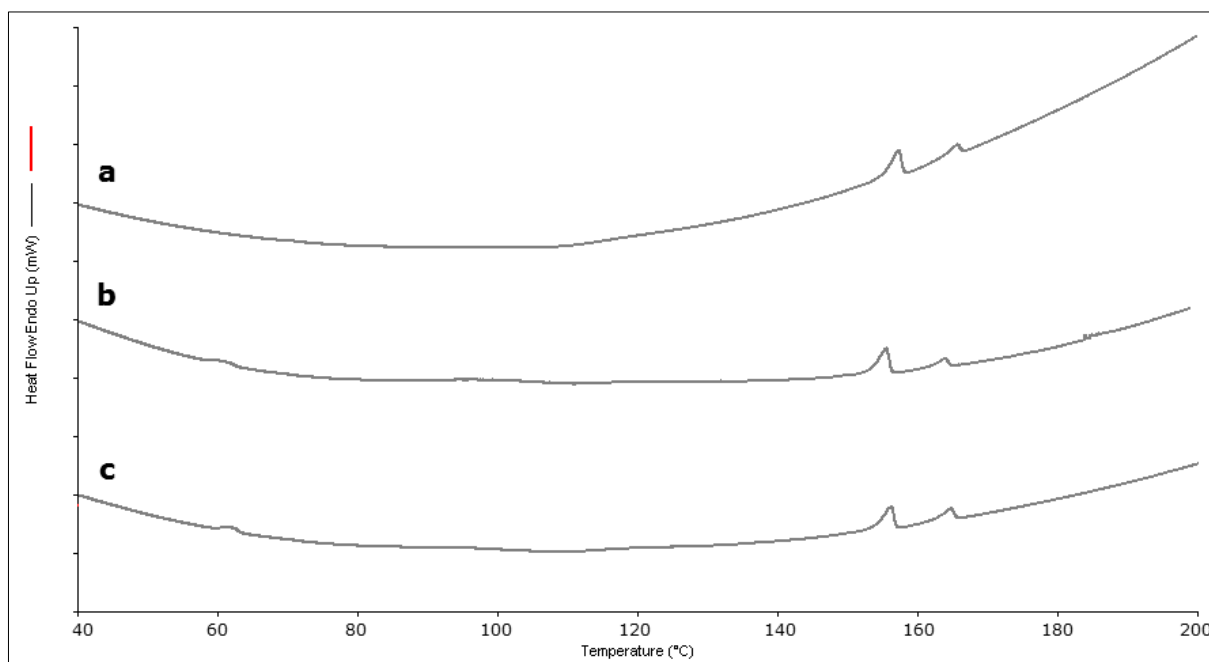


Figure IV.58. - Excerpts from DSC traces of HMG Trial B during the stability study; a) start, b) 6 months in open container, c) 6 months in closed container, analyses conducted from 30 - 200 °C after 2 min holding period at 30 °C; heating rate 3 K/min.

HMG Trial HP showed the same behaviour in the DSC over storage as can be seen in Figure IV.59.. Upon magnification, the T_g of ITR became more pronounced as explained above. "Cold crystallisation" was also detectable. The fact that the detected T_g signal was smaller than for HMG Trial A and B might have been related to more crystalline ITR being present, as also indicated by the higher second T_m around 165 °C compared to the polymorph around 155 °C (see section IV.6.). The previously presented results of the water content had indicated further recrystallisation of ITR during storage in HMG Trial HP. At the beginning of the stability study, the ratio between T_m one (polymorph) and two was 1:1.45. After six months of storage, this ratio rose to 1:1.85 and 1:2.15 for the open and closed PE bottle, respectively. This generally supported further recrystallisation. However, it also assumed total homogeneity of the samples after six months. Adding the fact that DSC measurements could only be conducted as single experiments, a substantial conclusion could not be drawn from the increase in the second endotherm.

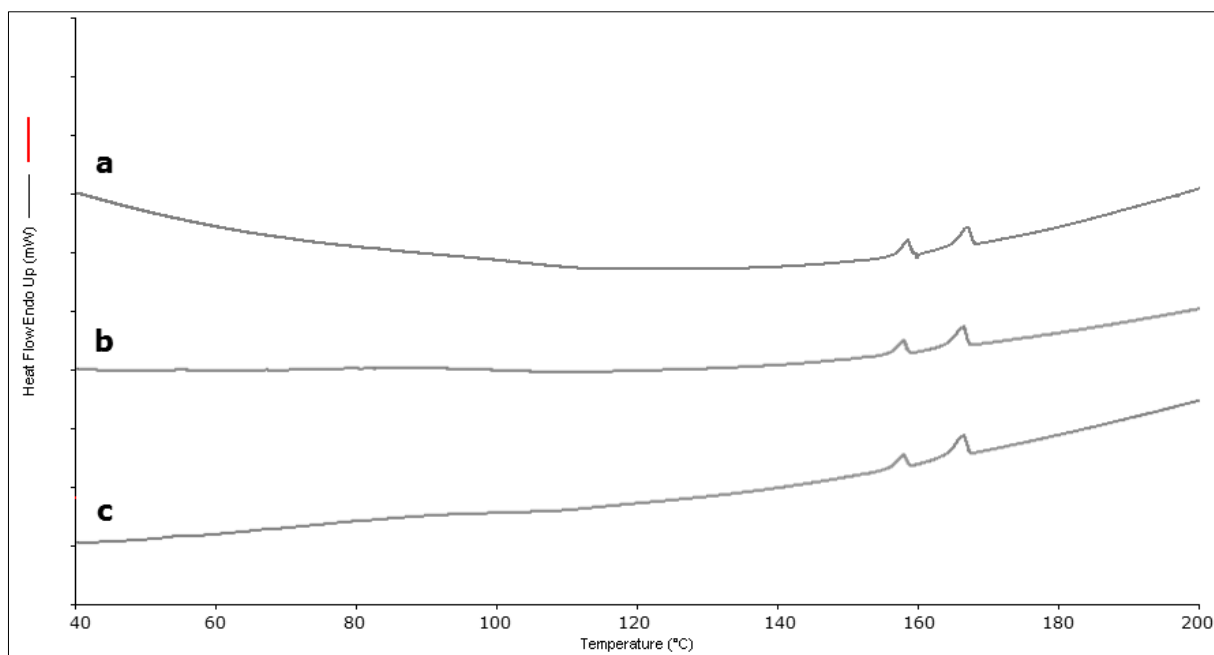


Figure IV.59. - Excerpts from DSC traces of HMG Trial HP during the stability study; a) start, b) 6 months in open container, c) 6 months in closed container, analyses conducted from 30 - 200 °C after 2 min holding period at 30 °C; heating rate 3 K/min.

DSC results of HMG Trial SOLU are shown in Figure IV.60.. Here, no ITR melting signal could be observed which clearly showed that SOLU as a matrix hindered the API's mobility and subsequently, recrystallisation.

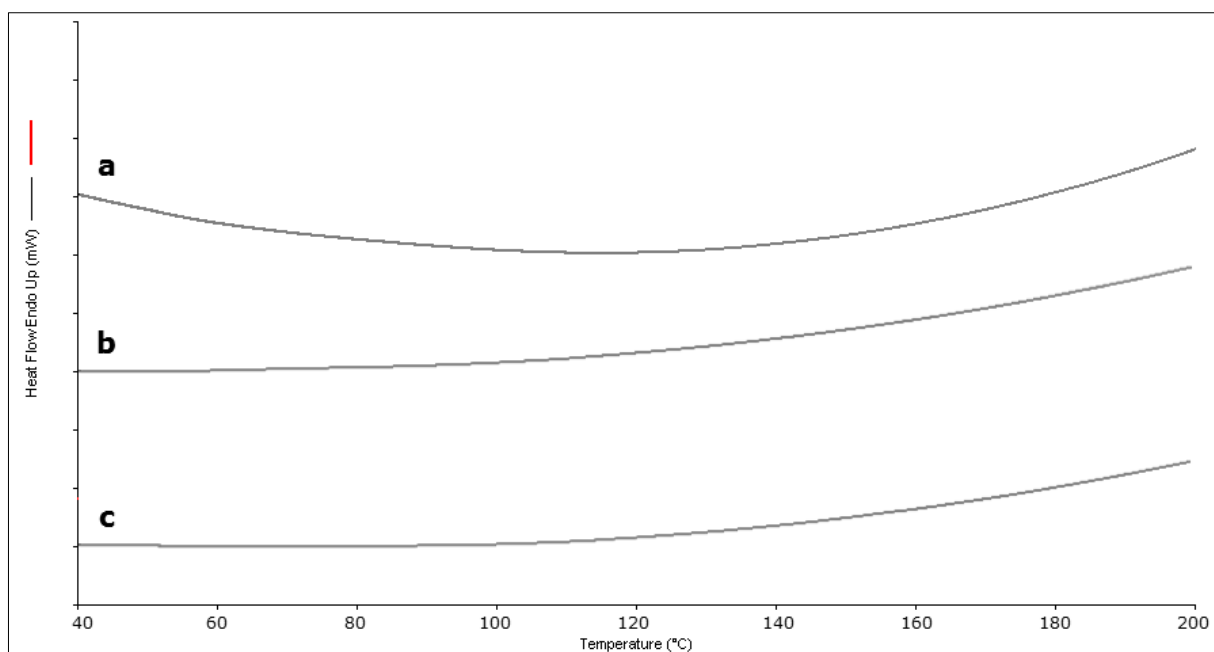


Figure IV.60. - Excerpts from DSC traces of HMG Trial SOLU during the stability study; a) start, b) 6 months in open container, c) 6 months in closed container, analyses conducted from 30 - 200 °C after 2 min holding period at 30 °C; heating rate 3 K/min.

With this used DSC technique, no T_g of ITR was detected, not even after six months of storage. On the one hand, this showed just how immobile SOLU kept ITR, suggesting the formation of a solid solution. But on the other hand, it might have indicated that the chosen DSC procedure for the stability study might not have been as specific as necessary for this sample. Lastly, SEMP was investigated by DSC analysis (Figure IV.61.). As was outlined in the corresponding section (section IV.8.), the DSC trace of SEMP had shown T_m corresponding to the PEG seal coating around 60 °C and an endothermic peak at 185.5 °C which was correlated to sucrose melting. Comparing the DSC trace at the beginning of the stability study with the DSC curve after six months of storage in closed containers, no difference was visible. The DSC trace of the open container showed a new event around 130 °C. One may suspect this to be an artefact in the DSC, however, this event was also observed in the SEMP sample stored at 25 °C/ambient humidity (data not shown) in the open container, only at a lower temperature, around 110 °C.

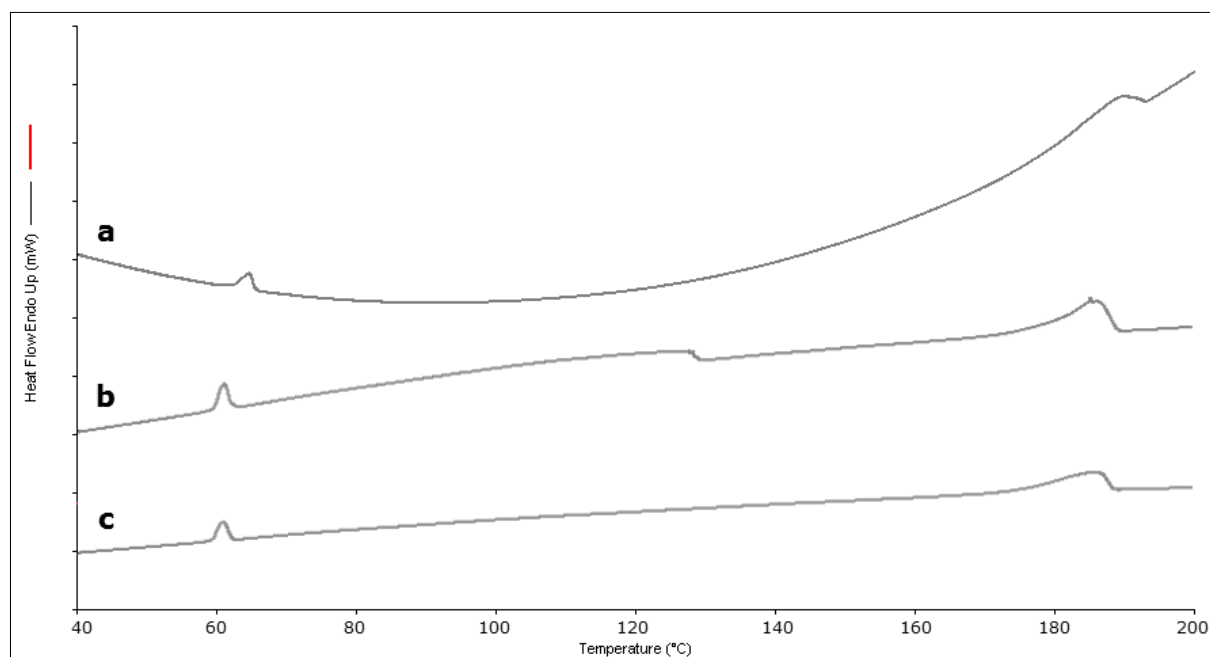


Figure IV.61. - Excerpts from DSC traces of SEMP during the stability study; a) start, b) 6 months in open container, c) 6 months in closed container, analyses conducted from 30 - 200 °C after 2 min holding period at 30 °C; heating rate 3 K/min.

This event might have been related to ITR recrystallising due to water adsorption during storage. The broad sucrose peak at 185.5 °C might have masked T_m of ITR. Also it had to be taken into account when comparing SEMP results to the melt-produced samples that this formulation is composed of many excipients that could all potentially influence the DSC curve. Therefore, it was not complete-

ly possible to ascribe this signal specifically to one formulation component. Enthalpy relaxation around the T_g of ITR could not be evaluated as this signal would have overlapped with T_m of PEG. Consequently, it could be concluded for the DSC measurements that all samples appeared generally stable after six months of storage. Possibly for HMG Trial HP, ITR had recrystallised further.

All self-produced samples were investigated for their ITR, β CD or (if appropriate) HP β CD content. SEMP, being an authorised marketed formulation was not examined for ITR content. The content was expected to stay in the acceptable range during the six months. Figure IV.62. to Figure IV.65 show the results of these analyses for HMG Trial A, B, HP and SOLU. Additionally, the ITR and CD contents at the beginning as well as at the end of the stability study are given in Table IV.31.. No substantial decrease in content of any component could be observed throughout the storage over six months, regardless if the used container was closed or not.

Table IV.31. - Summary of ITR and CD contents for the beginning and the end of the stability study for HMG Trial A, B, HP and SOLU.

Contents, %	HMG Trial A		HMG Trial B		HMG Trial HP		HMG Trial SOLU
	ITR	β CD	ITR	β CD	ITR	HP β CD	ITR
Beginning of stability study							
	97.59 ± 0.11	105.21 ± 0.37	93.00 ± 2.35	93.70 ± 1.93	100.20 ± 1.39	102.49 ± 2.62	96.04 ± 2.02
Ending of stability study							
Open container	100.69 ± 2.96	102.78 ± 0.52	98.36 ± 4.73	102.51 ± 0.56	96.18 ± 1.54	97.84 ± 6.45	93.54 ± 0.78
Closed container	97.18 ± 1.41	103.13 ± 0.87	100.32 ± 3.19	101.90 ± 2.47	98.74 ± 1.06	96.82 ± 2.06	95.17 ± 0.89

Some experimental values appeared too high, possibly due to inhomogeneous samples or by analytical error. This applied e.g. to ITR content of HMG Trial SOLU at two weeks (open), HMG Trial A at one month (closed), HMG Trial B at two weeks (open) and one month (open and closed) (see Figure IV.62., Figure IV.63., and Figure IV.65.). The results of HMG Trial B (see Figure IV.63.) also indicated that the initially detected ITR and β CD contents might have been outliers, revealing values too low. Additionally, it had to be taken into account that the crushed melt-granules were kept as a bulk in PE bottles. This might have negatively influence segregation of the components over storage time.

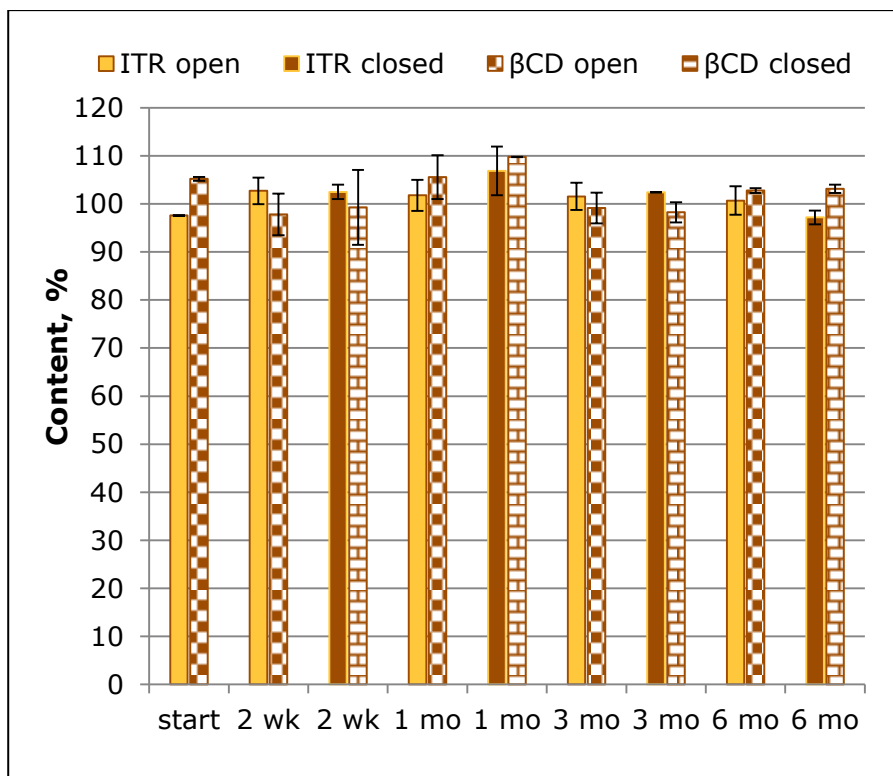


Figure IV.62. - Results of ITR and β CD content analyses of HMG Trial A during the stability study; n = 3; error bars = sd.

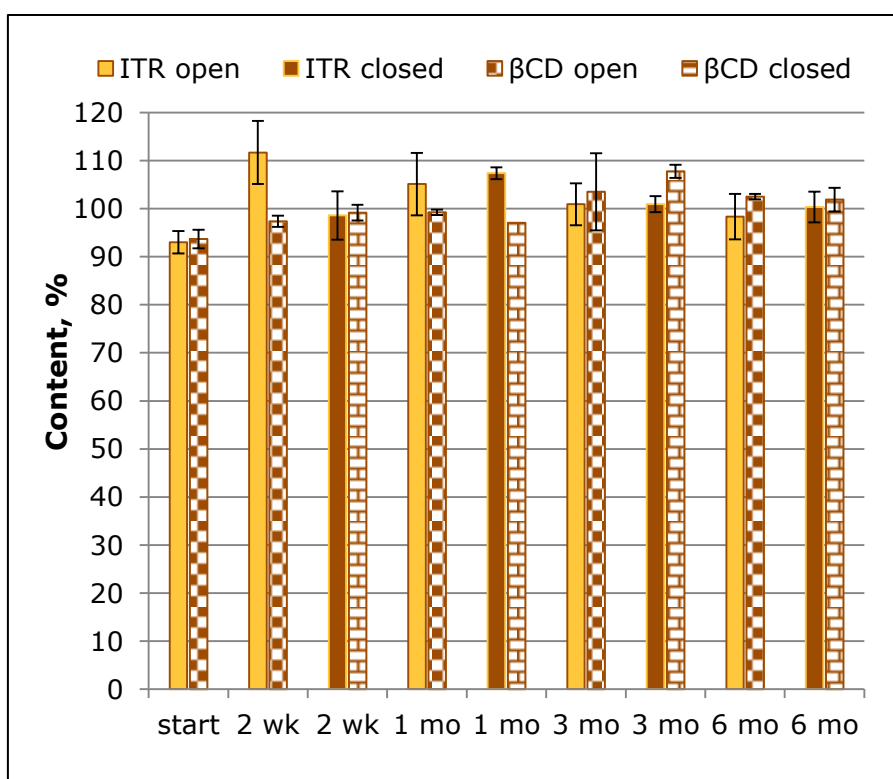


Figure IV.63. - Results of ITR and β CD content analyses of HMG Trial B during the stability study; n = 3; error bars = sd; β CD closed 1 mo n = 1 due to experimental issues.

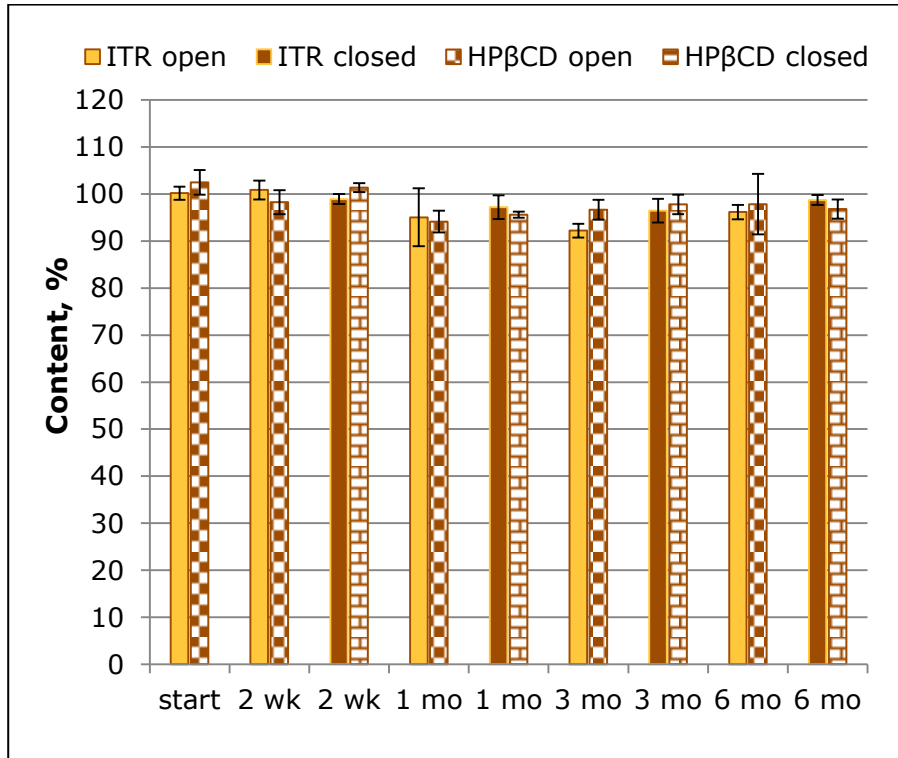


Figure IV.64. - Results of ITR and HPβCD content analyses of HMG Trial HP during the stability study; n = 3; error bars = sd.

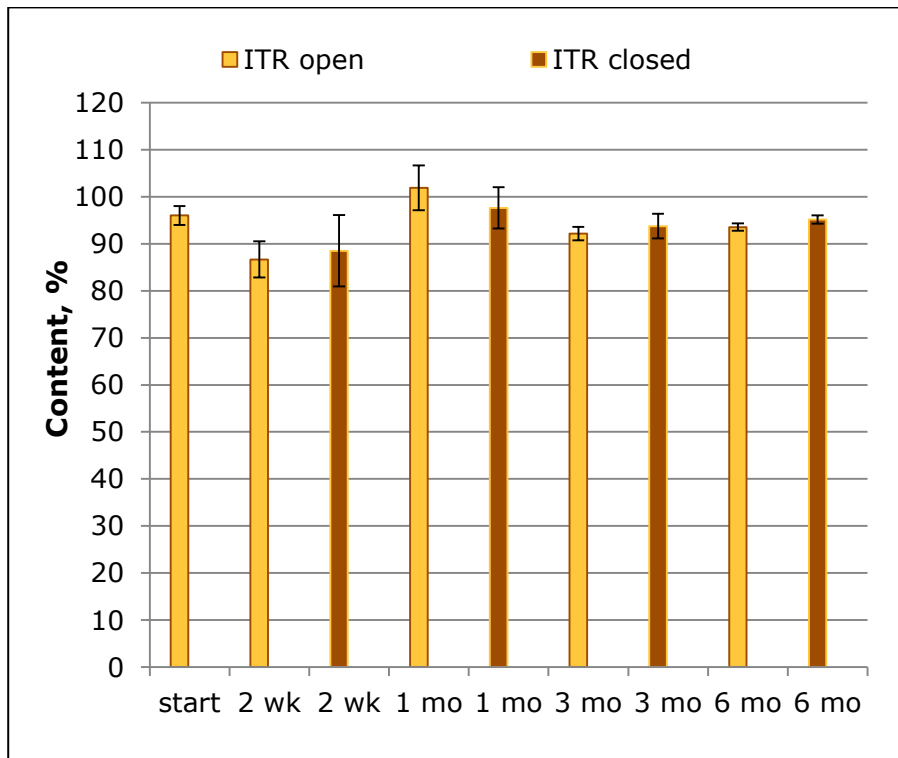


Figure IV.65. - Results of ITR content analyses for HMG Trial SOLU during the stability study; n = 3; error bars = sd.

To generally conclude the content analyses of the four self-produced samples, it could be stated that no degradation of either the API or the CD in question was observed and based on the attained content values, it seemed unlikely that deterioration had taken place during storage. Yet, as the sometimes very high sd indicated, content determination in triplicate might have been not ideal.

IV.10.2.2. Variations in Dissolution and ATR-FT-IR Spectroscopic Changes

The previous subsection revealed no substantial changes in all investigated samples' physico-chemical properties. In addition, all samples undergoing the stability study were investigated regarding their ITR dissolution rate. Furthermore, the self-produced specimen were examined by ATR-FT-IR spectroscopy to detect changes in the interactions of functional groups. Figure IV.66. shows exemplary ATR-FT-IR spectra of these measurements. The ATR-FT-IR spectra were evaluated for changes regarding the structure of the wave bands. Variabilities in intensity might have been ascribed to the unique sample and position in every single ATR-FT-IR run and thus, were not taken into account as indicators for changes in interaction.

HMG Trial A (1 and 2 in Figure IV.66.) did not indicate any transformation over the storage time. Both samples stored in open and closed containers exhibited the same spectra at all investigated sampling time points. For technical reasons, it was not possible to obtain an ATR-FT-IR spectrum of HMG Trial A and B after three months, but the results after six months of storage also showed no difference compared to earlier analyses for HMG Trial A. This was not always the case for HMG Trial B. Mostly, no differences were observed between the spectra as well, particularly comparing the start of the stability study with the six months results. But, when taking a closer look at the wave bands around 1030 cm^{-1} , the one month-measurements in 3 and 4 of Figure IV.66. presented not only one broadened signal with a shoulder on the right side but rather two small peak-like structures. This might have been ascribed to a higher amount of crystalline ITR in the sample or inhomogeneity of the investigated specimen. Despite differences in intensity, no distinct changes were detected for HMG Trial HP (5 and 6 in Figure IV.66.). Merely for the one month-measurement, the broad wave band around 1030 cm^{-1} presented two very small tips instead of one. Explanation for this might have also been a larger amount of crystalline ITR or inhomogeneity.

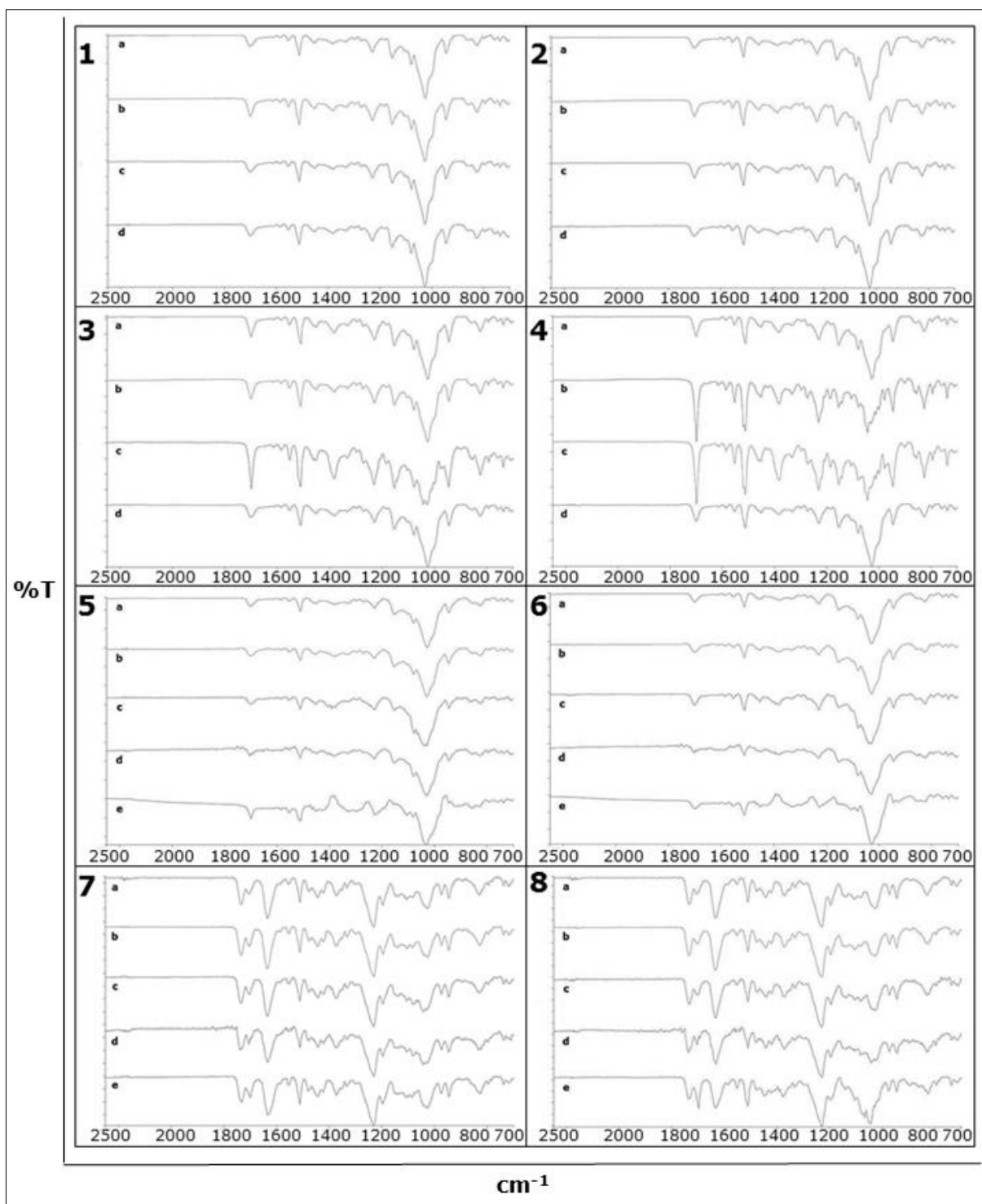


Figure IV.66. - Results of ATR-FT-IR spectroscopy during the stability study of 1) HMG Trial A open containers, 2) HMG Trial A closed containers, 3) HMG Trial B open containers, 4) HMG Trial B closed containers, 5) HMG Trial HP open containers, 6) HMG Trial HP closed containers, 7) HMG Trial SOLU open containers, 8) HMG Trial SOLU closed containers; from a) to e): start, 2 weeks, 1 month, 3 months, 6 months; $n = 3$; due to technical issues, no 3 months-measurement could be conducted for HMG Trial A and B.

The same held true for the results of HMG Trial SOLU. Here as well, no clear variabilities could be observed apart from slight changes in the region around 1050 cm^{-1} after one month of storage both in open and closed containers.

Generally, the ATR-FT-IR results could be viewed as partially inconclusive. Only small alterations could be seen but nothing that would have justified the assumption that any of the samples aged in an outstanding way.

Importantly, all five samples were investigated for their dissolution performance. On a general note, the following dissolution results were always calculated with the corresponding ITR content determined at that time point of the stability study.

Figure IV.67. and Figure IV.68. give the results of HMG Trial A in open and closed containers, respectively. Regarding the dissolution profiles of the samples stored in the open, only minor differences could be detected. The achieved dissolution after 4 h ranged from $86.50 \pm 1.46 \%$ (three months) to $93.55 \pm 1.57 \%$ (two weeks). During the first 30 min, all dissolution curves were nearly identical except the result of six months which presented a faster dissolution rate up until 45 min. All samples had reached 85 % of ITR dissolution after 120 min. The seen variabilities were in an expected range, due to inhomogeneities in the samples as well as natural fluctuations, especially when remembering that only duplicate experiments could be carried out.

The samples stored in closed containers showed related results. After 4 h, ITR dissolution differed between $84.58 \pm 0.91 \%$ (two weeks) and $98.73 \pm 0.85 \%$ (six months). The dissolution curve of the six months sample exhibited a faster dissolution rate than the other samples. It had to be kept in mind, however, that this sample was calculated with the lowest ITR content ($97.18 \pm 1.41 \%$). It might have well been that the derived ITR content was too low which would have subsequently meant that the calculated dissolution values in per cent were too high. The same had to be suspected for the one month-result, as the very high ITR content ($106.87 \pm 5.06 \%$) mathematically forced the dissolution curve down. For the calculated amount of ITR in the dissolution vessel, high variations during content analyses were not taken into account. This however, could also explain strong fluctuations of the dissolution curves.

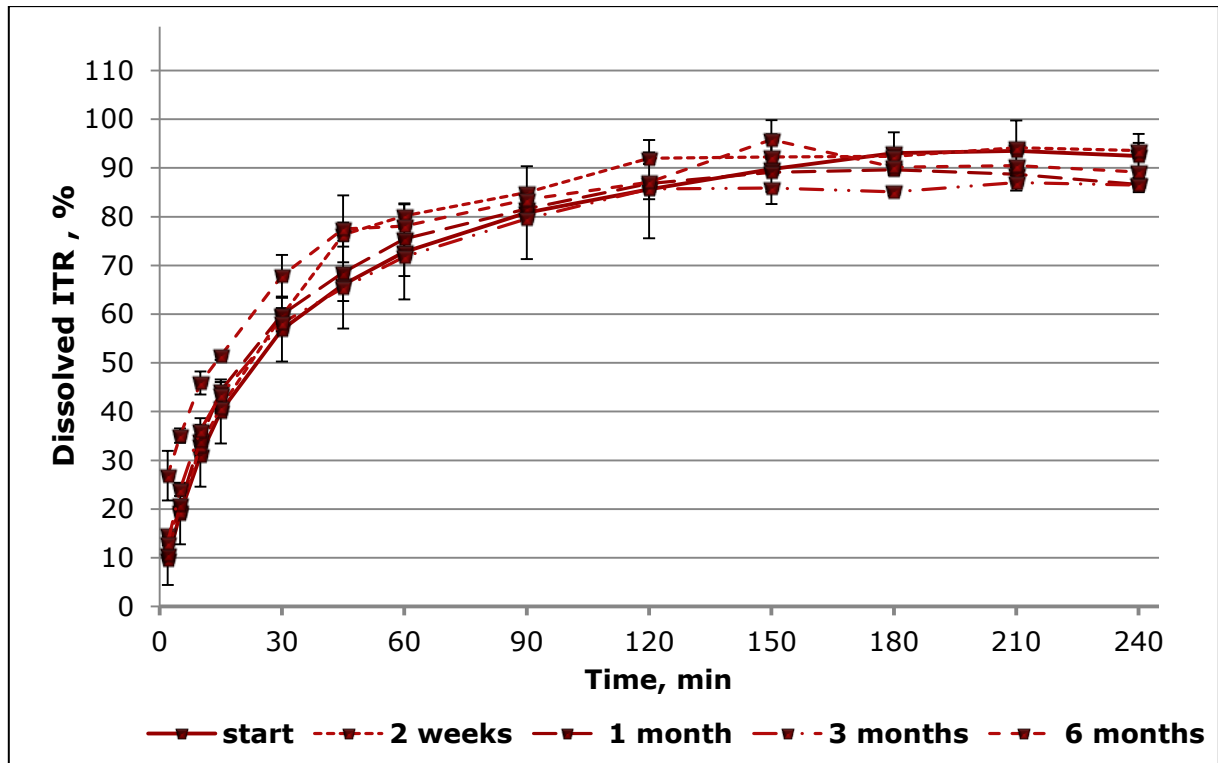


Figure IV.67. - Dissolution results of HMG Trial A stored in open containers during the stability study; n = 2; error bars = min/max.

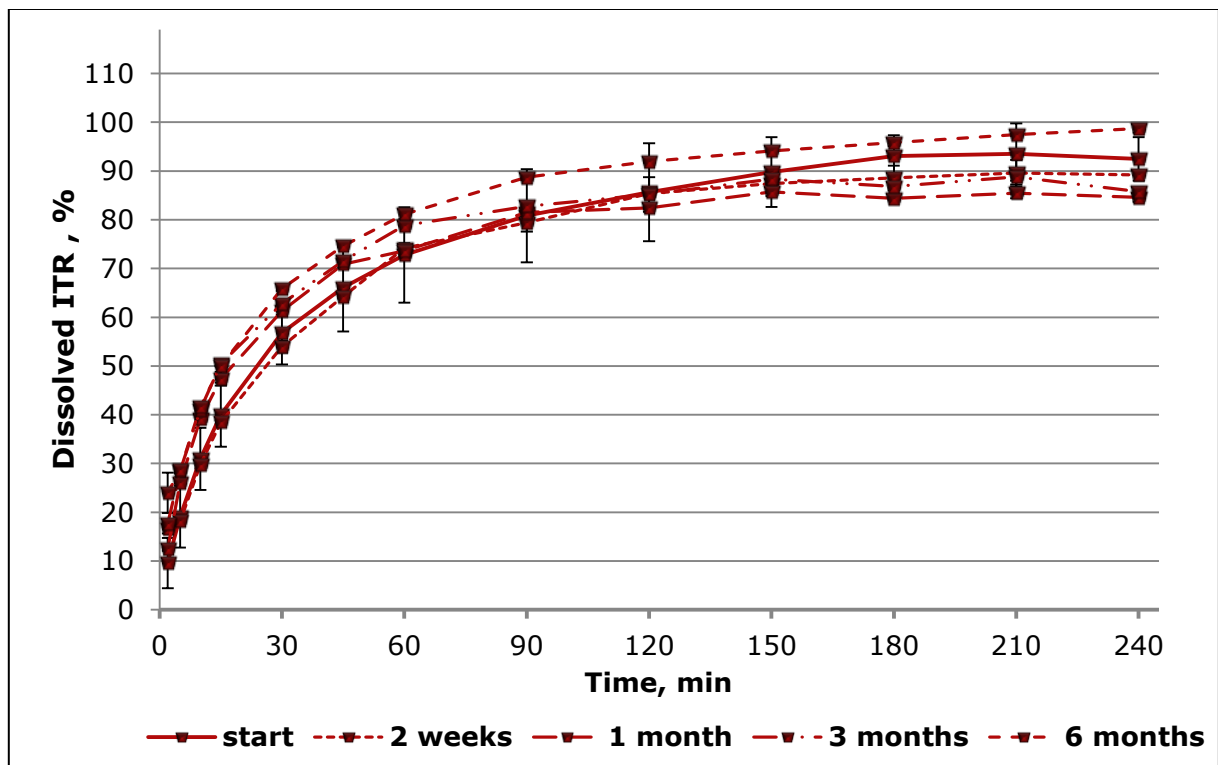


Figure IV.68. - Dissolution results of HMG Trial A stored in closed containers during the stability study; n = 2; error bars = min/max.

Figure IV.69. and Figure IV.70. present the dissolution results of HMG Trial B in open and closed containers. The detected variations here were stronger than for HMG Trial A. After storage in open PE bottles, the ITR dissolution after 4 h ranged from 83.20 ± 0.06 % (two weeks) to 98.46 ± 3.92 % (six months). The low results after two weeks and one month had to be ascribed to the high determined ITR contents (111.68 ± 6.56 % and 105.12 ± 6.51 %). The remaining three dissolution curves showed natural fluctuations. The same held true for the dissolution results in closed containers. Here, dissolution after 4 h spanned from 80.99 ± 0.56 % (one month) to 97.89 ± 2.39 % (start of the stability study). After six months, 95.86 ± 1.06 % of ITR dissolution was achieved. Results of the ITR content evaluation were also reflected in this dissolution analysis, especially in dropping down the curve for one month (ITR content 107.39 ± 1.25 %). Apart from this sample, all other dissolution curves reached 80 % of dissolution after 90 min.

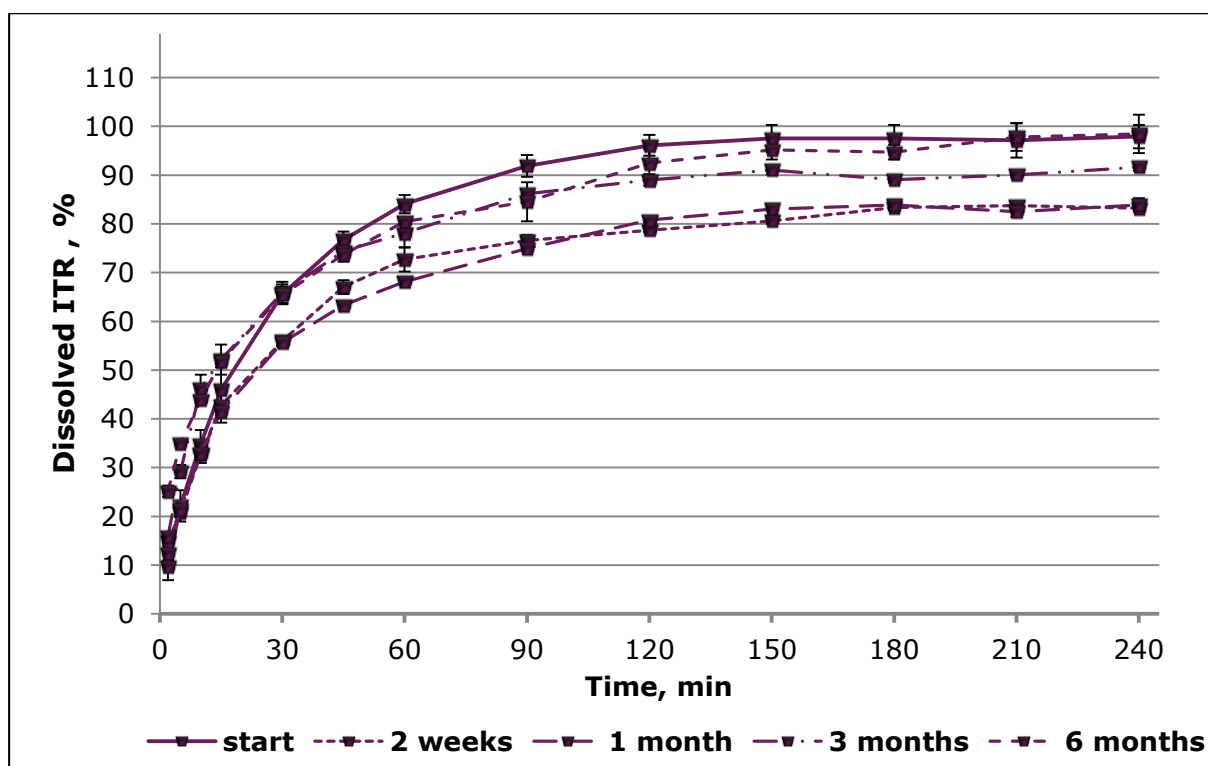


Figure IV.69. - Dissolution results of HMG Trial B stored in open containers during the stability study; $n = 2$; error bars = min/max.

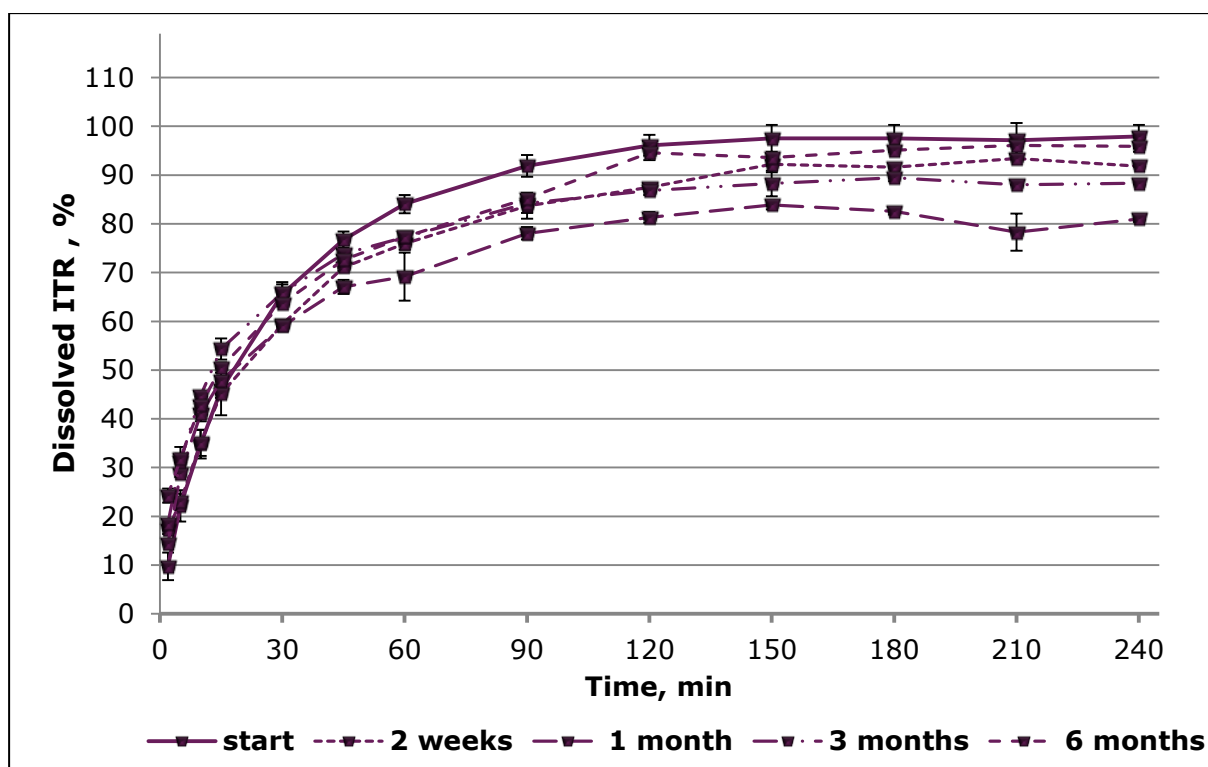


Figure IV.70. - Dissolution results of HMG Trial B stored in closed containers during the stability study; n = 2; error bars = min/max.

Figure IV.71. and Figure IV.72. present the dissolution profiles of HMG Trial HP stored in open and closed containers. The previously described curve fluctuations might have been proclaimed as minor. This, however, was not the case for HMG Trial HP. Dissolution in open and closed containers ranged from $73.66 \pm 3.99\%$ (three months) and $66.00 \pm 1.66\%$ (six months) to $91.31 \pm 0.35\%$ (one month) and $87.29 \pm 8.23\%$ (one month), respectively. This could not solely be explained by segregation within the storage container or falsely determined ITR content. It rather seemed as if the previously described results regarding the high ITR crystallinity as well as suspected inhomogeneities influenced these dissolution results.

The ITR content evaluation after one month in the open container had shown a high sd (6.16 %). This had indicated inhomogeneity of the sample and might have been the reason why this dissolution profile was always above all the other dissolution curves. It was probable that the assumed content for calculating the dissolution curve had been too low. No trend could be observed throughout the six months that would have suggested further ITR recrystallisation or degradation as causes for decreasing dissolution.

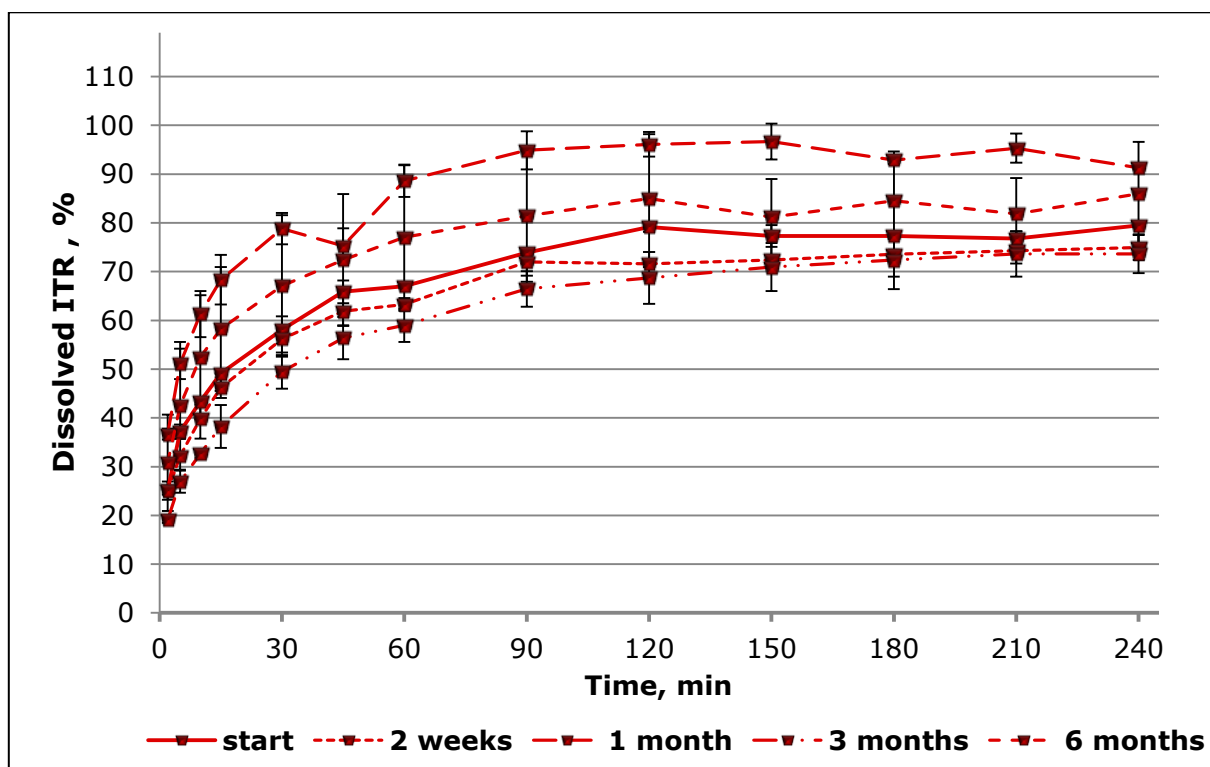


Figure IV.71. - Dissolution results of HMG Trial HP stored in open containers during the stability study; n = 2; error bars = min/max.

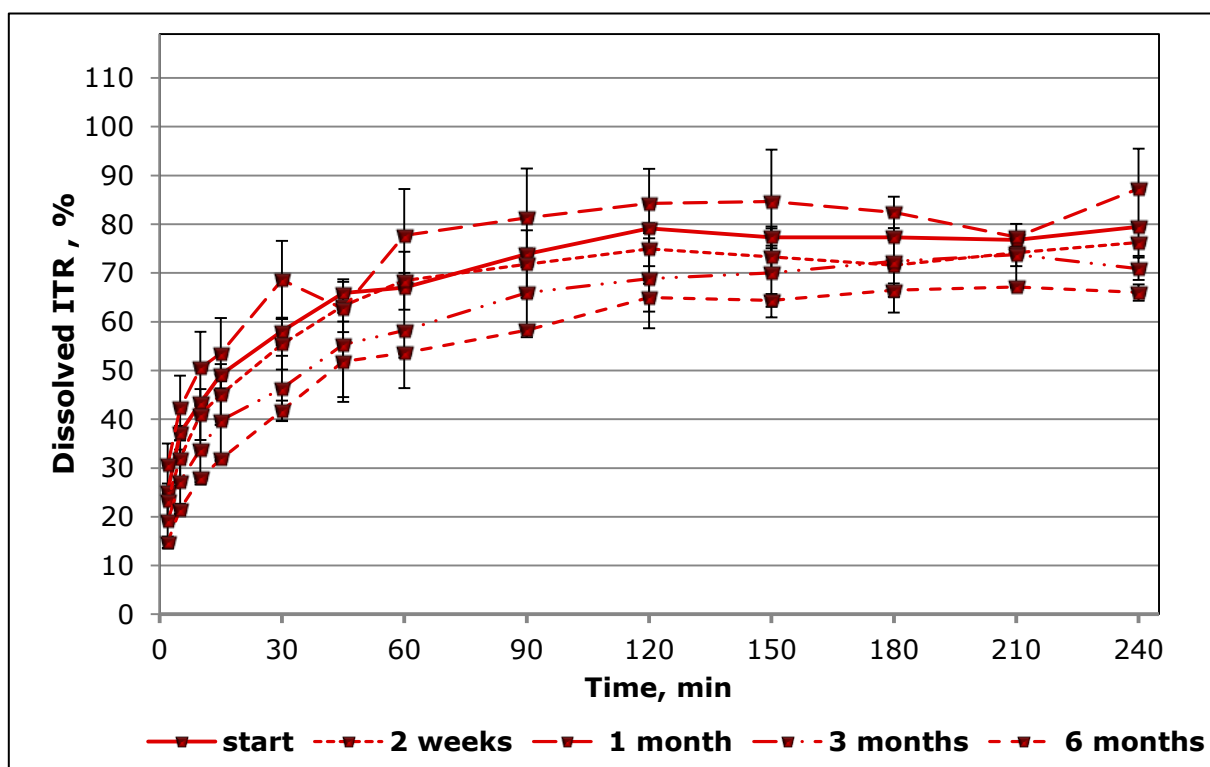


Figure IV.72. - Dissolution results of HMG Trial HP stored in closed containers during the stability study; n = 2; error bars = min/max.

The dissolution results of HMG Trial SOLU are shown in Figure IV.73. and Figure IV.74. for open and closely stored samples, respectively. Regarding the dissolution rate, all samples were identical. Right from the start, there was rapid ITR dissolution with the plateau phase reached after 10 min. The situation of the plateau phase, however, varied strongly for the samples. ITR dissolution ranged from $109.62 \pm 0.37 \%$ (two weeks) to $81.90 \pm 4.27 \%$ (one month) for the openly stored samples and from $87.70 \pm 3.40 \%$ (two weeks) to $100.44 \pm 0.37 \%$ (start) for the samples stored in closed containers.

ITR dissolution after six months was determined to be $101.92 \pm 2.76 \%$ and $98.62 \pm 2.41 \%$ after 4 h in open and closed containers, respectively. Even though content analyses had yielded high variations at some sampling points and had suggested too low results, the obtained dissolution curves could not be completely correlated to that. For example, the low ITR content after three months in the open PE bottle should have caused the dissolution curve to go up, however, this was the lowest dissolution curve. These results strongly hinted at inhomogeneities in the samples. The variabilities of the presented curves were more pronounced for the openly stored samples.

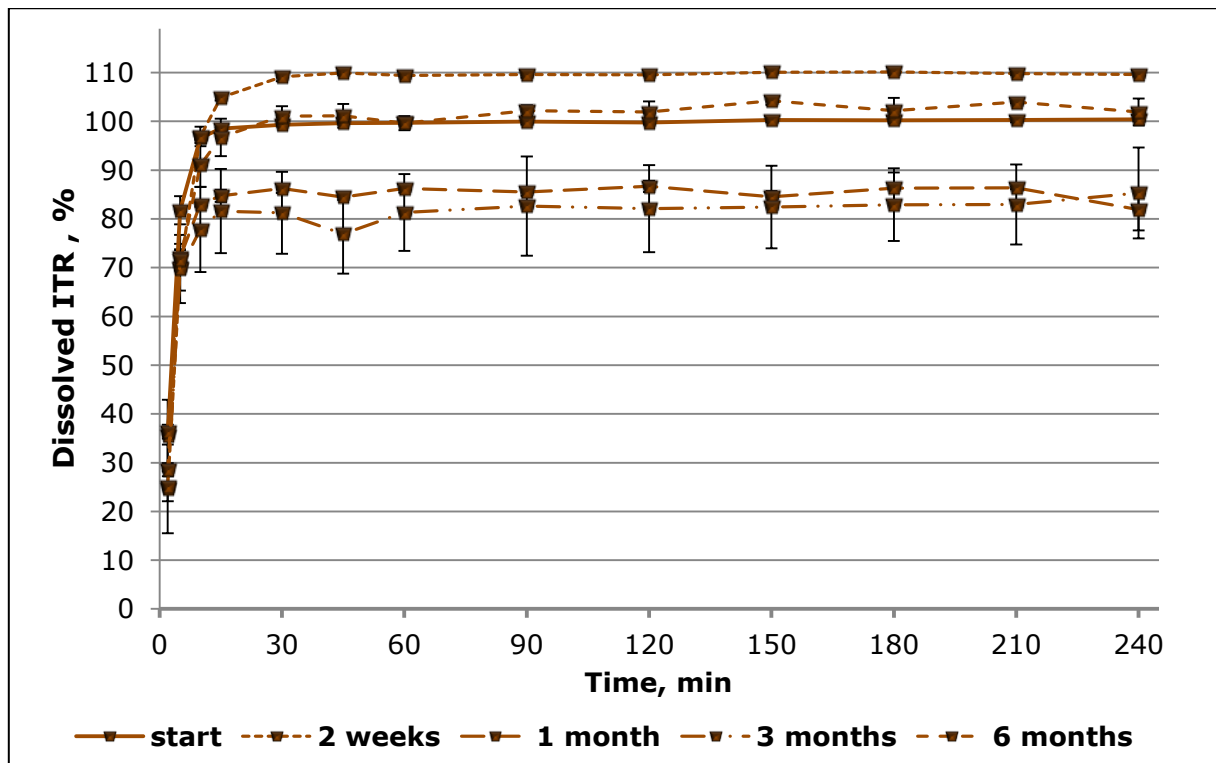


Figure IV.73. - Dissolution results of HMG Trial SOLU stored in open containers during the stability study; n = 2; error bars = min/max; start: n = 6.

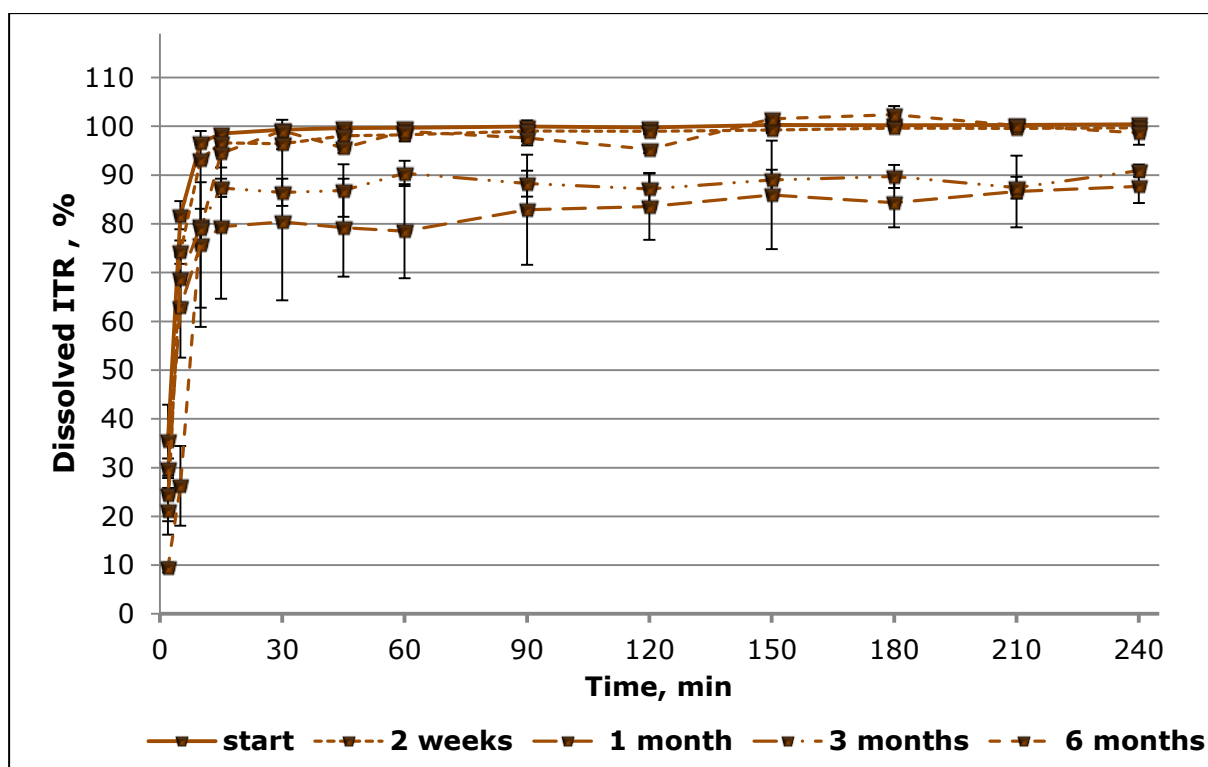


Figure IV.74. - Dissolution results of HMG Trial SOLU stored in closed containers during the stability study; n = 2; error bars = min/max; start: n = 6.

As presented before, HMG Trial SOLU was susceptible to water absorption. It is possible that this might have influenced the dissolution, e.g. by ITR recrystallisation in the dissolution vessel.

Lastly, the marketed formulation, SEMP, was investigated for ITR dissolution during storage. Changes in ITR content were not taken into account. Figure IV.75. and Figure IV.76. present the dissolution curves for the openly and closely stored samples. The results of the samples stored in open containers only showed minor fluctuations of the curves which could be ascribed to slightly differing ITR content (e.g. faster dissolution rate after three months). No difference in lag time was observed during storage as might have been expected due to the cracks in the PEG seal coating as previously reported. ITR dissolution after 4 h ranged from 95.07 ± 0.73 % (one month) to 105.80 ± 1.37 % (three months) for the openly stored samples and from 94.05 ± 1.94 % (six months) to 109.74 ± 3.92 % (three months) for the samples stored in the closed PE bottle. No trend regarding decreasing dissolution or solubility rate was observable. The ITR dissolution for the closed container differed more pronounced. However, no shortened lag time with longer storage could be observed.

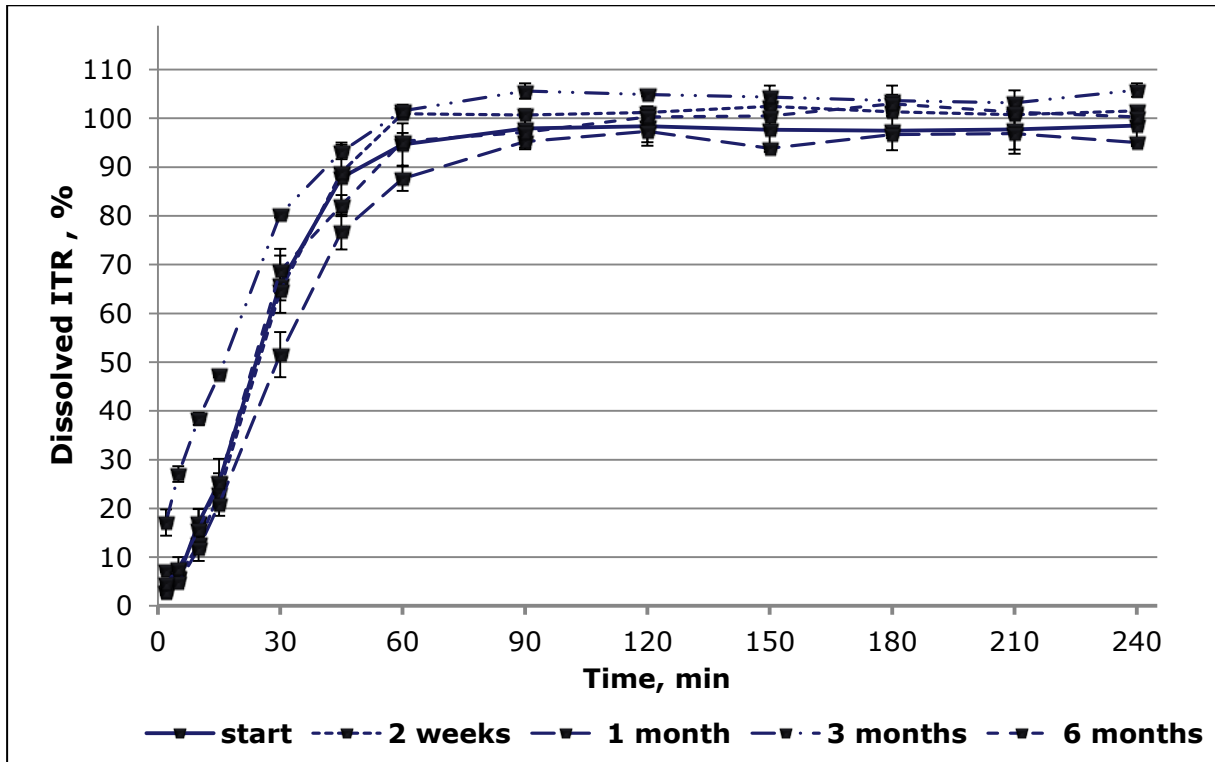


Figure IV.75. - Dissolution results of SEMP stored in open containers during the stability study; n = 2; error bars = min/max; start: n = 6.

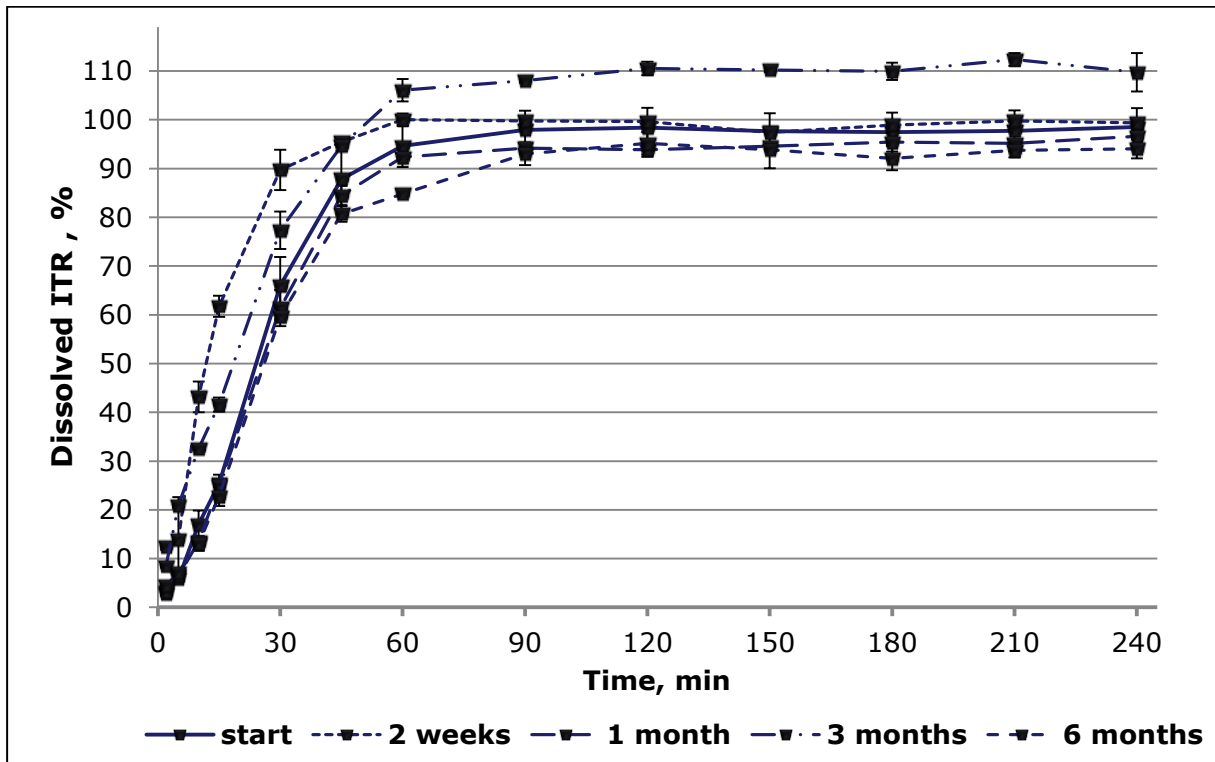


Figure IV.76. - Dissolution results of SEMP stored in closed containers during the stability study; n = 2; error bars = min/max; start: n = 6.

The dissolution rate after two weeks and after three months appeared faster than for the rest of the samples, which could have indicated that a substantial amount of the pellets used in this analysis exhibited disrupted seal coatings. Still, both of these samples reached their plateau phase after 60 min and did not show a decrease in absolute ITR dissolution. The fact that the sample after three months exhibited such high ITR dissolution well above 100 % must have been ascribed to the used sample. Even the marketed formulation allows ITR content to be in a certain range for the product to be regarded as specified. The used ITR amount during this experiment must have exceeded the previously determined ratio that 464 mg equalled 100 mg of ITR. Generally, the hypothesis that the marketed formulation would still show acceptable dissolution results after storage of six months had been proven right.

IV.10.3. Concluding Remarks about the Stability Study

In the previous subsections, results of the stability study of four self-produced samples and SEMP were shown. As suspected, SEMP stayed stable the whole time and no recrystallisation of ITR could be detected in the DSC. ITR dissolution stayed on satisfactory levels. HMG Trial A and B did not show substantial aging over six months. Even though the dissolution curves fluctuated which could be correlated to high variations in the content analyses, no decreasing trend was visible over six months. This also held true for the remaining two samples. However, when evaluating HMG Trial SOLU and HP, variabilities were seen in the dissolution experiments that could not be correlated to ITR content examination. This indicated stronger inhomogeneities in these samples.

Concluding the stability study, it can be said that both HMG Trial A and B proved to be the most stable of the self-produced samples. HMG Trial B showed higher dissolution fluctuations than HMG Trial A. However, the absolute dissolution of HMG Trial B was generally higher than of HMG Trial A, both in openly and closely stored samples. It could still be concluded that HMG Trial B, being produced at lower operating temperatures, seemed to be the most profitable binary β CD formulation *in-vitro*. Nonetheless, during this study, it was only possible to conduct content analyses in triplicate and dissolution experiments in duplicate. For statistically relevant results, this would have to be strongly expanded. That way, the vulnerability of the dissolution results to high content variations could be minimised. Moreover, it would allow obtaining valid statistical data.

Furthermore, the samples were all stored in PE bottles as bulk. It was possible that this had further enabled segregation during storage. Future stability studies should rather use pre-filled capsules or single doses (e.g. in sachets), to exclude this phenomenon from influencing later results. Moreover, it has to be added that a probable pharmaceutical product would most likely also be investigated for storage stability packaged in the chosen primary packaging as this is relevant for determining the later shelf life.

V. Comparative Summary and Overall Discussion

The previous chapters presented the results obtained in this project as well as discussions about specific observations. After the preformulation studies and the development of an HMG procedure to produce binary β CD/ITR melt-granules containing solid ICs, different formulation approaches were presented. The aim of this was to further optimise the firstly created specimen. The following chapter will take up the most important of the previously described data and put them into a wider scientific perspective to allow an encompassing conclusion of this work as a whole.

V.1. Hot-Melt Processes and Formulation Approaches

The foremost goal of the present study was the development of a binary hot-melt procedure that would yield solid ICs on the basis of β CD as matrix. Sections IV.2., IV.3. and IV.4. followed the development of this process, firstly, by employing HME with a self-built conical 6 mm die and secondly, by changing the focus to HMG which resulted in an equivalent product. It was presented that the HMG process was the most feasible procedure for this task. Different temperature profiles were investigated and HMG Trial B was chosen as the best compromise between product properties and coldest applicable temperature. The maximum temperature in this procedure was 180 °C. HMG Trial B showed the highest ITR dissolution after 4 h. ITR was at least mostly amorphous in the samples. Even though ATR-FT-IR results were inconclusive, comparing the dissolution against PMAITR as reference clearly showed interactions between β CD and ITR. Additionally, it was presented that the highest relative enhancement in dissolution compared to crystalline ITR (86 %) had occurred for HMG Trial D, the sample processed at the coldest temperatures, below T_m of ITR.

Sections IV.5., IV.6., IV.7. and IV.8. presented different approaches to optimise the reference formulation HMG Trial B. The marketed formulation SEMP was also investigated for comparative reasons. Furthermore, HP β CD and SOLU were examined as alternative matrices in HMG. In section IV.9., different case studies were described, utilising xylitol, PEG 6000 and HPMC 4000 either as matrix or ternary addition of 10 % and 20 % in mass. Xylitol and PEG 6000 failed to show any additive or synergistic effect on the formulation. The sample containing a

10 % mass fraction of HPMC, however, showed substantially faster ITR dissolution compared to the reference HMG Trial B.

Lastly, chosen samples underwent stability testing, presented in section IV.10.. Apart from segregation of the samples stored as bulk in PE containers, no substantial aging was observed.

The development of HME and later HMG procedures proved to be challenging as β CD lacks thermoplastic behaviour. The results in this thesis showed that β CD did not melt at all during the experiments and was either present in the solid state or degraded. Nevertheless, the resulting HMG process has to be regarded as innovative. The general use of CDs in hot-melt processes can only be referred to as restricted. There is a 2002 US patent dealing with HME of CDs and APIs without the further use of polymers [172]. However, a few facts about this patent are interesting in regard to this project. Firstly, they clearly state that the term "melting" should be interpreted "broadly", covering the possibility that one component does not melt. Secondly, even though β CD is directly mentioned, the presented practical examples in this patent only show the use of HP β CD and dimethyl- β CD. Rambali et al. investigated HME properties with ITR but they also chose HP β CD as matrix [110]. Thiry et al. prepared ternary ICs with different CDs with an mTSE. Yet, they also did not use β CD and their binary IC examples were not prepared by HME/HMG [87]. Yano and Kleinebudde compared wet and hot extrusion of indomethacin/HP β CD mixtures. They found improved indomethacin dissolution for both formulations. They concluded that the dissolution enhancement of the HME sample was most likely caused by API amorphisation and stressed the importance of HP β CD for wet extrusion [173]. Interestingly, it has previously been reported that β CD showed a slightly higher CE than HP β CD for indomethacin [174]. Section IV.1. also showed that ITR exhibited a higher CE with β CD than with HP β CD. Still, somehow there seem to be restraints in regard to the application of β CD as matrix in hot-melt processes.

Fukuda et al. investigated HME with sulfobutyl ether β CD (SBE₇- β CD) and ketoprofen. For comparative processes, they also examined β CD and found that their SBE₇- β CD extrudates showed a faster dissolution rate. However, as SBE₇- β CD is a hygroscopic substance, they saw definite decreases in dissolution after only seven days storage in open containers at 40 °C/75 % RH [81]. Unfortunately, they did not explain much about the HME process operability. Nonetheless, simi-

larities to the HME process described in this work could be found. The die size was also 6 mm and they employed molten API and solid β CD. However, the process developed in this work is more industry-oriented. Apart from the fact that Fukuda et al. only used a mSSE, they also operated their procedure with a ScS of 10 rpm which is considerably lower than 150 rpm as used for HMG Trial B. This comparative study between SBE₇- β CD and β CD was the only attainable report about HME with unmodified β CD. To the author's best knowledge, there are no reports about using β CD as sole matrix component in HMG.

Miller et al. discussed practical considerations that formulators should be aware of when utilising CDs. They mentioned two basic methods for producing solid ICs, coprecipitation and kneading with subsequent drying. Additionally, they reported two innovative approaches, dry grinding and steam granulation. However, they also stated that dry grinding has not proven to be a satisfactory technique in obtaining ICs [175]. This further highlights that the manufacturing of IC without the addition of solvent is an unusual and inventive approach. Cavallari et al. steam-granulated piroxicam and β CD. They used a one-step mixer-granulator-dryer with an electric boiler which supplied aqueous steam at a steady flow. By doing so, the additional use of water is not necessary. It is proposed that the steam diffuses faster into the powder and creates a better thermal balance during a fastened drying step. They found improved piroxicam dissolution rate for the steam-granulated samples and concluded steam-granulation to be a water-saving alternative to WG [176]. In some ways, the HMG procedure described in this thesis shared characteristics with steam-granulation. Water from the CD cavity was vaporised during HMG and also presented as steam before leaving mTSE. HMG Trial D, showing the highest relative dissolution enhancement, was produced at a maximum temperature of 100 °C. Although water vapour was not visible to the extent of the other samples, it might have had some effect. But, an important difference to steam-granulation is the complete lack of further addition of solvent and thus, no need for a drying step altogether. The developed HMG procedure must therefore be described as advancement to steam-granulation.

Regarding only the HMG process, this work clearly demonstrates that it was possible to operate β CD as matrix and gain sufficient results. A continuous, easily up-scalable and stable manufacturing process was developed. Nonetheless, especially the experimentation with different powder blends and formulation ap-

proaches indicated drawbacks of the used HMG equipment, such as the utilisation of only one volumetric feeding station.

Apart from the development of a newly HMG process, another important objective of this work was to gain a product with sufficient characteristics which contained ICs. Figure V.1. recaps all investigated samples in regard to their ITR dissolution after 4 h directly after production. Hereby, the amount of dissolved ITR after 4 h of the samples is juxtaposed with the respective dissolution reference as shown in the correlating sections. Samples processed above ITR T_m were evaluated against PMAITR, samples processed below ITR T_m against PM.

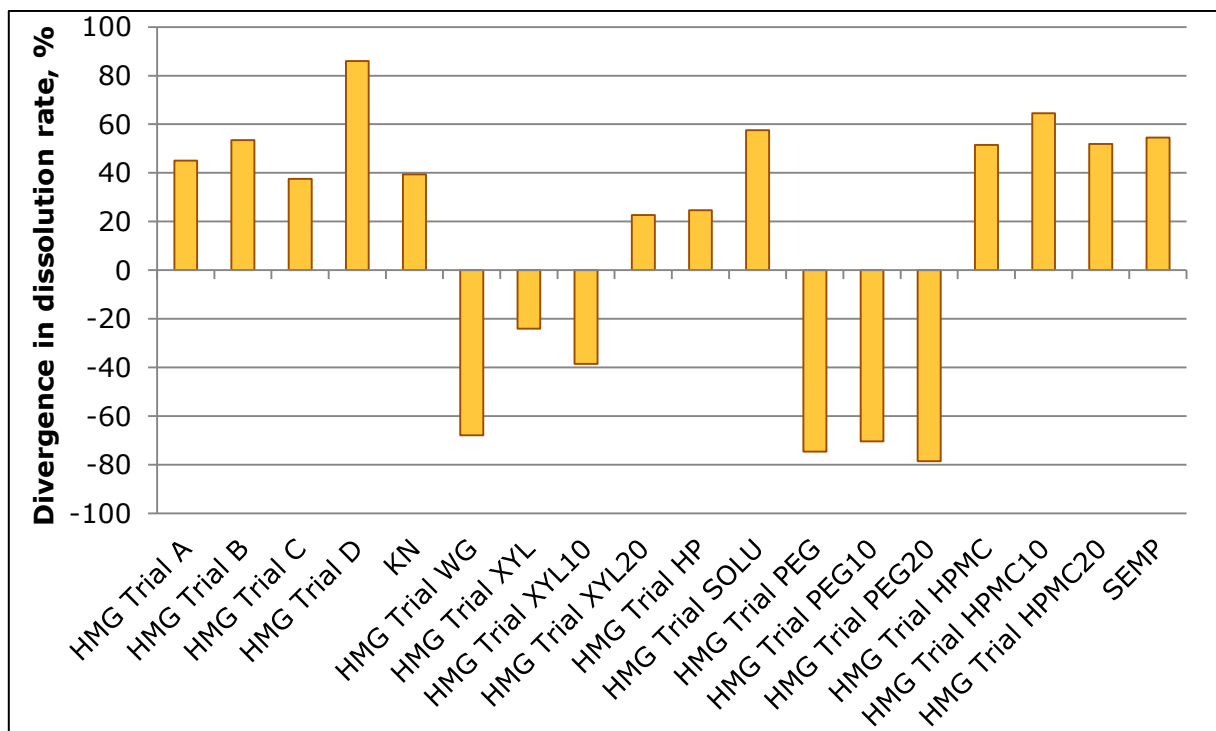


Figure V.1. - Deviations of ITR dissolution after 4 h compared to the respective reference formulation (PM or PMAITR) for all investigated samples in this project.

The presented overview cannot indicate the absolute solubility enhancement of ITR and also not give indications regarding the dissolution rate. In the results and discussion section, some produced samples were already shown to be effective for ITR dissolution. Figure V.2. summarises a selection of those samples as well as SEMP and PMAITR as references. The corresponding results sections showed that the determination of ICs with ATR-FT-IR was challenging if aITR was present. However, the synopsis of Figure V.1. strongly indicates ICF during HMG. All four binary HMG formulations HMG Trial A – D showed improved dissolution against their respective references. The same held true for HMG Trial HP and HMG Trial XYL20. The discrepancy in CE between β CD and HP β CD (see sec-

tion IV.1.) proved true as β CD showed further dissolution improvement than HP β CD. HMG Trial D showed distinct differences in ATR-FT-IR, further proving ICF.

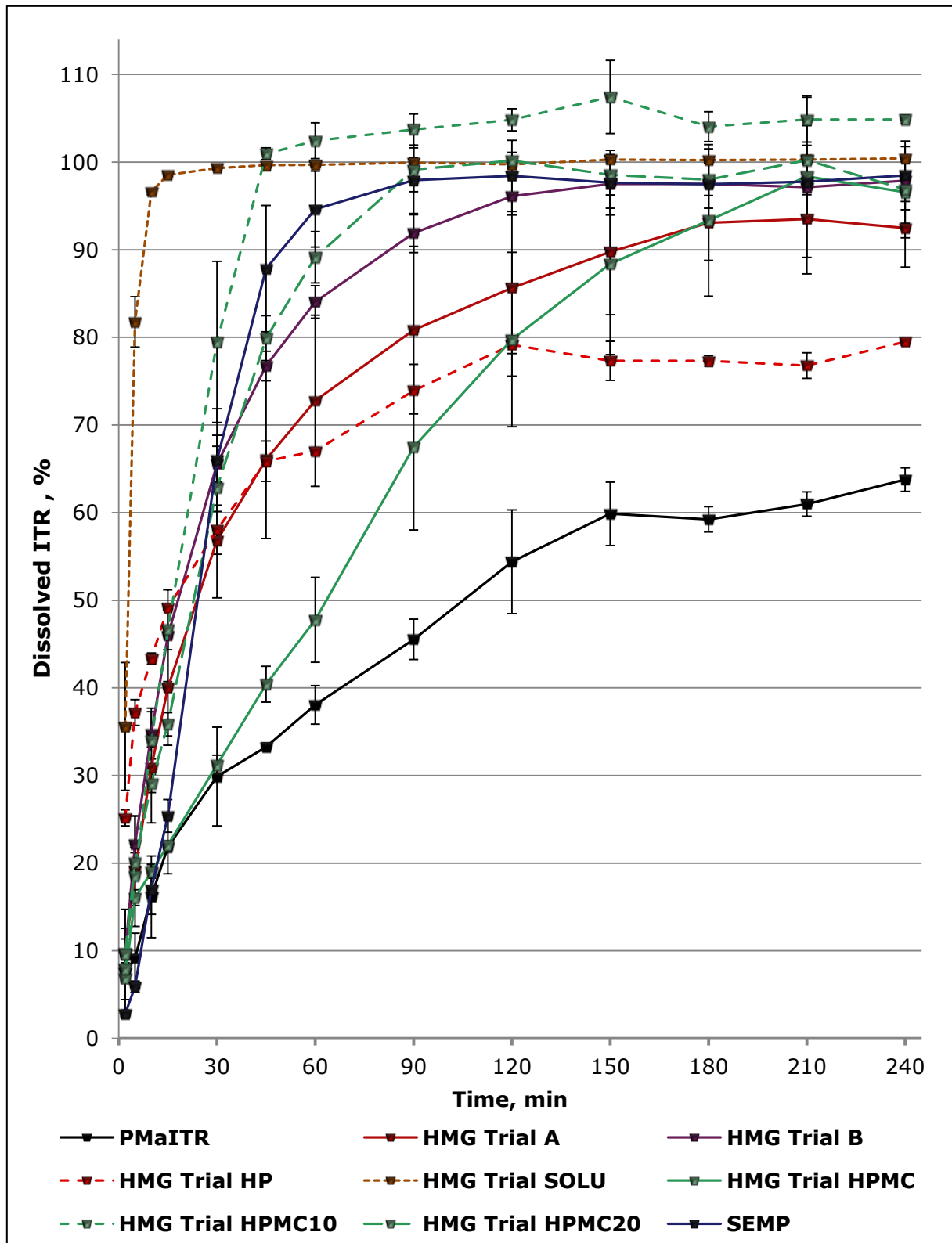


Figure V.2. - Dissolution results of PMAITR (n= 3) and SEMP (n= 6) as references, HMG Trial A (n = 2), B (n = 2), HP (n = 2), and SOLU (n = 6) as well as from the HPMC case study (n = 3); error bars = min/max.

ITR has been extensively studied both in respect to ICF and hot-melt processes. Since ITR is a perfect candidate for solubility enhancing attempts, a plethora of techniques and excipients have been examined and promoted to be the best suitable formulation available. Very often, the concept of solid dispersions is applied. To only name a few, ITR dissolution rate has been improved by spray drying, media milling, ITR salt formation, HME with different polymers or by ICF utilising supercritical carbon dioxide [46,150,177–182]. In recent times, one of the polymers most frequently used in these different research approaches is SOLU.

Guth et al. showed improved ITR *in-vitro* dissolution and *in-vivo* absorption in beagle dogs from SOLU extrudates compared to Sempera® [85]. The presented dissolution rate of SOLU was slower than described in this project, probably due to different experimental settings such as slower paddle rotation speed. As visible in Figure V.2., HMG Trial SOLU exhibited the fastest dissolution rate of all samples which could lead to the assumption that this formulation was best suited for a later industrial process. Thiry et al. examined extrudates with SOLU in binary and ternary form (addition of HP β CD or superdisintegrant) *in-vitro* by a previously reported biphasic dissolution method and *in-vivo* in rats. They found that the CD formulation exhibited highest and fastest ITR release *in-vitro*, whereas the SOLU/ITR/disintegrant formulation was the most favourable *in-vivo* [182,183]. Linn et al. investigated solid solutions of SOLU and ITR and found increased ITR absorption both in Caco-2 cells as well as in beagle dogs [82].

However, to the author's best knowledge, in early 2018, there still is no marketed formulation available containing SOLU. This can be explained by SOLU's regulatory status as a completely new pharmaceutical excipient. Even though there are toxicology studies ongoing, it is still hard to predict how regulatory agencies will respond to an application based on such a new substance. The very strong absorption enhancing and solubility enhancing properties of SOLU could prove to be disadvantageous in humans as is, for example, the case with methylated CDs. Depending on the amount of methylated groups, these CDs can be strongly cytotoxic, e.g. by extracting cholesterol from cell membranes [184]. Until there is no full toxicological profile of SOLU available or the substance has passed a regulatory inquiry, HMG Trial SOLU could not be regarded as the most favourable formulation prepared in this project. This conclusion was also backed up by the fact

that the operability of HMG with SOLU was not as sufficient as with the binary ITR/ β CD, especially regarding the sampling procedure at the granulation heel slide.

Figure V.1. further stresses the failure of the investigated ternary additives xylitol and PEG 6000. Apart from HMG Trial WG, these samples were the only ones showing negative deviations in regard to their reference. The only exception was HMG Trial XYL20 which showed the smallest increase of dissolution of all positive samples. The case study HPMC 4000, however, yielded interesting results. The addition of a 10 % mass fraction of HPMC 4000 to the binary β CD/ITR formulation strongly increased the dissolution rate. The sample even showed faster dissolution than SEMP. This sample combined fast ITR dissolution with the coldest applicable HMG temperatures based on HMG Trial B. The fast dissolution was due to the combination of ITR amorphisation, ICF and improved wettability or possibly complexation between ITR and HPMC 4000. Due to its size, it seemed unlikely that HPMC 4000 (or parts thereof) had become included in the β CD cavity.

Figure V.3. shows a magnification of the first 30 min of dissolution testing presented in Figure V.2.. Of all self-produced samples apart from HMG Trial SOLU, HMG Trial HP showed fastest dissolution during the first 15 min. HMG Trial HPMC10 exhibited higher ITR dissolution than SEMP during the whole 30 min. Before interpreting these data regarding the definition of the most optimal specimen produced during this work, the limitations of the presented results have to be considered. First of all, most dissolution studies could only be performed in duplicate. Nevertheless, all samples underwent stability testing and since no substantial aging was detected, the dissolution of the samples in question stayed on similar levels as presented in Figure V.2. and Figure V.3.. Secondly, all data provided only *in-vitro* information. The used dissolution method for ITR was a simple and traditional procedure. Even though it lacked complexity, it allowed discriminatory results. As mentioned previously, Thiry et al. developed a biphasic ITR dissolution method which supposedly should further mirror the GIT [183].

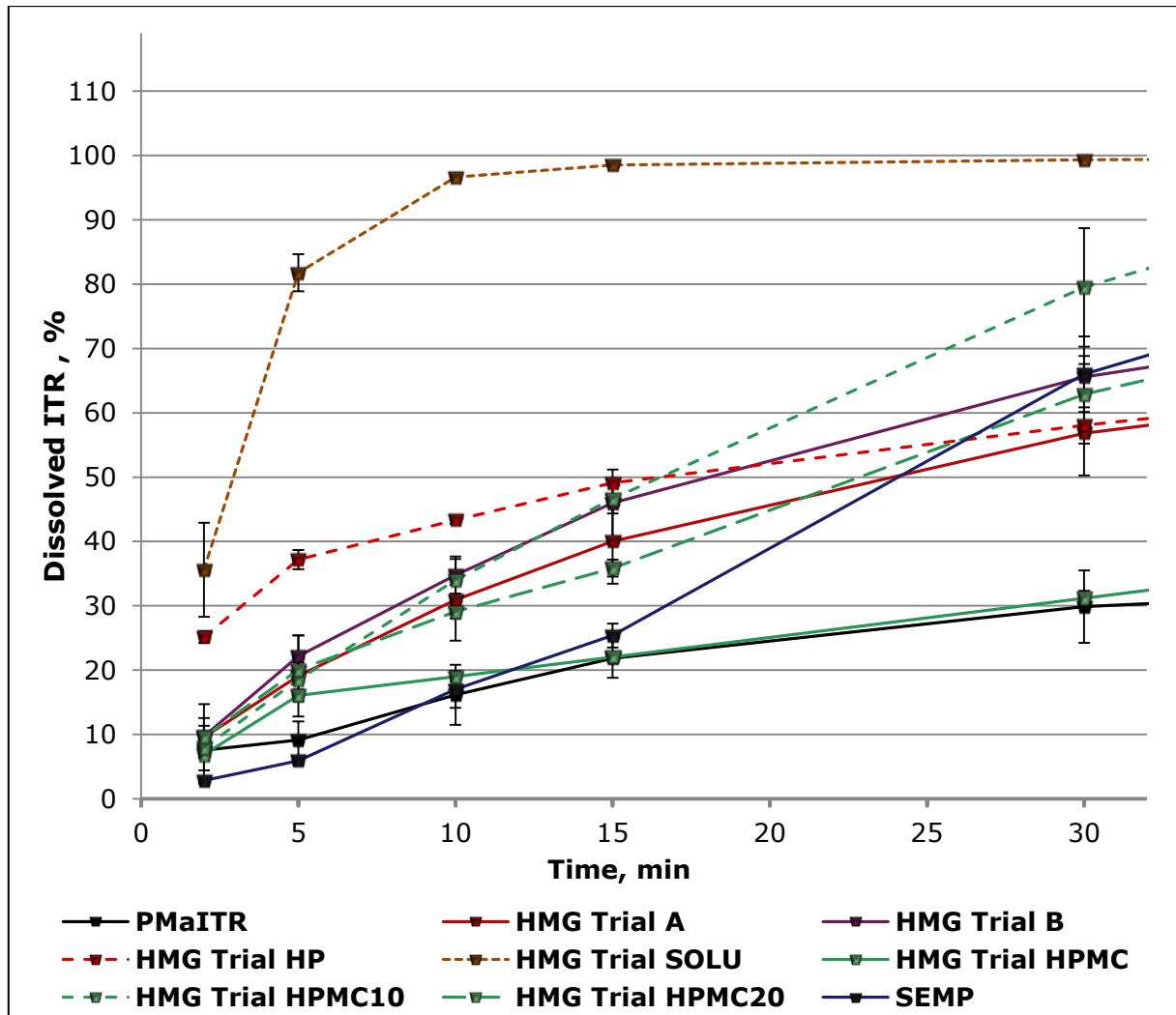


Figure V.3. - Dissolution results of PMAITR (n= 3) and SEMP (n= 6) as references, HMG Trial A (n = 2), B (n = 2), HP (n = 2), and SOLU (n = 6) as well as from the HPMC case study (n=3) during the first 30 min of the experiment; error bars = min/max.

However, as described in section III.1.2., the bioavailability of Sporanox[®] is situated at about 55 % even though dissolution results have shown quantitative ITR release. ITR is strongly protein bound and causes unpredictable individual absorption not only in humans, but also in birds, horses, reptiles or arthropods [185]. Yoo et al. investigated the different oral absorption of ITR in laboratory rats, rabbits and dogs and found strong variabilities [186]. Zimmermann et al. concluded after examining the influence of food on ITR absorption in humans that the influence was very strong but sometimes irregular and variable between individuals. Additionally, they found that ITR absorption was improved by long gastric retention times, low stomach pH, and a high fat content of the co-administered meals [187,188].

The presence of CDs can further complicate the circumstances for the drug in the human body. Stappaerts and Augustijns conducted *in-vitro* gastrointestinal transfer studies of ITR in the presence of HP β CD and different bile salts. They found that in the intestinal milieu, ITR was supersaturated depending on the excipients. However, displacement of ITR from the HP β CD cavity caused by bile salts was also observed. The consequently following ITR precipitation was not always seen, probably because ITR was emulsified by the present bile salts. They concluded that the supersaturated amount of ITR was rapidly absorbed and that the presence of CDs as well as different endogenous substances definitely impacted ITR absorption [167].

Another interesting study about ITR behaviour in gastric and intestinal milieus was carried out by Brouwers et al. (part I) and Berben et al. (part II). They investigated GIT precipitation of ITR in human volunteers after administering Sporanox[®] capsules and solution which contains HP β CD. Additionally, they reviewed precipitation and supersaturation of ITR from Sporanox[®] solution after intake with and without water. Their findings included that the solution showed faster and higher ITR dissolution in the stomach. But, in the small intestine, precipitation occurred. Generally, they observed high variabilities between their subjects. In part II of the study, they made the observation that even though ITR precipitation was higher after taking Sporanox[®] solution with water, the systemic exposure of ITR was nearly identical to the intake without water. They concluded that HP β CD in diluted form partially lost its encapsulation ability. But, even when more ITR was in solution, the included portion was not able to permeate through intestinal membranes [189,190]. This is a good example for the solubility-permeability interplay of an API. Just because the drug is dissolved does not automatically mean that the absorption will be high.

All these different case studies clearly show that it is almost impossible to predict ITR *in-vivo* behaviour after evaluation of *in-vitro* data, regardless of the investigated species. Also, they stress the individual variabilities of ITR absorption. This project majorly dealt with the general development of the β CD/ITR formulation. Although the obtained *in-vitro* results do not allow a distinct prediction of physical ITR absorption, they can indicate the theoretical dissolving of ITR. This also holds strong value, especially as a specification for determining the product quality.

Notwithstanding, transferring the results of Berben et al. to the dissolution results obtained in this project for HMG Trials B, HP and HPMC10, it has to be considered that the faster dissolution rate in the 30 min window may lead to higher ITR dissolution in the stomach but also to higher precipitation and less absorption due to the complexation [190]. On the other hand, Loftsson et al. concluded after reviewing different oral formulations with CDs that the necessary mechanism for drug absorption from the GIT should be dilution of the formulation to force the drug out of the IC and make it accessible to intestinal membranes. They strongly suggested that formulations should not contain excess CD as this would hamper dilution after intake [191]. This might explain the similar ITR plasma concentrations Berben et al. obtained for their two samples [190]. It appeared as if the amount of precipitated ITR was not relevant in this study for the efficacy in the patient. Brouwers et al. however showed much higher plasma concentrations for the oral solution than the oral capsule [189]. Even though it was suboptimal to compare a solution and a capsule, these results still suggested that the formulation with CD was superior to the polymer-based formulation.

Based on this, three self-produced formulations stood out to be potentially regarded as the most optimal exemplar, HMG Trial B, HP and HPMC10. HMG Trial HPMC10 showed the fastest absolute dissolution rate whereas HMG Trial HP showed the highest ITR dissolution in the first 15 min. Brouwers et al. showed t_{\max} values for the Sporanox[®] capsules and solution of 2.9 ± 1.6 h and 2.5 ± 0.7 h, respectively [189]. This supported a scenario where the faster dissolution rate would not be that important for the absolute drug absorption when evaluating the 4 h experimental set-up presented in this work. Thus, as HMG Trial HP exhibited lower absolute ITR dissolution, CE was lower than for β CD, and as it is a much costlier excipient, this sample was ruled out as optimal formulation. This choice was also supported by the fact that HMG Trial HP was the only sample where a dissolution influence due to small particle size in comparison to the other specimen could not have been excluded. Thus, the only advantage of this sample compared to the other two might have been a mere result of smaller particles and not ICF.

HMG Trial B and HPMC10 both reached nearly quantitative ITR dissolution after 4 h with HMG Trial HPMC10 showing the faster dissolution rate. However, the mixture of HMG Trial HPMC10 differed more strongly in ITR content due to seg-

regation. This forced the determined ITR dissolution above 100 %. With the used equipment, HMG Trial B had to be regarded as more stable. Nonetheless, provided different feeders were used, HMG Trial HPMC10 would be creatable in a more reproducible manner. Due to the presence of HPMC 4000, it was not possible to distinguish between ICF and dissolution improvement due to amorphisation or other mechanisms. Moreover, no stability data were obtained for the HPMC 4000 case study. Even though HPMC based SEMP did not show much signs of aging regarding the dissolution tests, this still could not be extrapolated towards HMG Trial HPMC10.

Therefore, taking into account all of the *in-vitro* results presented in this thesis, it could be confirmed that HMG Trial B entailed the best compromise between high ITR dissolution, low application temperature during HMG (maximum 180 °C) and storage stability. The product utilised a cost-effective, sustainable excipient. In ITR therapy against fungal infection with HMG Trial B (200 mg ITR/day), β CD intake would be 320 mg/day. Until October 2017, the NOAEL of β CD for adult humans was 500 mg/day. Then, the annex to the European Commission guideline on 'Excipients in the labelling and package leaflet of medicinal products for human use' was updated and proposed a limit of 20 mg/kg/day to be harmless [78,79]. This would also allow high dose ITR therapy in adults with HMG Trial B.

VI. Conclusion and Perspectives

VI.1. Final Denouement and Scientific Significance of the Developed Formulation

To finally conclude this work, it can be stated that it was possible to develop a novel polymer-free HMG process for binary β CD formulations. Simultaneously, it was possible to create ICs without addition of solvents.

HMG Trial B with a maximum processing temperature of 180 °C was selected to be the most favourable HMG formulation manufactured in this project. The comprehensive presentation and discussion about the development of the HMG procedure are useful examples regarding the overall strategy when creating a new hot-melt process. In addition, it was shown that the change from HME to HMG does not have to coincide with loss of desired product properties. In the course of the process development, a new 6 mm conical die was developed. Insights into the necessary inner die structures when operating without polymers are also of value for formulation scientists working in this field.

The present thesis provides continuous manufacturing procedures for β CD that can either result in improved API dissolution by the combination of amorphisation and ICF or solely by ICF. The mere processing of ITR at a temperature of 100 °C (HMG Trial D) showed the highest relative improvement in dissolution even though nearly no vaporisation of cavity water was observed.

With the development of the HMG process as well as different optimisation approaches and the conducting of a stability investigation, all previously defined objectives have been met. A comprehensive summary of the positive properties of the developed HMG procedure is given in Table VI.1..

Finally, it can be confirmed that the present work combines the development of a new HMG technique from scratch as well as the thorough characterisation of the produced samples. Important conclusions could be drawn from the given data, both for the application of CDs and HME/HMG. Nonetheless, there are yet future possibilities regarding the here-in presented research. These will be shortly discussed in the next subsection.

Table VI.1. - Favourable process characteristics of the developed HMG procedure.

Favourable Process Characteristics	
▼	<i>Stable, solvent- and polymer-free process was operated which holds strong industrial potential.</i>
▼	<i>Continuous manufacturing process would allow 24/7 production of a formulation with higher drug load than SEMP.</i>
▼	<i>Less production steps and excipients than SEMP as the binary product utilised only one cost-effective and sustainable excipient.</i>
▼	<i>ICF during HMG proven by dissolution results and by ATR-FT-IR for crystalline sample.</i>
▼	<i>Additional effects by amorphisation of ITR and ICF with βCD were proven.</i>
▼	<i>ITR only employed as model substance; technique generally suitable for any API, possibly even without the use of high temperatures, since greatest relative dissolution enhancement for a crystalline sample prepared below the T_m of ITR.</i>
▼	<i>Process can be regarded as novel model technique for solvent-free ICF. HMG could be entrenched as additional method for ICF in the solid state.</i>

VI.2. Future Possibilities

While reasonable explanations were found for emerging issues about the presented data, there were also some drawbacks defined which could be eradicated in future research. These are, mainly, the mTSE equipment as well as the statistical significance of the results. It was described that the used mTSE was operated with a volumetric feeding system which made it impossible to fully determine the throughput of the material during processing. Furthermore, the use of one single hopper promoted mixture segregation. The use of separate gravimetric feeders would allow constant throughput monitoring. This would also lower production costs as blending of the API with the matrix would not be necessary. Follow-up studies with more suitable HMG/HME equipment should be carried out to improve reproducibility of the results.

In addition, the sample characterisation should be conducted with a larger sampling size. In this work, statistical analyses of the results were left out due to

the small number of replications that were implementable. Additionally, the presented process should be conducted with different model APIs to gain far-reaching insights into the binary HMG of unmodified β CD. As the patent protection of Sporanox[®] capsules has already expired and many different generic formulations are available on the market, the realistic possibility for a new oral ITR formulation has to be considered slim. If ITR is authorised for additional indications such as the recently researched types of cancer (see section III.1.1.) this judgement may need to be revised. However, when considering ITR as model BCS class II API, it is likely that the innovative HMG process holds strong scientific value in formulation design of different BCS class II APIs, mainly NCEs. The water-free ICF method could possibly allow investigations with hydrolysis-sensitive drugs.

Lastly, to fully fathom the clinical significance of the developed process and subsequent formulation, *in-vivo* studies should be carried out regarding drug absorption. For the oral use of β CD, no toxic effects have to be expected.

Utilising parenterally harmless CDs in the HMG process such as HP β CD would be a possibility to continuously produce solids for later reconstitution and parenteral application. Having the right equipment at disposal, the new HMG process may be universally employed for a plethora of administrations, depending mostly only on the substances used.

VII. Appendices**VII.1. Abbreviations, Units and Variables**

%	mass fraction
[CD] _t	total cyclodextrin concentration in phase-solubility measurements
°2θ	degree of diffraction angle in XRPD
A	ampere
A	surface
ADI	acceptable daily intake
aITR	amorphous itraconazole
API	active pharmaceutical ingredient
ATR-FT-IR	attenuated total reflectance Fourier-transform infrared spectroscopy
βCD	beta-cyclodextrin
BCS	Biopharmaceutics Classification System
CE	complexation efficiency
C _s	saturation concentration
D:CD	drug : cyclodextrin ratio
<i>d</i>	diameter
d	day
D	extruder screw diameter
<i>D</i>	diffusion coefficient
DCS	Developability Classification System
dem.	demineralised

DSC	differential scanning calorimetry
D_t	total drug concentration in phase-solubility measurements
DR	dissolution rate
drug load	mass fraction of the API of a formulation
$\frac{dX}{dt}$	dissolved drug (dX) over a time period (dt)
EMA	European Medicines Agency
EV	Einschlussverbindung(en)
f1	difference factor
f2	similarity factor
FAO	Food and Agriculture Organisation of the United Nations
FB	formulation bulk
FDA	US Food and Drug Administration
GIT	gastrointestinal tract/Gastrointestinaltrakt
GRAS	generally recognised as safe
h	effective boundary layer thickness
Hh	Hedgehog pathway
HME	hot-melt extrusion
HMG	hot-melt granulation
HMG Trial A, B, C, D	samples of different HMG temperature profiles
HMG Trial HP	sample of HP β CD HMG case study
HMG Trial HPMC/10/20	samples of HPMC 4000 HMG case study
HMG Trial PEG/10/20	samples of PEG 6000 HMG case study

HMG Trial SOLU	sample of Soluplus® HMG case study
HMG Trial WG	sample of HMG process after WG
HMG Trial XYL/10/20	samples of xylitol HMG case study
HPβCD	hydroxy-propyl-beta-cyclodextrin
HPLC	high performance liquid chromatography
HPMC	hydroxy propyl methyl cellulose
i.v.	intravenous
IC	inclusion complex
ICF	inclusion complex formation
IFB	increase in bulk formulation
ITR	Itraconazole/Itraconazol
IVIVC	<i>in-vivo</i> – <i>in-vitro</i> correlation
IVIVR	<i>in-vivo</i> – <i>in-vitro</i> relationship
JECFA	Joint FAO/WHO Committee of Food Additives
KN	sample of kneading process
L	length of extruder screws
L/D ratio	ratio between length and diameter of extruder screws
M	mole per litre
mg/kg · bw	milligram per kilogram body weight
min	minute(s)
mo	month(s)
mPa · s	milli Pascal · second
mSSE	melt-single screw extruder

mTSE	melt-twin screw extruder
MWCD	molecular weight of cyclodextrin
MWdrug	molecular weight of drug
N	normality, $\frac{\text{molar concentration}}{\text{equivalence factor}}$
NCE	new chemical entity
NIC	non-inclusion complex
Nm	Newton metre
PAT	process analytical technology
PEG	Polyethylene glycol
Ph.Eur.	Pharmacopoeia Europaea
PM	physical mixture
PMaITR	physical mixture with amorphous itraconazole
PS	phase solubility
PSD	phase solubility diagram(s)
PSM	phase solubility measurements
PVPVA	polyvinyl pyrrolidone vinyl acetate
R ²	regression coefficient
H	relative humidity
rpm	rounds per minute
R _t	dissolution value of reference at time t
s	second(s)
ScS	screw speed
sd	standard deviation
SE	Schmelzextrusion

SEM	scanning electron microscopy
SEMP	marketed formulation Sempera®
SG	Schmelzgranulation
SOLU	Soluplus®
<i>t</i>	time point
TGA	thermogravimetric analysis
<i>T_t</i>	dissolution value of measurand at time <i>t</i>
UK	United Kingdom
US	United States of America
US\$	currency of the United States of America, US-dollar
USP	United States Pharmacopeia
wt/v %	weight per volume per cent
WG	sample of wet granulation process
WHO	World Health Organisation
WS	Wirkstoff
<i>V</i>	volume
V/V	volume per volume
<i>X_d</i>	amount of dissolved drug
XRPD	X-ray powder diffraction
XYL	xylitol
\bar{x}	arithmetic mean
yr/s	year/s

VII.2. Analyser Materials

Material	Manufacturer
Acetonitrile	Honeywell Riedel-de Haën™, Fisher Scientific GmbH, Germany
Argon 5.0	Linde AG, Germany
Bidistilled water	freshly produced with in-house Finn Aqua 75, San-Asalo-Sohlberg Corp., Finland
Citric Acid, mono hydrate	Carl Roth GmbH & Co. KG, Germany
Hydrochloric acid	AppliChem GmbH, Germany
Methanol, HPLC Grade	Avantor Performance Materials Poland S.A., Poland
Nitrogen 5.0	Linde AG, Germany

VII.3. Methods for Content Evaluation

VII.3.1. HPLC Method for Itraconazole Content Evaluation

Table VII.1. - HPLC method for ITR quantification

HPLC system	Agilent 1100 Series LC with diode array detector (Agilent Technologies Inc., US)
Software	HPChemstation (Agilent Technologies Inc.)
Column	LiChroCart® 125-4, LiChrospher® 100 RP18-5 (Merck KGaA, Germany) with precolumn
Mobile phase	80/20 V/V% acetonitrile/ bidistilled aqueous citric acid 1 %, pH adjusted to 3.2 - 3.3
Flow rate	2 mL/min
Oven temperature	20 °C
Detection wavelength	264 nm
Injection volume	100 µL
Run time	3.5 min

VII.3.2. HPLC Method for Cyclodextrin Content Evaluation

Table VII.2. - HPLC method for quantification of βCD and HPβCD

HPLC system	Agilent 1100 Series LC (Agilent Technologies Inc.) with RI detector (Shodex RI-101, Shoko Scientific Co., LTD., Japan)
Software	Clarity™ Chromatography Station 6.1 (DataApex, Czech Republic)
Column	LiChroCart® 250-4, LiChrospher® 100 RP18-5 (Merck KGaA) with precolumn
Mobile phase	10/90 V/V% methanol/bidistilled water
Flow rate	0.8 mL/min
Oven temperature	35 °C
Detector temperature	35 °C
Injection volume	100 µL
Run time	15 min

VII.3.3. Comparison of Methods for Itraconazole Content Evaluation

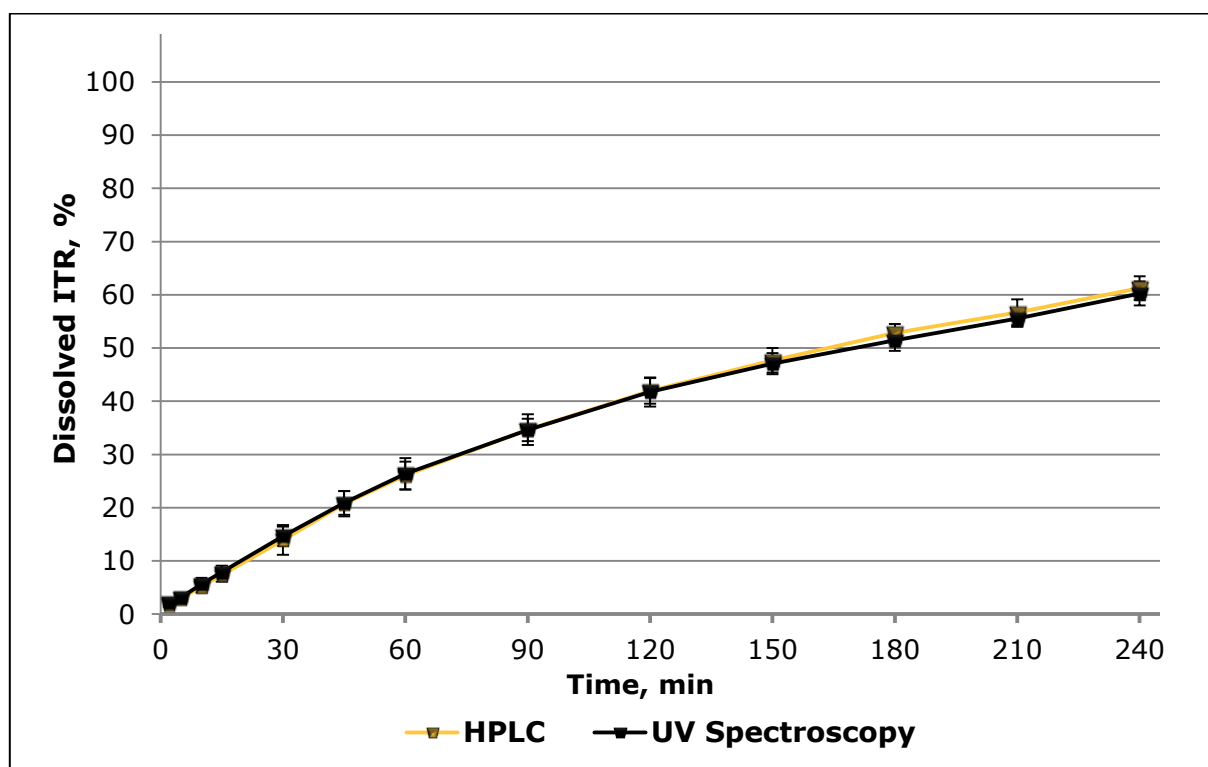


Figure VII.1. - Dissolution results of aITR measured by HPLC and UV spectroscopy; n = 12; error bars = sd.

VIII. Literature References

- [1] A. Fahr, X. Liu, Drug delivery strategies for poorly water-soluble drugs, *Expert opinion on drug delivery* 4 (2007) 403–416.
- [2] G.L. Amidon, H. Lennernäs, V.P. Shah, J.R. Crison, A theoretical basis for a biopharmaceutical drug classification: The correlation of in vitro drug product dissolution and in vivo bioavailability, *Pharmaceutical research* 12 (1995) 413–420.
- [3] C.W. Pouton, Formulation of poorly water-soluble drugs for oral administration: Physicochemical and physiological issues and the lipid formulation classification system, *European journal of pharmaceutical sciences official journal of the European Federation for Pharmaceutical Sciences* 29 (2006) 278–287.
- [4] J. Cook, W. Addicks, Y.H. Wu, Application of the biopharmaceutical classification system in clinical drug development--an industrial view, *The AAPS journal* 10 (2008) 306–310.
- [5] Y.S.R. Krishnaiah, *Pharmaceutical Technologies for Enhancing Oral Bioavailability of Poorly Soluble Drugs*, JBB 02 (2010).
- [6] A. Shahiwala, Formulation approaches in enhancement of patient compliance to oral drug therapy, *Expert opinion on drug delivery* 8 (2011) 1521–1529.
- [7] E. Mutschler, *Mutschler Arzneimittelwirkungen: Lehrbuch der Pharmakologie und Toxikologie mit einführenden Kapiteln in die Anatomie, Physiologie und Pathophysiologie*, 9., vollst. neu bearb. und erw. Aufl. ed., Wissenschaftliche Verlagsgesellschaft, Stuttgart, 2008.
- [8] Y. Kawabata, K. Wada, M. Nakatani, S. Yamada, S. Onoue, Formulation design for poorly water-soluble drugs based on biopharmaceutics classification system: Basic approaches and practical applications, *International journal of pharmaceutics* 420 (2011) 1–10.
- [9] K. Plumb, Continuous Processing in the Pharmaceutical Industry, *Chemical Engineering Research and Design* 83 (2005) 730–738.
- [10] FDA, Sporanox (itraconazole) Oral Solution: Reference ID: 2886744, <https://www.accessdata.fda.gov/drugsatfda.../020657s032lbl.pdf>, accessed 6 September 2017.
- [11] E.M.M. Del Valle, Cyclodextrins and their uses: A review, *Process Biochemistry* 39 (2004) 1033–1046.
- [12] J.M. Butler, J.B. Dressman, The developability classification system: Application of biopharmaceutics concepts to formulation development, *Journal of pharmaceutical sciences* 99 (2010) 4940–4954.
- [13] J.M. Butler, The optimal use of biorelevant media & simple modelling for the prediction of in-vivo oral behaviour, 2011.
- [14] Y. Perrie, T. Rades, Themed issue: Improve dissolution, solubility and bioavailability of poorly soluble drugs, *The Journal of pharmacy and pharmacology* 62 (2010) 1517–1518.
- [15] Leuner, C., Dressman, J., Improving drug solubility for oral delivery using solid dispersions, *European journal of pharmaceutics and biopharmaceutics*

- official journal of Arbeitsgemeinschaft für Pharmazeutische Verfahrenstechnik e.V 50 (2000) 47–60.
- [16] H. Egermann, K.H. Bauer, B.C. Lippold, Lehrbuch der pharmazeutischen Technologie: Mit einer Einführung in die Biopharmazie ; mit 95 Tabellen, 8., durchges. und aktualisierte Aufl. ed., Wiss. Verl.-Ges, Stuttgart, 2006.
- [17] J.B. Dressman, C. Reppas, In vitro-in vivo correlations for lipophilic, poorly water-soluble drugs, European journal of pharmaceutical sciences official journal of the European Federation for Pharmaceutical Sciences 11 Suppl 2 (2000) 73-80.
- [18] W.L. Chiou, S. Riegelman, Pharmaceutical Applications of Solid Dispersion Systems, Journal of pharmaceutical sciences 60 (1971) 1281–1302.
- [19] S. Janssens, G. van den Mooter, Review: Physical chemistry of solid dispersions, The Journal of pharmacy and pharmacology 61 (2009) 1571–1586.
- [20] K. Kolter, M. Karl, A. Gryczke, Hot-melt extrusion with BASF pharma polymers: Extrusion compendium, 2., rev. and enl. ed. ed., BASF, Ludwigshafen, 2012.
- [21] M.M. Crowley, F. Zhang, M.A. Repka, S. Thumma, S.B. Upadhye, S.K. Battu, J.W. McGinity, C. Martin, Pharmaceutical applications of hot-melt extrusion: Part I, Drug development and industrial pharmacy 33 (2007) 909–926.
- [22] M. Wilson, M.A. Williams, D.S. Jones, G.P. Andrews, Hot-melt extrusion technology and pharmaceutical application, Therapeutic Delivery 3 (2012) 787–797.
- [23] S. Shah, M.A. Repka, Chapter 1 Melt Extrusion in Drug Delivery: Three Decades of Progress, in: M.A. Repka, N. Langley, J. DiNunzio (Eds.), Melt extrusion: Materials, technology and drug product design, Springer, New York, 2013, pp. 3–47.
- [24] J. Breitenbach, Melt extrusion: From process to drug delivery technology, European journal of pharmaceuticals and biopharmaceutics official journal of Arbeitsgemeinschaft für Pharmazeutische Verfahrenstechnik e.V 54 (2002) 107–117.
- [25] M. Maniruzzaman, J.S. Boateng, M.J. Snowden, D. Douroumis, A review of hot-melt extrusion: Process technology to pharmaceutical products, ISRN pharmaceuticals 2012 (2012) 436763.
- [26] D. Treffer, P. Wahl, D. Markl, G. Koscher, E. Roblegg, J.G. Khinast, Chapter 15 Hot Melt Extrusion as a Continuous Pharmaceutical Manufacturing Process, in: M.A. Repka, N. Langley, J. DiNunzio (Eds.), Melt extrusion: Materials, technology and drug product design, Springer, New York, 2013, pp. 363–397.
- [27] M.A. Repka, S. Shah, J. Lu, S. Maddineni, J. Morott, K. Patwardhan, N.N. Mohammed, Melt extrusion: Process to product, Expert opinion on drug delivery 9 (2012) 105–125.
- [28] N. Follonier, E. Doelker, E.T. Cole, Evaluation of hot-melt extrusion as a new technique for the production of polymer-based pellets for sustained

- release capsules containing high loadings of freely soluble drugs, *Drug development and industrial pharmacy* 20 (2008) 1323–1339.
- [29] Z. Ghalanbor, M. Körber, R. Bodmeier, Improved lysozyme stability and release properties of poly(lactide-co-glycolide) implants prepared by hot-melt extrusion, *Pharmaceutical research* 27 (2010) 371–379.
- [30] M.M. Crowley, B. Schroeder, A. Fredersdorf, S. Obara, M. Talarico, S. Kucera, J.W. McGinity, Physicochemical properties and mechanism of drug release from ethyl cellulose matrix tablets prepared by direct compression and hot-melt extrusion, *International journal of pharmaceutics* 269 (2004) 509–522.
- [31] M.A. Repka, S.K. Battu, S.B. Upadhye, S. Thumma, M.M. Crowley, F. Zhang, C. Martin, J.W. McGinity, Pharmaceutical applications of hot-melt extrusion: Part II, *Drug development and industrial pharmacy* 33 (2007) 1043–1057.
- [32] M.A. Repka, T.G. Gerding, S.L. Repka, J.W. McGinity, Influence of plasticizers and drugs on the physical-mechanical properties of hydroxypropyl-cellulose films prepared by hot melt extrusion, *Drug development and industrial pharmacy* 25 (1999) 625–633.
- [33] C. Vervaet, J.P. Remon, Continuous granulation in the pharmaceutical industry, *Chemical Engineering Science* 60 (2005) 3949–3957.
- [34] T.W. Wong, W.S. Cheong, P.W.S. Heng, Melt Granulation and Pelletization, in: D.M. Parikh (Ed.), *Handbook of pharmaceutical granulation technology*, 2nd ed., Taylor & Francis, Boca Raton, 2005, pp. 385–406.
- [35] M. Richter, Dry granulation as a twin-screw process in pharmaceutical applications: Application Note No. LR-79.
- [36] A. Batra, D. Desai, A.T.M. Serajuddin, Investigating the Use of Polymeric Binders in Twin Screw Melt Granulation Process for Improving Compactibility of Drugs, *Journal of pharmaceutical sciences* 106 (2017) 140–150.
- [37] R.L. Carrier, L.A. Miller, I. Ahmed, The utility of cyclodextrins for enhancing oral bioavailability, *Journal of controlled release official journal of the Controlled Release Society* 123 (2007) 78–99.
- [38] T. Loftsson, P. Jarho, M. Másson, T. Järvinen, Cyclodextrins in drug delivery, *Expert opinion on drug delivery* 2 (2005) 335–351.
- [39] J. Szejtli, Cyclodextrin Complexed Generic Drugs are Generally not Bioequivalent with the Reference Products: Therefore the Increase in Number of Marketed Drug/Cyclodextrin Formulations is so Slow, *J Incl Phenom Macrocycl Chem* 52 (2005) 1–11.
- [40] T. Loftsson, M.E. Brewster, M. Másson, Role of Cyclodextrins in Improving Oral Drug Delivery, *American Journal of Drug Delivery* 2 (2004) 261–275.
- [41] T. Loftsson, M.E. Brewster, Pharmaceutical applications of cyclodextrins: Effects on drug permeation through biological membranes, *The Journal of pharmacy and pharmacology* 63 (2011) 1119–1135.
- [42] H. Yoshii, T. Kometani, T. Furuta, Y. Watanabe, Y.-Y. Linko, P. Linko, Formation of Inclusion Complex of Cyclodextrin in Organic Solvents and Alcohols under Anhydrous Conditions, in: J.J.T. Labandeira, J.L. Vila-Jato

- (Eds.), Proceedings of the Ninth International Symposium on Cyclodextrins, Springer Netherlands, Dordrecht, 1999, pp. 635–638.
- [43] P.J. Salústio, G. Feio, J.L. Figueirinhas, H.M. Cabral-Marques, P.C. Costa, J.F. Pinto, Release profile of ibuprofen in β -cyclodextrin complexes from two different solid dosage forms, *Powder Technology* 221 (2012) 245–251.
- [44] M. Pedersen, S. Pedersen, A.M. Sørensen, Polymorphism of miconazole during preparation of solid systems of the drug and β -cyclodextrins, *Pharmaceutica Acta Helvetiae* 68 (1993) 43–47.
- [45] A.H. Al-Marzouqi, I. Shehatta, B. Jobe, A. Dowaidar, Phase solubility and inclusion complex of itraconazole with beta-cyclodextrin using supercritical carbon dioxide, *Journal of pharmaceutical sciences* 95 (2006) 292–304.
- [46] H.A. Hassan, A.H. Al-Marzouqi, B. Jobe, A.A. Hamza, G.A. Ramadan, Enhancement of dissolution amount and in vivo bioavailability of itraconazole by complexation with beta-cyclodextrin using supercritical carbon dioxide, *Journal of pharmaceutical and biomedical analysis* 45 (2007) 243–250.
- [47] L. Liu, Q.-X. Guo, The Driving Forces in the Inclusion Complexation of Cyclodextrins, *J Incl Phenom Macrocycl Chem* 42 (2002) 1–14.
- [48] Y. Matsui, T. Nishioka, T. Fujita, Quantitative structure-reactivity analysis of the inclusion mechanism by cyclodextrins, in: F.L. Boschke, M.J.S. Dewar, J.D. Dunitz, K. Hafner, E. Heilbronner, S. Ito, J.-M. Lehn, K. Niedenzu, K.N. Raymond, C.W. Rees, F. Vögtle, G. Wittig (Eds.), *Biomimetic and Bioorganic Chemistry*, Springer Berlin Heidelberg, Berlin, Heidelberg, 1985, pp. 61–89.
- [49] T. Loftsson, M.E. Brewster, Pharmaceutical applications of cyclodextrins: Basic science and product development, *The Journal of pharmacy and pharmacology* 62 (2010) 1607–1621.
- [50] V.J. Stella, V.M. Rao, E.A. Zannou, V.V. Zia, Mechanisms of drug release from cyclodextrin complexes, *Advanced drug delivery reviews* 36 (1999) 3–16.
- [51] R.A. Rajewski, V.J. Stella, Pharmaceutical applications of cyclodextrins. 2. In vivo drug delivery, *Journal of pharmaceutical sciences* 85 (1996) 1142–1169.
- [52] V. Law, C. Knox, Y. Djoumbou, T. Jewison, A.C. Guo, Y. Liu, A. Maciejewski, D. Arndt, M. Wilson, V. Neveu, A. Tang, G. Gabriel, C. Ly, S. Adamjee, Z.T. Dame, B. Han, Y. Zhou, D.S. Wishart., *Drugbank 5.0: Itraconazole*, 2017.
- [53] G.E. Pierard, J.E. Arrese, C. Pierard-Franchimont, Itraconazole, *Expert opinion on pharmacotherapy* 1 (2000) 287–304.
- [54] J.M. Zuckerman, A.R. Tunkel, Itraconazole: A new triazole antifungal agent, *Infection control and hospital epidemiology* 15 (1994) 397–410.
- [55] J.A. Como, W.E. Dismukes, Oral azole drugs as systemic antifungal therapy, *The New England journal of medicine* 330 (1994) 263–272.
- [56] J. Kim, J.Y. Tang, R. Gong, J. Kim, J.J. Lee, K.V. Clemons, C.R. Chong, K.S. Chang, M. Fereshteh, D. Gardner, T. Reya, J.O. Liu, E.H. Epstein, D.A. Stevens, P.A. Beachy, Itraconazole, a commonly used antifungal that in-

- hibits Hedgehog pathway activity and cancer growth, *Cancer cell* 17 (2010) 388–399.
- [57] National Library of Medicine (NLM) at National Institutes of Health (NIH), www.clinicaltrials.gov.
- [58] ROTE LISTE 2017 Buchausgabe Aboausgabe: Arzneimittelverzeichnis für Deutschland (einschließlich EU-Zulassungen und bestimmter Medizinprodukte), 1. Auflage ed., Rote Liste Service GmbH, Frankfurt am Main, 2017.
- [59] Itraconazol: Monographie, in: Europäisches Arzneibuch DVD-ROM 8. Ausgabe, Grundwerk 2014 (Ph. Eur. 8.0) inkl. 1. bis 8. Nachtrag (Ph.Eur. 8.1 bis 8.8): Amtliche deutsche Ausgabe, 1st ed., Deutscher Apotheker Verlag, Stuttgart, 2016, pp. 3739–3741.
- [60] K. Six, T. Daems, J. de Hoon, A. van Hecken, M. Depre, M.-P. Bouche, P. Prinsen, G. Verreck, J. Peeters, M.E. Brewster, G. van den Mooter, Clinical study of solid dispersions of itraconazole prepared by hot-stage extrusion, *European journal of pharmaceutical sciences official journal of the European Federation for Pharmaceutical Sciences* 24 (2005) 179–186.
- [61] B. Lang, J.W. McGinity, R.O. Williams, Dissolution enhancement of itraconazole by hot-melt extrusion alone and the combination of hot-melt extrusion and rapid freezing--effect of formulation and processing variables, *Molecular pharmaceuticals* 11 (2014) 186–196.
- [62] K. Zhang, H. Yu, Q. Luo, S. Yang, X. Lin, Y. Zhang, B. Tian, X. Tang, Increased dissolution and oral absorption of itraconazole/Soluplus extrudate compared with itraconazole nanosuspension, *European journal of pharmaceuticals and biopharmaceutics official journal of Arbeitsgemeinschaft für Pharmazeutische Verfahrenstechnik e.V* 85 (2013) 1285–1292.
- [63] T. Taupitz, J.B. Dressman, C.M. Buchanan, S. Klein, Cyclodextrin-water soluble polymer ternary complexes enhance the solubility and dissolution behaviour of poorly soluble drugs. Case example: Itraconazole, *European journal of pharmaceuticals and biopharmaceutics official journal of Arbeitsgemeinschaft für Pharmazeutische Verfahrenstechnik e.V* 83 (2013) 378–387.
- [64] E. Cevher, A. Acma, G. Sinani, B. Aksu, M. Zloh, L. Mulazimoglu, Bioadhesive tablets containing cyclodextrin complex of itraconazole for the treatment of vaginal candidiasis, *International journal of biological macromolecules* 69 (2014) 124–136.
- [65] I.A. Alsarra, F.K. Alanazi, S.M. Ahmed, A.A. Bosela, S.S. Alhamed, H.A. Mowafy, S.H. Neau, Comparative study of itraconazole-cyclodextrin inclusion complex and its commercial product, *Archives of pharmacal research* 33 (2010) 1009–1017.
- [66] P.M.V. Gilis, De Condé, Valentin F. V., R.P.G. Vandecruys, Beads having a core coated with an antifungal and a polymer, US005633015A (1993).
- [67] P.M.V. Gilis, De Conde, Valentin Florent Victor, R.P.G. Vandecruys, Pellets having a core coated with an antifungal and a polymer, US006663901B1 (1999).
- [68] T. Loftsson, D. Duchêne, Cyclodextrins and their pharmaceutical applications, *International journal of pharmaceuticals* 329 (2007) 1–11.

- [69] H. Leemhuis, R.M. Kelly, L. Dijkhuizen, Engineering of cyclodextrin glucanotransferases and the impact for biotechnological applications, *Applied microbiology and biotechnology* 85 (2010) 823–835.
- [70] S.V. Kurkov, T. Loftsson, Cyclodextrins, *International journal of pharmaceuticals* 453 (2013) 167–180.
- [71] M.E. Brewster, T. Loftsson, Cyclodextrins as pharmaceutical solubilizers, *Advanced drug delivery reviews* 59 (2007) 645–666.
- [72] T. Loftsson, M.E. Brewster, Pharmaceutical applications of cyclodextrins. 1. Drug solubilization and stabilization, *Journal of pharmaceutical sciences* 85 (1996) 1017–1025.
- [73] T. Irie, K. Uekama, Pharmaceutical applications of cyclodextrins. III. Toxicological issues and safety evaluation, *Journal of pharmaceutical sciences* 86 (1997) 147–162.
- [74] S. Gould, R.C. Scott, 2-Hydroxypropyl-beta-cyclodextrin (HP-beta-CD): A toxicology review, *Food and chemical toxicology an international journal published for the British Industrial Biological Research Association* 43 (2005) 1451–1459.
- [75] Hydroxypropylbetadex: Monographie, Nachtrag 8.2, in: *Europäisches Arzneibuch DVD-ROM 8. Ausgabe, Grundwerk 2014 (Ph. Eur. 8.0) inkl. 1. bis 8. Nachtrag (Ph.Eur. 8.1 bis 8.8): Amtliche deutsche Ausgabe, 1st ed., Deutscher Apotheker Verlag, Stuttgart, 2016, pp. 5815–5817.*
- [76] Betadex: Monographie, in: *Europäisches Arzneibuch DVD-ROM 8. Ausgabe, Grundwerk 2014 (Ph. Eur. 8.0) inkl. 1. bis 8. Nachtrag (Ph.Eur. 8.1 bis 8.8): Amtliche deutsche Ausgabe, 1st ed., Deutscher Apotheker Verlag, Stuttgart, 2016, pp. 7188–7190.*
- [77] A. Mortensen, F. Aguilar, R. Crebelli, A. Di Domenico, B. Dusemund, M.J. Frutos, P. Galtier, D. Gott, U. Gundert-Remy, J.-C. Leblanc, O. Lindtner, P. Moldeus, P. Mosesso, D. Parent-Massin, A. Oskarsson, I. Stankovic, I. Waalkens-Berendsen, R.A. Woutersen, M. Wright, M. Younes, P. Boon, D. Chrysafidis, R. Gürtler, P. Tobback, D. Arcella, A.M. Rincon, C. Lambré, Re-evaluation of β -cyclodextrin (E 459) as a food additive, *EFS2* 14 (2016).
- [78] European Medicines Agency, Annex to the European Commission guideline on 'Excipients in the labelling and package leaflet of medicinal products for human use', 2017.
- [79] European Medicines Agency, Background review for cyclodextrins used as excipient, 2014.
- [80] Roquette Frères S.A., Kleptose® Betacyclodextrins and HPBCD, 2006.
- [81] M. Fukuda, D.A. Miller, N.A. Peppas, J.W. McGinity, Influence of sulfobutyl ether beta-cyclodextrin (Captisol) on the dissolution properties of a poorly soluble drug from extrudates prepared by hot-melt extrusion, *International journal of pharmaceuticals* 350 (2008) 188–196.
- [82] M. Linn, E.-M. Collnot, D. Djuric, K. Hempel, E. Fabian, K. Kolter, C.-M. Lehr, Soluplus(R) as an effective absorption enhancer of poorly soluble drugs in vitro and in vivo, *European journal of pharmaceutical sciences official journal of the European Federation for Pharmaceutical Sciences* 45 (2012) 336–343.

- [83] M. Beneš, T. Pekárek, J. Beránek, J. Havlíček, L. Krejčík, M. Šimek, M. Tkadlecová, P. Doležal, Methods for the preparation of amorphous solid dispersions – A comparative study, *Journal of Drug Delivery Science and Technology* 38 (2017) 125–134.
- [84] BASF SE, Technical Information Soluplus: Pharma Ingredients and Services, 2010.
- [85] F. Guth, M. Becker, Buesen, R., Kolter, K., Bioavailability Enhancement of Itraconazole with Solid Solutions Based on Soluplus®, 39th CRS Annual Meeting, Québec City, Canada, 2012.
- [86] Y. Zhong, G. Jing, B. Tian, H. Huang, Y. Zhang, J. Gou, X. Tang, H. He, Y. Wang, Supersaturation induced by Itraconazole/Soluplus® micelles provided high GI absorption in vivo, *Asian Journal of Pharmaceutical Sciences* 11 (2016) 255–264.
- [87] J. Thiry, F. Krier, S. Ratwatte, J.-M. Thomassin, C. Jerome, B. Evrard, Hot-melt extrusion as a continuous manufacturing process to form ternary cyclodextrin inclusion complexes, *European journal of pharmaceutical sciences official journal of the European Federation for Pharmaceutical Sciences* 96 (2017) 590–597.
- [88] L.L.C. MP Biomedicals, Chemical structure of PEG, 2017, <https://www.mpbio.com/product.php?pid=02151910&country=81>.
- [89] R. Voigt, A. Fahr, *Pharmazeutische Technologie: Für Studium und Beruf ; 109 Tabellen, 10., überarb. und erw. Aufl. ed., Dt. Apotheker-Verl., Stuttgart, 2006.*
- [90] S. Stavchansky, W.G. Gowan, Evaluation of the bioavailability of a solid dispersion of phenytoin in polyethylene glycol 6000 and a commercial phenytoin sodium capsule in the dog, *Journal of pharmaceutical sciences* 73 (1984) 733–736.
- [91] G. Trapani, M. Franco, A. Latrofa, M.R. Pantaleo, M.R. Provenzano, E. Sanna, E. Maciocco, G. Liso, Physicochemical characterization and in vivo properties of Zolpidem in solid dispersions with polyethylene glycol 4000 and 6000, *International journal of pharmaceutics* 184 (1999) 121–130.
- [92] W.L. Chiou, Pharmaceutical applications of solid dispersion systems: X-ray diffraction and aqueous solubility studies on griseofulvin-polyethylene glycol 6000 systems, *Journal of pharmaceutical sciences* 66 (1977) 989–991.
- [93] S. Verheyen, P. Augustijns, R. Kinget, G. van den Mooter, Melting behavior of pure polyethylene glycol 6000 and polyethylene glycol 6000 in solid dispersions containing diazepam or temazepam: A DSC study, *Thermochimica Acta* 380 (2001) 153–164.
- [94] A.M. Rabasco, J.M. Ginés, M. Fernández-Arévalo, M.A. Holgado, Dissolution rate of diazepam from polyethylene glycol 6000 solid dispersions, *International journal of pharmaceutics* 67 (1991) 201–205.
- [95] Clariant International AG, Your universally applicable polymer: POLYGLYKOL (2013).
- [96] I.S.M. Rafiqul, A.M.M. Sakinah, Processes for the Production of Xylitol—A Review, *Food Reviews International* 29 (2013) 127–156.

- [97] V. Law, C. Knox, Y. Djoumbou, T. Jewison, A.C. Guo, Y. Liu, A. Maciejewski, D. Arndt, M. Wilson, V. Neveu, A. Tang, G. Gabriel, C. Ly, S. Adamjee, Z.T. Dame, B. Han, Y. Zhou, D.S. Wishart., Drugbank 5.0: D-Xylitol, 2017.
- [98] J.N. Pawar, R.A. Fule, M. Maniruzzaman, P.D. Amin, Solid crystal suspension of Efavirenz using hot melt extrusion: Exploring the role of crystalline polyols in improving solubility and dissolution rate, *Materials science & engineering. C, Materials for biological applications* 78 (2017) 1023–1034.
- [99] E.M. Schwarz, V.V. Grundstein, A.F. Ievins, Thermal investigation of polyols, *Journal of Thermal Analysis* 4 (1972) 331–337.
- [100] A. Kaizawa, N. Maruoka, A. Kawai, H. Kamano, T. Jozuka, T. Senda, T. Akiyama, Thermophysical and heat transfer properties of phase change material candidate for waste heat transportation system, *Heat Mass Transfer* 44 (2008) 763–769.
- [101] Royal Society of Chemistry 2015, ChemSpider: Structure of Xylitol.
- [102] Cellulose & Pharmaceutical Excipients Department, METOLOSE: Water soluble cellulose ethers, 2005.
- [103] A. Makó, G. Csóka, E. Pásztor, S. Marton, G. Horvai, I. Klebovich, Formulation of thermoresponsive and bioadhesive gel for treatment of oesophageal pain and inflammation, *European journal of pharmaceutics and biopharmaceutics official journal of Arbeitsgemeinschaft fur Pharmazeutische Verfahrenstechnik e.V* 72 (2009) 260–265.
- [104] S. Verma, S. Kumar, R. Gokhale, D.J. Burgess, Physical stability of nanosuspensions: Investigation of the role of stabilizers on Ostwald ripening, *International journal of pharmaceutics* 406 (2011) 145–152.
- [105] F. Sadeghi, J.L. Ford, M.H. Rubinstein, A.R. Rajabi-Siahboomi, Comparative study of drug release from pellets coated with HPMC or Surelease, *Drug development and industrial pharmacy* 26 (2000) 651–660.
- [106] C. de Brabander, C. Vervaet, J.P. Remon, Development and evaluation of sustained release mini-matrices prepared via hot melt extrusion, *Journal of Controlled Release* 89 (2003) 235–247.
- [107] M.M. Al-Tabakha, HPMC capsules: Current status and future prospects, *Journal of pharmacy & pharmaceutical sciences a publication of the Canadian Society for Pharmaceutical Sciences, Societe canadienne des sciences pharmaceutiques* 13 (2010) 428–442.
- [108] K. Six, H. Berghmans, C. Leuner, J. Dressman, K. van Werde, J. Mullens, L. Benoist, M. Thimon, L. Meublât, G. Verreck, J. Peeters, M. Brewster, G. van den Mooter, Characterization of solid dispersions of itraconazole and hydroxypropylmethylcellulose prepared by melt extrusion, Part II, *Pharmaceutical research* 20 (2003) 1047–1054.
- [109] G. Verreck, K. Six, G. van den Mooter, L. Baert, J. Peeters, M.E. Brewster, Characterization of solid dispersions of itraconazole and hydroxypropylmethylcellulose prepared by melt extrusion—part I, *International journal of pharmaceutics* 251 (2003) 165–174.
- [110] B. Rambali, G. Verreck, L. Baert, D.L. Massart, Itraconazole formulation studies of the melt-extrusion process with mixture design, *Drug development and industrial pharmacy* 29 (2003) 641–652.

- [111] S. Rajarajan, B. Baby, K. Ramesh, D. Singh, Preparation and Evaluation of Ternary Mixing Itraconazole Solid Dispersions by Spray Drying Method, *Journal of Pharmaceutical Sciences and Research* 1 (2009) 22–25.
- [112] Willy A. Bachofen AG, Maschinenfabrik, Muttentz, Switzerland, Turbula - Three-dimensional shaker-mixer.
- [113] M. Wilson, M.A. Williams, D.S. Jones, G.P. Andrews, Hot-melt extrusion technology and pharmaceutical application, *Therapeutic Delivery* 3 (2012) 787–797.
- [114] Brabender Technologie GmbH&Co.KG, Betriebsanleitung MT-S HYD (2013).
- [115] H.F. Giles, J.R. Wagner, E.M. Mount, *Extrusion: The definitive processing guide and handbook*, William Andrew Pub, Norwich NY, 2005.
- [116] S. Shah, S. Maddineni, J. Lu, M.A. Repka, Melt extrusion with poorly soluble drugs, *International journal of pharmaceutics* 453 (2013) 233–252.
- [117] Thermo Electron (Karlsruhe) GmbH, Part of Thermo Fisher Scientific, Betriebsanleitung: Pharma 11 Doppelschnecken-Extruder. Version 1.02 (2013).
- [118] T. Higuchi, K.A. Connors, Phase-Solubility Techniques, *Advances in Analytical Chemistry and Instrumentation* 117–212.
- [119] T. Loftsson, D. Hreinsdóttir, M. Másson, Evaluation of cyclodextrin solubilization of drugs, *International journal of pharmaceutics* 302 (2005) 18–28.
- [120] T. Loftsson, M. Másson, M.E. Brewster, Self-association of cyclodextrins and cyclodextrin complexes, *Journal of pharmaceutical sciences* 93 (2004) 1091–1099.
- [121] T. Loftsson, D. Hreinsdóttir, M. Másson, The complexation efficiency, *J Incl Phenom Macrocycl Chem* 57 (2007) 545–552.
- [122] T. Loftsson, M. Másson, J.F. Sigurjónsdóttir, Methods to enhance the complexation efficiency of cyclodextrins, *S.T.P. Pharma Sci.* (1999) 237–242.
- [123] R.K. Khankari, D. Law, D.J.W. Grant, Determination of water content in pharmaceutical hydrates by differential scanning calorimetry, *International journal of pharmaceutics* 82 (1992) 117–127.
- [124] R.A. Storey, I. Ymen, *Solid state characterization of pharmaceuticals*, John Wiley & Sons, Chichester, UK, 2011.
- [125] D.A. Skoog, F.J. Holler, S.R. Crouch, *Instrumentelle Analytik: Grundlagen - Geräte - Anwendungen*, 6., vollst. überarb. erw. Aufl. 2014 ed., Springer, Berlin, 2014.
- [126] P. Matejtschuk, C. Duru, K. Malik, E. Ezeajughi, E. Gray, S. Raut, F. Mawas, Use of Thermogravimetric Analysis for Moisture Determination in Difficult Lyophilized Biological Samples, *AJAC* 07 (2016) 260–265.
- [127] S.K. Parikh, A.D. Patel, J.B. Dave, C.N. Patel, D.J. Sen, Development and Validation of UV Spectrophotometric Method for Estimation of Itraconazole Bulk Drug and Pharmaceutical Formulation, *Int J. Drug Dev. & Res.* (2011) 324–328.
- [128] M. Trinadha Rao, J. Vijaya Ratna, Y. Srinivas Rao, T. Hemant Kumar, Development and Validation of RP-HPLC Method for the Determination of Itraconazole in Bulk and Capsule Dosage Form, *International Journal of Pharmaceutical Sciences Review and Research* (2015) 221–225.

- [129] US Department of Health and Human Services, Food and Drug Administration, Center for Drug Evaluation and Research, Guidance for industry: dissolution testing of Immediate Release Solid Oral Dosage Forms, 1997.
- [130] B. Shah, V.K. Kakumanu, A.K. Bansal, Analytical techniques for quantification of amorphous/crystalline phases in pharmaceutical solids, *Journal of pharmaceutical sciences* 95 (2006) 1641–1665.
- [131] G. Rücker, M. Neugebauer, G.G. Willems, *Instrumentelle Analytik für Pharmazeuten: Lehrbuch zu spektroskopischen, chromatografischen, elektrochemischen und thermischen Analysenmethoden*, 4., durges. und akt. Aufl. ed., Wissenschaftliche Verlagsgesellschaft, Stuttgart, 2008.
- [132] PerkinElmer Life and Analytical Sciences, FT-IR Spectroscopy: Attenuated Total Reflectance (ATR). Technical Note (2005).
- [133] P. Mura, Analytical techniques for characterization of cyclodextrin complexes in the solid state: A review, *Journal of pharmaceutical and biomedical analysis* 113 (2015) 226–238.
- [134] N. Kumar, S. Goindi, B. Saini, G. Bansal, Thermal characterization and compatibility studies of itraconazole and excipients for development of solid lipid nanoparticles, *J Therm Anal Calorim* 115 (2014) 2375–2383.
- [135] D.I. Nesseem, Formulation and evaluation of itraconazole via liquid crystal for topical delivery system, *Journal of pharmaceutical and biomedical analysis* 26 (2001) 387–399.
- [136] A.A. Al-Badr, H.I. El-Subbagh, Itraconazole: Comprehensive Profile, in: Elsevier, 2009, pp. 193–264.
- [137] S. Gunasekaran, B. Anita, Spectral investigation and normal coordinate analysis of piperazine, *IJPAP* 46 (2008) 833–838.
- [138] B. Nickerson, R. Löbenberg, C. Tong, Y. Mao, Q. Wang, T. Mirza, R. Lozano, V. Gray, The Value of In Vitro Dissolution in Drug Development: A Position Paper from the AAPS In Vitro Release and Dissolution Focus Group, *Pharmaceutical Technology* 33 (2009).
- [139] B. Nickerson, C.K. Brown, H.P. Chokshi, R.A. Reed, B.R. Rohrs, P.A. Shah, Acceptable Analytical Practises for Dissolution Testing of Poorly Soluble Compounds, *Pharmaceutical Technology* 28 (2004) 56–65.
- [140] Wirkstofffreisetzung aus festen Arzneiformen: Methode der pharmazeutischen Technologie, in: *Europäisches Arzneibuch DVD-ROM 8. Ausgabe*, Grundwerk 2014 (Ph. Eur. 8.0) inkl. 1. bis 8. Nachtrag (Ph.Eur. 8.1 bis 8.8): Amtliche deutsche Ausgabe, 1st ed., Deutscher Apotheker Verlag, Stuttgart, 2016, pp. 7367–7375.
- [141] H.S. Ghazal, A.M. Dyas, J.L. Ford, G.A. Hutcheon, In vitro evaluation of the dissolution behaviour of itraconazole in bio-relevant media, *International journal of pharmaceutics* 366 (2009) 117–123.
- [142] INTERNATIONAL CONFERENCE ON HARMONISATION OF TECHNICAL REQUIREMENTS FOR REGISTRATION OF PHARMACEUTICALS FOR HUMAN USE, ICH HARMONISED TRIPARTITE GUIDELINE: STABILITY TESTING OF NEW DRUG SUBSTANCES AND PRODUCTS Q1A(R2) (2003).

- [143] E. Gökbulut, N. Özdemir, Enhancement of Solubility of Itraconazole by Complexation with beta Cyclodextrin Derivatives, *FABAD J. Pharm. Sci.* 42 (2017) 1–6.
- [144] K. Kumari, V. Sharma, B. Philip, K. Pathak, Preparation and evaluation of binary and ternary inclusion complex of Itraconazole, *Der Pharmacia Lettre* 2 (2010) 144–155.
- [145] F.K. Alanazi, S.M. Ahmed, S.S. Alhamed, H.A. Mowafy, I.A. Alsarra, M.A. Bayomi, Inclusion complexation of Itraconazole with cyclodextrin derivatives: phase solubility and physicochemical characterization, *Mansoura J. Pharm. Sci.* 23 (2007) 177–194.
- [146] J. Peeters, P. Neeskens, J.P. Tollenaere, P. van Remoortere, M.E. Brewster, Characterization of the interaction of 2-hydroxypropyl-beta-cyclodextrin with itraconazole at pH 2, 4, and 7, *Journal of pharmaceutical sciences* 91 (2002) 1414–1422.
- [147] S.S. Shah, T.Y. Pasha, A.K. Behera, A. Bhandari, Solubility enhancement and physicochemical characterization of inclusion complexes of itraconazole, *Der Pharmacia Lettre* 4 (2012) 354–366.
- [148] P. Li, S.E. Tabibi, S.H. Yalkowsky, Combined effect of complexation and pH on solubilization, *Journal of pharmaceutical sciences* 87 (1998) 1535–1537.
- [149] F. Giordano, C. Novak, J.R. Moyano, Thermal analysis of cyclodextrins and their inclusion compounds, *Thermochimica Acta* 380 (2001) 123–151.
- [150] K. Six, C. Leuner, J. Dressman, G. Verreck, J. Peeters, N. Blaton, P. Augustijns, R. Kinget, G. van den Mooter, Thermal Properties of Hot-Stage Extrudates of Itraconazole and Eudragit E100: Phase separation and polymorphism, *J Therm Anal Calorim* 68 (2002) 591–601.
- [151] S. Kumar, J. Shen, D.J. Burgess, Nano-amorphous spray dried powder to improve oral bioavailability of itraconazole, *Journal of controlled release official journal of the Controlled Release Society* 192 (2014) 95–102.
- [152] S. Zhang, T.W.Y. Lee, A.H.L. Chow, Crystallization of Itraconazole Polymorphs from Melt, *Crystal Growth & Design* 16 (2016) 3791–3801.
- [153] J. Werling, M.J. Doty, C.L. Rebbeck, J.C.T. Wong, J.E. Kipp, Polymorphic Form of Itraconazole, *US 7,193,084 B2* (August 5).
- [154] K. Six, G. Verreck, J. Peeters, K. Binnemans, H. Berghmans, P. Augustijns, R. Kinget, G. van den Mooter, Investigation of thermal properties of glassy itraconazole: Identification of a monotropic mesophase, *Thermochimica Acta* 376 (2001) 175–181.
- [155] S. Janssens, H.N. de Armas, J.P. Remon, G. van den Mooter, The use of a new hydrophilic polymer, Kollicoat IR, in the formulation of solid dispersions of Itraconazole, *European journal of pharmaceutical sciences official journal of the European Federation for Pharmaceutical Sciences* 30 (2007) 288–294.
- [156] A.H. Al-Marzouqi, H.M. Elwy, I. Shehadi, A. Adem, Physicochemical properties of antifungal drug-cyclodextrin complexes prepared by supercritical carbon dioxide and by conventional techniques, *Journal of pharmaceutical and biomedical analysis* 49 (2009) 227–233.

- [157] J. Liu, L. Qiu, J. Gao, Y. Jin, Preparation, characterization and in vivo evaluation of formulation of baicalein with hydroxypropyl-beta-cyclodextrin, *International journal of pharmaceutics* 312 (2006) 137–143.
- [158] A. Singh, A. Bharati, P. Frederiks, O. Verkinderen, B. Goderis, R. Cardinaels, P. Moldenaers, J. van Humbeeck, G. van den Mooter, Effect of Compression on the Molecular Arrangement of Itraconazole-Soluplus Solid Dispersions: Induction of Liquid Crystals or Exacerbation of Phase Separation?, *Molecular pharmaceutics* 13 (2016) 1879–1893.
- [159] S.G. Kapsi, J.W. Ayres, Processing factors in development of solid solution formulation of itraconazole for enhancement of drug dissolution and bioavailability, *International journal of pharmaceutics* 229 (2001) 193–203.
- [160] National Center for Biotechnology Information. PubChem Compound Database; CID=5988, <https://pubchem.ncbi.nlm.nih.gov/compound/5988> (accessed Oct. 25, 2017).
- [161] A. Sarnes, M. Kovalainen, M.R. Häkkinen, T. Laaksonen, J. Laru, J. Kiesvaara, J. Ilkka, O. Oksala, S. Rönkkö, K. Järvinen, J. Hirvonen, L. Peltonen, Nanocrystal-based per-oral itraconazole delivery: Superior in vitro dissolution enhancement versus Sporanox® is not realized in in vivo drug absorption, *Journal of controlled release official journal of the Controlled Release Society* 180 (2014) 109–116.
- [162] X. Wang, A. Michoel, G. van den Mooter, Study of the phase behavior of polyethylene glycol 6000-itraconazole solid dispersions using DSC, *International journal of pharmaceutics* 272 (2004) 181–187.
- [163] S. Janssens, H.N. de Armas, W. D'Autry, A. van Schepdael, G. van den Mooter, Characterization of ternary solid dispersions of Itraconazole in polyethylene glycol 6000/polyvidone-vinylacetate 64 blends, *European journal of pharmaceutics and biopharmaceutics official journal of Arbeitsgemeinschaft fur Pharmazeutische Verfahrenstechnik e.V* 69 (2008) 1114–1120.
- [164] H. Valizadeh, A. Nokhodchi, N. Qarakhani, P. Zakeri-Milani, S. Azarmi, D. Hassanzadeh, R. Löbenberg, Physicochemical characterization of solid dispersions of indomethacin with PEG 6000, Myrj 52, lactose, sorbitol, dextrin, and Eudragit E100, *Drug development and industrial pharmacy* 30 (2004) 303–317.
- [165] S. Janssens, H.N. de Armas, C.J. Roberts, G. van den Mooter, Characterization of ternary solid dispersions of itraconazole, PEG 6000, and HPMC 2910 E5, *Journal of pharmaceutical sciences* 97 (2008) 2110–2120.
- [166] T. Loftsson, H. Frikdriksdóttir, A.M. Sigurkdardóttir, H. Ueda, The effect of water-soluble polymers on drug-cyclodextrin complexation, *International journal of pharmaceutics* 110 (1994) 169–177.
- [167] J. Stappaerts, P. Augustijns, Displacement of itraconazole from cyclodextrin complexes in biorelevant media: In vitro evaluation of supersaturation and precipitation behavior, *International journal of pharmaceutics* 511 (2016) 680–687.
- [168] T. Loftsson, The effect of water-soluble polymers on aqueous solubility of drugs, *International journal of pharmaceutics* 127 (1996) 293–296.

- [169] J. Savolainen, K. Järvinen, H. Taipale, P. Jarho, T. Loftsson, T. Järvinen, Co-Administration of a Water-Soluble Polymer Increases the Usefulness of Cyclodextrins in Solid Oral Dosage Forms, *Pharmaceutical research* 15 (1998) 1696–1701.
- [170] J.C.d. Miranda, T.E.A. Martins, F. Veiga, H.G. Ferraz, Cyclodextrins and ternary complexes: Technology to improve solubility of poorly soluble drugs, *Braz. J. Pharm. Sci.* 47 (2011) 665–681.
- [171] J.K. Lee, J.Y. Hwang, Erasure Behavior of Isothermal Physical Aging Effect below Glass Transition Temperature in a Fully Cured Epoxy Resin. Differential Scanning Calorimetry Measurement, *Polym J* 35 (2003) 191–196.
- [172] L. E. C. Baert, J. Peeters, G. Verreck, SOLID MIXTURES OF CYCLODEXTRINS PREPARED VIA MELTEXTRUSION, US 6,365,188 B1 (May 20th, 1998).
- [173] H. Yano, P. Kleinebudde, Improvement of dissolution behavior for poorly water-soluble drug by application of cyclodextrin in extrusion process: Comparison between melt extrusion and wet extrusion, *AAPS PharmSciTech* 11 (2010) 885–893.
- [174] M.A. Halim Mohamed, A.A. Mahmoud, Formulation of indomethacin eye drops via complexation with cyclodextrins, *Current eye research* 36 (2011) 208–216.
- [175] L.A. Miller, R.L. Carrier, I. Ahmed, Practical considerations in development of solid dosage forms that contain cyclodextrin, *Journal of pharmaceutical sciences* 96 (2007) 1691–1707.
- [176] C. Cavallari, B. Abertini, M.L. González-Rodríguez, L. Rodriguez, Improved dissolution behaviour of steam-granulated piroxicam, *European journal of pharmaceutics and biopharmaceutics official journal of Arbeitsgemeinschaft fur Pharmazeutische Verfahrenstechnik e.V* 54 (2002) 65–73.
- [177] T. Tao, Y. Zhao, J. Wu, B. Zhou, Preparation and evaluation of itraconazole dihydrochloride for the solubility and dissolution rate enhancement, *International journal of pharmaceutics* 367 (2009) 109–114.
- [178] S.-Y. Lee, I.-I. Jung, J.-K. Kim, G.-B. Lim, J.-H. Ryu, Preparation of itraconazole/HP- β -CD inclusion complexes using supercritical aerosol solvent extraction system and their dissolution characteristics, *The Journal of Supercritical Fluids* 44 (2008) 400–408.
- [179] B. van Eerdenbrugh, M. van Speybroeck, R. Mols, K. Houthoofd, J.A. Martens, L. Froyen, J. van Humbeeck, P. Augustijns, G. van den Mooter, Itraconazole/TPGS/Aerosil200 solid dispersions: Characterization, physical stability and in vivo performance, *European journal of pharmaceutical sciences official journal of the European Federation for Pharmaceutical Sciences* 38 (2009) 270–278.
- [180] J.-Y. Jung, S.D. Yoo, S.-H. Lee, K.-H. Kim, D.-S. Yoon, K.-H. Lee, Enhanced solubility and dissolution rate of itraconazole by a solid dispersion technique, *International journal of pharmaceutics* 187 (1999) 209–218.
- [181] K. Six, G. Verreck, J. Peeters, M. Brewster, G. van den Mooter, Increased physical stability and improved dissolution properties of itraconazole, a

- class II drug, by solid dispersions that combine fast- and slow-dissolving polymers, *Journal of pharmaceutical sciences* 93 (2004) 124–131.
- [182] J. Thiry, M.G.M. Kok, L. Collard, A. Frère, F. Krier, M. Fillet, B. Evrard, Bio-availability enhancement of itraconazole-based solid dispersions produced by hot melt extrusion in the framework of the Three Rs rule, *European journal of pharmaceutical sciences official journal of the European Federation for Pharmaceutical Sciences* 99 (2017) 1–8.
- [183] J. Thiry, G. Broze, A. Pestieau, A.S. Tatton, F. Baumans, C. Damblon, F. Krier, B. Evrard, Investigation of a suitable in vitro dissolution test for itraconazole-based solid dispersions, *European journal of pharmaceutical sciences official journal of the European Federation for Pharmaceutical Sciences* 85 (2016) 94–105.
- [184] T. Kiss, F. Fenyvesi, I. Bácskay, J. Váradi, E. Fenyvesi, R. Iványi, L. Szente, A. Tósaki, M. Vecsernyés, Evaluation of the cytotoxicity of beta-cyclodextrin derivatives: Evidence for the role of cholesterol extraction, *European journal of pharmaceutical sciences official journal of the European Federation for Pharmaceutical Sciences* 40 (2010) 376–380.
- [185] E.M. Bunting, N. Abou-Madi, S. Cox, T. Martin-Jimenez, H. Fox, G.V. Kollias, Evaluation of oral itraconazole administration in captive Humboldt penguins (*Spheniscus humboldti*), *Journal of zoo and wildlife medicine official publication of the American Association of Zoo Veterinarians* 40 (2009) 508–518.
- [186] S.D. Yoo, E. Kang, B.S. Shin, H. Jun, S.-H. Lee, K.C. Lee, K.-H. Lee, Inter-species comparison of the oral absorption of itraconazole in laboratory animals, *Archives of pharmacal research* 25 (2002) 387–391.
- [187] T. Zimmermann, R.A. Yeates, H. Laufen, G. Pfaff, A. Wildfeuer, Influence of concomitant food intake on the oral absorption of two triazole antifungal agents, itraconazole and fluconazole, *European journal of clinical pharmacology* 46 (1994) 147–150.
- [188] T. Zimmermann, R.A. Yeates, M. Albrecht, H. Laufen, A. Wildfeuer, Influence of concomitant food intake on the gastrointestinal absorption of fluconazole and itraconazole in Japanese subjects, *International journal of clinical pharmacology research* 14 (1994) 87–93.
- [189] J. Brouwers, S. Geboers, R. Mols, J. Tack, P. Augustijns, Gastrointestinal behavior of itraconazole in humans - Part 1: Supersaturation from a solid dispersion and a cyclodextrin-based solution, *International journal of pharmaceutics* 525 (2017) 211–217.
- [190] P. Berben, R. Mols, J. Brouwers, J. Tack, P. Augustijns, Gastrointestinal behavior of itraconazole in humans - Part 2: The effect of intraluminal dilution on the performance of a cyclodextrin-based solution, *International journal of pharmaceutics* (2017).
- [191] T. Loftsson, M.D. Moya-Ortega, C. Alvarez-Lorenzo, A. Concheiro, Pharmacokinetics of cyclodextrins and drugs after oral and parenteral administration of drug/cyclodextrin complexes, *The Journal of pharmacy and pharmacology* 68 (2016) 544–555.

IX. Curriculum Vitae

Personal data

Name: Annika Kristin Heel
Date of birth: February 9th 1988
Place of birth: Lübeck
Nationality: German

Basic and secondary school education

June 2007 Abitur
1998-2007 Oberschule zum Dom, Lübeck
1994-1998 Albert-Schweitzer-Schule, Lübeck

University education

Aug. 2013 Licensure as pharmacist
Aug. 2013 3rd state examination
Jan. 2013-June 2013 pharmacist in training at Kant-Apotheke, Lübeck
June 2012-Dec. 2012 pharmacist in training at KVP Pharma + Veterinär
Produkte GmbH, Kiel in the department of Quality
Assurance
May 2012 2nd state examination
March 2010 1st state examination
April 2008-May 2012 pharmaceutical sciences studies at Kiel University

Work experience

Since Aug. 2014 pharmacist at Kant-Apotheke, Lübeck
April 2014-April 2018 as doctoral candidate: Supervision of student training
- Tableting and powder technology (1 year)
- Galenics (1.5 years)
- Coating, drying and innovative dosage forms (1 year)
- Parenteral dosage forms (6 months)
Since April 2014 doctoral candidate at department of Pharmaceu-
tics and Biopharmaceutics at Kiel University
Sept. 2013-March 2014 research associate at department of Pharmaceu-
tics and Biopharmaceutics at Kiel University

X. Declaration

Erklärung nach § 8 der Promotionsordnung

Hiermit erkläre ich gemäß § 8 der Promotionsordnung der Mathematisch-Naturwissenschaftlichen Fakultät der Christian-Albrechts-Universität zu Kiel, dass ich die vorliegende Arbeit, abgesehen von der Beratung durch meinen Betreuer, selbstständig und ohne fremde Hilfe verfasst habe. Weiterhin habe ich keine anderen als die angegebenen Quellen oder Hilfsmittel benutzt und die den benutzten Werken wörtlich oder inhaltlich entnommenen Stellen als solche kenntlich gemacht. Die vorliegende Arbeit ist unter Einhaltung der Regeln guter wissenschaftlicher Praxis entstanden und wurde bei keiner anderen Universität zur Begutachtung eingereicht.

Annika Kristin Heel

Danksagung

Der Lebensabschnitt „Promotion“ neigt sich nun dem Ende zu und damit auch eine sehr spannende, lehrreiche, herausfordernde und vor allem schöne Zeit, die ich am Pharmazeutischen Institut verbringen durfte, das in den letzten zehn Jahren während meines Studiums und meiner Doktorandenzeit fast zu einem zweiten Zuhause geworden ist. Die letzten Worte dieser Dissertation möchte ich nun dafür nutzen, all den Menschen aufs Herzlichste zu danken, die an ihrem Entstehen beteiligt waren.

Zuallererst ist mein Doktorvater Herr Prof. Dr. Hartwig Steckel zu nennen. Schon während des Studiums motivierten mich seine Vorlesungen und Praktika und festigten mein Interesse an der Pharmazeutischen Technologie, wofür ich ihm sehr dankbar bin. Zudem möchte ich ihm für die Aufnahme in seinen Arbeitskreis danken und die Übergabe eines äußerst spannenden Forschungsthemas zwischen Studium und Promotion, das es mir bereits möglich machte, mit Schmelzextrusion zu arbeiten. Des Weiteren bin ich ihm sehr dankbar für mein interessantes Promotionsthema, dessen Gestaltung er stets unterstützend begleitete, mir aber dennoch sehr viel Raum ließ.

Auch Frau Prof. Dr. Regina Scherließ möchte ich herzlich danken. Sie stand mir immer als Ansprechpartnerin mit Rat und Tat zur Seite und ermöglichte es mir, meine Forschungsergebnisse auf verschiedenen Konferenzen zu präsentieren. Auch ihr bin ich sehr dankbar für die freundliche Aufnahme in ihren Arbeitskreis und ihre Unterstützung in den letzten Jahren.

Bedanken möchte ich mich bei der Firma Roquette Frères, die mit ihrer großzügigen β -Cyclodextrin-Spende einen entscheidenden Beitrag zu meiner Forschung geleistet hat. Zudem danke ich Dr. Nicole Pienack für das Durchführen von XRPD-Messungen im Institut für Anorganische Chemie der CAU Kiel.

Die Entstehung dieser Arbeit wäre nicht möglich gewesen ohne die guten Geister unserer Abteilung, die TAs. Anna, Hanna, Maren, Regina K., Rüdiger, Simone, ihr wart immer sehr hilfsbereit. Wenn man euch gebraucht hat, habt ihr nie gezögert, mir sofort zu Hilfe zu eilen! Ohne eure Süßigkeitenschublade hätte ich die vielen späten Abende, an denen ich diese Arbeit erstellt habe, nicht überlebt. Maren, dir bin ich besonders dankbar, wie genau und geduldig du mich in die HPLC-Analytik eingearbeitet hast. Regina K., meinen herzlichsten Dank für deine Unterstützung bei meinen Analysen, du hast mir damit sehr geholfen. Anna, dir danke ich für die vielen, vielen Freisetzungen und anderweitigen Versuche während unseres gemeinsamen Projektes, du hast mir damit den Rücken freigehalten. Simone, du hattest immer den perfekten Substanzenüberblick, nicht nur bezüglich des Praktikums, danke dafür!

Danksagung

Hanna, ich weiß gar nicht, wo ich anfangen soll. Niemand freut sich so schön über den perfekten Peak wie du und ich bin sehr froh, dass ich das Vergnügen hatte, mit dir zusammen HPLC-Analytik machen zu können. Du hattest immer ein offenes Ohr für mich und alle großen und kleineren Sorgen und hast mir mit tatkräftiger Unterstützung zur Seite gestanden. Bonnie und Clyde waren bei dir in den perfekten Händen. Mir werden insbesondere die gemeinsamen Mittagessen und die begleitenden, wichtigen Diskussionen fehlen, vor allem donnerstags. Vielen Dank!

Rüdi, dir danke ich für deine unendliche Unterstützung während meiner Zeit am Institut. Du hast es immer geschafft mich aufzumuntern und man konnte mit niemandem so gut philosophieren wie mit dir. Ich bin dir auch sehr dankbar für die vielen schönen Abbildungen, die du in den letzten Jahren für mich erstellt hast. Deine Kreativität bleibt unübertroffen.

Denissa, auch dir möchte ich herzlich danken. Dein „kritischer“ Styling-Blick jeden Morgen war immer der perfekte Start in den Tag. Bei allen bürokratischen, organisatorischen Angelegenheiten konnte man immer auf dich zählen!

Liebe IT, Detlef und Volkmar, auf euch konnte man sich vollkommen verlassen und bei jedem Problem wart ihr immer schnell zur Stelle und habt geholfen, wo es nur ging. Vielen Dank dafür! Kalle, auch dir gehört mein Dank. Deine Reparaturkünste haben mir nicht nur im Praktikum sehr geholfen.

Lieber Dirk, dein technischer Einfallsreichtum ist unerschöpflich! Ich konnte stets auf dich zählen und insbesondere bei der Düsenentwicklung für den Schmelzextruder warst du mir eine riesige Hilfe. Was du in deiner Werkstatt alles gezaubert hast war ganz großes Kino und ich bin dir sehr, sehr dankbar dafür.

Einen großen Rahmen während meiner Promotionszeit nahmen die Praktika in Anspruch, die ich in der Gesellschaft vieler talentierter Köpfe betreuen durfte. Kirsten, Judith, Dorothea, Friederike, Mats, Tobias und Marie, mit euch allen konnte ich zusammen die verschiedenen Praktikumsstationen betreuen und wir hatten nicht nur während der Versuche, sondern auch Drumherum sehr viel Spaß! Vom Game-of-Thrones-Tuesday über Vanilletabletten zu bunten Zäpfchen wurde uns nie langweilig! Bedanken möchte ich mich aber natürlich auch bei allen, die ich nicht namentlich genannt habe und die zwar nicht direkt mit mir gemeinsam, aber dennoch auf anderen Stationen die Studenten betreuten und die Semester gestaltet haben.

Ebenfalls danken möchte ich Mathias, Mats und Tobias für das Anfertigen der REM-Aufnahmen.

Des Weiteren danke ich allen meinen Wahlpflichtfachstudentinnen und -studenten sowie Hiwis, die während meiner Promotion viele interessante Ergebnisse herausbekommen haben und sehr oft eine helfende Hand waren.

Ich bedanke mich bei dem „alten“ Arbeitskreis, in den ich damals so offen mit einem „Duplo“ aufgenommen wurde und auch bei allen neuen Kollegen für die spannende Zeit am Institut. Besonders zu nennen an dieser Stelle sind Dr. Katharina Paulsen, der ich sehr dankbar bin, dass sie so viel von ihrem Schmelzextrusionswissen mit mir geteilt hat, und Dr. Ann-Kathrin Menge. Nicht nur während unserer gemeinsamen Zeit am Institut konnte man sich immer sehr gut mit dir unterhalten, auch während unserer Spaziergänge an der Förde war dein klarer Blick auf die Dinge eine wichtige Stütze. Dr. Andrea Arntz danke ich für ihre fröhliche Art, die mich immer mitgerissen hat. Dein spezieller Flair hat die Arbeitsatmosphäre hier sehr viel bunter gemacht.

Besonderer Dank gilt meinen Korrekturlesern, Desirée, Friederike, Judith, Niklas und Dorothea, die mich nicht nur während meiner gesamten Schreibphase mit aller Kraft motiviert und unterstützt haben.

Liebe Desi, wir kennen uns seit unserem ersten Semester, was inzwischen über zehn Jahre her ist, und du hast mich bis zu deiner eigenen Promotion 2017 hier am Institut begleitet. Ich möchte deine Freundschaft nicht einen Tag missen und bin dir so dankbar, dass du die Zeit zum Korrekturlesen gefunden hast.

Liebe Fritzi, danke, dass du trotz des eigenen Promotionsstresses meine Arbeit Korrektur gelesen hast. Wir hatten wirklich wundervolle Jahre hier am Institut und ich schätze deine offene, ehrliche und direkte Art. Wir haben so viele Dinge erlebt und die letzten 4,5 Jahre so mit Leben gefüllt. Ich bin so stolz, dass wir gemeinsam diesen Lebensabschnitt beenden und ich hoffe sehr, dass du auch im nächsten mit von der Partie bist.

Liebe Judith, deine Motivation und Hingabe was Korrigieren, Praktikum, Forschen, ja eigentlich alles angeht, sind unglaublich. Auch wir hatten die letzten Jahre wahnsinnig viel Spaß und nicht zuletzt unsere beiden Praktikumsabenteuer bleiben mir in sehr guter Erinnerung. Vielen Dank, dass du meine Arbeit Korrektur gelesen und mir so viele hilfreiche Ratschläge gegeben hast. Dein eigener Endspurt wird ein Weltrekord, das weiß ich!

Lieber Niklas, deine trockene Art zu korrigieren war genau das Richtige. Vielen Dank, dass du dir während des anstrengenden Arbeitslebens so viel Zeit genommen hast. Vielen Dank auch für die gemeinsame Zeit am Institut! Den „Unfall“ im Abzug werde ich nie vergessen und die „Fotodokumentation“ davon in allen Ehren halten.

Danksagung

Liebe Thea, auch dir bin ich unendlich dankbar, dass du neben dem Arbeitsalltag Zeit hattest, meine Arbeit zu lesen. Du warst die beste Büronachbarin, die man sich wünschen konnte. Du hattest immer ein offenes Ohr und einen Ratschlag und konntest mich auch wieder einnorden, wenn es mal sein musste. Bleib so, wie du bist!

Bedanken möchte ich mich auch bei dem „Bachelor-Club“, der sich in den Jahren meiner Promotion zu einer richtigen Tradition entwickelt hat, von der ich hoffe, dass sie auch noch viele Jahre in unserem Arbeitskreis bestehen bleibt. Der Mittwochabend war immer das Highlight der Woche. Mats und Nancy, vielen Dank, dass ihr uns dabei öfters mit euren Waffeln verpflegt habt, ihr habt euch beide definitiv eine Rose verdient!

Liebe Marie, ich fühle mich sehr alt, wenn ich dich jetzt als Doktorandin sehe, der ich früher noch selbst auf der Sterilstation auf die Finger geguckt habe... Auch dir möchte ich für die gemeinsame Zeit am Institut danken, insbesondere für die vielen intensiven Gespräche kurz vor Feierabend und unsere zahlreichen Tatortabende, bei denen uns auch hinterher nie der Diskussionsstoff ausging.

Diese Arbeit wäre niemals fertig geworden ohne Schokoladenkekse, Beethovens 9., den Soundtrack von Game of Thrones, sowie die unerschütterlich glücklich machenden Liedtexte von Helene Fischer, die mich immer wieder aus meinen „atemlosen“ Phasen der Schreibblockade hervorlocken konnten. Aber vor allem wäre diese Arbeit nicht fertig geworden ohne drei entscheidende Menschen.

Ich bedanke mich aus tiefstem Herzen bei meinem Freund Florian. Du bist immer für mich da und stärkst mir den Rücken. Du hast mich jedes Mal aufgefangen wenn ich schlecht drauf war. Deine Geduld mit mir und deine Nachsichtigkeit wenn ich wieder bis in die Puppen im Labor rumgehangen habe, waren absolut nicht selbstverständlich. Du trägst einen großen Anteil am Gelingen dieser Arbeit und ich bin unendlich dankbar dafür, dass es dich gibt.

Abschließend möchte ich den beiden wichtigsten Personen danken, ohne die diese Arbeit niemals möglich gewesen wäre, meinen Eltern Sibylle und Kai-Detlef Heel. Ihr habt mich von Tag eins an gefördert, ich durfte sein und werden was ich wollte und konnte mich absolut frei entfalten. Egal, was ich auch gemacht habe, eure Unterstützung und Liebe waren mir sicher. Ihr seid in jeder Lebenslage immer für mich da und ich kann kaum in Worte fassen, wie sehr ich euch dankbar bin für das, was aus meinem Leben bislang so geworden ist. Diese Arbeit ist aus gutem Grunde euch gewidmet, ihr habt den Grundstein gelegt und mich seitdem mein ganzes Leben lang kräftig mit Mörtel und Steinen versorgt. Vielen Dank!

Kiel, April 2018